

GEOLOGICA ULTRAIECTINA

Mededelingen van de
Faculteit Aardwetenschappen
Universiteit Utrecht

No. 218

**Relationship between dynamic recrystallization,
grain size distribution and rheology**

Jan ter Heege

Cover:

Evolution of microstructure and flow stress with progressive deformation in Carrara marble (front) and synthetic polycrystalline halite (back), illustrated by the axial shortening of a sample.

This research was carried out at:

HPT laboratory
Faculty of Earth Sciences
Utrecht University
Budapestlaan 4
3584 CD Utrecht
The Netherlands

http://www.geo.uu.nl/Research/HPT_lab/

The research falls within the research program of the
Vening Meinesz Research School of Geodynamics

ISBN: 90-5744-075-X

Relationship between dynamic recrystallization, grain size distribution and rheology

Relatie tussen dynamische rekristallisatie, korrelgrootteverdeling en rheologie

(met een samenvatting in het Nederlands)

Proefschrift

ter verkrijging van de graad van doctor
aan de Universiteit Utrecht,
op gezag van de Rector Magnificus, Prof. Dr. W.H. Gispen,
ingevolge het besluit van het College voor Promoties
in het openbaar te verdedigen op
maandag 4 maart 2002 des middags te 12:45 uur

door

Johannes Hendrik ter Heege

Geboren op 14 februari 1972, te Rossum

PROMOTOR: Prof. Dr. C.J. Spiers
Faculty of Earth Sciences
Utrecht University

CO-PROMOTOR: Dr. J.H.P. de Bresser
Faculty of Earth Sciences
Utrecht University

This is not a black and white world
To be alive
I say the colors must swirl
and I believe
That maybe today
We will all get to appreciate

The beauty of gray

Live (from the album Mental Jewelry)

"Some men see things as they are and say, 'Why ?'
I dream of things that never were and say, 'Why not?'"

Robert F. Kennedy, after George Bernard Shaw

Aan mijn ouders

MEMBERS OF THE DISSERTATION COMMITTEE:

Prof. Dr. B. Evans
Massachusetts Institute of Technology, Cambridge, U.S.A.

Prof. Dr. J. Tullis
Brown University, Providence, U.S.A.

Prof. Dr. J.L. Urai
Aachen University of Technology, Germany

Dr. I. Shimizu
University of Tokyo, Japan

Dr. M.R. Drury
Utrecht University, The Netherlands

Table of contents

Summary.....	11
Chapter 1: General introduction, problem statement and aims.....	13
1.1 General scope and motivation: Rheology in geodynamic processes.....	13
1.2 Rheology, composite flow laws and grain size distributions.....	13
1.3 The effect of dynamic recrystallization on grain size distribution and rheology.....	14
1.4 Models for dynamic recrystallization.....	14
1.4.1 Theoretical background.....	14
1.4.2 The <i>Twiss</i> model.....	15
1.4.3 The <i>Derby and Ashby</i> model.....	16
1.4.4 The <i>Shimizu</i> model.....	17
1.4.5 The <i>De Bresser et al.</i> hypothesis.....	18
1.4.6 Comparison of the models.....	19
1.5 Previous experimental data.....	19
1.5.1 Review of data.....	19
1.5.2 Temperature dependence of d_{rx} - σ relations.....	21
1.5.3 Stress dependence of d_{rx} - σ relations.....	21
1.5.4 Field boundary for olivine and calcite.....	22
1.6 Implications of the models for dynamic recrystallization.....	25
1.6.1 Implications for paleo-stress estimation.....	25
1.6.2 Implications for rheological weakening.....	25
1.7 Research aims.....	27
1.8 Methodology and organization of the thesis.....	27
Chapter 2: Composite flow laws for crystalline materials with continuously distributed grain size: Theory and application to olivine.....	29
2.1 Introduction.....	29
2.2 Model Development.....	30
2.2.1 Composite flow law for a single-valued grain size.....	33
2.2.2 Composite flow law for discrete grain size distributions.....	33
2.2.3 Composite flow laws for a continuous grain size distribution.....	34

2.3 Discussion.....	39
2.3.1 Universal deformation maps and the effect of distributed grain size.....	39
2.3.2 Effect of grain size distribution on the rheology of olivine.....	42
2.3.3 Implications for the rheology of rock materials in general.....	46
2.4 Summary and conclusions.....	49

Chapter 3: The influence of dynamic recrystallization on the grain size distribution and rheological behaviour of Carrara marble deformed in axial compression.....

3.1 Introduction.....	51
3.2 Experimental procedure.....	53
3.2.1 Material and sample preparation.....	53
3.2.2 Experiments, data acquisition and processing.....	54
3.2.3 Microstructural analysis.....	54
3.3 Results.....	55
3.3.1 Mechanical data.....	55
3.3.2 Qualitative microstructural observations.....	57
3.3.3 Quantitative microstructural results.....	61
3.4 Discussion.....	68
3.4.1 Flow behaviour and deformation mechanisms.....	68
3.4.2 Evolution of flow stress with strain.....	70
3.4.3 Evolution of dynamically recrystallizing microstructure.....	72
3.4.4 Comparison with high strain torsion experiments.....	73
3.4.5 Geodynamical implications.....	74
3.5 Summary and conclusions.....	75

Chapter 4: The effect of dynamic recrystallization on rheology, microstructure and grain size distribution: Inferences from experiments on polycrystalline halite

4.1 Introduction.....	77
4.2 Experimental procedure.....	78
4.2.1 Sample preparation.....	78
4.2.2 Apparatus, experimental procedure and data acquisition.....	79
4.2.3 Microstructural analysis.....	80

4.3 Results.....	80
4.3.1 Mechanical data.....	80
4.3.2 Microstructure.....	84
4.3.3 Grain size distributions.....	89
4.4 Discussion.....	94
4.4.1 Deformation mechanisms.....	94
4.4.2 Flow behavior and microstructural evolution.....	95
4.4.3 Comparison with previous studies.....	98
4.4.4 Grain size distributions in relation to deformation conditions.....	100
4.4.5 Calibration of a recrystallized grain size piezometer.....	101
4.4.6 General implications.....	104
4.6 Summary and conclusions.....	107
Chapter 5: A model relating grain size distribution to the rheology of dynamically recrystallizing rock materials.....	109
5.1 Introduction.....	109
5.2 Model Development.....	110
5.3 Evaluation of the model using data on wet polycrystalline halite.....	113
5.3.1 Deformation mechanism maps of grain size versus stress including a distribution term.....	114
5.3.2 Deformation mechanism maps of stress versus strain rate.....	115
5.4 Discussion.....	117
5.4.1 Consequences of incorporating standard deviation in σ - d relations.....	117
5.4.2 Implications for rheological weakening.....	119
5.4.3 Final remarks.....	119
5.5 Conclusions.....	120
Chapter 6: Conclusions and recommendations for further research.....	121
6.1 General conclusions and innovative aspects.....	121
6.2 Recommendations for further research.....	122
References.....	125
Papers and abstracts.....	134

Samenvatting (summary in Dutch)	135
Korte samenvatting voor de leek.....	138
Dankwoord.....	139
Curriculum Vitae.....	141

Summary

The solid state flow behavior (rheology) of materials constituting the Earth's mantle and crust is of key importance in controlling large scale geodynamic processes. Flow laws that are calibrated using laboratory experiments provide constraints on the rheology of rock materials under natural conditions, given that all active deformation mechanisms and microphysical processes affecting rheology are accounted for. Rocks invariably exhibit a distributed grain size, with small grains that may deform by grain size sensitive (GSS) deformation mechanisms and large grains that may deform by grain size insensitive (GSI) deformation mechanisms. Moreover, dynamic recrystallization can affect the rheology of rock materials by extensively modifying the grain size distribution. This means that flow laws must account for combined operation of grain size sensitive and grain size insensitive deformation mechanisms in order to accurately describe rheology and to allow the effects of dynamic recrystallization to be assessed. However, conventional flow laws are either fully empirical or based on a single deformation mechanism, and if grain size is included, it is represented as a constant single value.

This thesis aims to provide an improved description of the effect of grain microstructure on rheology by incorporating distributed grain size and multiple deformation mechanisms into flow laws. It further aims to assess the influence of dynamic recrystallization on the evolution of grain size distribution and on composite flow behavior.

In chapter 1, problems concerning the description of rheology using flow laws are outlined. It is shown that the effect of dynamic recrystallization on the rheology of Earth materials has not yet been adequately addressed, notwithstanding the substantial body of previous work on this topic. A framework is thus established for the present study.

In chapter 2, a theoretical diffusion (GSS) creep equation incorporating a lognormal grain size distribution is derived and combined with a theoretical dislocation (GSI) creep equation in order to formulate composite dislocation-diffusion flow laws for materials with a distributed grain size. The flow laws allow systematic investigation of the influence of the grain size distribution parameters, i.e. the median and standard deviation of the lognormal distribution, on rheology. Application of these flow laws to polycrystalline olivine under natural conditions reveals that strain rates can change by orders of magnitude due to variation in standard deviation at fixed median grain size. This is unaccounted for by conventional flow laws incorporating a single-valued grain size. The new flow laws thus provide an improved basis for the extrapolation of mechanical data to nature, the interpretation of experimental data in terms of deformation mechanisms and the assessment of the effect of dynamic recrystallization on rheology.

Chapter 3 describes an experimental investigation into the effect of dynamic recrystallization on the grain size distribution and rheological behavior of natural Carrara marble. In this investigation, samples have been systematically deformed to natural strains of 0.15-0.90 in axial compression at constant strain rates of 3.0×10^{-6} - $4.9 \times 10^{-4} \text{ s}^{-1}$, temperatures of 700-990°C, and a confining pressure of 150 or 300 MPa, yielding stresses of 15-65 MPa. The microstructure and grain size distribution of the starting material and each deformed sample have been analyzed in detail. The deformed samples show widespread evidence for dislocation creep and dynamic recrystallization by grain boundary migration and progressive subgrain rotation. The average grain size of the deformed samples was progressively reduced with increasing natural strain above 0.15, associated with minor rheological weakening. No microstructural or mechanical steady state was reached. From the observed evolution of the grain size distribution as a function of strain, it is inferred that recrystallization involved a competition between grain growth and grain size reduction. It is suggested that the relative importance of grain size sensitive creep mechanisms with respect to dislocation mechanisms

increases as the average grain size is reduced with strain, causing the minor weakening observed. This is quantitatively supported by calculations of weakening caused by changes in grain size distribution, performed using composite GSS-GSI flow laws (as derived in chapter 2). It is inferred that the weakening associated with grain size reduction is probably insufficient to cause strain localization.

Chapter 4 deals with a similar experimental investigation, now using dry and wet synthetic polycrystalline halite to study the influence of dynamic recrystallization on microstructure, grain size distribution and rheology, under conditions where dislocation creep mechanisms and solution-precipitation processes are expected to operate. Experiments are reported on wet samples, deformed at strain rates of 5×10^{-7} - $1 \times 10^{-4} \text{ s}^{-1}$, temperatures of 75-240°C, and 50 MPa confining pressure, yielding stresses of 7-22 MPa. Dry samples were deformed at a strain rate of $\sim 5 \times 10^{-7} \text{ s}^{-1}$, a temperature of 125 or 175°C, and 50 MPa confining pressure, yielding stresses of 20 or 15 MPa. Again, the microstructure and grain size distribution of the starting material and of each deformed sample have been analyzed. The results for the wet samples show that microstructural development was dominated by dynamic recrystallization involving fluid-assisted grain boundary migration, resulting in minor rheological weakening. The dry samples show limited progressive subgrain rotation recrystallization. Based on the application of composite GSI-GSS flow laws that include grain size distribution (chapter 2), it is inferred that deformation of wet polycrystalline halite occurred by a combination of dislocation and solution-precipitation creep mechanisms. Recrystallized grain size data of wet polycrystalline halite are found to depend on stress as well as temperature. The data are best described by a model that assumes that dynamic recrystallization adjusts grain size and rheology so that these are constrained to the boundary between the grain size sensitive (diffusion) creep and grain size insensitive (dislocation) creep fields.

In chapter 5, a modified model for dynamic recrystallization that incorporates grain size distribution is presented. This model is also based on the assumption that dynamic recrystallization adjusts grain size and rheology to the boundary between the GSS and GSI fields. It relates recrystallized grain size to rheology by equating the theoretical strain rate expression for diffusion creep, including distribution parameters, to the theoretical strain rate expression for dislocation creep (chapter 3). The model is evaluated against the experimental results on wet polycrystalline halite (chapter 4). The data support the model, showing that recrystallized grain size cannot be uniquely related to stress and temperature without taking the width of the grain size distribution into account.

Chapter 1

General introduction, problem statement and aims

1.1 General scope and motivation: Rheology in geodynamic processes

Large scale geodynamic processes are strongly influenced by the solid state flow behavior (rheology) of materials constituting the Earth's mantle and crust. Various numerical models demonstrate a key role of rheology in controlling the dynamics of geodynamic processes, such as mantle convection, subduction, mountain building and basin formation [e.g. *Bassi, 1991; Furlong, 1993; Govers and Wortel, 1995; Ranalli, 1995; Van den Berg, 1995; Zhong, 1995; Beaumont et al., 1996; Fernández and Ranalli, 1997*]. Constraints on the rheology of materials playing a role in these processes may come from flow laws that are calibrated using laboratory deformation experiments [*Kirby, 1980; Carter and Tsenn, 1987; Kohlstedt et al., 1995*]. As application of flow laws to natural conditions usually requires substantial extrapolation in deformation conditions, flow laws need to account for all microphysical processes that may influence rheology. This means that flow laws should incorporate all active deformation mechanisms and include effects of processes that might change the rheological behavior of materials during ongoing deformation. One such process is dynamic (syntectonic) recrystallization, which can extensively modify the microstructure (grain shape and size) of a material. In this thesis, the relationship between dynamic recrystallization, grain size distribution and rheology is investigated. In this first chapter, the background of the study will be described, previous work related to dynamic recrystallization and rheology will be summarized and problems concerning the quantitative description of rheology will be identified. It will be shown that the effect of dynamic recrystallization on rheology has not yet been adequately addressed and that there is scope for improvement in the calibration of flow laws.

1.2 Rheology, composite flow laws and grain size distributions

In most rock deformation studies, mechanical data are fitted to a single constitutive rate equation, usually a standard (Dorn type) power law with three independent parameters, i.e. a rate constant, a stress exponent and an apparent activation energy [see for example *Kirby, 1983; Carter and Tsenn, 1987; Evans and Kohlstedt, 1995* for reviews]. The resulting flow law may accurately describe the mechanical data for the range of investigated conditions, but is fully empirical and the flow law parameters may in fact represent multiple active deformation mechanisms. Despite this fact, mechanical data are often used to make inferences on active deformation mechanisms by comparing the empirical flow law parameters with theoretical values for a single deformation mechanism. If multiple deformation mechanisms were active, such inferences are meaningless. At conditions relevant for deformation in nature, rock materials may deform by a combination of grain size sensitive (GSS) deformation mechanisms, such as lattice or grain boundary diffusion creep or grain boundary sliding, and grain size insensitive (GSI) deformation mechanisms, such as climb or cross slip controlled dislocation creep [*Karato and Wu, 1993; Dell'Angelo and Olgaard, 1995; Rutter, 1995*]. Therefore, flow laws should account for possible composite GSS-GSI flow behavior.

The notion that rocks invariably exhibit a grain size distribution [e.g. *Ranalli, 1984*], with small grains that may deform by GSS mechanisms and large grains that may deform by

GSI mechanisms, further emphasizes the need to employ composite flow laws. In materials with a distributed grain size, the overall rate of deformation will depend on the relative contribution of GSS and GSI deformation, determined by the characteristics of the grain size distribution [Raj and Ghosh, 1981; Freeman and Ferguson, 1986; Wang, 1994]. Conventional flow laws incorporate grain size as a single value (i.e. average or median grain size) and cannot account for variations in width of the distribution. Freeman and Ferguson [1986] have shown that in a material deforming by a combination of GSS and GSI flow, a change in width of the grain size distribution may have a marked effect on the rheology of materials. Considering the fact that the width of grain size distributions may vary considerably between otherwise similar rock materials [Michibayashi, 1993; Newman, 1994; Dijkstra, 2001], conventional flow laws will predict erroneous stresses and strain rates because width is unaccounted for. In addition, flow laws may result in significant over- or underestimation of stresses and strain rates associated with the deformation of rocks in nature if the width of the grain size distribution of the rock is different from that of the material used to calibrate the flow law under laboratory conditions. This will be particularly important if the grain size distribution is syntectonically modified, for example by dynamic recrystallization or grain growth. The above considerations illustrate the need for composite GSS-GSI flow laws that can account for variations in the width of the grain size distribution. However, routinely applicable flow laws with these specific features are lacking.

1.3 The effect of dynamic recrystallization on grain size distribution and rheology

Dynamic recrystallization can modify the microstructure of materials and accordingly may alter the grain size distribution. By systematically monitoring the evolution of the grain size distribution and flow stress with strain, detailed information on the effect of dynamic recrystallization on the microstructure and rheology may be obtained [cf. Pieri *et al.*, 2001a]. As mentioned in the previous section, a change in grain size distribution may affect rheology by changing the distribution parameters (e.g. the width and median or average grain size). Therefore, accurate quantification of changes in rheology of materials due to dynamic recrystallization requires analysis of the complete grain size distribution. It also requires flow laws that incorporate the distribution parameters. However, studies that systematically investigate the effect of dynamic recrystallization for a range of strains and deformation conditions, including analysis of the complete grain size distribution are lacking. Such an investigation may be used to evaluate recent claims that dynamic recrystallization may not produce the rheological weakening required for strain localization [De Bresser *et al.*, 1998] as often proposed in the past [White *et al.*, 1980; Rutter and Brodie, 1988; Karato and Wu, 1993]. The next section deals with the theoretical background and literature review of experimental data on dynamic recrystallization, explaining the basis for these claims.

1.4 Models for dynamic recrystallization

1.4.1 Theoretical background

Dynamic recrystallization may alter the grain size of materials during deformation by grain boundary migration or formation of new high angle grain boundaries [Poirier, 1985; Drury and Urai, 1990; Humphreys and Hatherly, 1996]. It has long been recognized in deformation experiments that recrystallized grain size is inversely related to flow stress [Luton and Sellars, 1969; Mercier *et al.*, 1977; Schmid *et al.*, 1980]. Such a relation has been

observed in numerous experimental studies on metals, ceramics and rock materials [Takeuchi and Argon, 1976; Twiss, 1977; Drury et al., 1985]. These studies relate the mean recrystallized grain size (d_{rx}) to flow stress (σ) by a relation of the type

$$d_{rx} = K_I \sigma^{-p} \quad (1.1)$$

where K_I and p (typically 0.7-1.6) are material- and mechanism-specific constants. However, most published relations of this type are empirical, i.e. the relations are calibrated using flow stress and recrystallized grain size data obtained from deformation experiments under laboratory conditions, but lack a sound theoretical basis [e.g. Poirier, 1985]. Such a basis is a requirement if relations of the type (1.1) are to be reliably extrapolated to natural conditions and applied as a paleo-piezometers, using the mean recrystallized grain size of natural tectonites to estimate flow stress [White, 1979; Christie and Ord, 1980; Etheridge and Wilkie, 1981].

Next, existing quantitative models for dynamic recrystallization are reviewed that underpin relation (1.1) and may provide the necessary microphysical basis for the application of recrystallized grain size-stress relations to nature. The basic difference between existing models for dynamic recrystallization lies in assumptions regarding the recrystallization mechanisms. The models can be divided into (1) a model for rotation recrystallization [Shimizu, 1998; Shimizu, 1999], (2) a model for migration recrystallization [Derby and Ashby, 1987; Derby, 1990] and (3) models that do not specify the recrystallization mechanism [Twiss, 1977; De Bresser et al., 1998]. Rheology is incorporated in some of the models using constitutive rate equations for diffusion and dislocation creep. The creep rate for diffusion creep ($\dot{\epsilon}_{diff}$) is expressed by an equation of the type

$$\dot{\epsilon}_{diff} = A \left(\frac{\sigma}{d^m} \right) \exp \left(\frac{-Q_{diff}}{RT} \right) \quad (1.2)$$

where A and m are constants, d is the grain size, and Q_{diff} is the activation energy for the process controlling the diffusion creep rate (i.e. $m=2$ and $Q_{diff}=Q_v$ for lattice diffusion, or $m=3$ and $Q_{diff}=Q_{gb}$ for grain boundary diffusion). The creep rate for dislocation creep ($\dot{\epsilon}_{disl}$) is expressed by a conventional power law (Dorn) equation of the type

$$\dot{\epsilon}_{disl} = B \sigma^n \left(\frac{-Q_{disl}}{RT} \right) \quad (1.3)$$

where B and n are constants, and Q_{disl} is the activation energy for the process controlling the dislocation creep rate.

1.4.2 The Twiss model

The model presented by Twiss [1977] is based on the assumption that there exists a unique (sub)grain size at which the total strain energy of dislocations ordered in a subgrain boundary or in a recrystallized grain boundary is equal to the stored energy of the dislocations in the enclosed volume. The flow stress σ is introduced into the model through the usual relationship with dislocation density $\sigma \propto \rho^{0.5}$ [Nabarro, 1987]. Using equations for boundary

and volume energies for an idealized, cubic (sub)grain structure, with all boundaries being simple tilt walls and all dislocations being of edge type, the following equation resulted

$$d^* = K_2 \sigma^{-p} \quad \text{with } p = \left(\frac{2\phi - 1}{\phi} \right) \quad (1.4)$$

where d^* represents either subgrain or recrystallized grain size, K_2 is a constant and ϕ is the ratio of total dislocation length in the (sub)boundary to that in the enclosed volume. The value of the parameter ϕ is the only difference between the subgrain and recrystallized grain size models. *Twiss* argues that if ϕ is smaller than 1, dislocations in the enclosed volume will increase their energy rather than decrease if moving into the boundary, hence the boundary will not form. If it is assumed that the subgrain size d_s that forms is the smallest possible stable size, ϕ must be taken as 1, yielding

$$d_s = K_3 \sigma^{-1} \quad (1.5)$$

Recrystallized grains are thought to develop by expansion of dislocation loops, moving outward to form grain boundaries. Only those dislocations originally present in the enclosed volume at the time of recrystallization are involved in the grain boundary formation. In that way, ϕ is minimized and the produced recrystallized grains are dislocation-free and remain so. Thus, it is assumed that the smallest stable grain size is the one that develops. Values for ϕ are estimated to be $1.4 \leq \phi \leq 2$, resulting in

$$d_{rx} = K_4 \sigma^{-p} \quad \text{with } 1.3 \leq p \leq 1.5 \quad (1.6)$$

where d_{rx} is the recrystallized grain size and K_4 is a constant.

1.4.3 The Derby and Ashby model

Derby and Ashby [1987] and *Derby* [1990] present a model for dynamic recrystallization by grain boundary migration. A steady state mean grain size d_{rx} is achieved by competition between grain nucleation by bulging at grain boundaries, and grain growth events. An estimate of the mean grain size d_{rx} is obtained by balancing the rate of bulge nucleation with the mean boundary migration rate, reasoning that at steady state there should be one nucleation event in a volume of $(d_{rx})^3$ in the time required for a moving grain boundary to sweep out a similar volume. The driving force for both bulge nucleation and grain boundary migration is related to the energy stored in subgrain walls formed during deformation at elevated temperature. The number of nuclei (per unit area) is related to the strain of the material during one cycle of recrystallization, hence the nucleation rate is directly related to the strain rate during the cycle time. The rate of grain boundary migration depends linearly on the driving force via a mobility term that includes the boundary thickness and grain boundary diffusion coefficient. Assuming that the mean strain rate during recrystallization is the same as determined by the steady state creep behavior of the material (cf. (1.3), assuming creep is controlled by lattice diffusion), the following relation between d_{rx} and σ resulted

$$d_{rx} = K_5 \exp\left(\frac{Q_v - Q_{gb}}{2RT}\right) \sigma^{-n/2} \quad (1.7)$$

where K_5 is a constant, Q_v and Q_{gb} are the activation energies for lattice and grain boundary diffusion, respectively, and n is again the stress exponent in the power law creep equation given by (1.3). The *Derby and Ashby* model critically depends on differences in sub-boundary spacing between neighboring grains. Note, however, that the derivation of equation (1.7) does not include use of a subgrain size-stress relation of the type given by (1.5).

1.4.4 The Shimizu model

In the model put forward by *Shimizu* [1998], new grains ‘nucleate’ via progressive misorientation (rotation) of subgrains. A steady state recrystallized grain size d_{rx} is formed because of a balance between the rate of nucleation and the (radial) growth rate of the newly created grains. This is similar to the foundation of the *Derby and Ashby* model for migration recrystallization. However, *Shimizu’s* approach takes into account the fact that real materials undergoing recrystallization show a distribution of grain sizes rather than a single value [see also *Shimizu*, 1999], and the characteristic grain size parameter d_{rx} is accordingly defined as the maximum frequency in a logarithmic frequency diagram.

The nucleation rate in *Shimizu’s* model depends on the number of nucleation sites (subgrains) per unit volume and the time required to develop new grain nuclei by subgrain rotation. The nuclei are assumed to be spherical and to have the same size as subgrains. The density of potential nucleation sites (subgrains) can be independently specified for intracrystalline nucleation and nucleation at grain boundaries, making use of the inverse relation between d_s and σ given by (1.5). The time required for subgrains to become nuclei is determined by the flux of dislocations climbing into the subgrain boundaries, i.e. by the product of the free dislocation density ρ and the climb velocity of the dislocations.

The radial growth rate is assumed constant by *Shimizu* and depends on the grain boundary mobility, hence the grain boundary diffusion coefficient, in the same way as implemented by *Derby and Ashby* [1987]. In order to obtain a d_{rx} - σ relationship, stress is introduced through the expression $\sigma \propto \rho^{0.5}$ and the above mentioned $d_s \propto \sigma^{-1}$ relation given by (1.5). The result is

$$d_{rx} = K_6 \sigma^{-1.25} \exp\left(\frac{Q_v - Q_{gb}}{4RT}\right) \quad (1.8)$$

for intracrystalline nucleation, and

$$d_{rx} = K_7 \sigma^{-1.33} \exp\left(\frac{Q_v - Q_{gb}}{3RT}\right) \quad (1.9)$$

for grain boundary nucleation. Here, Q_v is the activation energy for lattice diffusion, which controls dislocation climb towards sub-boundaries, but not necessarily controls creep. Note that the model implies that recrystallized grains nucleated from subgrains are always larger than the original subgrains.

1.4.5 The De Bresser et al. hypothesis

The *Derby and Ashby* model for migration recrystallization as well as the *Shimizu* model for rotation recrystallization incorporates a dynamic balance between grain size reduction (via nucleation of new grains) and grain growth, both driven by dislocation stored energy. These models should be regarded as end-members of a range of potential combinations of the two basic recrystallization mechanisms that can accompany dislocation creep [see also *Drury and Urai*, 1990]. During dynamic recrystallization, new grains might be sufficiently small to deform by grain size sensitive mechanisms. However, grain surface energy may then become a driving force for grain boundary migration in addition to dislocation stored energy, resulting in grain growth. This reasoning was used by *De Bresser et al.* [1998] to argue that the grain size of a dynamically recrystallizing material will tend to organize itself so that deformation proceeds in the boundary between the grain size insensitive (GSI) dislocation creep field and the grain size sensitive (GSS) diffusion creep field. The hypothesis is briefly reviewed below.

If a single phase material has a sufficiently fine starting grain size, deformation will initially be grain size sensitive. However, the grains will then grow under the action of surface energy until dislocation processes become significant. At that point, bulge nucleation and/or progressive subgrain rotation processes will produce fine new grains, re-promoting GSS flow mechanisms. Conversely, in an initially coarse material, bulge nucleation and/or rotation recrystallization accompanying dislocation (GSI) creep will lead to grain size reduction. This will promote GSS mechanisms, which will in turn be counteracted by grain growth. On this basis, it was suggested by *De Bresser et al.* that, in materials in which grain size reduction is sufficiently effective, dynamic recrystallization should lead to a steady state balance between grain size reduction and grain growth processes set up in the boundary region between the dislocation (GSI) and diffusion (GSS) creep field. The boundary can be located using the relation for diffusion creep given by (1.2), plus that for dislocation creep given by (1.3). Near the boundary, both dislocation and diffusion creep will contribute to the overall steady state creep rate ($\dot{\epsilon}_{rx}$). Because the mechanisms are parallel-concurrent, their strain rates are additive, so that

$$\dot{\epsilon}_{rx} = \dot{\epsilon}_{diff} + \dot{\epsilon}_{disl} \quad (1.10)$$

At the boundary both mechanisms contribute equally to the overall creep rate, and $\dot{\epsilon}_{diff} = \dot{\epsilon}_{disl}$. However, the mean recrystallized grain size d_{rx} might adjust itself to a different relative contribution of dislocation and diffusion creep, defined

$$\dot{\epsilon}_{diff} / \dot{\epsilon}_{disl} = U \quad (1.11)$$

Here, U may depend upon stress and temperature but can be assumed constant for sufficiently small ranges of these variables. Taking now $d=d_{rx}$, i.e. assuming a steady state recrystallized grain size, and combining equations (1.2), (1.3), (1.10) and (1.11) results in

$$d_{rx} = K_8 \sigma^{-(n-1/m)} \exp\left(\frac{Q_{disl} - Q_{diff}}{mRT}\right) \quad (1.12)$$

with $K_8 = (A/UB)^{1/m}$, where U takes the value 1 for exact correspondence with the mechanism boundary.

1.4.6 Comparison of the models

The model of the stress-dependence of both subgrain and recrystallized grain size advanced by *Twiss* [1977] has been criticized in the literature [*Poirier*, 1985; *Derby*, 1990], because it rests on an incorrect application of equilibrium thermodynamics to what is clearly a non-equilibrium, dynamic process as both subgrains and new grains are cyclically formed and removed during syntectonic recrystallization. The stable grain size predicted by *Twiss* is the smallest grain size possible; the system, however, can always lower its energy by allowing these small grains to grow [*Poirier*, 1985]. Although widely applied in the past, the *Twiss* model must therefore be regarded as a lower bound only [see also *Twiss and Sellars*, 1978], and the model cannot accordingly be generally used.

The recrystallized grain size versus stress relations of *Derby and Ashby* [1987] given by (1.7), of *Shimizu* [1998] given by (1.8) and (1.9), and of *De Bresser et al.* [1998] given by (1.12) have similar forms. Most importantly, all three contain activation energy terms. Given that, in general, $Q_{gb} \approx 0.6Q_v$ [*Frost and Ashby*, 1982; *Evans and Kohlstedt*, 1995], the d_{rx} - σ relationships for nucleation by both grain boundary bulging (*Derby/Ashby*) and progressive subgrain rotation (*Shimizu*) are expected to be (weakly) temperature dependent. At high temperature, the steady state recrystallized grain size will then be smaller than at lower temperature at the same stress. In the case of the field boundary equation (given by (1.12), covering both migration and rotation recrystallization), a temperature dependence is also expected, except when GSS and dislocation (GSI) creep are both controlled by lattice diffusion (i.e. $(Q_{disl}=Q_v)=Q_d$). At high temperature (at constant stress), the recrystallized grain size d_{rx} will be smaller than at low temperature if $\Delta Q > 0$, i.e. if $Q_{disl} > Q_{diff}$ (cf. *Derby/Ashby* and *Shimizu's* relations) whereas the opposite would hold if $\Delta Q < 0$, i.e. if $Q_{disl} < Q_{diff}$. The latter would be the case if, for example, diffusion (GSS) creep is controlled by lattice diffusion, while recovery (GSI) creep is controlled by dislocation cross slip. Note that p (cf. 1.1) in the *Derby/Ashby* and *De Bresser et al.* equations depends on the creep behavior, whereas it is a material independent constant in *Shimizu's* relations.

1.5 Previous experimental data

1.5.1 Review of data

In table 1.1, a compilation is presented of p -values from experimentally calibrated d_{rx} - σ relations obtained for a range of metals, rocks and rock analogues by fitting (1.1) to the experimental data (i.e. either fitted at constant temperature or assuming no dependence on temperature). We distinguish between rotation and migration recrystallization only if explicitly differentiated in the respective study. Added to the table are values for the power law stress exponent n (cf. 1.3), as reported in the same study or other literature.

Table 1.1. Compilation of p -values from experimentally calibrated D - σ relations for a range of materials. Values for the power law stress exponent n (c.f. 1.3) as reported in the same study or other literature. p -values obtained by fitting (1.1) to the experimental data. In some studies, D - σ data were graphed without giving actual values for p and/or n . In those cases, a best fit regression analysis was performed; these results are given in italics.

Material	$p1^*$	$p2^\dagger$	$p3^\ddagger$	n	References
Albitic feldspar			0.66	3.1	<i>Post and Tullis [1999]</i>
Calcite (Carrara marble)		0.89		7.6	<i>Schmid et al. [1980], regime 2</i>
Calcite (Carrara marble)		0.97		4.2	<i>Schmid et al. [1980], regime 3</i>
Calcite (Carrara marble)		1.14	1.12	7.6	<i>Rutter [1995]; Schmid et al. [1980]</i>
Calcite gouge	1.42			4.7	<i>Friedman and Higgs [1981]; Schmid et al. [1980]</i>
Cu	1.24			4.8	<i>Derby and Ashby [1987]; Frost and Ashby [1982]</i>
Cu (0-8% Al)	1.52			4.8	<i>Twiss [1977]; Frost and Ashby [1982]</i>
α -Fe	1.59			6.9	<i>Luton and Sellars [1969]; Frost and Ashby [1982]</i>
α -Fe (vacuum melted)	1.41			4.1	<i>Glover and Sellars [1973]</i>
Halite single crystals		1.18	1.28	4.4	<i>Guillopé and Poirier [1979]</i>
Ice	0.85			3.5	<i>Jacka and Li Jun [1994]</i>
Ice	1.37			3.0	<i>Derby and Ashby [1987]; Frost and Ashby [1982]</i>
Magnox (Mg alloy)	1.28			4.5	<i>Drury et al. [1985]</i>
Magnox (Mg alloy)	1.23			4.3	<i>De Bresser et al. [1998]</i>
NaNO ₃		1.54	1.54	4.4	<i>Tungatt and Humphreys [1984]</i>
Ni	1.33			5.7	<i>Luton and Sellars [1969]</i>
Ni	2.00			5.6	<i>Sah et al. [1974]</i>
Olivine (Åheim dunite, wet)			1.19	4.48	<i>Van der Wal [1993]; Van der Wal et al. [1993]; Chopra and Paterson [1984]</i>
Olivine (Anita Bay dunite, wet)			0.88	3.35	<i>Van der Wal [1993]; Van der Wal et al. [1993]; Chopra and Paterson [1984]</i>
Olivine (San Quintin Baja, dry)	1.23			3.0	<i>Mercier et al. [1977]; Kirby and Raleigh [1973]</i>
Olivine (Mt. Burnet dunite, wet)	0.89			3.0	<i>Post [1977]</i>
Olivine (Mt. Burnet dunite, wet)	0.82			3.0	<i>Ross et al. [1980]; Post [1977]</i>
Olivine (Mt. Burnet dunite, dry)	0.75			3.6	<i>Post [1977]</i>
Olivine (Mt. Burnet dunite, dry)	1.27			3.8	<i>Ross et al. [1980]; Post [1977]</i>
Olivine single crystals	1.18			3.6	<i>Karato et al. [1980]; Durham and Goetze [1977]</i>
Pyrite	1.10			7	<i>Cox et al. [1981]</i>
Pyroxene (diopside, dry)	0.90			4.3	<i>Avé Lallemant [1978]</i>
Pyroxene (enstatite, wet)	0.85			3	<i>Ross and Nielson [1978]</i>
Quartzite (novaculite)			0.61	2.6	<i>Bishop in: Post and Tullis [1999]; Kronenberg and Tullis [1984]</i>
Quartzite (wet Canyon Creek)	1.40			2.6	<i>Mercier et al. [1977]; Parrish et al. [1976]</i>
Quartzite (flint, novaculite)	0.59			2.65	<i>Koch [1983]; Hacker et al. [1990]; Christie et al. [1980]</i>
Steel (mild, Al killed)	1.70			6.3	<i>Cepeda et al. [1989]</i>

* Unspecified recrystallization mechanism, \dagger Rotation recrystallization, \ddagger Migration recrystallization

1.5.2 Temperature dependence of d_{rx} - σ relations

The comparison of model predictions in the previous section shows that the recrystallized grain size versus stress relations are in general expected to show a temperature dependence. Evidence for an effect of temperature has so far been reported for only a few materials. *Mercier et al.* [1977] mention that recrystallized grain size versus stress data for wet quartzite and dunite appear to show a weak negative temperature dependence of grain size (i.e. the recrystallized grain size becomes smaller at higher temperature), although the relevant data points are not shown. *Ross et al.* [1980] report a weak positive temperature dependence for wet dunite, with larger recrystallized grain sizes developing at higher deformation temperature. A positive effect of temperature on d_{rx} can also be deduced from the results of *Tungatt and Humphreys* [1984] for polycrystalline sodium nitrate. These authors demonstrate that the D - σ relation depends on strain rate; if compared at the same stress level this implies variations in recrystallized grain size related to temperature. Finally, the work of *De Bresser et al.* [1998] on a magnesium alloy, Magnox Al80, showed a decrease in recrystallized grain size with increasing temperature and good agreement with the field boundary hypothesis. From the above, it follows that although evidence exists for a modest temperature dependence of recrystallized grain size versus stress relations in a few materials, widespread support is lacking. This might reflect (1) that the influence of temperature in fact is very limited, implying small differences in the activation energies (ΔQ) appearing in the model equations; (2) that the scatter in the experimental results for individual materials is usually too large to recognize any effect; or (3) that the experimental program did not systematically explore the possible role of temperature. With respect to point (3), we note that, to investigate a wide enough stress range at laboratory accessible strain rates, the majority of previously obtained d_{rx} - σ relations were calibrated by combining low temperature/high stress data with high temperature/low stress data, assuming no influence of temperature and therefore obscuring any such effect.

1.5.3 Stress dependence of d_{rx} - σ relations

The comparison of model predictions in the previous section also shows that the models may be discriminated on the basis of p , which is dependent on the creep behavior in the *Derby/Ashby* and *De Bresser et al.* models, but is a material independent constant in the *Shimizu* model. Values for the exponents p and n in table 1.1 are plotted against each other in fig. 1.1. Included in the figures are the trends as predicted by the various models considered above. The results show considerable spread, with p varying between 0.6 and 2. Although the scatter is substantial, some inferences can be made. The data show little support for the *Derby and Ashby* model given by (1.7); at almost any given n -value, the measured p -exponent is smaller than predicted. Only the data for ice (quoted in *Derby and Ashby* [1987]), wet Canyon creek quartzite and San Quentin Baja dunite (both in *Mercier et al.* [1977]) fall close to the *Derby/Ashby* prediction. Turning to the *Shimizu* model, this falls midway in the range of observed p -values, but does not reproduce the tendency for p to increase with n apparent in the data (fig. 1.1). It is probably not realistic to distinguish in practice between grains explicitly resulting from rotation or migration recrystallization, as new grains developed by rotation recrystallization may subsequently grow and become indistinguishable from grains developed by migration recrystallization. Dynamic recrystallization in real materials generally involves components of both recrystallization mechanisms. Nonetheless, a few values for p are quoted to represent ‘rotation’ recrystallization in table 1.1; these mostly lie below the values predicted by *Shimizu’s* model, given by (1.8) and (1.9). Like the *Shimizu* model, the

Twiss predictions ($p=1.3-1.5$) fall midway in the range of observed values (fig. 1.1). However, in the light of the flaws in this model, an agreement appears to be fortuitous, and again the tendency of p to increase with n is not reproduced. Comparison with the predictions of the *De Bresser et al.* model demonstrates that the majority of the data points falls close to the range defined by this model given by (1.12), assuming m -values in the range between $m=2$ and $m=3$. Note from table 1.1 that not enough systematic p versus n data are available to resolve with confidence any trends pertaining to individual materials.

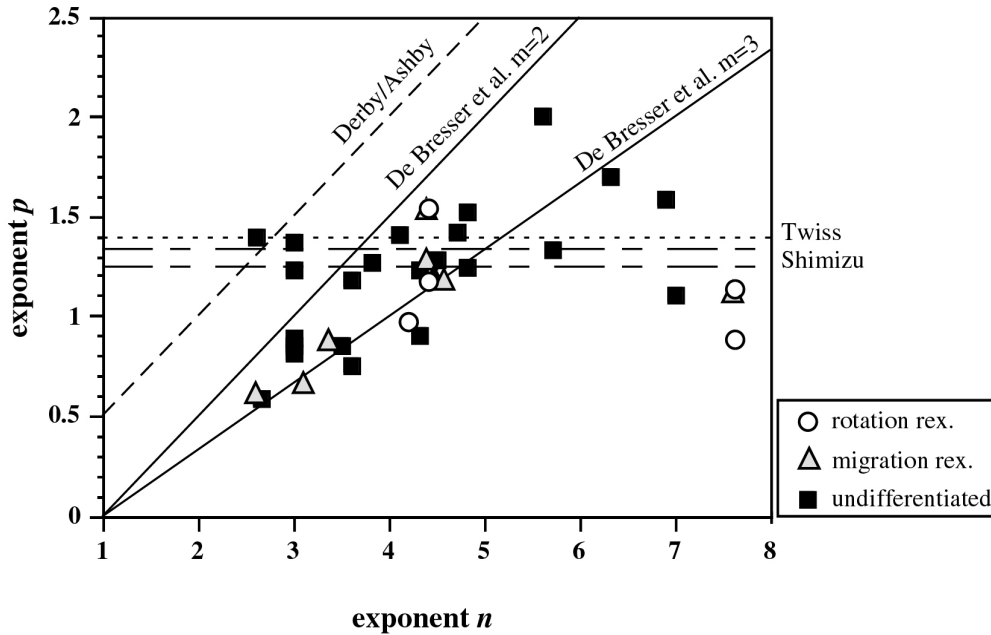


Figure 1.1. Values for p in the recrystallized grain size versus stress relations plotted against the (Dorn) power law stress exponent n for a wide range of materials, after table 1.1. Added to the plot are the trends predicted by (1.6) (*Twiss* model for recrystallized grain size versus stress), (1.7) (*Derby/Ashby* model), (1.8) and (1.9) (*Shimizu* model), and (1.12) (*De Bresser et al.* model with $m=2$ for lattice diffusion, and $m=3$ for grain boundary diffusion).

1.5.4 Field boundary for olivine and calcite

A further test of the *De Bresser et al.* model using the available experimental data may come from plotting recrystallized grain size versus stress data on a deformation map for a given material. Such a test is performed for two important Earth materials, namely olivine and calcite. The maps are drawn for a given temperature using experimentally determined flow laws to outline the GSS and GSI deformation fields in grain size versus stress space [*Frost and Ashby*, 1982]. Ideally, one would prefer to use $d_{rx}-\sigma$ data derived from the same set of experimentally deformed samples as used to derive the GSI and GSS flow laws. In practice, no study exists in which the same set of experiments has been used to explore both the dislocation creep and the diffusion creep behavior, and for which the $d_{rx}-\sigma$ relationship has also been calibrated. Thus, we have to rely on the merging of data and flow laws from different starting materials and/or experiments. An additional problem is the question of whether or not microstructural and mechanical steady state was reached in the various

experiments merged. Note that natural strains larger than 0.6 were required to obtain stable grain sizes in Magnox [Drury *et al.*, 1985]. In constructing the deformation mechanism maps, composite flow laws embodying GSI and GSS creep were used [e.g. Freeman and Ferguson, 1986], resulting in gently curved strain rate contours.

Various studies have investigated d_{rx} - σ relationships and calibrated flow laws for diffusion and dislocation creep for different types of olivine rock material [Post, 1977; Karato *et al.*, 1980; Ross *et al.*, 1980; Chopra and Paterson, 1981; Chopra and Paterson, 1984; Karato *et al.*, 1986; Van der Wal *et al.*, 1993; McDonnell, 1997]. From these studies, the d_{rx} - σ data from Van der Wal *et al.* [1993] obtained from experiments in a gas apparatus and the flow laws given by (1.2) and (1.3) with flow law parameters depicted in table 1.2 were taken as an example [see De Bresser *et al.*, 2001 for other examples and more details]. The map shows a close correspondence between the plotted d_{rx} - σ data and the GSS-GSI transition region, in agreement with the De Bresser *et al.* model (fig. 1.2a).

There also exist various studies that have investigated d_{rx} - σ relationships and calibrated flow laws for diffusion and dislocation creep for different types of calcite rock material [Schmid *et al.*, 1980; Friedman and Higgs, 1981; Walker *et al.*, 1990; Rutter, 1995]. From these studies, the d_{rx} - σ data from Rutter [1995] and the flow laws given by (1.2) and (1.3) with flow law parameters depicted in table 1.2 were taken as an example [see De Bresser *et al.*, 2001 for other examples and more details]. The d_{rx} - σ data are consistently positioned within the GSS-GSI transition region in this example, although the position of the data with respect to the GSS-GSI transition region is more dependent on the choice of flow laws than for olivine.

The Derby/Ashby and Shimizu models addressing the relationship between dynamically recrystallized grain size and flow stress comprise end-member models for rotation and migration recrystallization. In the De Bresser *et al.* model (field boundary hypothesis), both recrystallization mechanisms may be involved whereas grain size is determined in relation to the mechanical behavior. The experimental data compiled in figs. 1.1 and 1.2 lend support to the De Bresser *et al.* model rather than to the end-member models. However, uncertainties and scatter in the available (literature) data preclude definitive statements.

Table 1.2. Overview of experimentally derived flow laws for olivine and calcite employed in the construction of the deformation mechanism maps of fig. 1.2a and 1.2b.

Material	A, B (MPa ⁻ⁿ $\mu\text{m}^m \text{s}^{-1}$)	Q (kJ/mol)	m	n	References
Olivine (fig. 1.2a)					
Anita Bay dunite (wet), GSI	9.55×10^2	444	-	3.4	Chopra and Paterson [1981, 1984]
Synthetic San Carlos (wet), GSS	1.50×10^6	250	3	1	Karato <i>et al.</i> [1986]
Calcite (fig. 1.2b)					
Carrara marble, GSI	1.26×10^8	428	-	4.2	Schmid <i>et al.</i> [1980], regime 3
Synthetic calcite, GSS	8.51×10^4	190	1.87	1.7	Walker <i>et al.</i> [1990], low σ , high T

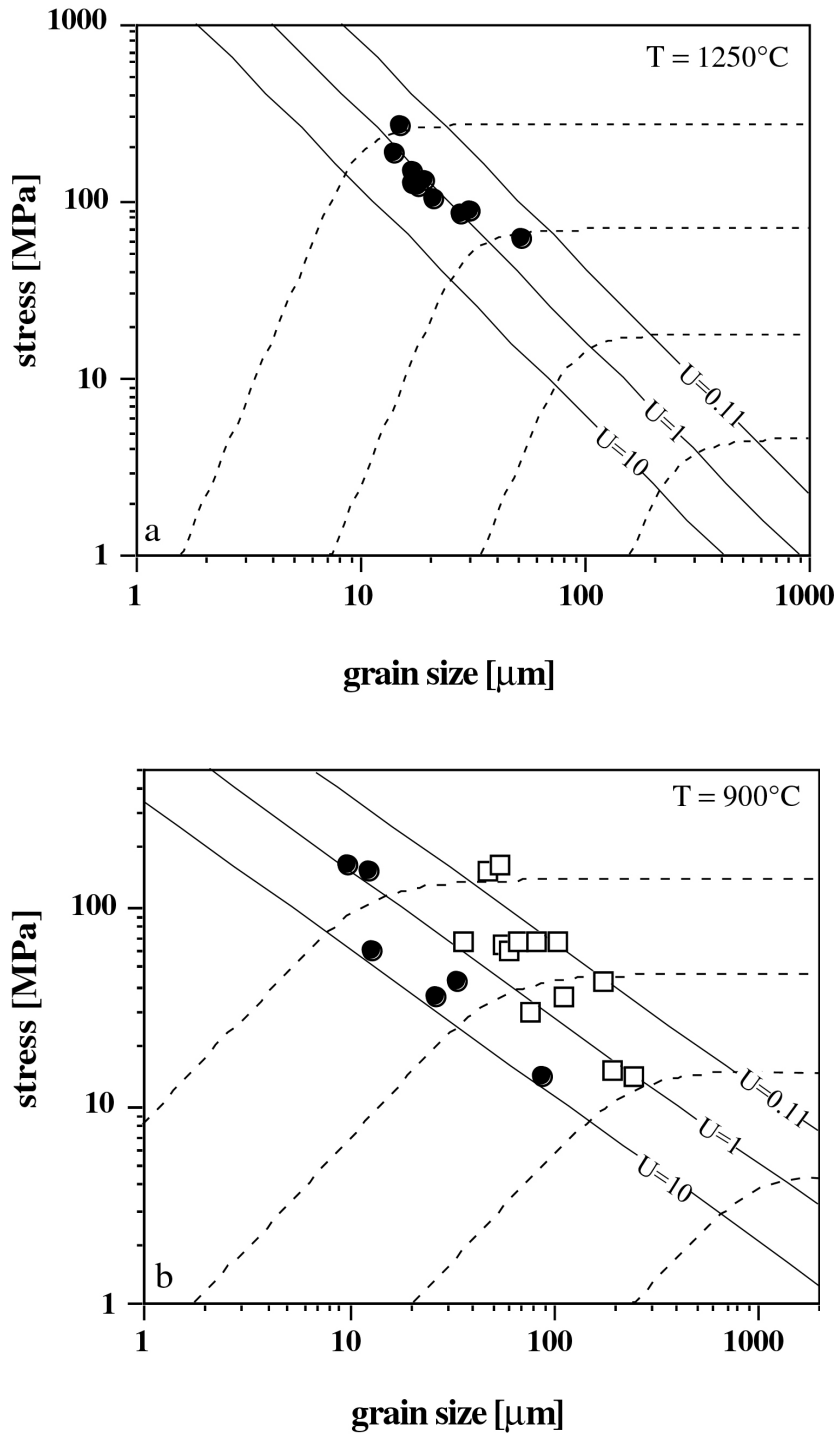


Figure 1.2. Deformation mechanism maps plotted using the constitutive creep equations tabulated in table 1.2 for (a) wet olivine at $T=1250^\circ\text{C}$ with contours for strain rates of 10^{-3} , 10^{-5} , 10^{-7} and 10^{-9} s^{-1} (dashed lines) and D - σ data for $T=1200$ - 1300°C obtained for Anita Bay dunite by Van der Wal et al. [1993] and (b) calcite at $T=900^\circ\text{C}$ with contours for strain rates of 10^{-2} , 10^{-4} , 10^{-6} and 10^{-8} s^{-1} (dashed lines) and D - σ data for $T=800$ - 1000°C obtained for rotation recrystallized (closed circles) and migration recrystallized (open circles) grain size of Carrara marble by Rutter [1995]. Straight solid lines for $U=0.11$, $U=1$, $U=10$ indicate the relative contributions of GSS and GSI creep to the overall creep rate in the mechanism transition region, see (1.10) and (1.11).

1.6 Implications of the models for dynamic recrystallization

1.6.1 Implications for paleo-stress estimation

Experimentally calibrated $d_{rx}-\sigma$ relationships have frequently been used for estimating paleo-stresses in naturally deformed rocks [e.g. *Kohlstedt and Weathers*, 1980; *Pfiffner*, 1982; *Ord and Christie*, 1984; *Hacker et al.*, 1992; *Fliervoet*, 1995). Invariably, the applied $d_{rx}-\sigma$ relations did not include temperature as an environmental variable. In view of the above discussion on (1) the role of temperature in the various recrystallization models, and (2) the available, though limited, experimental evidence for the influence of temperature, this may have been erroneous. Because natural deformation usually occurs at lower temperatures than applied during experimental calibration of most piezometric relations, paleo-stresses calculated from existing piezometers may represent over- or underestimates, depending on the relative values of the activation energy terms appearing in the relevant model equations. For the *De Bresser et al.* model depicted by (1.12), the temperature dependence drops out if GSS creep and dislocation creep are rate controlled by the same mechanism, e.g. by lattice diffusion. However, if grain boundary diffusion controls GSS creep, then $Q_{gb} \approx 0.6Q_{disl}$ [*Frost and Ashby*, 1982; *Evans and Kohlstedt*, 1995], and paleo-stresses estimated without taking temperature into account will be underestimates compared with the true values.

All models and experimental data regard grain size as a single value, whereas rocks invariably exhibit a grain size distribution that may vary in width or standard deviation as well as median or average grain size [*Ranalli*, 1984; *Freeman and Ferguson*, 1986; *Michibayashi*, 1993]. Variations in the width of grain size distribution can have important effects on the rheology of materials [*Raj and Ghosh*, 1981; *Freeman and Ferguson*, 1986; *Wang*, 1994]. In view of the relation between rheology and recrystallized grain size, explicitly predicted by the *Derby/Ashby* and *De Bresser et al.* models, variations in width accordingly may have important effects on piezometric relations, but have not been taken into account thus far.

In the review of experimental data in the previous section, all values for recrystallized grain size were taken as face value. As a consequence, recrystallized grain size versus stress relations using different grain size measurement, stereological corrections and averaging techniques have been treated on equal footing. This makes direct comparison of the data from different studies difficult. Recrystallized grain size often shows a lognormal distribution [e.g. *Ranalli*, 1984, *Newman*, 1994, *Dijkstra*, 2001], hence grain size may be best described by the median (geometric mean) and the standard deviation of logarithmic grain size.

It is emphasized that revision of piezometric relations, involving a consistent approach to measure grain size, a systematic investigation of the role of temperature and standard deviation of the grain size distribution, and reaching true steady state is required. If evaluated against a sound theoretical model for dynamic recrystallization, this would provide the proper basis for reliable application of piezometric relation to estimate deformation conditions of rocks in nature.

1.6.2 Implications for rheological weakening

It is often proposed that dynamic recrystallization may lead to major rheological weakening due to a switch in deformation mechanism from GSI to GSS creep, caused by grain size reduction [*White et al.*, 1980; *Rutter and Brodie*, 1988; *Karato and Wu*, 1993]. This requires crosscutting of the recrystallized grain size versus stress relation with the GSI-GSS field boundary (fig. 1.3), which is in contradiction with the field boundary hypothesis underlying the *De Bresser et al.* model.

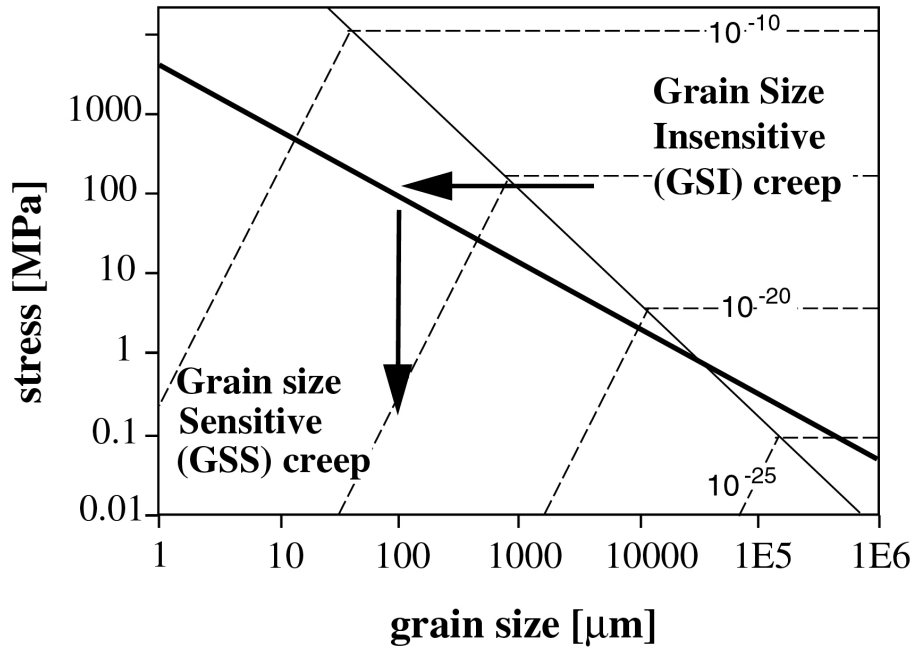


Figure 1.3. Empirical stress versus recrystallized grain size relation (heavy line) for olivine extrapolated into a deformation mechanism map drawn for a temperature of 600°C. Redrawn after Rutter and Brodie [1988]. Strain rate contours in s^{-1} . The arrows illustrate the notion of rheological weakening resulting from a switch in deformation mechanism associated with grain size reduction by dynamic recrystallization, at constant strain rate.

If the latter hypothesis is correct, this has major implications for rheological weakening. Using (1.10), (1.11) and (1.3), the steady state creep rate during dynamic recrystallization can be written as

$$\dot{\epsilon}_{rx} = \dot{\epsilon}_{diff} + \dot{\epsilon}_{disl} = (U + 1)\dot{\epsilon}_{disl} = (U + 1)B\sigma^n \exp\left(\frac{-Q_{disl}}{RT}\right) \quad (1.13)$$

The steady state creep during dynamic recrystallization thus can be expressed using a grain size insensitive constitutive rate equation. Compared with dislocation creep before pervasive recrystallization given by (1.3), only minor weakening is therefore possible as a result of grain size reduction by dynamic recrystallization. This is seen from (1.13) which shows that, at constant stress, the strain rate is enhanced by a factor of only $(U+1)$. If both dislocation and diffusion creep contribute equally to the total strain rate, $U=1$ (see 1.11) and the strain rate at the boundary will be just twice as fast as before recrystallization. The above implies that, at constant temperature, grain size reduction by dynamic recrystallization is not expected to result in a major change in strength or effective viscosity of a material deforming in steady state. These findings will influence numerical modeling performed to determine the conditions under which strain localization takes place [e.g. Kameyama *et al.*, 1997; Braun *et al.*, 1999; Gueydan *et al.*, 2001]. These conditions play an important role in large scale models of lithosphere deformation and mantle flow. The experimental data seems to support the De Bresser *et al.* model. However, the model so far lacks a detailed microphysical basis. Such a basis should come from a model that includes expressions describing the effect of

microphysical processes, such as rotation and migration recrystallization, on grain size as well as the mechanisms controlling the creep rate (GSI and GSS mechanisms). In addition, if firm conclusions regarding rheological weakening due to dynamic recrystallization are to be made, further experimental support is required, ideally consisting of well constrained flow laws for GSS and GSI deformation in combination with recrystallized grain size data for the same material.

1.7 Research aims

The considerations and review of models and data in the previous sections clearly show the need for a better description of the rheology of dynamically recrystallizing materials, providing a more reliable basis for extrapolation of data obtained at laboratory conditions to conditions prevailing in nature. The general aim of this study is to provide an improved description of the effect of dynamic recrystallization on rheology and microstructure. Within this broad aim, we focus on:

1. Derivation of routinely applicable composite flow laws describing grain size sensitive (diffusion) creep and grain size insensitive (dislocation) creep that incorporate grain size distribution.
2. Assessment of the influence of dynamic recrystallization on rheology and microstructure, with emphasis on the effect on grain size distribution and composite flow behavior.
3. Evaluation of previous models for dynamic recrystallization using new, systematic experimental data on recrystallized grain size of rock materials with particular emphasis on the role of temperature and strain.
4. Incorporation of distributed grain size into a model that directly relates recrystallized grain size distribution to the rheological behavior of a material.

1.8 Methodology and organization of the thesis

This study combines theoretical work and experimental deformation, both performed to achieve the specific aims mentioned above. In the theoretical part (chapter 2), composite diffusion-dislocation flow laws for materials with a lognormal grain size distribution are derived that incorporate the standard deviation as well as the median of the distribution. The model is used to determine the effect of varying grain size distribution on the rheology of olivine.

In the experimental part (chapters 3 and 4), the natural calcite rock Carrara marble [see for example *Schmid et al.*, 1980; *Rutter*, 1995; *Covey-Crump*, 1998; *Pieri et al.*, 2001a] and synthetic polycrystalline halite [see for example *Urai et al.* 1986; *Peach and Spiers*, 1996; *Watanabe and Peach*, 2002] have been deformed for a systematic range of strains, strain rates, stresses and temperature at elevated pressure. The experiments have been performed to investigate the effect of dynamic recrystallization on the rheology, microstructure and grain size distribution, focusing on the calibration of accurate flow laws, microstructural alteration, variations in grain size distribution, interpretation of microstructures and mechanical data in terms of active deformation mechanisms, calibration of piezometers and rheological

weakening. The materials serve as key examples of possible responses of rock materials to deformation accompanied by dynamic recrystallization, i.e. in Carrara marble, dynamic recrystallization is known to result in progressive grain size reduction with minor rheological weakening during deformation under laboratory conditions [Rutter, 1998; Pieri *et al.*, 2001a], and in wet polycrystalline halite dynamic recrystallization is known to be dominated by fluid-assisted grain boundary migration accompanied by a marked increase grain size, minor rheological weakening and oscillating flow stress at constant strain rate [Watanabe and Peach, 2002]. However, a systematic study of the effect of dynamic recrystallization for a range of strains and deformation conditions, including analysis of the complete grain size distribution is lacking for both materials.

Finally, the composite flow laws derived in chapter 2 are used in chapter 5 in combination with the field boundary hypothesis of *De Bresser et al.* [1998; 2001] (section 1.4) to relate the median and standard deviation of a lognormal recrystallized grain size distribution to temperature and stress using the flow law parameters for diffusion and dislocation creep. The resulting model is tested against the experimental data obtained on polycrystalline halite (chapter 4).

Besides the use of Carrara marble and synthetic polycrystalline halite as key materials to investigate the relation between dynamic recrystallization and rheology, there is also considerable interest in the deformation behavior of both materials in association with large scale geodynamical processes. Marble is often observed to accommodate high-strain deformation in nature (e.g. Glarus thrust in the Alps, *Schmid* [1975]) and the rheology of marble may be expected to play an important role in mountain building processes. The rheology of polycrystalline halite is of key interest in studying salt tectonics and the development of salt diapirs [Talbot and Rogers, 1980; Talbot and Jackson, 1987; Carter *et al.*, 1993]. The results for polycrystalline halite will also be relevant for some geoengineering applications, such as nuclear waste disposal in salt domes, hydrocarbon trapping and borehole closure [see for example *Aubertin and Hardy Jr.*, 1998 and references therein].

Chapter 2

Composite flow laws for crystalline materials with continuously distributed grain size: Theory and application to olivine

Abstract. Conventional steady state flow laws describing combined grain size insensitive dislocation creep and grain size sensitive diffusion creep incorporate grain size as a single (mean) value. However, rocks exhibit distributed grain size and variations in the shape of the distribution, such as its width, will accordingly affect rheological behavior. To evaluate this effect, we have derived composite dislocation-diffusion flow laws describing upper and lower bounds on the rate of deformation of materials showing a grain size distribution of the commonly observed lognormal type. The upper and lower bound flow laws obtained allow systematic investigation of the influence of the grain size distribution parameters, i.e. the median and standard deviation, on composite rheology. The results demonstrate major effects of distribution width as well as median value. Application to polycrystalline olivine, deforming by grain boundary diffusion creep and power law dislocation creep, reveals significant implications for interpreting deformation experiments and modeling flow in the Earth's mantle. The flow laws also provide an improved basis for understanding and modeling the consequences of dynamic recrystallization and grain growth in the crust and mantle.

2.1 Introduction

In formulating steady state flow laws for polycrystalline materials, the microstructure of the material is usually regarded as fixed, with a constant, single-valued (mean) grain size [Tsenn and Carter, 1987; Rutter and Brodie, 1992; Kohlstedt *et al.*, 1995]. However, rocks invariably exhibit a grain size distribution [Ranalli, 1984; Michibayashi, 1993; Molli *et al.*, 2000; Dijkstra, 2001]. Small grains within such a distribution may deform by grain size sensitive mechanisms such as diffusion creep, while larger grains may deform by grain size insensitive dislocation creep. This means that differences in grain size distribution parameters between otherwise similar rock materials or samples could have major effects on rheology [Heilbronner and Bruhn, 1998]. To evaluate such effects, a composite grain size sensitive (GSS) and grain size insensitive (GSI) rate equation is needed, in which the grain size distribution parameters explicitly determine the relative (volumetric) contributions of GSI versus GSS mechanisms [Raj and Ghosh, 1981; Freeman and Ferguson, 1986; Wang, 1994].

The importance of the above lies in the application of laboratory flow laws to model the deformation behavior of rocks under natural conditions. First, if mechanical data obtained from laboratory experiments are fitted to a GSS or composite GSS-GSI creep law incorporating the grain size distribution parameters, rather than to a conventional creep law assuming a single-valued grain size, the constitutive parameter values obtained (e.g. diffusion coefficients, activation energies and power law stress exponents) will be physically more meaningful. This will allow better interpretation of laboratory data in terms of deformation mechanisms, and accordingly better interpretation of microstructures exhibited by natural tectonites. Second, more reliable extrapolation of laboratory flow laws to nature will be possible if the effects of grain size distribution can be incorporated, because the grain size distribution of natural tectonites can differ widely from that of the material used to determine the flow law. Third, changes in grain size distributions must be taken into account in composite flow laws, if we are to understand the effects of dynamic recrystallization and grain growth on rheology and strain localization [Rutter and Brodie, 1988]. In this context, note that the grain size distribution of dynamically recrystallizing materials can be expected to

evolve towards a characteristic steady state form, in a manner analogous to the characteristic subgrain size distribution that develops during steady state dislocation creep [Stone, 1991], and must play a role in determining the steady state rheology.

A first treatment of the effect of distributed grain size on the composite GSS-GSI rheology of polycrystalline materials was presented by *Raj and Ghosh* [1981]. Assuming uniform strain rate in all grains, they investigated the effect of varying bimodal and simple multimodal grain size distributions, using both analytical and numerical methods. *Wang* [1994] later extended their analysis to investigate the effect of varying bimodal grain size distributions on apparent power law parameters, such as stress exponent (n), grain size exponent and activation energy, for the cases of uniform strain rate and uniform stress. Both studies demonstrated marked effects of varying grain size distribution. However, rock materials usually exhibit continuous, unimodal grain size distributions rather than (discrete) bimodal or multimodal distributions. Using numerical methods, *Freeman and Ferguson* [1986] investigated the effects of variations in geologically realistic grain size distributions, namely discrete lognormal and bimodal distributions, again considering both uniform strain rate and uniform stress cases. They showed that for distributions with similar mean grain size, variations in distribution type and width have substantial effects on flow strength and on the width of the zone, in stress-temperature space, where both GSS and GSI mechanisms contribute significantly to the overall strain rate. However, their model, being entirely numerical, does not lend itself to routine analysis of experimental data, to obtain parameters such as n -values or activation energies, or to analysis of natural microstructures.

In the present paper, we derive combined GSS-GSI creep equations for materials showing a continuous grain size distribution of the lognormal type commonly observed in rocks [Kretz, 1966; Ranalli, 1984; Michibayashi, 1993; Miralles *et al.*, 2000; Dijkstra, 2001]. The effect of the distribution appears explicitly in terms of the median grain size and standard deviation. Composite flow equations are derived, assuming either the applied stress or strain rate to be homogeneous throughout the material. These equations respectively describe lower and upper bounds for the rate of deformation, in a manner analogous to the Reuss and Voigt bounds for elastic behavior [Hashin, 1964; Hill, 1965; Tullis *et al.*, 1991]. After a general derivation, we focus on grain boundary diffusion (Coble) creep and dislocation creep. Though several approximations are made, our flow laws possess the advantage of algebraic form allowing systematic investigation of the effect of the distribution parameters on rheology. In addition, they can be applied to any material deforming under experimental or natural conditions in more or less the same way as conventional flow laws, provided the grain size distribution is of a lognormal type and the distribution parameters have been analyzed. We apply our results to describe the rheological behavior of polycrystalline olivine, using realistic flow law parameters [Karato *et al.*, 1986]. Our results show that varying the standard deviation of the grain size distribution at constant median grain size and temperature can yield order of magnitude changes in flow stress or strain rate, as well as switches between dislocation and diffusion dominated creep with associated rheological softening or hardening.

2.2 Model Development

Our model addresses a single-phase polycrystalline material, with lognormally distributed grain size, undergoing steady state, axi-symmetric deformation by GSS and GSI mechanisms, operating as independent, parallel-concurrent processes [Poirier, 1985]. In the latter stages of our treatment, we restrict attention to solid state grain boundary diffusion creep [Coble, 1963] and power law, recovery-controlled dislocation creep [Weertman, 1968; Frost and Ashby, 1982], but the analysis can easily be modified to incorporate other GSS

mechanisms, such as lattice diffusion creep [Nabarro, 1948; Herring, 1950], superplastic flow mechanisms [e.g. Nieh *et al.*, 1997], pressure solution [e.g. De Meer and Spiers, 1999], or other GSI mechanisms. We follow a three-step approach. In the first step, a composite diffusion-dislocation flow law for a single-valued grain size (fig. 2.1a, b) is obtained [Frost and Ashby, 1982; Poirier, 1985]. In the second step, composite flow laws for discrete grain size distributions (fig. 2.1c, d) are derived, making end member assumptions that stress or strain rate is distributed homogeneously throughout the material. The average bulk strain rate or stress is obtained by summing the values associated with individual grain size classes according to their volume fraction (i.e. by volume averaging) following Raj and Ghosh [1981]. In the third step, a continuous lognormal grain size distribution [Aitchison and Brown, 1957] is incorporated into the composite flow law (fig. 2.1d). All symbols used in our analysis are defined in table 2.1.

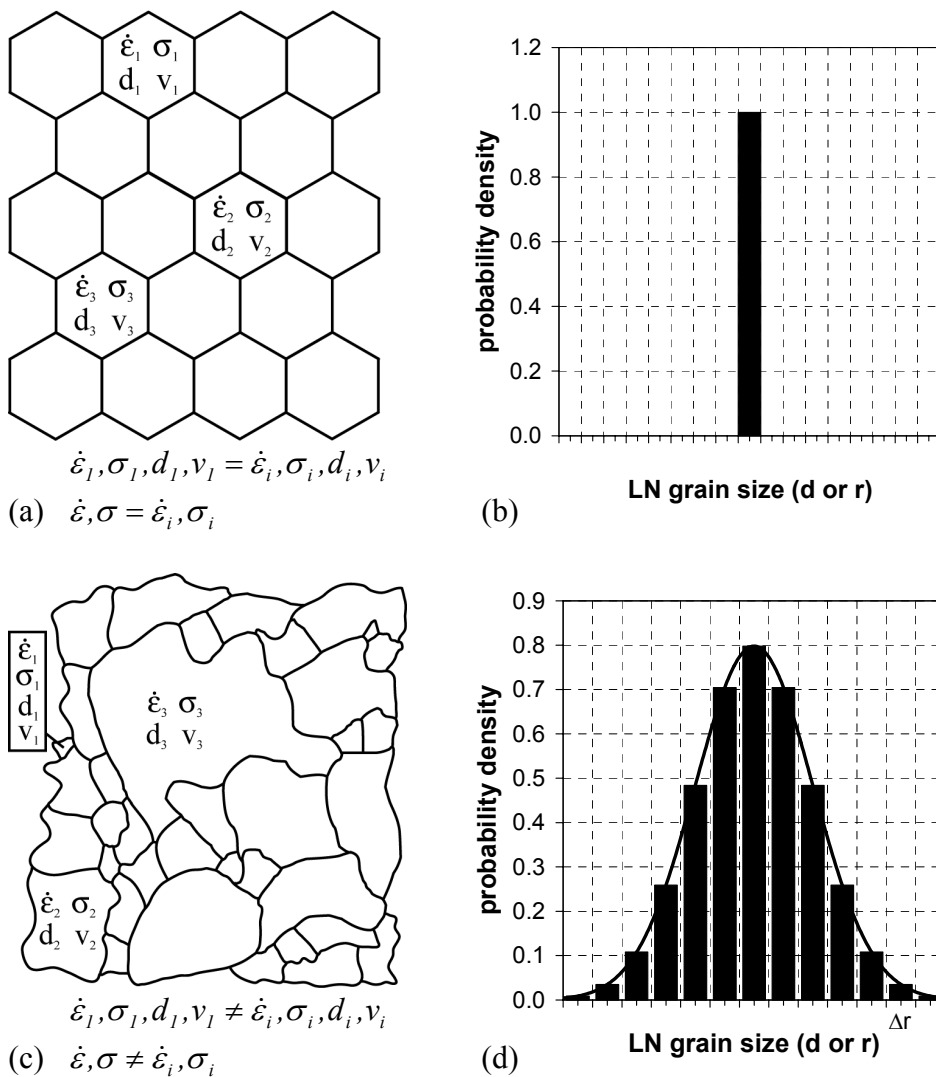


Figure 2.1. Schematic diagrams of polycrystalline aggregates with a single-valued grain size (a) and a distributed grain size (c), plus corresponding probability density distributions (b) and (d). For the distributed grain size (c), discrete and continuous lognormal probability density distributions are shown (d). Note that the local strain rate $\dot{\epsilon}_i$, stress σ_i and grain size d_i vary from grain to grain (interval to interval) in (c) but are uniform in (a). Grain size distributions can be viewed as distributions of grain diameter d or radius $r=d/2$.

Table 2.1. List of symbols used with description and S.I. units.

symbol*	description, expression, units
$A(T), B(T)$	temperature dependent material parameter diffusion creep, $\text{m}^{\text{m}}.\text{s}^{-1}$, dislocation creep, s^{-1}
A	rate constant
b	magnitude of Burgers' Vector, m
C	normalized factor containing material parameters, distribution parameters and temperature
d	grain size (diameter), $d = 2r$, m
dr	grain size interval in a continuous distribution, m
D_0, D	(pre-exponential) diffusion coefficient [†] , $D = D_0 \exp\left[\frac{-Q}{RT}\right]$, $D_{diff} = D_v + \frac{\pi\delta}{b} D_b$, $\text{m}^2.\text{s}^{-1}$
$F(\bar{\sigma}_{\dot{\epsilon}}^*, \phi, n, m)$	empirical fitted function
i, j	grain size class number, total number of grain size classes in a discrete distribution
k	Boltzmann's constant, J.K^{-1}
K	shape factor, $K = \frac{4}{3}\pi$ for spherical grains
m, n	grain size exponent, power law stress exponent
N_t	total number of grains in a polycrystalline material
p, q	constants
Q	activation energy, J.mol^{-1}
r	grain radius, $r = \frac{1}{2}d$, m
R	gas constant, $\text{J.mol}^{-1}.\text{K}^{-1}$
S	normalized strain rate
T	absolute temperature, K
v	volume fraction
V_t	total volume of material, m^3
X	grain size (distribution) term, m
z	substitution variable
α, β, γ	empirical constants in function $F(\bar{\sigma}_{\dot{\epsilon}}^*, \phi, n, m)$
δ	diffusive thickness of a grain boundary, m
Δ	error in strain rate between $\dot{\epsilon}_{\dot{\epsilon}}^{\text{rough}}$ and $\dot{\epsilon}_{\dot{\epsilon}}^{\text{true}}$, %
Δr	width of a grain size class in a discrete distribution, m
$\dot{\epsilon}$	strain rate, s^{-1}
ϕ	standard deviation of a lognormal grain size distribution
μ	shear modulus [†] , Pa
π	constant pi
$\sigma, \bar{\sigma}, \bar{\sigma}^*$	stress, Pa, normalized stress, $\bar{\sigma} = (\sigma / \mu)$, normalized relative to $\bar{\sigma}_{\sigma}^{\text{int}}$, $\bar{\sigma}_{\sigma}^* = \bar{\sigma}_{\sigma} / \bar{\sigma}_{\sigma}^{\text{int}}$
$\Lambda(r)$	probability density function of grains in a continuous distribution

*Sub- or superscript *diff*- for pure diffusion creep (single mechanism), e.g. $A_{diff}, D_{diff}, D_{0diff}, Q_{diff}, \dot{\epsilon}_{diff}, \bar{\sigma}_{diff}, \dot{\epsilon}_{\dot{\epsilon}}^{\text{diff}}$

Sub- or superscript *disl*- for pure dislocation creep (single mechanism), e.g. $A_{disl}, D_{disl}, D_{0disl}, Q_{disl}, \dot{\epsilon}_{disl}, \bar{\sigma}_{\dot{\epsilon}}^{\text{disl}}$

Subscript *b*- grain boundary diffusion, e.g. D_b, Q_b , subscript *v*- lattice diffusion, e.g. D_v, Q_v

Subscript *i*- for grains in class *i* of a discrete distribution, e.g. $d_i, r_i, v_i, \dot{\epsilon}_i, \sigma_i, \bar{\sigma}_i$

Subscript *j*- for grains in the last class of a discrete distribution, e.g. $v_j, \dot{\epsilon}_j, \bar{\sigma}_j$

Subscript *med*- median of a continuous lognormal distribution, e.g. d_{med}, r_{med}

Subscript $\dot{\epsilon}$ - for a continuous lognormal distribution assuming uniform strain rate, e.g. $\dot{\epsilon}_{\dot{\epsilon}}, \sigma_{\dot{\epsilon}}, \bar{\sigma}_{\dot{\epsilon}}$

Subscript σ - for a continuous lognormal distribution assuming uniform stress, e.g. $\dot{\epsilon}_{\sigma}, \sigma_{\sigma}, \bar{\sigma}_{\sigma}$

Superscript *rough, approx, true*- rough, approximated, true value, e.g. $\dot{\epsilon}_{\dot{\epsilon}}^{\text{rough}}, \dot{\epsilon}_{\dot{\epsilon}}^{\text{approx}}, \dot{\epsilon}_{\dot{\epsilon}}^{\text{true}}$

Superscript *int*- at the pure diffusion-dislocation creep intersection (single mechanisms), e.g. $\bar{\sigma}_{\sigma}^{\text{int}}$

(*r*)- for grains of radius *r* in a lognormal distribution, e.g. $\dot{\epsilon}(r), \bar{\sigma}(r)$

[†]Frost and Ashby [1982]

2.2.1 Composite flow law for a single-valued grain size

We use the following theoretical rate equation for diffusion creep of a polycrystalline material characterized by a single-valued grain size d (see fig. 2.1a, b)

$$\dot{\epsilon}_{diff} = \frac{A_{diff} b D_{diff} \mu}{kT} \left(\frac{b}{d} \right)^m \left(\frac{\sigma}{\mu} \right) \quad (2.1)$$

This represents grain boundary diffusion creep [Coble, 1963] if $m=3$ and $D_{diff}=\pi\delta D_b/b$ (see table 2.1), or lattice diffusion creep [Nabarro, 1948; Herring, 1950] if $m=2$ and $D_{diff}=D_v$. For power law dislocation creep, we use [Frost and Ashby, 1982]

$$\dot{\epsilon}_{disl} = \frac{A_{disl} b D_{disl} \mu}{kT} \left(\frac{\sigma}{\mu} \right)^n \quad (2.2)$$

Microphysical models for climb-controlled dislocation creep typically predict n -values of 3 or 4.5, and possibly up to 6 [Weertman, 1968; Poirier, 1985]. However, other values of n are often found experimentally, and although it is doubtful if (2.2) can be applied when $n > 5$, it can usually be used to describe the creep rate accurately if $3 \leq n \leq 5$ [Poirier, 1985]. Since the above GSS and GSI mechanisms contribute independently to the overall strain rate, summation gives the composite flow law

$$\dot{\epsilon} = \left[\frac{A_{diff} b D_{diff} \mu}{kT} \left(\frac{b}{d} \right)^m \left(\frac{\sigma}{\mu} \right) \right] + \left[\frac{A_{disl} b D_{disl} \mu}{kT} \left(\frac{\sigma}{\mu} \right)^n \right] \quad (2.3)$$

2.2.2 Composite flow law for discrete grain size distributions

Consider a polycrystalline material characterized by a discrete grain size distribution consisting of j grain radius classes, each centered about a radius $r_i=d_i/2$ and of width Δr (fig. 2.1c, d). For an individual grain size class in such a distribution, (2.3) yields

$$\dot{\epsilon}_i = \frac{A(T)}{r_i^m} \bar{\sigma}_i + B(T) \bar{\sigma}_i^n \quad (2.4)$$

where $A(T) = \frac{A_{diff} b^{m+1} D_{diff} \mu}{2^m kT}$, $B(T) = \frac{A_{disl} b D_{disl} \mu}{kT}$ and $\bar{\sigma}_i = \frac{\sigma_i}{\mu}$

In order to derive equations for the overall creep rate of our material, we now make the following assumptions: (i) the morphology of grains does not change between individual classes and (ii) either stress or strain rate is uniform throughout the sample. These assumptions also underlie (2.1) and (2.2). Together with (2.3), assumption (ii) implies that strain rate or stress must vary abruptly from grain to grain according to grain size [Raj and Ghosh, 1981; Freeman and Ferguson, 1986]. In real polycrystals, strain compatibility and stress equilibrium are maintained by more continuous stress and strain rate gradients, analogous to the distribution of stress and strain between different phases in polyphase materials [Tullis et al., 1991].

If the stress is assumed uniform throughout a material with discretely distributed grain size, (2.4) requires that the grains in different grain size classes will deform at different rates. We assume that the contribution of each grain size class to the bulk strain rate ($\dot{\epsilon}_\sigma$) is determined by the volume fraction v_i of the grains in that class [Tullis *et al.*, 1991]. In other words, the bulk creep rate under given conditions can be obtained by volume-averaging the strain rates as given by (2.4) for the individual grain size classes [Raj and Ghosh, 1981; Freeman and Ferguson, 1986], so that

$$\dot{\epsilon}_\sigma = \dot{\epsilon}_1 v_1 + \dot{\epsilon}_2 v_2 + \dots + \dot{\epsilon}_j v_j = \sum_{i=1}^{i=j} \dot{\epsilon}_i v_i = \sum_i \left(\frac{A(T)}{r_i^m} \bar{\sigma}_i + B(T) \bar{\sigma}_i^n \right) v_i \quad (2.5a)$$

If the strain rate is assumed to be uniform throughout the material, the normalized bulk stress $\bar{\sigma}_\dot{\epsilon}$ can be similarly obtained by volume-averaging the stresses $\bar{\sigma}_i$ for the individual grain size classes given by (2.4), so that

$$\bar{\sigma}_\dot{\epsilon} = \bar{\sigma}_1 v_1 + \bar{\sigma}_2 v_2 + \dots + \bar{\sigma}_j v_j = \sum_i \bar{\sigma}_i v_i \quad (2.5b)$$

Here, $\bar{\sigma}_i$ is the root of (2.4) for each grain size class at the imposed strain rate. Equations (2.5a, b) constitute bulk $\sigma - \dot{\epsilon}$ relations, which can be investigated numerically, as did Freeman and Ferguson [1986], by inserting v_i values reflecting specific discrete grain size distributions.

2.2.3 Composite flow laws for a continuous grain size distribution

For continuous distributions, the number of grain size classes $j \rightarrow \infty$ and the class interval $dr \rightarrow 0$. If an appropriate probability density function $\Lambda(r)$ is chosen to describe the grain radius distribution (cf. fig. 2.1d) and the total number of grains in volume V_t is N_t , then the number of grains falling in a radius interval dr of $\Lambda(r)$ is $\Lambda(r)drN_t$. Since the volume of each grain is Kr_i^3 (where K is a shape factor, equal to $\frac{4}{3}\pi$ for spherical grains), the volume fraction of grains falling in the radius interval dr is $(\Lambda(r)drN_tKr^3)/V_t$. For a continuously distributed grain size, (2.5a, b) can hence be re-written in the form

$$\dot{\epsilon}_\sigma = \int_0^\infty \dot{\epsilon}(r) \left(\frac{\Lambda(r)N_tKr^3}{V_t} \right) dr \quad (2.6a) \quad \text{and} \quad \bar{\sigma}_\dot{\epsilon} = \int_0^\infty \bar{\sigma}(r) \left(\frac{\Lambda(r)N_tKr^3}{V_t} \right) dr \quad (2.6b)$$

Grain size is commonly lognormally distributed both in nature [Ahrens, 1957; Kretz, 1966; Ranalli, 1984; Michibayashi, 1993; Miralles *et al.*, 2000; Dijkstra, 2001] and experiment [Post and Tullis, 1999]. In addition, a lognormal grain size distribution is predicted to result from both dynamic recrystallization [Shimizu, 1999] and grain growth [Humphreys and Hatherly, 1996; Wang *et al.*, 1999]. We therefore assume that $\Lambda(r)$ can be described by the standard lognormal probability density distribution

$$\Lambda(r) = \frac{1}{\sqrt{2\pi}\phi r} \exp \left[-\frac{(\ln r - \ln r_{med})^2}{2\phi^2} \right] \quad (2.7)$$

for which the area beneath the curve is unity, i.e. $\int_0^{\infty} \Lambda(r) dr = 1$ [Aitchison and Brown, 1957; Kurtz and Carpay, 1980]. The parameters characterizing the distribution are the median grain radius (r_{med}) and standard deviation (ϕ). For this distribution, the total volume of grains can be expressed as

$$V_t = \int_0^{\infty} N_t K r^3 \Lambda(r) dr = \frac{N_t K}{\sqrt{2\pi}} \int_0^{\infty} \frac{r^2}{\phi} \exp\left[-\frac{(\ln r - \ln r_{med})^2}{2\phi^2}\right] dr \quad (2.8)$$

Putting $z = (\ln r - \ln r_{med})/\phi$ then leads to

$$V_t = \frac{N_t K}{\sqrt{2\pi}} r_{med}^3 \int_{-\infty}^{\infty} \exp\left[-\frac{1}{2}z^2 + 3\phi z\right] dz \quad (2.9)$$

which using the standard integral given by *Gradshteyn and Ryzhik* [1980]

$$\int_{-\infty}^{\infty} \exp[-p^2 z^2 \pm qz] dz = \frac{\sqrt{\pi}}{p} \exp\left[\frac{q^2}{4p^2}\right] \text{ for } p > 0 \quad (2.10)$$

reduces to

$$V_t = N_t K r_{med}^3 \exp\left[\frac{9}{2}\phi^2\right] \quad (2.11)$$

Flow law assuming homogeneous stress

The overall creep rate $\dot{\epsilon}_\sigma$ of a polycrystalline material with a lognormal grain size distribution, for the case that the stress $\bar{\sigma} = \sigma/\mu$ is uniform (i.e. constant) throughout the aggregate, can now be found by putting (2.11), (2.7) and the expression for $\dot{\epsilon}(r)$ embodied by (2.4) into (2.6a). This yields

$$\dot{\epsilon}_\sigma = \frac{1}{\sqrt{2\pi} \phi \exp\left[\frac{9}{2}\phi^2\right] r_{med}^3} \int_0^{\infty} \left(A(T) r^{2-m} \bar{\sigma} + B(T) r^2 \bar{\sigma}^n \right) \left(\exp\left[-\frac{(\ln r - \ln r_{med})^2}{2\phi^2}\right] \right) dr \quad (2.12)$$

which, using the aforementioned substitution $z = (\ln r - \ln r_{med})/\phi$, and standard integral (2.10) reduces to

$$\dot{\epsilon}_\sigma = \left[\frac{A_{diff} b D_{diff} \mu}{kT} \left(\frac{b}{\exp\left[\left(3 - \frac{1}{2}m\right)\phi^2\right] d_{med}} \right)^m \left(\frac{\sigma_\sigma}{\mu} \right) \right] + \left[\frac{A_{disl} b D_{disl} \mu}{kT} \left(\frac{\sigma_\sigma}{\mu} \right)^n \right] \quad (2.13)$$

Note that the first term on the right of this equation gives the strain rate (flow law) for diffusion creep in materials with a lognormal grain size distribution, assuming homogeneous stress (cf. equation 2.1).

Flow law assuming homogeneous strain rate

The derivation of a flow law under the assumption that the strain rate $\dot{\epsilon}$ is uniform throughout a polycrystalline material is more difficult, since it requires finding an expression for $\bar{\sigma} = \bar{\sigma}(\dot{\epsilon}, r, T) = r$ in (2.6b), i.e. for the stress in individual grains of radius $r (=d/2)$. This is not straightforward as it means solving for $\bar{\sigma} = \sigma / \mu$ in (2.3) - an n^{th} -order polynomial in $\bar{\sigma}$ where n is the power law stress exponent taking values between 3 and 5. The problem can be tackled by first evaluating (2.6b) separately for dislocation and diffusion creep. An expression for $\bar{\sigma}(\dot{\epsilon}, r, T)$ when deformation takes place by diffusion creep alone in a single grain is given by (2.1) as

$$\bar{\sigma}_{diff} = \frac{kT\dot{\epsilon}_{diff}}{A_{diff}bD_{diff}\mu} \left(\frac{d}{b}\right)^m = \frac{\dot{\epsilon}_{diff}r^m}{A(T)} \quad (2.14)$$

where $d=2r$ and $A(T)$ is defined as in (2.4). Putting (2.7), (2.11) and (2.14) into (2.6b) and again using our substitution $z=(\ln r - \ln r_{med})/\phi$ plus standard integral (2.10), now yields

$$\bar{\sigma}_{\dot{\epsilon}}^{diff} = \frac{\dot{\epsilon}_{\dot{\epsilon}}^{diff}}{A(T)\sqrt{2\pi}\phi \exp\left[\frac{\phi}{2}\phi^2\right] r_{med}^3} \int_0^{\infty} r^{m+2} \exp\left[-\frac{(\ln r - \ln r_{med})^2}{2\phi^2}\right] dr = \frac{\left(\exp\left[\left(3 + \frac{1}{2}m\right)\phi^2\right] r_{med}\right)^m \dot{\epsilon}_{\dot{\epsilon}}^{diff}}{A(T)} \quad (2.15)$$

This is the volume averaged stress for a material with lognormal grain size distribution deforming by diffusion creep at uniform strain rate $\dot{\epsilon}_{\dot{\epsilon}}^{diff}$. When deformation occurs by pure dislocation creep, $\bar{\sigma}$ in (2.6b) is independent of grain size and is uniform in all grains, as described by (2.2). Rearranging (2.2) and using the definition of $B(T)$ given in (2.4), this yields

$$\bar{\sigma}_{\dot{\epsilon}}^{disl} = \left(\frac{\dot{\epsilon}_{\dot{\epsilon}}^{disl}}{B(T)}\right)^{\frac{1}{n}} \quad (2.16)$$

for the volume averaged (uniform) stress when deformation occurs by dislocation creep at a homogeneous strain rate $\dot{\epsilon}_{\dot{\epsilon}}^{disl}$. Rearranging (2.15) and (2.16) to give $\dot{\epsilon}_{\dot{\epsilon}}$, putting $\bar{\sigma}_{\dot{\epsilon}}^{diff} = \bar{\sigma}_{\dot{\epsilon}}^{disl} = \bar{\sigma}_{\dot{\epsilon}}$ and summing now gives the following rough expression for the bulk creep rate of a polycrystalline material for the case that strain rate is homogeneously distributed in all grains:

$$\dot{\epsilon}_{\dot{\epsilon}}^{rough} = \frac{A(T)}{\left(\exp\left[\left(3 + \frac{1}{2}m\right)\phi^2\right] r_{med}\right)^m} \bar{\sigma}_{\dot{\epsilon}} + B(T)\bar{\sigma}_{\dot{\epsilon}}^n \quad (2.17)$$

Note that the first term on the right here gives an expression for strain rate in terms of bulk stress, which is in fact a diffusion creep law for materials with a lognormally distributed grain size, assuming homogeneous strain rate (cf. 2.15). This expression and the first term on the

right of (2.13), which assumes homogeneous stress, give upper and lower bounds for the diffusion creep rate of materials with a lognormally distributed grain size. These expressions account for variations in standard deviation as well as median grain size and can be used in their own right to describe or analyze the behavior of materials undergoing pure diffusion creep.

Equation (2.17) closely approximates the exact relationship between bulk homogeneous strain rate $\dot{\epsilon}$ and bulk stress $\bar{\sigma}_{\dot{\epsilon}}$ only if one mechanism dominates. The true solution for $\dot{\epsilon}_{\dot{\epsilon}} = \dot{\epsilon}_{\dot{\epsilon}}(\bar{\sigma}_{\dot{\epsilon}})$ can be determined iteratively, by first determining $\bar{\sigma} = \sigma / \mu$ from (2.3) at fixed strain rate and fixed T , for a large range of realistic r -values. Subsequently, the integral in (2.6b) is evaluated by incrementally summing with respect to r , yielding $\bar{\sigma}_{\dot{\epsilon}}$. The whole operation is then repeated for different strain rates. The discrepancy or error in strain rate between the rough solution, given by (2.17), and the true strain rate ($\dot{\epsilon}_{\dot{\epsilon}}^{true}$) is defined here as

$$\Delta = \left(\frac{\dot{\epsilon}_{\dot{\epsilon}}^{true} - \dot{\epsilon}_{\dot{\epsilon}}^{rough}}{\dot{\epsilon}_{\dot{\epsilon}}^{true}} \right) \times 100\% \quad (2.18)$$

This error will be negligible towards low and high normalized stresses, where diffusion creep or dislocation creep respectively dominates, but large when both mechanisms contribute significantly to $\dot{\epsilon}_{\dot{\epsilon}}$. In addition, Δ will be small for small standard deviations, because the term $\exp[(3+m/2)\phi^2]$ in (2.17) then approaches unity (single-valued grain size). The error Δ is dependent on all quantities appearing on the right hand side of (2.17), i.e. on $A(T)$, $B(T)$, r_{med} , ϕ , n , m and $\bar{\sigma}_{\dot{\epsilon}}$, but the error for a given material (fixed n , m , $A(T)$, $B(T)$) with constant grain size distribution (fixed r_{med} , ϕ) deforming at fixed conditions is only dependent on $\bar{\sigma}_{\dot{\epsilon}}$. The effects of $A(T)$, $B(T)$ and r_{med} can be removed by normalizing $\bar{\sigma}_{\dot{\epsilon}}$ with respect to $\bar{\sigma}_{\dot{\epsilon}}^{int}$, the normalized stress at the intersection between the diffusion and dislocation creep terms in (2.17) (i.e. the stress at which both terms contribute equally to the overall strain rate), using $\bar{\sigma}_{\dot{\epsilon}}^* = \bar{\sigma}_{\dot{\epsilon}} / \bar{\sigma}_{\dot{\epsilon}}^{int} = \sigma_{\dot{\epsilon}} / \sigma_{\dot{\epsilon}}^{int}$. When this is done, all curves of Δ versus $\bar{\sigma}_{\dot{\epsilon}}^*$ coincide for given n , ϕ and m , because the curves become independent of material parameters $A(T)$ and $B(T)$, temperature T and median grain radius r_{med} . The resulting Δ vs. $\bar{\sigma}_{\dot{\epsilon}}^*$ master-curve is roughly bell-shaped, peaking near $\bar{\sigma}_{\dot{\epsilon}}^{int}$. The function has been explored numerically by varying $\bar{\sigma}_{\dot{\epsilon}}^*$, n and ϕ through reasonable ranges, for both $m=2$ and $m=3$. This procedure showed (see results for $m=3$ in table 2.2) that Δ can be accurately approximated by the exponential distribution function

$$F(\bar{\sigma}_{\dot{\epsilon}}^*, \phi, n, m) = \exp\left(\alpha + \beta \bar{\sigma}_{\dot{\epsilon}}^{*0.5} \ln(\bar{\sigma}_{\dot{\epsilon}}^*) + \gamma (\ln(\bar{\sigma}_{\dot{\epsilon}}^*))^2\right) \quad (2.19)$$

in which α , β and γ are 3 independent parameters. Using this in the relation (cf. 2.18)

$$\dot{\epsilon}_{\dot{\epsilon}}^{approx} = \dot{\epsilon}_{\dot{\epsilon}}^{rough} \left(\frac{1}{1 - F(\bar{\sigma}_{\dot{\epsilon}}^*, \phi, n, m)} \right) \quad (2.20)$$

allows $\dot{\epsilon}_{\dot{\epsilon}}^{true}$ to be approximated by $\dot{\epsilon}_{\dot{\epsilon}}^{approx}$. This yields as a final result for the overall creep rate of a polycrystalline material with a lognormal grain size distribution, for the case that strain rate is uniform (i.e. constant) throughout the aggregate

$$\dot{\epsilon}_{\dot{\epsilon}}^{approx} = \left\{ \left[\frac{A_{diff} b D_{diff} \mu}{kT} \left(\frac{b}{\exp\left[\left(3 + \frac{1}{2} m\right) \phi^2\right] d_{med}} \right) \left(\frac{\sigma_{\dot{\epsilon}}}{\mu} \right) \right]^m + \left[\frac{A_{disl} b D_{disl} \mu}{kT} \left(\frac{\sigma_{\dot{\epsilon}}}{\mu} \right)^n \right] \right\} \left\{ \frac{1}{1 - F(\bar{\sigma}_{\dot{\epsilon}}^*, \phi, n, m)} \right\}$$

where $\bar{\sigma}_{\dot{\epsilon}}^* = \bar{\sigma}_{\dot{\epsilon}} / \bar{\sigma}_{\dot{\epsilon}}^{int} = \sigma_{\dot{\epsilon}} / \sigma_{\dot{\epsilon}}^{int}$ with $\bar{\sigma}_{\dot{\epsilon}}^{int} = \left(\frac{A_{diff} D_{diff}}{A_{disl} D_{disl}} \right)^{\frac{1}{n-1}} \left(\frac{b}{\exp\left[\left(3 + \frac{1}{2} m\right) \phi^2\right] d_{med}} \right)^{\frac{m}{n-1}}$ (2.21)

We further focus on grain boundary diffusion (Coble) creep with $m=3$ [cf. Karato *et al.* 1986]. Values for the parameters α , β and γ for $m=3$ are given in table 2.2 (the entire range of $\bar{\sigma}_{\dot{\epsilon}}^*$ from pure diffusion creep to pure dislocation creep was covered in the numerical exploration, taking $3 \leq n \leq 5$ and $0 \leq \phi \leq 1.2$). Using these values for $m=3$, $\dot{\epsilon}_{\dot{\epsilon}}^{true}$ is approximated by $\dot{\epsilon}_{\dot{\epsilon}}^{approx}$ within a factor of 0.9-1.1 for $n=3$ and $\phi=1.2$, and within a factor of 0.5-1.5 for $n=5$ and $\phi=1.2$, which is adequate for most purposes.

standard deviation	expression $\alpha = (a + b e^{-n})^{-1}$	expression $\beta = a + b n$	expression $\gamma = (a + b / n^2)^{-1}$
0.1	$a=-0.335$ $b=0.4619$	$a=1.13082$ $b=-0.5664$	$a=0.2339$ $b=-19.96$
0.2	$a=-0.581$ $b=1.203$	$a=0.6056$ $b=-0.3515$	$a=0.1760$ $b=-25.93$
0.3	$a=-0.919$ $b=2.434$	$a=0.4155$ $b=-0.2459$	$a=0.1316$ $b=-36.37$
0.4	$a=-1.41$ $b=4.499$	$a=0.3025$ $b=-0.1780$	$a=0.05871$ $b=-52.12$
0.5	$a=-2.14$ $b=8.046$	$a=0.2256$ $b=-0.1305$	$a=-0.06970$ $b=-75.29$
0.6	$a=-3.28$ $b=14.29$	$a=0.1697$ $b=-0.09589$	$a=-0.2600$ $b=-109.4$
0.7	$a=-5.12$ $b=25.50$	$a=0.1279$ $b=-0.07032$	$a=-0.5423$ $b=-159.0$
0.8	$a=-8.18$ $b=45.96$	$a=0.09565$ $b=-0.05110$	$a=-0.8690$ $b=-232.0$
0.9	$a=-13.5$ $b=84.11$	$a=0.06933$ $b=-0.03635$	$a=-1.352$ $b=-336.0$
1.0	$a=-22.8$ $b=155.7$	$a=0.05172$ $b=-0.02595$	$a=-1.333$ $b=-500.6$
1.1	$a=-39.5$ $b=285.9$	$a=0.03773$ $b=-0.01821$	$a=-0.1743$ $b=-761.9$
1.2	$a=-69.4$ $b=512.3$	$a=0.02767$ $b=-0.01277$	$a=4.304$ $b=-1201$

Table 2.2. Expressions for parameters α , β and γ versus stress exponent n (quoted in table heading) with constants a and b used in the expression for each standard deviation ϕ . Parameters α , β and γ evaluated for $m=3$ (grain boundary diffusion creep). With α , β and γ , the empirical function $F(\bar{\sigma}_{\dot{\epsilon}}^*, \phi, n, m)$, given by (2.19), can be used to reduce the error in strain rate to acceptable levels for deformation assuming homogeneous strain rate. The expressions can be used to estimate α , β and γ and determine $F(\bar{\sigma}_{\dot{\epsilon}}^*, \phi, n, m)$ for any stress exponent in the range $n=3-5$ and any standard deviation in the range $\phi=0-1.2$ by linear interpolation between the quoted values.

2.3 Discussion

We have derived constitutive equations describing composite diffusion plus dislocation creep for polycrystalline materials with a lognormally distributed grain size, assuming that either stress or strain rate is uniform throughout the aggregate. The two equations (2.13 and 2.21) allow investigation of the effect of varying grain size distribution on the rheology of materials deforming by these mechanisms. Note that the two equations represent upper and lower bounds for the rate of deformation in composite diffusion-dislocation creep of materials with a lognormal grain size distribution [see also *Raj and Ghosh, 1981; Freeman and Ferguson, 1986; Tullis et al., 1991*]. We will now explore the differences between our composite flow laws and composite flow laws based on a single-valued grain size, first in a general sense and then using polycrystalline olivine as an example. We focus attention on grain boundary diffusion and dislocation creep, for which the composite equation (2.21) has been fully explored. Finally, the implications for the rheology of other rock materials and for the application of flow laws to modeling and interpretation of natural rock deformation are discussed.

2.3.1 Universal deformation maps and the effect of distributed grain size

In order to make general inferences about the effect of distributed grain size on the rheology of polycrystalline materials, the flow laws for a single-valued grain size (2.3) and a lognormally distributed grain size assuming homogeneous stress (2.13) or homogeneous strain rate (2.21) are written in dimensionless form, i.e. in terms of normalized strain rate S . This yields

$$S = \left[C \left(\frac{\sigma}{\mu} \right) + \left(\frac{\sigma}{\mu} \right)^n \right] \left[\frac{1}{1 - F(\bar{\sigma}^*, \phi, n, m)} \right] \quad (2.22)$$

$$\text{where } S = \frac{\dot{\epsilon} k T}{A_{disl} b D_{disl} \mu} \quad \text{and} \quad C = \frac{A_{diff} D_{0diff}}{A_{disl} D_{0disl}} \left(\frac{b}{X} \right)^m \exp \left(\frac{Q_{disl} - Q_{diff}}{RT} \right)$$

Here, $X=d$ and $F(\bar{\sigma}^*, \phi, n, m) = 0$ for a single-valued grain size (cf. 2.3). For a lognormally distributed grain size and homogeneous stress (cf. 2.13), $X = \exp[(3-m/2)\phi^2] d_{med}$ and $F(\bar{\sigma}^*, \phi, n, m) = 0$. For a lognormally distributed grain size, homogeneous strain rate and grain boundary diffusion creep (cf. 2.21), $m=3$, $X = \exp[(3+m/2)\phi^2] d_{med}$ and $F(\bar{\sigma}^*, \phi, n)$ is given by (2.19). The advantage of the dimensionless flow laws given in (2.22) is that they can be used to construct universal deformation mechanism maps with pre-set C/n -contours that apply to any material and any set of deformation conditions. In one map, different materials and differences in deformation conditions or grain size (distribution) are represented by different C/n -contours and can be investigated in the same map. In contrast, conventional maps [*Frost and Ashby, 1982*] apply to a single material with constant grain size, temperature, stress or strain rate, depending on the type of map (e.g. stress-temperature, grain size-stress, etc.).

In fig. 2.2, such a universal deformation mechanism map is given for materials with a single-valued grain size. In this map, dimensionless strain rate S is plotted versus dimensionless stress $\bar{\sigma}$ for different combinations of power law stress exponents ($n=3, 4, 5$) and values of the constitutive parameter C . The slope of individual curves (individual C/n -contours) reflects the stress exponent of the dominant deformation mechanism. All contours

change in slope from $3 \leq n \leq 5$ at high normalized stresses to 1 at low normalized stresses, representing dominant dislocation creep and diffusion creep, respectively. In general, C will decrease with increasing temperature and grain size (see 2.22), so that at constant $\bar{\sigma}$ the normalized strain rate S will also decrease and power law dislocation creep will become increasingly important (fig. 2.2).

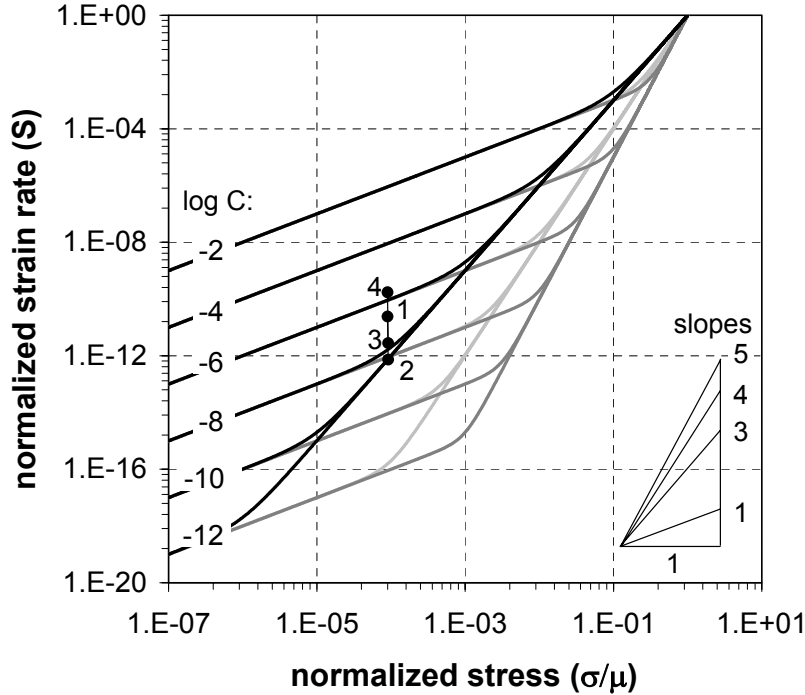


Figure 2.2. Universal deformation mechanism map for materials with a single-valued grain size, deforming by combined diffusion and power law dislocation creep. The map shows contours of C in logarithmic space of normalized (dimensionless) strain rate S versus normalized (dimensionless) stress $\bar{\sigma}$ for material with a lognormal grain size distribution and a power law stress exponent n of 3, 4 or 5. The slope of the contours reflects n . Point 1 \rightarrow 2 shows the effect of changing temperature ($T=1073 \rightarrow 1473$ K) at constant grain size ($d=500 \mu\text{m}$) and point 3 \rightarrow 4 shows the effect of changing grain size ($d=500 \rightarrow 100 \mu\text{m}$) at constant temperature ($T=1273$ K) for olivine deforming by dislocation and grain boundary diffusion creep [Karato et al., 1986] at a normalized stress of 1×10^{-4} .

Expressions for S and C for general materials with a lognormal grain size distribution, given by (2.22), incorporate the standard deviation (ϕ) and median grain size (d_{med}) of the distribution. As a consequence, the value of C and hence the rheology of a material changes if a distribution is used instead of a single-valued grain size. If homogeneous stress is assumed, the shape and position of the C/n -contours remains the same as in fig. 2.2, since the second main term in (2.22) remains unity. If homogeneous strain rate is assumed, the detailed shape of the C/n -contours is determined by the function $F(\bar{\sigma}^*, \phi, n, m)$. Figure 2.3 shows the contours for the homogeneous strain rate case and homogeneous stress case at specific values of C and n , taking $m=3$, i.e. for the case of grain boundary diffusion and dislocation creep. The difference between the homogeneous stress (thick) and homogeneous strain rate (thin) contours increases with increasing ϕ , being largest at the mechanism transition where both diffusion and dislocation creep contribute significantly to the overall strain rate. The contours

merge towards low and high normalized stress, where either diffusion or dislocation creep is dominant. When $\phi=0$, which is equivalent to a single-valued grain size, both stress and strain rate are distributed homogeneously throughout the material and the contours for homogeneous stress and strain rate coincide.

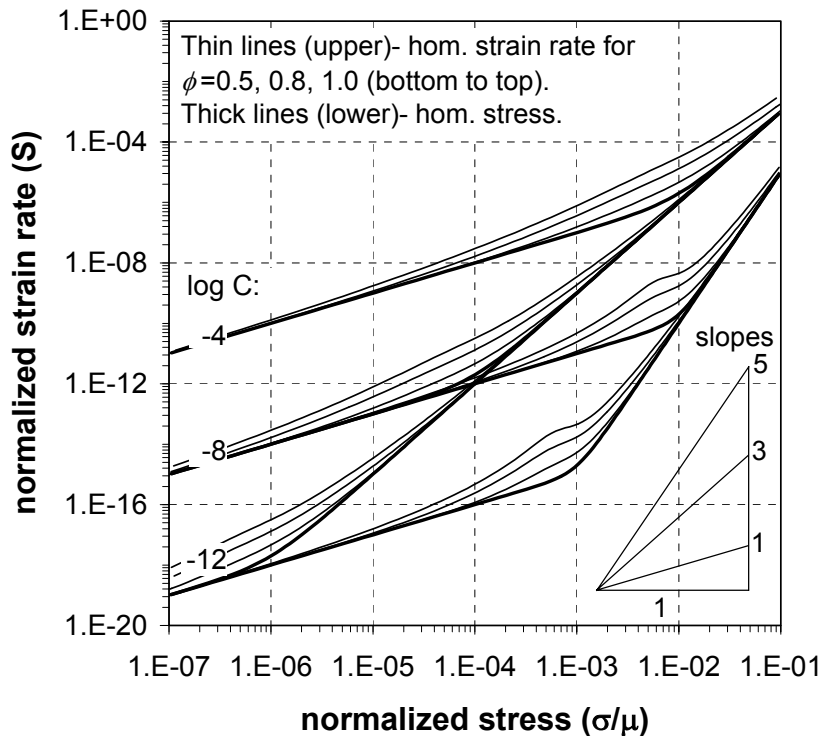


Figure 2.3. Universal deformation mechanism map for materials with a distributed grain size, deforming by combined grain boundary diffusion and power law dislocation creep. The map shows contours of C in log normalized strain rate S versus log normalized stress $\bar{\sigma}$ space for material with a lognormal grain size distribution and a power law stress exponent n of 3 or 5. The slope of the contours reflects n . The contours for homogeneous stress are represented by thick lines. Those for homogeneous strain rate are represented by thin lines, corresponding to standard deviations ϕ of 0.5, 0.8 and 1.0 (from bottom to top for each set of contours). The irregularity in the homogeneous strain rate contours for $n=5$ is due to the residual error in strain rate, which is highest for the largest stress exponent and standard deviation. Note that all strain rates for $n=3-5$ and $\phi=0-1.2$ are accurate within a factor of 2 or better.

The influence of temperature and median grain size on the rheology of materials with a lognormal grain size distribution is analogous to the influence of temperature and grain size on materials with a single-valued grain size as described above (fig. 2.2). This is evident from the expression for C in (2.22). At constant stress, increasing temperature and median grain size lead to a decrease in C and hence S , and power law creep will become increasingly important (fig. 2.3, cf. fig. 2.2). The influence of standard deviation can be seen from (2.22) as well. With increasing ϕ at a given d_{med} at constant stress, the volume fraction of grains deforming by dislocation creep increases, which is accompanied by a decrease in C and S . The range in $\bar{\sigma}$ covering the transition between diffusion and dislocation creep for constant C and homogeneous strain rate, changes from approximately one order of magnitude for small ϕ to more than 5 orders of magnitude for $\phi > 1.0$ and $n=3$ (fig. 2.3). Thus, the region where the

two deformation mechanisms contribute significantly to the overall strain rate expands considerably in a material with distributed grain size when strain rate is homogeneous.

The above results for a continuous lognormal grain size distribution are in agreement with previous studies on the effect of distributed grain sizes on rheology by *Raj and Ghosh* [1981], who showed a broadening of the transition zone with increasing separation between two discrete grain size classes. *Freeman and Ferguson* [1986] also showed a broadening of the transition zone with increasing dispersion around the mean of the discrete lognormal and bimodal distributions investigated.

2.3.2 Effect of grain size distribution on the rheology of olivine

We now apply the above flow laws and universal deformation mechanism maps to examine the rheological behavior of wet olivine during deformation by grain boundary diffusion creep ($m=3$) and power law dislocation creep ($n=3$). To do so, we use the experimental data of *Karato et al.* [1986] for the rheology of wet olivine (table 2.3), assuming this to apply for single-valued grain size (although the data were of course derived from experiments on olivine rock with distributed grain size). Note that *Karato et al.* [1986] inferred deformation to occur by dislocation creep at high stress and grain boundary diffusion (Coble) creep at low stress.

Table 2.3. Constants and flow law parameters for olivine from *Karato et al.* [1986] and *Frost and Ashby* [1982].

parameter	value	dimensions	remarks*
$A_{diff} \frac{\pi\delta}{b} D_{0diff}$	0.251	-	calculated from rate constant quoted in <i>Karato et al.</i> [1986] and values from <i>Frost and Ashby</i> [1982]
$A_{disl} D_{0disl}$	2.80×10^{-4}	-	calculated from rate constant quoted in <i>Karato et al.</i> [1986] and D_{0disl} value from <i>Frost and Ashby</i> [1982]
b	6.0×10^{-10}	m	<i>Frost and Ashby</i> [1982]
k	1.381×10^{-23}	J.K ⁻¹	
m	3	-	<i>Karato et al.</i> [1986]
n	3	-	<i>Karato et al.</i> [1986]
μ	7.10×10^{10} 6.83×10^{10} 6.57×10^{10}	Pa	for $T=1073$ K temperature-dependent, for $T=1273$ K data and equations in for $T=1473$ K <i>Frost and Ashby</i> [1982] used
Q_{diff}	250000	J.mol ⁻¹	<i>Karato et al.</i> [1986]
Q_{disl}	420000	J.mol ⁻¹	<i>Karato et al.</i> [1986]
R	8.314	J.mol ⁻¹ .K ⁻¹	

* Note that the data from *Karato et al.* [1986] are for grain boundary diffusion (Coble) creep and dislocation creep of wet hot-pressed San Carlos olivine and the data from *Frost and Ashby* [1982] are from various sources.

We consider two cases for olivine with a single-valued grain size:

- (1) $d=500 \mu\text{m}$, $T=1073 \rightarrow 1473$ K
- (2) $T=1273$ K, $d=500 \rightarrow 100 \mu\text{m}$

Using equation (2.22) and the parameters given in table 2.3, the change in temperature at constant grain size in case (1) results in a decrease in C from 3×10^{-7} to 2×10^{-9} (fig. 2.4)

and hence a decrease in S from 3×10^{-11} to 1×10^{-12} at a normalized stress of 1×10^{-4} . This means that strain rate increases from 9×10^{-14} to $8 \times 10^{-10} \text{ s}^{-1}$ at a stress of ~ 7 MPa. In addition, a switch in deformation mechanism from diffusion creep to power law dislocation creep ($n=3$ for olivine) occurs (point 1 \rightarrow 2 in fig. 2.2). The change in grain size at constant temperature in case (2) results in an increase in C from 1×10^{-8} to 2×10^{-6} (fig. 2.4) and an increase in S from 2×10^{-12} to 2×10^{-10} at a normalized stress of 1×10^{-4} (~ 7 MPa), which means strain rate increases from 9×10^{-12} to $7 \times 10^{-10} \text{ s}^{-1}$ for olivine. In addition, an increase in the importance of diffusion creep occurs (point 3 \rightarrow 4 in fig. 2.2). Similar trends can be found on the basis of conventional flow laws and deformation mechanism maps [Frost and Ashby, 1982; Karato *et al.*, 1986]. However, the present approach has the advantage that the influence of temperature and grain size on the rheology of any material can be investigated in a single diagram.

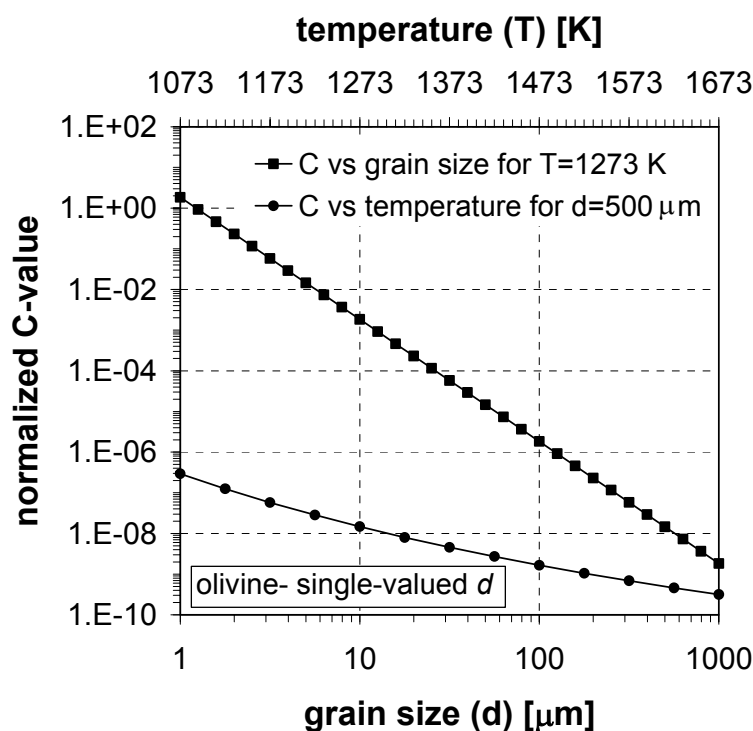


Figure 2.4. Variation of C in (2.22) with single-valued grain size d and temperature T for wet olivine, assuming grain boundary diffusion creep described by the parameters listed in table 2.3 [Karato *et al.*, 1986].

We will now evaluate the effect of varying the standard deviation on the rheology of olivine rock with a distributed grain size using the GSS and GSI flow parameters depicted in table 2.3. Lognormal grain size distributions with the same median grain size (d_{med}) and varying standard deviation (ϕ) are used. Figure 2.5 shows C/n -contours in a deformation mechanism map (cf. fig. 2.3) calculated for olivine ($n=3$) from (2.22) for deformation at $T=1273$ K, using the lognormal distributions depicted in the inset. As ϕ decreases from 1.2 to 0 (single-valued grain size), C increases from 3×10^{-9} for homogeneous stress or 7×10^{-15} for homogeneous strain rate to 2×10^{-6} (fig. 2.6). For olivine deforming at a normalized stress of 7.4×10^{-5} (~ 5 MPa), this means that S increases by more than 2 orders of magnitude from 6×10^{-13} (homogeneous stress) or 4×10^{-13} (homogeneous strain rate) to 1×10^{-10} , equivalent to an increase in absolute strain rate of more than two orders of magnitude from 2×10^{-12} to $5 \times 10^{-10} \text{ s}^{-1}$. In addition, a switch in rheological behavior from dominantly dislocation to dominantly diffusion creep occurs, as shown at 5 MPa in fig. 2.5.

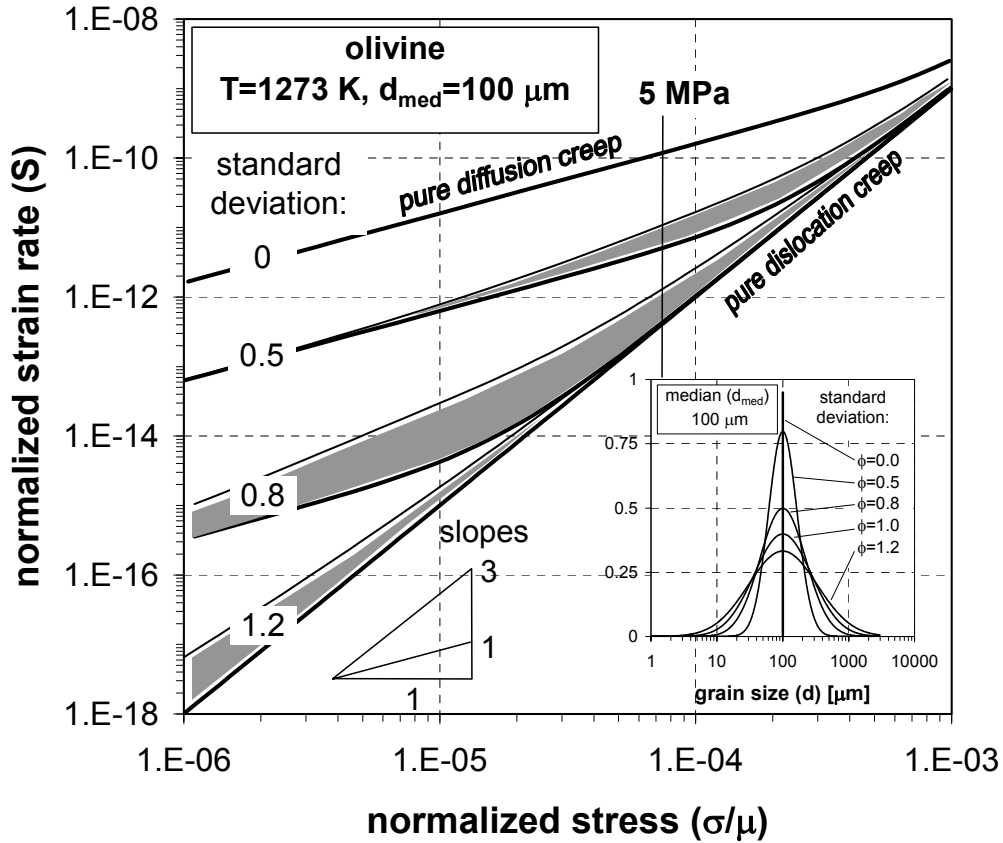


Figure 2.5. Deformation map for wet olivine, deforming by grain boundary diffusion creep and power law dislocation creep described by the parameters listed in table 2.3 [Karato et al., 1986]. The map shows contours of C in log normalized strain rate S versus log normalized stress $\bar{\sigma}$ space, assuming a lognormal grain size distribution having a fixed median and varying standard deviation, as depicted in the inset. Values of C vary from 1.6×10^{-6} for $\phi=0$ to 6.6×10^{-15} for $\phi=1.2$. For each standard deviation ϕ , the true normalized strain rate S falls between the homogeneous stress (lower thick lines) and the homogeneous strain rate (upper thin lines) bounds (shaded area). For $T=1273$ K, the normalized stress equivalent to 5 MPa is indicated.

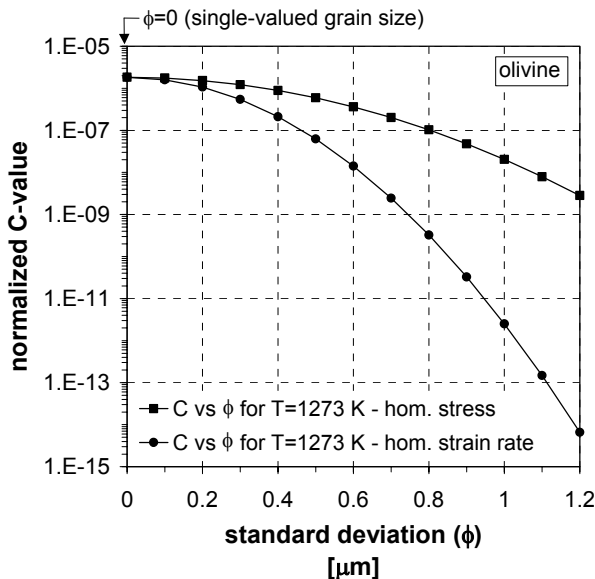


Figure 2.6. Variation of C in (2.22) with standard deviation (ϕ) of the lognormal grain size distribution for wet olivine assuming homogeneous stress and homogeneous strain rate, calculating C for the case of grain boundary diffusion creep (table 2.3).

Figure 2.7 illustrates the effect of decreasing ϕ on absolute strain rate (in s^{-1}) for olivine deforming at ~ 5 MPa and 1273 K in detail. The increase in strain rate is even greater towards lower stresses, but decreases towards higher stresses where grain size insensitive dislocation creep becomes more important. The influence of d_{med} and T on the rheology of olivine rock with a distributed grain size is similar to the influence of d and T for a single-valued grain size described above as the dependence of C and S on these parameters is the same - see (2.22).

The above example for olivine (fig. 2.5-2.7) demonstrates a substantial change in strain rate of wet polycrystalline olivine (with fixed d_{med}) deforming at a given stress if the width of the grain size distribution changes. Conventional flow laws that regard grain size as single-valued do not account for this effect and would predict strain rates similar to the strain rate at $\phi=0$ for the entire range in ϕ (fig. 2.7). It should be noted, however, that the flow parameters of olivine used (table 2.3) are determined for olivine with a specific (unreported) grain size distribution, but fitted to a flow law for a single-valued grain size [Karato *et al.*, 1986]. Strictly then, these parameters should not be used in flow laws for a distributed grain size. Rather, true flow law parameters should be determined independently by fitting flow laws for distributed grain size to mechanical data obtained for materials with a known grain size distribution. Only then can the absolute changes in $\dot{\epsilon}$ related to a change in ϕ be accurately evaluated. The present example (fig. 2.5-2.7) nonetheless illustrates that variation in standard deviation can have a major effect on the rheology of materials such as olivine.

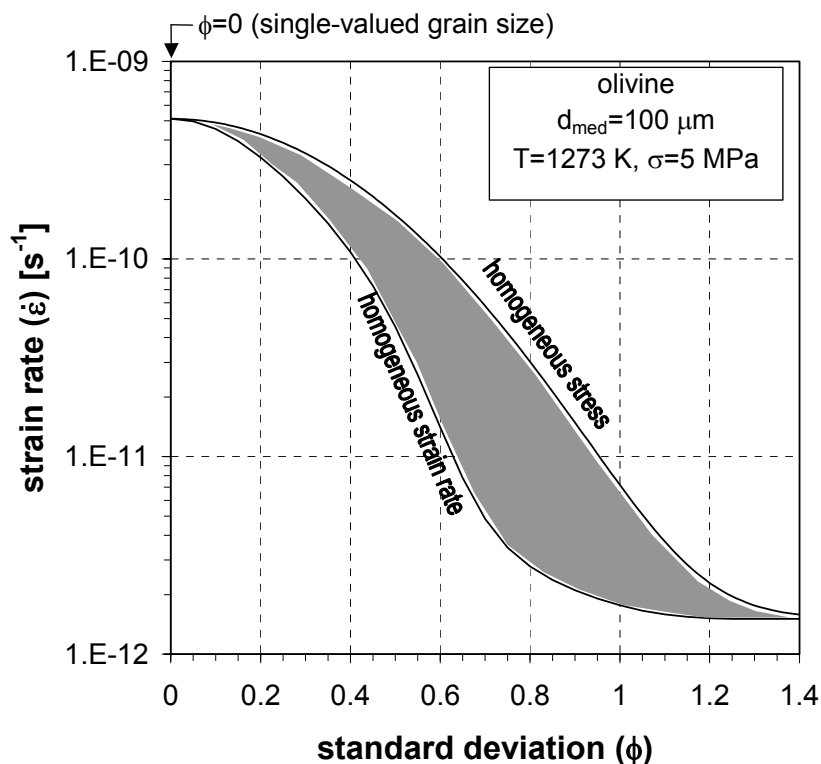


Figure 2.7. Variation of absolute strain rate $\dot{\epsilon}$ (s^{-1}) with standard deviation of the lognormal grain size distribution ϕ for wet olivine deforming at $T=1273$ K and $\sigma=5$ MPa. The true strain rate falls in between the homogeneous stress (lower line) and homogeneous strain rate (upper line) bounds (shaded area). Flow law parameters used for olivine are from Karato *et al.* [1986] (table 2.3).

2.3.3 Implications for the rheology of rock materials in general

We now address the question of what the general implications of the present model are for the rheology of materials in nature and experiment. From the foregoing, it is evident that four inter-related points need consideration:

- (1) The calibration of flow laws using laboratory data,
- (2) The interpretation of mechanical data and microstructures in experiment and nature in terms of deformation mechanisms,
- (3) The extrapolation of laboratory data to natural conditions using flow laws,
- (4) The influence of syn-tectonic modifications of the microstructure, e.g. by dynamic recrystallization or grain growth.

Calibration of flow laws

Conventional flow laws used to describe the rheology of materials in nature regard grain size as single-valued but have been “calibrated” in laboratory experiments using materials with some specific grain size distribution. In addition, laboratory data are often fitted to a single mechanism flow law, while in most cases the grain size distributions of materials consist of small grains that may deform by GSS deformation mechanisms and large grains that may deform by GSI deformation mechanisms. This means that a conventional single-mechanism flow law cannot be used to accurately predict the rheology of materials that have a grain size distribution with a different standard deviation than the material that was used to calibrate the flow law. Instead, composite GSS-GSI flow laws that account for a distributed grain size are needed. This requires the materials used in laboratory experiments to be well characterized in terms of their grain size distribution as well as their mechanical behavior. It also requires n -dimensional, two-mechanism regression analysis of mechanical data obtained in deformation experiments [Parrish and Gangi, 1981].

In general, grain size distributions in polycrystalline materials are characterized using grain areas or linear intercepts measured in a 2-D section [Underwood, 1970; Heilbronner and Bruhn, 1998]. Grain areas or intercepts measured in a 2-D section are often lognormally distributed [Ranalli, 1984; Michibayashi, 1993], whereas our flow laws assume that grain size is lognormally distributed in 3-D. Calibration of flow laws therefore requires that sectioning effects are accounted for by converting grain size distributions from 2-D sections to 3-D distributions. Several methods have been described in the literature to convert linear intercept or grain area distributions measured in 2-D sections to 3-D grain size distributions [Underwood, 1970; Thorvaldsen, 1997; Han and Kim, 1998; Heilbronner and Bruhn, 1998]. Fortunately, comparison of the 2-D and 3-D distributions indicates that the calculated 3-D distributions are very similar to the measured 2-D distributions [Heilbronner and Bruhn, 1998] and that lognormality is maintained upon conversion to 3-D [Schückher, 1968], so that incorporation of distribution parameters into flow laws is possible from 2-D measurements.

The influence of grain size distribution parameters on flow behavior has important implications for the determination of flow parameters from deformation experiments. In some studies, the conventional single-valued grain size flow laws, given by (2.1) or (2.2), are used to estimate diffusion coefficients and the associated activation energy by systematically investigating the influence of temperature on mechanical behavior [e.g. Frost and Ashby, 1982; Wang and Ji, 2000]. However, if grain size is distributed, mixed mechanisms may operate. The implication is that true (as opposed to apparent) diffusion coefficients and associated activation energies cannot be determined accurately from the mechanical behavior of materials with a distributed grain size and should really be determined independently by direct diffusion or electrical conductivity studies investigating the diffusion of atomic species

[e.g. *Jaoul*, 1990; *De Meer and Spiers*, 2002]. These diffusion coefficients can then be used as input for composite flow laws that incorporate distribution parameters, such as those given by (2.13) or (2.21). In order to determine accurate flow law parameters, new ways to measure individual parameters in theoretical flow laws need to be explored in the future.

Interpretation of deformation mechanisms

Depending on the standard deviation, the transition between diffusion and dislocation creep for materials with a lognormal grain size distribution may spread out over several orders of magnitude in (normalized) stress (cf. fig. 2.3). Since most experimental studies are restricted to a relatively narrow range of (normalized) stress in this transition zone (cf. fig. 2.5 for olivine), this can greatly complicate the interpretation of mechanical data. If a conventional single mechanism, single grain size flow law is fitted to mechanical data collected in the transition zone, apparent flow laws parameters, such as apparent diffusion coefficient, activation energy, stress exponent and grain size exponent, will be intermediate in value between the parameters for diffusion and dislocation creep. For example, apparent stress exponents that are dependent on the relative contribution of diffusion and dislocation creep may be misinterpreted as the true stress exponents for pure dislocation creep and given mechanistic significance. Such difficulties may explain some of the discrepancies between flow law parameters obtained in different studies, because grain size distributions of the materials used in experiments and hence the width of the transition zone may vary. Some of the discrepancies between theoretical models and experimental data may be likewise explained [cf. *Parrish and Gangi*, 1981]. Consider, for example, the fact that stress exponents predicted by microphysical models for diffusion ($n=1$) and dislocation ($n=3, 4.5$ or 5) creep are often different from stress exponents quoted in experimental studies. Further, the combination of mechanisms predicted by our distributed grain size models may give rise to microstructures that seem to contradict mechanical behavior observed in experiments. For example, microstructures indicative of diffusion creep have been reported in samples showing mechanical behavior with a high stress exponent [e.g. *Wolfenstine et al.*, 1993; *Bilde-Sørensen and Smith*, 1994; *Langdon*, 2000]. Some of the controversy existing in metallurgy regarding the mechanical and microstructural evidence for diffusion creep might be related to composite flow behavior and distributed grain size.

Microstructures in nature and experiment are often used in an attempt to determine the dominant deformation mechanism on the basis of prevailing microstructural features. In order to constrain rheological behavior in nature, natural microstructures are compared to microstructures from deformation experiments, in which the rheological behavior has been determined. We note two problems with this. First, the prevailing microstructural features in individual grains are not necessarily caused by the dominant deformation mechanism, i.e. the mechanism accommodating most strain [*Knipe*, 1989]. Second, if grain size is distributed, different grains may deform by different deformation mechanisms (as already indicated) and the most easily observed mechanism may not be most important in controlling flow. In this case, the rheological behavior of the material is dependent on the relative contribution of diffusion and dislocation creep to the overall creep rate. Conventional single mechanism, single grain size flow laws, determined empirically from rheological behavior using the apparently dominant deformation mechanism and average grain size, disregard the contribution of grains deforming by other potentially important mechanisms. This problem can be solved by using composite flow laws, such as those given in (2.13) and (2.21), that allow a flow law to be obtained incorporating the median grain size and standard deviation of the grain size distribution.

Extrapolation of experimental data to nature

When conventional flow laws based on a single-valued grain size are applied (extrapolated) to evaluate flow in natural rocks, differences in grain size distribution are not taken into account. Nevertheless, grain size distributions in naturally deformed rocks show a wide range of standard deviations ($\phi=0.7-1.2$ for $\ln d$, estimated from grain size distribution reported in [Michibayashi, 1993; Newman, 1994; Molli *et al.*, 2000; Dijkstra, 2001]). As shown in section 2.3.2, variations in the standard deviation of grain size distributions may have a large effect on the strain rate at a given stress. Therefore, predictions of stresses and strain rates in nature made using conventional flow laws may be significantly over- or underestimated, depending on the difference in width (expressed as ϕ) of the grain size distribution between the natural rock under investigation and the material used for calibration of the flow law. This effect is illustrated in fig. 2.8 for the example of wet olivine with $d_{med}=100 \mu\text{m}$, deforming by grain boundary diffusion ($m=3$) creep plus dislocation creep at $\sigma=5 \text{ MPa}$ and $T=1273 \text{ K}$ (cf. fig. 2.7). Figure 2.8 shows the extent to which the strain rate $\dot{\epsilon}_1$ of a natural olivine rock, with ϕ_1 , varies with respect to the strain rate $\dot{\epsilon}_2$ predicted when it is assumed that the natural rock has the same standard deviation (ϕ_2) as the olivine rock material used in the laboratory to calibrate the flow law. In this example, we take $\phi_2=0.5$ and a varying standard deviation of the olivine rock in nature of $\phi_1=0-1.4$, and calculate ratio's of $\dot{\epsilon}_1 / \dot{\epsilon}_2$ using the flow laws in (2.13) and (2.21). Figure 2.8 emphasizes that conventional single grain size flow laws predict identical strain rates ($\dot{\epsilon}_1 / \dot{\epsilon}_2=1$) regardless of differences in standard deviation between the natural and laboratory olivine rock (i.e. if $\phi_1 \neq \phi_2$). However, this would significantly underestimate (for $\phi_1 > \phi_2$) or overestimate (for $\phi_1 < \phi_2$) the strain rate, because variations as large as $\dot{\epsilon}_1 / \dot{\epsilon}_2 \sim 0.1-100$ are predicted by the flow laws that take variations in the width of the distribution into account (given in 2.13 and 2.21). In other words, conventional flow laws may overestimate the strain rate in this realistic example by a factor up to 10 if $\phi_1 < \phi_2$ or underestimate it by a factor up to 100 if $\phi_1 > \phi_2$.

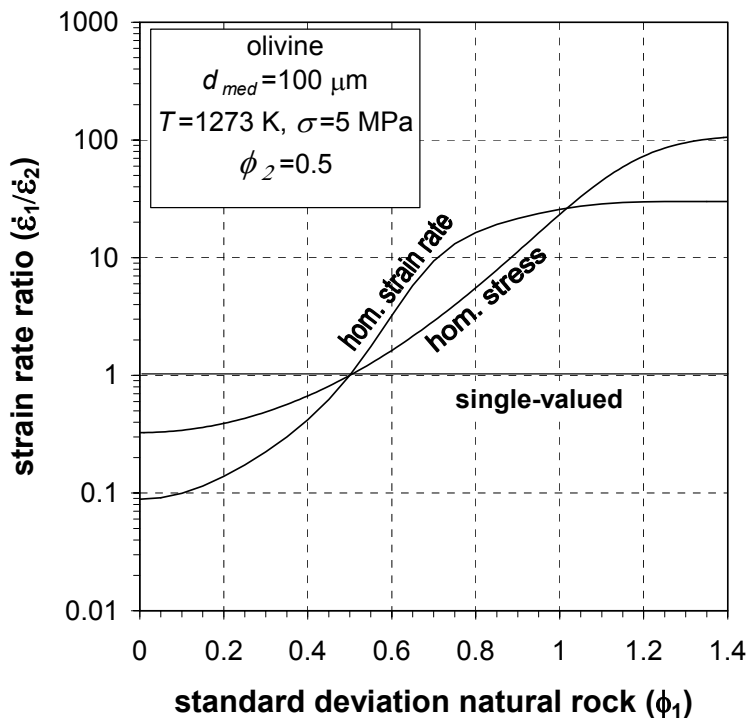


Figure 2.8. Example of the possible variation in strain rate (expressed as the ratio $\dot{\epsilon}_1 / \dot{\epsilon}_2$) due to differences in standard deviation between the olivine rock in nature (with ϕ_1) and the olivine rock material used in the laboratory to calibrate the flow law (with ϕ_2). In this example, $T=1273 \text{ K}$, $\sigma=5 \text{ MPa}$ and $d_{med}=100 \mu\text{m}$ (cf. fig. 2.7), $\phi_2=0.5$ and $\phi_1=0-1.4$ with $\dot{\epsilon}_1$ representing the strain rate for of the natural rock and $\dot{\epsilon}_2$ the strain rate of the laboratory material with $\phi_2=0.5$. A flow law for a single-valued grain size may overestimate the strain rate by a factor ~ 10 ($\dot{\epsilon}_1 / \dot{\epsilon}_2=0.1$) or underestimate it by a factor ~ 100 ($\dot{\epsilon}_1 / \dot{\epsilon}_2=100$) for this example.

The above implies that geodynamic models using conventional single grain size flow laws to describe rheology may largely over- or underestimate the flow rate in the Earth's crust or mantle. The flow laws, presented in this paper, that include the distribution parameters may be used to better constrain on stress and strain rate in the Earth. Accordingly, the flow laws may be expected to improve geodynamic models that use the rheology of materials, for example in the form of strength profiles [Kirby, 1980; Kohlstedt *et al.*, 1995], such as models for plate movement and subduction [Zhong and Gurnis, 1995; Van Hunen *et al.*, 2000], mantle flow [Van den Berg *et al.*, 1993] and the evolution of shear zones [Braun *et al.*, 1999; Gueydan *et al.*, 2001].

Effect of dynamic recrystallization and grain growth

It has been widely recognized that microstructures of materials deforming by diffusion or dislocation creep may be altered by normal grain growth or dynamic recrystallization [e.g. Rutter and Brodie, 1988; Humphreys and Hatherly, 1996]. These processes of microstructural modification result in the alteration of grain size distribution (e.g. median *and* standard deviation). Examples have been demonstrated in natural shear zones in quartz and carbonate rocks [Michibayashi, 1993; Newman, 1994] and in deformation experiments on olivine, feldspar and calcite aggregates [Post and Tullis, 1999; Zhang *et al.*, 2000; Pieri *et al.*, 2001a]. If changes in the width of the distribution are not taken into account, rheological weakening or strengthening associated with dynamic recrystallization or grain growth may be over- or underestimated. In addition, dynamic recrystallization may cause rheological weakening by lowering the width of the grain size distribution, providing a possible mechanism for strain localization. Note that the mechanism causing rheological weakening is different from the often-proposed switch in deformation mechanism [e.g. Rutter and Brodie, 1988], because grains that deform by dislocation creep can still be present in the material after narrowing the distribution width. The weakening is due to a lowering in the relative contribution of grains deforming by dislocation creep to the overall creep rate.

Several recent studies have attempted to relate dynamic recrystallization to rheological behavior using models based on a balance between grain growth and grain size reduction [Derby, 1991; Shimizu, 1998; De Bresser *et al.*, 2001]. In accordance with such models, dynamic recrystallization leads to a specific grain size distribution, characteristic of the microstructural state. During dynamic recrystallization, the evolution of the microstructure towards steady state can be monitored through changes in the distribution parameters d_{med} and ϕ , which can be regarded as microstructural state variables. The effect of dynamic recrystallization on rheology can therefore be described with the flow laws presented in this paper using models that describe the evolution of d_{med} and ϕ . For an accurate assessment of rheological weakening and associated strain localization, composite flow laws that incorporate grain size distribution parameters are accordingly essential.

2.4 Summary and conclusions

1. Constitutive flow equations describing deformation of materials generally are grain size insensitive (dislocation creep) or include grain size as a single value (e.g. diffusion creep). However, materials invariably exhibit a grain size distribution, implying that in the same aggregate small grains may deform by a different mechanism than large grains.

2. We have derived theoretical composite diffusion-dislocation creep laws for materials with a continuous lognormal grain size distribution for the assumption that either stress or strain rate is uniform in the material. The flow laws describe lower and upper bounds for the rate of deformation in materials with a distributed grain size and allow systematic investigation of the effect of varying the grain size distribution on rheology. In the flow laws, grain size distribution is characterized by the median grain size and standard deviation. The flow laws contain expressions that can be used to evaluate the role of grain size distribution in pure diffusion creep.
3. Composite flow laws that incorporate parameters characterizing the grain size distribution provide better constraints on rheology and on the interpretation of active deformation mechanisms in natural rocks, thereby helping to improve geodynamic models. This is due to the following aspects:
 - (a) Conventional flow laws calibrated in the laboratory are generally of empirical character. The composite expressions presented in this study allow calibration of flow laws with a microphysical basis, combining theoretical diffusion and dislocation creep models with realistic grain size distributions. Difficulties with the interpretation of apparent values for flow parameters resulting from fitting experimental data to single flow laws can be largely avoided. We emphasize, however, that constraints on flow laws parameters such as diffusion coefficients need to be measured independently (e.g. by direct diffusion studies or electrical conductivity) in order to obtain physically meaningful flow laws.
 - (b) Extrapolation of experimentally calibrated flow laws to nature can be done more reliably, because differences between the grain size distribution of naturally deformed rocks and that of the materials tested in the laboratory can be accounted for.
 - (c) The effect of dynamic recrystallization or grain growth on rheology can be investigated by assessing progressive changes in grain size distribution during deformation, using the median and standard deviation as microstructural state variables.
4. After expressing the flow laws in dimensionless form, universal deformation mechanism maps can be constructed that apply to any material and any set of realistic deformation conditions. A single map can then be used to compare deformation characteristics of different materials and grain size distributions.
5. Whereas the flow law for uniform stress is routinely applicable in a manner similar to conventional flow laws, routine application of the flow law for uniform strain rate requires an approximation in which parameters for a single diffusion creep mechanism are used. We focused in this paper on the application of the flow laws to olivine, deforming by a combination of dislocation and grain boundary diffusion creep. This showed that for a realistic range of standard deviations ($\phi=0-1.2$), the strain rate can change by orders of magnitude with increasing standard deviation. In some cases even a switch in rheological behavior from dominant diffusion creep to dominant dislocation creep or vice versa can be induced. Conventional flow laws based on a single-valued grain size significantly over- or underestimate strain rates or stresses in nature if the grain size distribution of the natural rock differs from that of the material used in laboratory experiments to calibrate the flow law.

Chapter 3

The influence of dynamic recrystallization on the grain size distribution and rheological behavior of Carrara marble deformed in axial compression

Abstract. Strain localization and associated rheological weakening are often attributed to grain size reduction resulting from dynamic recrystallization. Most studies investigating rheological changes due to dynamic recrystallization regard recrystallized grain size as a single value that is uniquely related to stress during steady state deformation. However, rock materials invariably exhibit a grain size distribution with distribution parameters that may be altered by dynamic recrystallization during transient deformation, affecting the rheological behavior. This study aims to investigate the effect of deformation conditions on the evolution of grain size distribution and rheological behavior during dynamic recrystallization in the approach to steady state. To study this, we have deformed Carrara marble to natural strains of 0.15-0.90 in axial compression at temperatures of 700-990°C, stresses of 15-65 MPa, strain rates of 3.0×10^{-6} - $4.9 \times 10^{-4} \text{ s}^{-1}$ and a confining pressure of 150 or 300 MPa, and analysed the grain size distribution of each sample. The results show that during dynamic recrystallization, grain size distributions evolve by a competition between grain growth and grain size reduction. The relative importance of grain size sensitive creep increases as the average grain size is reduced with strain. Minor weakening is observed, which is probably insufficient to cause strain localization in nature.

3.1 Introduction

It is commonly observed that deformation in natural rocks tends to localize in relatively narrow zones. Localized deformation is often found in calcite rocks that are believed to act as weak rocks accommodating large scale displacements along major thrusts in mountain belts, such as the Glarus thrust in the Alps [Schmid, 1975]. One of the key issues in rock deformation studies is the cause of the rheological weakening necessary for strain localization. It has been frequently proposed that dynamic recrystallization may produce the rheological weakening required for strain localization by inducing sufficient grain size reduction to cause a switch in deformation mechanism from dislocation to diffusion creep [White *et al.*, 1980; Rutter and Brodie, 1988; Karato and Wu, 1993]. However, this requires that the reduced grain size remains constant during diffusion creep, which may only occur when grain growth is prevented, for example if inhibited by second phases [Olgaard, 1990]. For single phase materials, grain growth during diffusion creep may drive deformation back to the boundary between the diffusion and dislocation creep fields, where dynamic recrystallization and grain size reduction associated with dislocation creep become important again. This notion has led to the hypothesis that for single phase materials, the recrystallized grain size tends to organize itself in the boundary between the dislocation and diffusion creep field during steady state deformation [De Bresser *et al.*, 1998; 2001]. This boundary hypothesis model, like most models describing dynamic recrystallization, treats recrystallized grain size as a single value and implicitly assumes steady state deformation. However, most rock materials exhibit some grain size distribution with distribution parameters, such as median and standard deviation, which may be altered during dynamic recrystallization. These alterations can be expected to cause changes in rheological behavior [Freeman and Ferguson, 1986]. In addition, recent torsion experiments on rock materials such as anhydrite [Stretton and Olgaard, 1997], olivine [Bystricky *et al.*, 2000] and calcite [Paterson and Olgaard, 2000; Pieri *et al.*, 2001a; b] reveal that high strains are required to reach microstructural and

mechanical steady state. Therefore, models describing the rheology of rock materials under natural conditions, which may have been deformed to a range of strains, must account for the evolution of grain size distribution and rheological behavior during transient deformation in the approach to steady state. This requires a detailed understanding of the influence of dynamic recrystallization on microstructural evolution and mechanical behavior. So far, only very few experimental deformation studies have been carried out that systematically contribute to this understanding [Covey-Crump, 1998; Bystricky *et al.*, 2000; Pieri *et al.*, 2001a]. The broad aim of this study is to provide a systematic investigation that helps to fill in this gap, concentrating on the important rock forming mineral calcite.

Calcite is one of the best studied materials in rock deformation and experiments on polycrystalline calcite aggregates, such as marble, date back to the early days of experimental rock deformation studies [Griggs, 1936]. Since these early studies, the mechanical behavior of calcite rocks has been explored by numerous studies, which demonstrated that different calcite rocks at a wide range of conditions dominantly deform by intracrystalline plastic flow accompanied by dynamic recrystallization, in particular at temperatures above $\sim 600^\circ\text{C}$ [e.g. Yule marble-*Heard and Raleigh*, 1972; Solnhofen limestone-*Rutter*, 1974; *Schmid et al.*, 1977 and Carrara marble-*Rutter*, 1974; *Schmid et al.*, 1980; *Covey-Crump*, 1998]. Only at low stresses and small grain size was grain size sensitive flow observed in calcite rocks, presumably controlled by grain boundary sliding accommodated by dislocation or diffusional processes [Solnhofen limestone-*Schmid et al.*, 1977, hot pressed synthetic calcite aggregates-*Walker et al.*, 1990]. Except for some extensional tests [*Rutter*, 1995; *Rutter*, 1998], samples were deformed in axial compression in these studies, which limited the amount of strain that could be attained. Higher strains have been reached by means of simple shear experiments on a diagonal saw cut assembly containing calcite rock slices [*Kern and Wenk*, 1983; *Schmid et al.*, 1987] and more recently by high strain torsion experiments [*Casey et al.*, 1998; *Pieri et al.*, 2001a; b]. Axial compression tests are often used to make inferences on steady state recrystallized grain size and rheological behavior of calcite rocks, despite the limited strain reached. In view of the large strains required to reach true steady state (shear strain well over 10, *Pieri et al.* [2001a]) compared to the strains attainable in axial compression (equivalent to shear strains of ~ 0.7), it is questionable if this approach is justified. Within the broad aim defined above, the specific objectives of this study are to systematically investigate (1) the evolution of the grain size distribution and rheological behavior of Carrara marble with increasing strain as a function of temperature during transient deformation and (2) the influence of stress and temperature on the grain size distribution that has developed at selected strains.

To investigate this, cylindrical samples of Carrara marble have been deformed to natural strains of 0.20-0.90 in axial compression at temperatures in the range of $700\text{-}990^\circ\text{C}$, stresses of 15-65 MPa, strain rates of 3.0×10^{-6} - $4.9 \times 10^{-4} \text{ s}^{-1}$ and a confining pressure of 150 or 300 MPa. Microstructural analysis of undeformed and deformed samples was conducted, applying quantitative image analysis techniques. Compared with previous studies on calcite deformed in axial compression, this research has the following new elements: (1) Instead of determining a single value representing the average grain size, complete grain size distributions have been analysed. This approach provides important additional information on the evolution of different sized grains during recrystallization. (2) The evolution of grain size distribution and rheological behavior in the approach to steady state gives insight into the processes altering the grain size distribution, both during transient and steady state deformation. (3) The influence of deformation conditions on the relative importance of processes altering the microstructure and their effect on the characteristics of the grain size distribution is investigated by analysis of samples deformed to selected strains at a range of stresses, temperatures and strain rates.

3.2 Experimental procedure

3.2.1 Material and sample preparation

The marble investigated in this study originates from a block of Carrara marble ('Lorano Bianco' type) that is selected as a laboratory standard for deformation experiments on marble. The structural elements, chemical composition and material properties of the marble are well characterized and the structure, stratigraphy and tectonic setting of the source of the block in the area near Carrara in the Apuane Alps in Italy have been well documented [Molli *et al.*, 2000; Pieri *et al.*, 2001a]. Microscopic analysis in combination with chemical analysis of minor and trace elements using X-ray fluorescence (XRF) and inductively coupled plasma (ICP) spectroscopy (table 3.1) reveal that the marble consists of ~99% pure calcite with few grains of muscovite, quartz, dolomite and graphite.

Samples were cored in an arbitrary but constant direction from the block of Carrara marble. Sample ends were machined and polished in such a way that they were parallel (to within 0.02 mm) to each other and perpendicular ($\leq 1^\circ$) to the sample axis. Measurements of grain aspect ratios (see result section) revealed that the starting material had a weak shape preferred orientation. Samples were cored in a direction of $\sim 20^\circ$ to the longest axis of grains in the starting material. Samples with a length of 25, 16 and 11 mm and a diameter of 9.9, 8.0 and 8.0 mm were used for the experiments to ~ 0.15 , ~ 0.30 , ~ 0.40 natural strain respectively. The samples, together with Al₂O₃ ceramic spacers for the samples shorter than 25 mm, were jacketed in a 0.2 mm thick copper tube with one copper cup at each end, which were welded together creating a gas tight copper capsule.

Table 3.1. Chemical analysis of Carrara marble ('Lorano Bianco' type)

	XRF*	ICP†		XRF‡	ICP§		XRF‡	ICP§
	wt.%	wt.%		ppm	ppm		ppm	ppm
CaO	56.86	55.11	Mg	-	2250	Zr	<6	27
MgO	0.85	0.82	Sr	122	97	P	-	6
SiO ₂	-	0.07	Mn	-	27	Cu	5	<1
Al ₂ O ₃	-	0.05	Ti	-	24	K	-	4
P ₂ O ₅	0.07	trace	Nd	<14	-	Pb	<4	-
Fe ₂ O ₃	0.07	0.01	V	<12	<0.8	Nb	3	-
Na ₂ O	0.04	trace	Fe	-	12	Ni	3	-
K ₂ O	0.02	trace	Ba	11	-	Y	3	1.3
TiO ₂	0.008	trace	La	10	-	As	<3	-
MnO	0.002	trace	Cr	<10	27	Ga	<3	-
LOI"	44.00	42.83	Sn	<9	1.5	U	<3	-
			Th	<9	-	Rb	<2	-
Total	101.92	98.88	Sc	8	-	Zn	1	-
			Ce	-	7	Be	-	<0.2

* XRF on fused glass bead-this study, † ICP (average)-Pieri *et al.* [2001a],

‡ XRF on pressed powder pellets-this study, § ICP-Rutter [1995],

" LOI- Lost On Ignition

3.2.2 Experiments, data acquisition and processing

The samples were deformed in axial compression by constant displacement rate tests in a constant volume, internally heated argon gas medium apparatus, consisting of a water cooled 1 GPa pressure vessel with a three zone Kanthal-AF wire furnace. The vessel is mounted in a horizontally placed Instron 1362 servo controlled testing machine. Piston displacement was controlled by an Instron actuator and measured externally with a linear variable differential transformer (LVDT, 2 μm resolution). Sample shortening was calculated by correcting piston displacement for apparatus distortion. Axial force was applied to the sample by displacement of a dynamically sealed deformation piston against a stationary reaction piston and measured both internally, using a Heard type internal force gauge (100 kN full scale, ~ 20 N resolution), and externally, using an Instron 100 kN load cell (accurate to 0.1 % of the full scale output or 0.5 % of the indicated load, whichever is greater). Confining pressure was measured using a strain gauge type pressure transducer (10^5 Pa resolution). In general, pressure remained constant within 2 MPa during the experiments, but in some overnight experiments small variations in pressure (< 5 MPa) occurred. Stress on the sample was calculated from the internal axial force, corrected for pressure variations and copper jacket strength, assuming constant volume and homogeneous deformation. Temperature was measured using three Pt/10%Rh (type S) thermocouples located next to the capsule wall. The temperature gradient along the sample was determined to be in the order of 1° or 2° [see *McDonnell, 1997; McDonnell et al., 1999* for a detailed description of the apparatus]. At the end of each experiment the furnace was immediately shut down, resulting in rapid cooling of the sample (1000°C to 100°C in ~ 13 min.). All measurements are estimated to be accurate to within 5%. However, taking into account inaccuracies caused by slight heterogeneous straining of the samples due to piston friction, the error in stress, strain and strain rate is estimated to be $< 10\%$, based on microstructural observations.

Samples were deformed to natural strains of 0.15-0.40 at strain rates of 3.0×10^{-6} - 4.9×10^{-4} s^{-1} , temperatures of 700 - 990°C and a confining pressure of 150 and 300 MPa resulting in flow stresses in the range 14.6-65.0 MPa (table 3.2). One sample was deformed to a natural strain of ~ 0.90 in three subsequent tests on the same sample (36LM900/0.90). This required removing the sample twice from the gas apparatus and jacket and after re-polishing and re-jacketing, inserting the sample into the apparatus again and heating to 900°C before restoring the load.

3.2.3 Microstructural analysis

Microstructural analysis was carried out on ultrathin (~ 5 - 10 μm) optical sections using a Leica DMRX light microscope, equipped with a Sony DXC-950P colour video camera. For grain size analysis, a mosaic covering an area of 3 - 12 mm^2 in the middle of the sample was made of colour photographs taken in transmitted light at $5\times$ magnification under crossed-polarized light. Grains in the photographs were traced manually on transparencies. Quantitative analysis of the area (A_{grain}) and perimeter (P_{grain}) of individual grains, the total grain boundary area (A_{gb}) (i.e. the total area made up by the traced boundary in 2-D section) and 22.5° ferets (i.e. the orthogonal distance between a pair of parallel tangents to the grain at angles of 22.5° intervals) was conducted on the scanned transparencies using the image analysing program Leica QWin Pro Version 2.2 [1997]. The thickness of the manually traced grain boundary in the 2-D section was added to the area of individual grains using $A_{\text{cor}} = A_{\text{grain}} + (P_{\text{grain}}/P_{\text{tot}}) \times A_{\text{gb}}$, with P_{tot} , the total measured grain perimeter and A_{cor} , the corrected area of individual grains in 2-D section. Grain size was calculated and presented as equivalent circular diameters (ECD), using the corrected grain area A_{cor} without any

(stereological) correction for sectioning effects. With this method, the number of grains in the lowest class (detection limit: 5-9 μm , equivalent to 1 pixel size) tends to be overestimated, because part of the grains smaller than the detection limit is incorporated in the lowest class. For all samples, the logarithmic ECD frequency distribution (referred to as grain size distribution) and the distribution of area fraction occupied by a given ECD class (referred to as area distribution) is given in a single histogram with a bin size of 0.1.

Delta-histograms have been constructed by subtracting two histograms with the same class intervals. Delta-histograms show differences in ECD frequency or area fraction of grains between samples and they can be used to investigate evolution of the grain size distribution with strain or during heating. When logarithmic grain size histograms of two samples deformed to different strains are used to construct a delta-histogram, grain areas A_{cor} have been corrected to account for out-of-plane strain, which causes a reduction of grain area in 2-D section unrelated to grain size reduction due to the recrystallization process. In axial symmetric straining, the three principal stretches s_1 , s_2 and s_3 (with s_3 parallel to the compression direction) are related by $s_1 = s_2 = \sqrt{I/s_3}$ if the volume of the deformed sample is constant. This means that a spherical grain with diameter d with maximum area in thin section of $\frac{1}{4}\pi d^2$ flattens to an ellipsoid with diameter $d_1=d_2>d_3$ and a maximum area in thin section of $\frac{1}{4}\pi d_1 d_3 = \frac{1}{4}\pi (ds_1)(ds_3) = \frac{1}{4}\pi d^2 \sqrt{s_3}$. Hence, A_{cor} needs to be corrected by a factor $\sqrt{s_3}$ to estimate the true influence of dynamic recrystallization on 2-D microstructural modification. An estimate of the minimum amount of recrystallized area as seen in 2-D section (A_{RXmin}) has been obtained by summing the negative area fraction differences (=area reduction) of the larger grain size classes (i.e. the area made up by the larger grains in the distribution that are reduced in size). A_{RXmin} is a minimum estimate since growth of (recrystallized) grains results in an increase of the area fraction difference in the larger grain size classes of the delta-histograms. This means area reduction due to dynamic recrystallization in these classes is underestimated. Grain aspect ratios were calculated by dividing the feret measured perpendicular to the compression direction by the feret measured parallel to the compression direction.

3.3 Results

3.3.1 Mechanical data

Table 3.2 lists test conditions and characteristics of all performed experiments. Note that test numbers are used, with approximate stress, temperature and final natural strain (if not ~ 0.4) as the first, second and third number respectively. Selected, representative stress (σ) versus strain (ε) curves are depicted in fig. 3.1. The flow stresses increase with increasing strain rate and decreasing temperature. Most curves show a peak stress or plateau in flow stress at $\varepsilon=0.1-0.2$ followed by weakening at higher strains. Experiments 15LM950, 36LM900/0.15 and 36LM900/0.30 weaken after a peak at a lower value of strain. However, the duplication experiment 36LM900/0.15r, which shows a peak stress at $\varepsilon=0.11$, indicates that peaks at lower strains are an exception rather than a general feature. The amount of weakening tends to increase with increasing temperature. Experiment 36LM900/0.90 (23% total weakening) shows that weakening continues at least up to $\varepsilon=0.90$. As a consequence, the observed weakening in the other samples, deformed to lower strains, should be regarded as a minimum value. In none of the experiments true steady state was achieved.

Table 3.2. Characteristics of all experiments.

test [*]	stress at peak [MPa]	strain at peak	strain rate at peak [s ⁻¹]	flow stress [†] [MPa]	strain rate [†] [s ⁻¹]	T [†] [°C]	P [†] [MPa]	natural strain	exp. duration [hr]	weakening (peak- end) [‡] [%]
starting material	-	-	-	-	-	-	-	-	-	-
start 1hr at 900°C	-	-	-	-	-	-	-	-	-	-
15LM950	24.9	0.03	2.7 · 10 ⁻⁶	14.6	4.2 · 10 ⁻⁶	962	150	0.446	39.07	41
23LM900	25.4	0.19	2.9 · 10 ⁻⁶	21.8	3.9 · 10 ⁻⁶	906	303	0.424	38.12	14
23LM990	28.1	0.13	3.5 · 10 ⁻⁵	25.0	4.6 · 10 ⁻⁵	992	299	0.386	2.89	11
36LM830/0.15	38.5	0.15	3.0 · 10 ⁻⁶	36.7	3.0 · 10 ⁻⁶	829	301	0.170	17.41	5
36LM830/0.30	43.9	0.19	3.2 · 10 ⁻⁶	39.6	3.4 · 10 ⁻⁶	830	299	0.291	27.95	10
36LM830	43.4	0.13	2.8 · 10 ⁻⁶	38.7	4.0 · 10 ⁻⁶	835	299	0.446	40.09	11
36LM900/0.15	37.4	0.01	3.1 · 10 ⁻⁵	34.1	3.7 · 10 ⁻⁵	903	305	0.158	1.70	9
36LM900/0.15r [§]	37.8	0.11	3.5 · 10 ⁻⁵	37.4	3.5 · 10 ⁻⁵	899	301	0.141	1.42	1
36LM900/0.30	35.6	0.02	3.2 · 10 ⁻⁵	32.9	4.0 · 10 ⁻⁵	901	303	0.269	2.14	8
36LM900/0.30	heated	for	~ 1 hr	At	900°C					
36LM900	39.9	0.16	3.7 · 10 ⁻⁵	36.3	4.5 · 10 ⁻⁵	898	299	0.399	2.98	9
36LM900/0.90a [¶]	33.9	0.16	3.5 · 10 ⁻⁵	33.5	3.5 · 10 ⁻⁵	900	299	0.161	1.37	-
36LM900/0.90b [¶]	-	-	-	31.9	4.6 · 10 ⁻⁵	900	302	0.299	2.07	-
36LM900/0.90c [¶]	-	-	-	26.2	7.1 · 10 ⁻⁵	902	306	0.437	2.20	23
36LM950/0.15	36.7	0.06	3.3 · 10 ⁻⁴	35.2	3.6 · 10 ⁻⁴	960	302	0.157	0.08	4
36LM950/0.30	38.5	0.07	3.3 · 10 ⁻⁴	32.5	4.1 · 10 ⁻⁴	957	300	0.298	0.23	16
36LM950	42.6	0.15	3.6 · 10 ⁻⁴	31.6	4.9 · 10 ⁻⁴	949	301	0.464	0.33	26
50LM730	58.5	0.18	3.0 · 10 ⁻⁶	52.2	3.9 · 10 ⁻⁶	726	298	0.436	39.56	11
50LM730r [§]	59.4	0.15	2.9 · 10 ⁻⁶	52.1	3.9 · 10 ⁻⁶	731	298	0.435	39.40	12
50LM780	55.6	0.13	3.5 · 10 ⁻⁵	47.3	4.7 · 10 ⁻⁵	776	298	0.429	3.21	15
50LM830	62.6	0.13	3.5 · 10 ⁻⁴	53.3	4.7 · 10 ⁻⁴	835	297	0.438	0.33	15
65LM700	73.5 ⁱ	0.23 ⁱ	3.1 · 10 ⁻⁶	65.0	3.8 · 10 ⁻⁶	698	299	0.431	39.44	12 ⁱ

* For convenience in comparing tests, stress (first number) and temperature (second number) are quoted in the test numbers. For samples deformed to natural strains less or more than ~0.4, the last number in the name gives the approximate natural strain.

† Flow stress, temperature (T), strain rate and pressure (P) averaged over a strain of 0.01 at the end of the test are quoted.

‡ Weakening is calculated by $((\sigma_{peak} - \sigma_{end}) / \sigma_{peak}) \times 100\%$ with σ_{peak} and σ_{end} the flow stress at the peak or at the end of the experiment.

§ Samples broke during removal from gas apparatus or jacket, no grain size distributions determined. Tests are quoted to give an indication of the reproducibility of the mechanical data.

¶ Three-step experiment, sample removed from apparatus and re-polished and re-jacketed after each step (twice in total). In total a natural strain of 0.897 was reached. See text for details.

ⁱ Value is influenced by dip in stress-strain curve due to day-night fluctuation of the pressure vessel cooling-water temperature affecting the internal load cell signal. Peak stress is likely to be slightly higher (~74 MPa) and strain at peak lower (~0.16) if temperature fluctuations of cooling-water are corrected for.

Duplication of selected experiments (i.e. 36LM900/0.15r and 50LM730r) indicates that flow stress at a given ε can be reproduced within ~10% (table 3.2). Flow stresses, which are the result of test conditions chosen on the basis of a previous study on the same material [De Bresser, 1996], are grouped into five sets of broadly constant stress, namely 15, 23.4 ± 1.6 , 35.6 ± 4.0 , 50.3 ± 3.0 and 65 MPa (table 3.2).

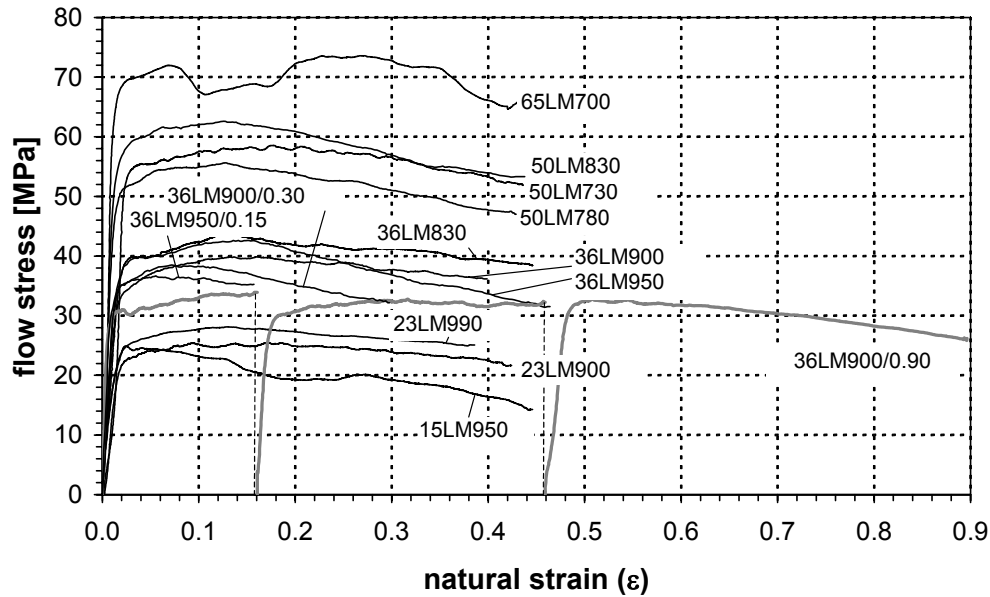
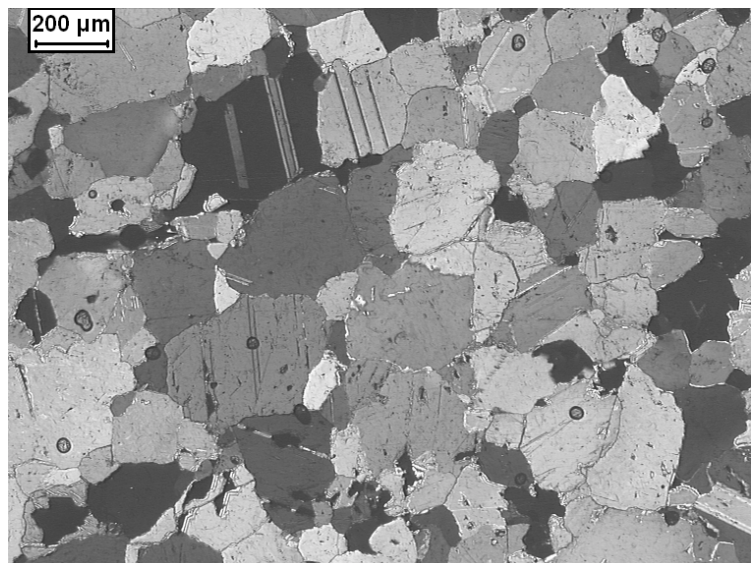


Figure 3.1. Typical stress-strain curves for Carrara marble deformed in axial compression showing the influence of stress and temperature on the flow stress. Sample 36LM900/0.90 was deformed to a strain of 0.9 in three subsequent steps (thick lines). The sudden dip in flow stress in experiment 65LM700 is due to day-night fluctuation of the pressure vessel cooling-water temperature affecting the internal load cell signal. This effect was corrected in all other overnight experiments. The experimental conditions and results of all tests are depicted in table 3.2.

3.3.2 Qualitative microstructural observations

Microscopic observations of the Carrara Marble starting material (fig. 3.2a) indicated that grain size is fairly homogeneous in the sample. The grains have a weak shape preferred orientation, but lack indications of intracrystalline deformation, such as undulose extinction, deformation lamellae or lattice preferred orientation. Within individual grains, thin twins with straight boundaries were recognized. Grain boundaries are generally straight or only gently curved, and preferentially intersect at triple point junctions with angles of $\sim 120^\circ$, although 90° junctions are present as well.

Figure 3.2a. Microstructure of undeformed Carrara marble (starting material) showing straight twins, straight or gently curved grain boundaries and triple point junctions intersecting at 120° or 90° .



Qualitatively, the microstructure of the starting material does not change significantly after heating for ~ 1 hr at 900°C (equivalent to the time needed to reach a stable temperature in the experiments).

Figure 3.2b. Overview of sample 65LM700 showing large flattened grains with small, recrystallized grains at the grain boundaries forming a core-mantle structure. Compression direction vertical.

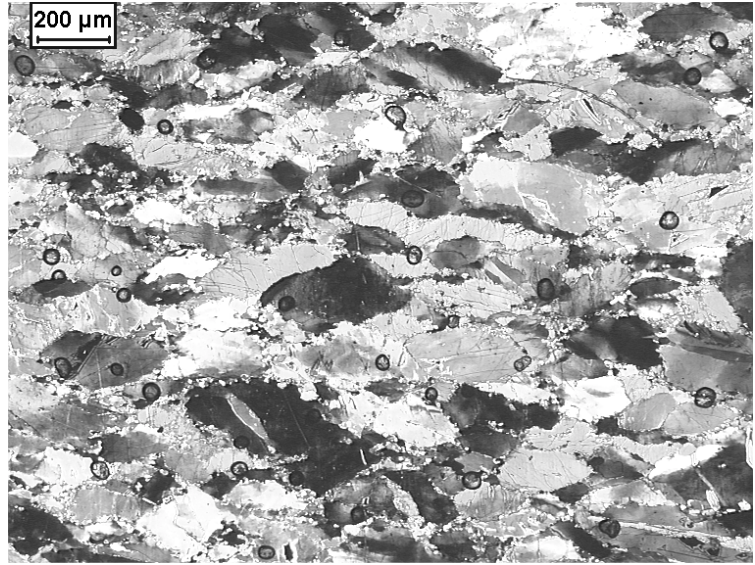


Figure 3.2c. Overview of sample 36LM950 showing grain flattening and irregular grain boundaries and shapes. Compression direction vertical.

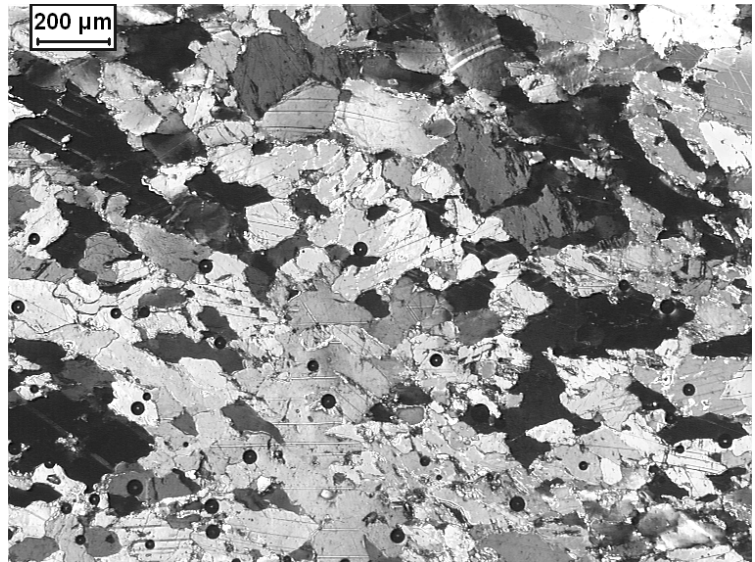
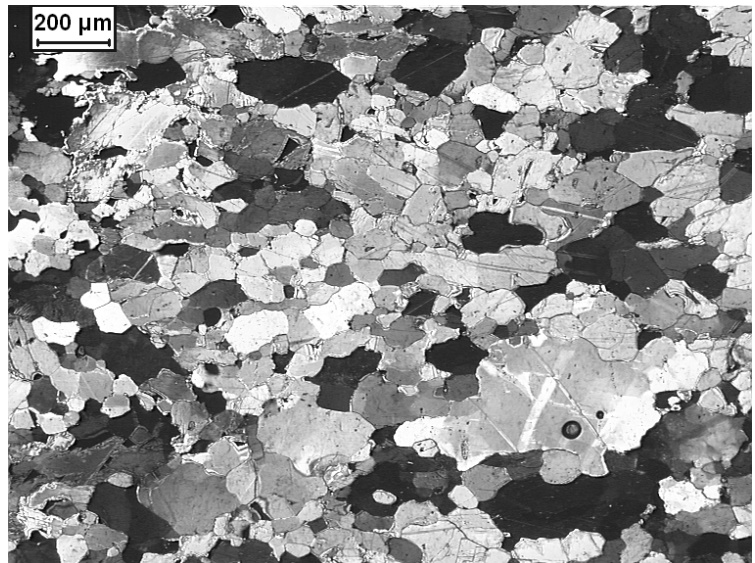


Figure 3.2d. Overview of sample 15LM950 showing extensive grain boundary migration leading recovery in grains and regular grains with gently curved grain boundaries. Compression direction vertical.



The influence of strain on the microstructure is inferred from samples 36LM830/0.15 to 36LM950 (table 3.2) deformed to strains of 0.15-0.90 in the temperature range 830-950°C at a near-constant stress of 35.6 ± 4.0 MPa. The samples deformed to a strain of ~ 0.15 show very minor grain flattening and an increase in grain size. At strains above ~ 0.15 , grain shapes become more irregular and grains become more flattened with increasing strain with the long axis perpendicular to the compression direction (fig. 3.2b). In addition, grain boundaries become more irregular and curved, and intersection of grain boundaries in triple junctions at an angle of $\sim 120^\circ$ is less common. Following the nomenclature described in *Passchier and Trouw* [1996], the grain aggregates change from inequigranular-polygonal in the starting material to seriate-interlobate after deformation to a strain of ~ 0.4 . With increasing strain, deformation bands, undulose extinction and deformation lamellae become more apparent. Thin twins with straight boundaries remain present as internal grain features, but thick twins with serrated twin boundaries tend to occur more frequently with increasing strain. All the above features are also apparent in sample 36LM900/0.90 deformed in three subsequent steps to a total strain of ~ 0.9 , but grains are more flattened. In addition, grain size is smaller and clusters of very small equi axed grains are present. Qualitatively, the microstructure of 36LM900/0.30 does not change significantly after heating for ~ 1 hr at 900°C.

In all samples deformed to a strain of ~ 0.4 (fig. 3.2b-h), grain size is reduced with respect to the starting material. Grain size reduction is most apparent in the samples deformed at high stress and low temperature (e.g. 50LM730 and 65LM700), where a core-mantle structure has developed consisting of large flattened grains with smaller grains at the grain boundaries (fig. 3.2b). Three distinctive types of microstructural features associated with grain size reduction could be identified:

- (1) Subgrains in individual grains or occasionally near twins. In addition, grains similar in size to the subgrains are present within larger grains or at grain boundaries (fig. 3.2e). These grains locally form clusters of equi axed grains with gently curved grain boundaries. Some of the grains inside larger grains have irregular shapes and grain boundaries (fig. 3.2f).
- (2) Irregular grain boundaries forming bulges. Near such boundaries, grains that are similar in size and shape as the bulges are present (fig. 3.2g).
- (3) Large relict grains that can be recognized by pervasive calcite twins running through several adjacent grains (fig. 3.2h). The relict grains are dissected by grain boundaries across larger parts of the grains or by large grains or arrays of small grains cross cutting the relict grains.

Microstructures of type (1) and (2) are found in all samples and tend to occur more frequently with increasing stress and decreasing temperature. Both types are most apparent in 65LM700 (fig. 3.2b), but are less developed in 15LM950 where grain boundaries are mostly gently curved without bulges, and internal grain structures do not show many subgrains (fig. 3.2d). Features accompanying features (1) and (2), such as deformation bands, undulose extinction and deformation lamellae occur more frequently with increasing stress and decreasing temperature and are most apparent in sample 65LM700 (fig. 3.2b). Microstructure of type (3) is most apparent in samples deformed at relatively high temperature and low stress where relict grains can be identified, such as 23LM990 and 36LM950 (fig. 3.2h). Thin twins with straight boundaries as well as thick twins with irregular boundaries are present in all samples. With increasing stress, the larger grains become more flattened with the long axis perpendicular to the compression direction and grain boundaries tend to be more irregular and aligned. At relatively low stress (~ 23 and ~ 36 MPa) and high temperature ($T=830-990^\circ\text{C}$), the microstructure does not seem to vary significantly with increasing temperature. At relatively high stress (~ 50 MPa) and low temperature ($T=700-830^\circ\text{C}$), the microstructure changes from

a core-mantle type structure to a microstructure with intensely flattened interlobate to amoeboid grains.

Figure 3.2e. Detail of the microstructure of sample 23LM990 showing progressive rotation of subgrains leading to the nucleation of new grains.

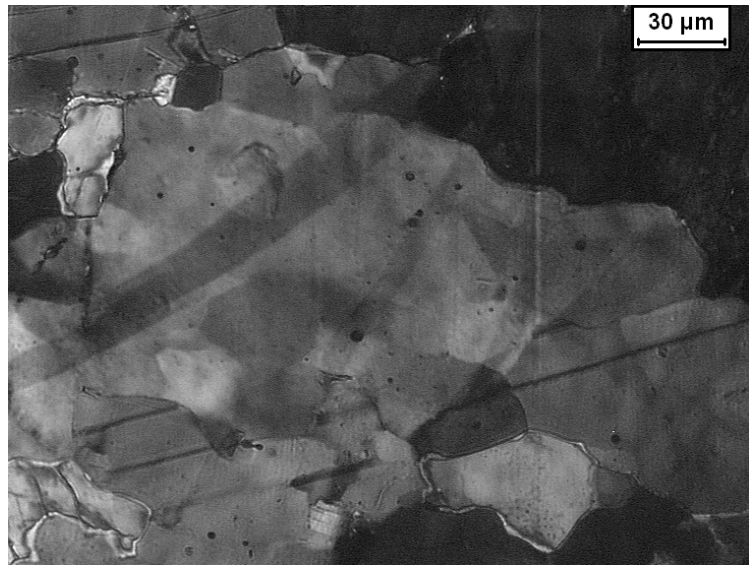


Figure 3.2f. Detail of the microstructure of sample 36LM950 showing irregular grain boundaries due to (sub)grain boundary migration in grains nucleated by subgrain rotation. Sub vertical stripes are related to sectioning or polishing.

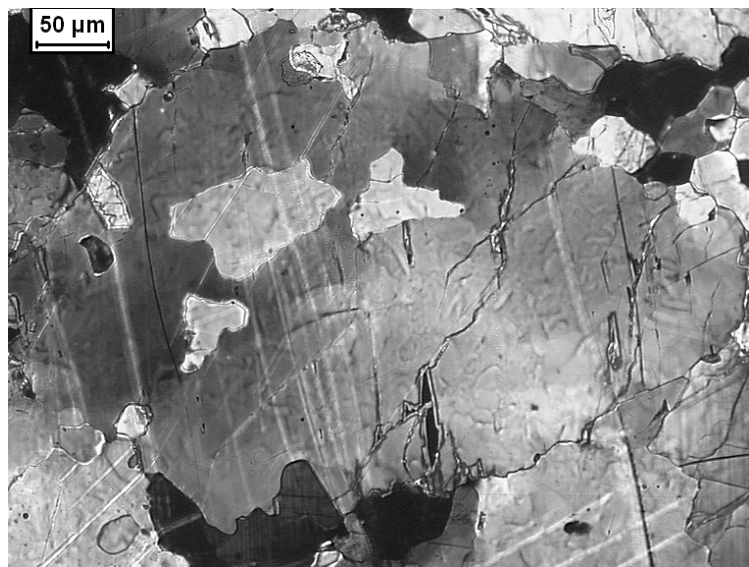


Figure 3.2g. Detail of the microstructure of sample 50LM780 showing bulge migration recrystallization with nucleation of new grains at grain boundary bulges caused by grain boundary migration.

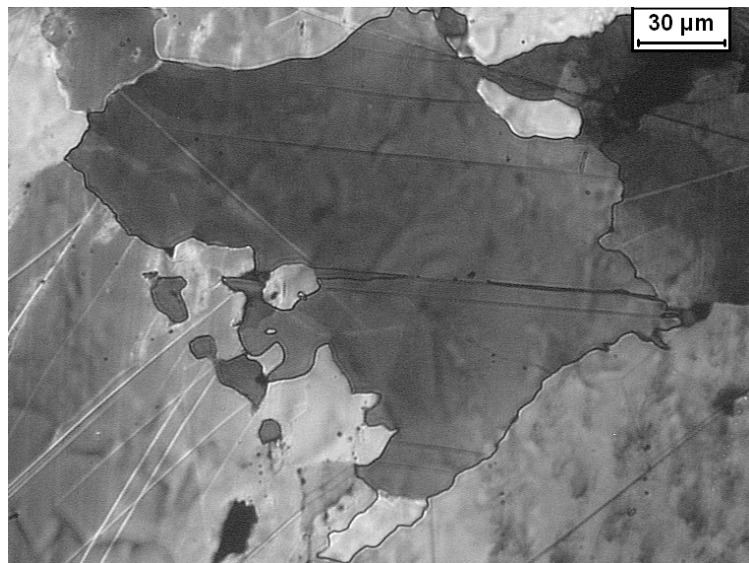
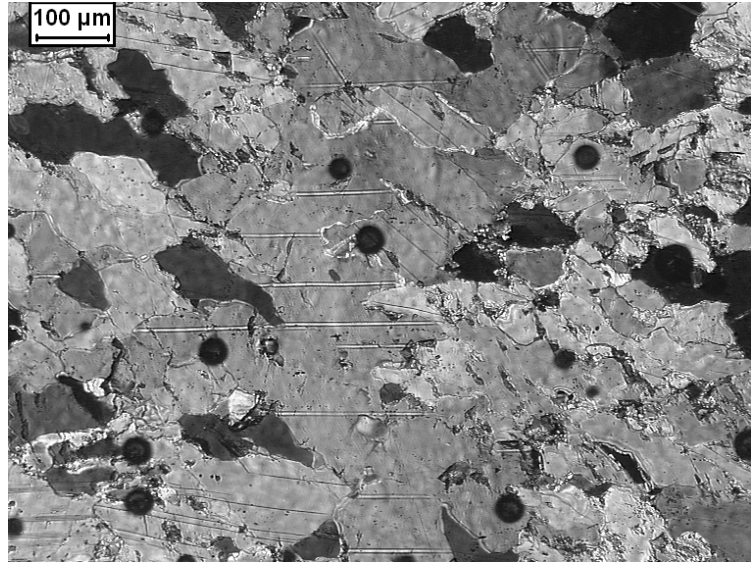


Figure 3.2h. Detail of the microstructure of sample 36LM950 showing grain size reduction by the formation of new grain boundaries dissecting large parts of a relict grain and by grain boundary migration of adjacent grains consuming a relict grain.



3.3.3 Quantitative microstructural results

All histograms with ECD frequency and area fraction distributions per individual grain size (ECD) class are depicted in fig. 3.3 and 3.4. In addition, fig. 3.5 shows delta-histograms illustrating the difference in ECD frequency and area fraction of grains for deformed samples, for the starting material heated for ~1hr at 900°C or the sample re-heated for ~1hr at 900°C after deformation. Statistical descriptors characterizing the grain size distributions are given in table 3.3. Standard deviation, skewness and kurtosis (of $\log d$) are plotted in fig. 3.6. Fig. 3.7 shows plots of the median and average grain size versus strain or temperature.

Starting material

The grain size distribution of the starting material is positively skewed, platykurtic (negative kurtosis) to bimodal with modes at 20 and 100 μm (fig. 3.3a, table 3.3). Although the starting material originates from the same block of Carrara Marble as used by *Pieri et al.* [2001a; b], the grain size distribution is different from that analysed by these authors, who found a unimodal grain size distribution with a mode at 178 μm . This may be due to natural variations in the grain size distribution of the Carrara marble [*Molli et al.*, 2000], or an artefact of the approach in grain size analysis. Note that grain sizes smaller than 30 μm were not analysed by *Pieri et al.* [2001a; b]. A bimodal distribution thus might have been overlooked, since the bimodal character of the starting material used in this study becomes apparent only at grain sizes smaller than 45 μm . The area distribution is unimodal with 90% of the area in section taken up by grains larger than 100 μm and a peak at 251 μm . The grains have an average aspect ratio of 1.30 with the long axis of the grains at an angle of $\sim 20^\circ$ with respect to the sample axis. If measured perpendicular to the sample axis, this shape preferred orientation results in an average aspect ratio of 1.16 (table 3.3). The starting material remains bimodal during heating for ~1 hr at 900°C (equivalent to the time needed to reach a stable temperature in the experiments), although the two modes have shifted to slightly higher values of 25 and 158 μm (fig. 3.3b). The delta-histogram (fig. 3.5a) shows that classes with grains of 22-282 μm increase in frequency and area fraction, while frequency or area fraction decrease in the other classes. This implies that the modification of microstructure during heating is caused by growth of grains smaller than 22 μm reducing the grain size of grains larger than 282 μm (possibly due to a higher surface energy of the small grains). The overall result is an increase

in the average and median grain size (table 3.3). The average grain aspect ratio slightly decreases during heating (table 3.3).

Table 3.3. Microstructural characteristics of all samples.

test*	median grain size [μm]	av. grain size [μm]	av. grain size log-space [μm] (log)	stand. dev. (log <i>d</i>)	min.-max. grain size [μm]	skewness (log <i>d</i>)	kurtosis (log <i>d</i>)	av. aspect ratio [§]	number of grains	min. RX area [%]
starting material	35	68	41 (1.62)	0.43	11-405	0.39	-1.02	1.16	1363	-
start 1hr at 900°C	47	78	52 (1.72)	0.40	11-385	0.11	-1.15	1.10	1155	-
15LM950	42	54	42 (1.62)	0.31	9-265	-0.06	-0.58	1.33	1797	38
23LM900	29	36	29 (1.46)	0.28	9-300	0.24	-0.21	1.31	3962	50
23LM990	32	48	35 (1.54)	0.33	8-450	0.55	0.04	1.34	1669	20
36LM830/0.15	58	85	60 (1.77)	0.38	10-502	0.02	-0.72	1.37	969	-
36LM830/0.30	52	80	52 (1.72)	0.41	10-614	0.06	-0.85	1.29	1114	9
36LM830	45	62	48 (1.68)	0.31	10-467	0.18	-0.48	1.46	2202	22
36LM900/0.15	80	100	69 (1.84)	0.41	10-479	-0.35	-0.86	1.32	805	-
36LM900/0.30	71	97	67 (1.82)	0.40	10-481	-0.29	-0.78	1.29	802	-
36LM900/0.30	35	66	43 (1.63)	0.40	11-435	0.37	-0.92	1.38	1462	-
36LM900	68	85	63 (1.80)	0.35	11-481	-0.20	-0.57	1.59	1090	15
36LM900/0.90c [¶]	22	29	24 (1.37)	0.26	6-288	0.69	0.79	1.40	2737	36
36LM950/0.15	103	118	90 (1.95)	0.35	9-372	-0.65	-0.12	1.30	565	-
36LM950/0.30	72	90	69 (1.84)	0.33	10-434	-0.22	-0.54	1.30	1127	8
36LM950	42	58	42 (1.62)	0.35	10-371	0.06	-0.58	1.51	2189	19
50LM730	27	39	30 (1.47)	0.30	6-243	0.65	0.04	1.36	1416	31
50LM780	32	42	33 (1.52)	0.30	8-306	0.14	-0.53	1.42	3094	52
50LM830	41	50	40 (1.61)	0.29	10-326	-0.01	-0.52	1.45	3588	46
65LM700	20	31	23 (1.36)	0.29	5-294	1.08	1.26	1.40	1871	30

*For convenience in comparing tests, stress (first number) and temperature (second number) are quoted in the test numbers. For samples deformed to natural strains less or more than ~0.4, the last number in the name gives the approximate natural strain. [§]Average measured grain aspect ratio perpendicular to the compression direction is quoted. [¶]Three-step experiment, sample removed from apparatus and re-polished and re-jacketed after each step (twice in total). In total a natural strain of 0.897 was reached. See text for details.

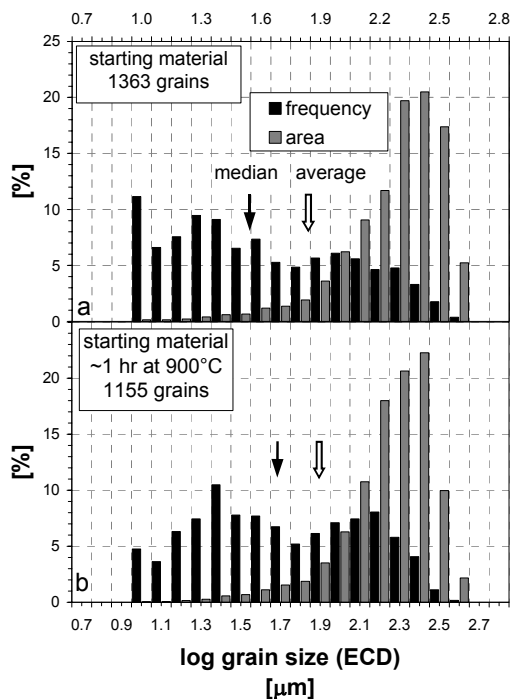


Figure 3.3. Logarithmic grain size (equivalent circular diameter-ECD) distributions showing ECD frequency (black bars) and area fraction (grey bars) of the undeformed samples. Sample number, median (closed arrow) and average (open arrow) grain size are indicated. (a) Carrara marble starting material. (b) Starting material heated for ~1 hr at 900°C. See table 3.3 and fig. 3.6 for statistical descriptors and other details on the experiments.

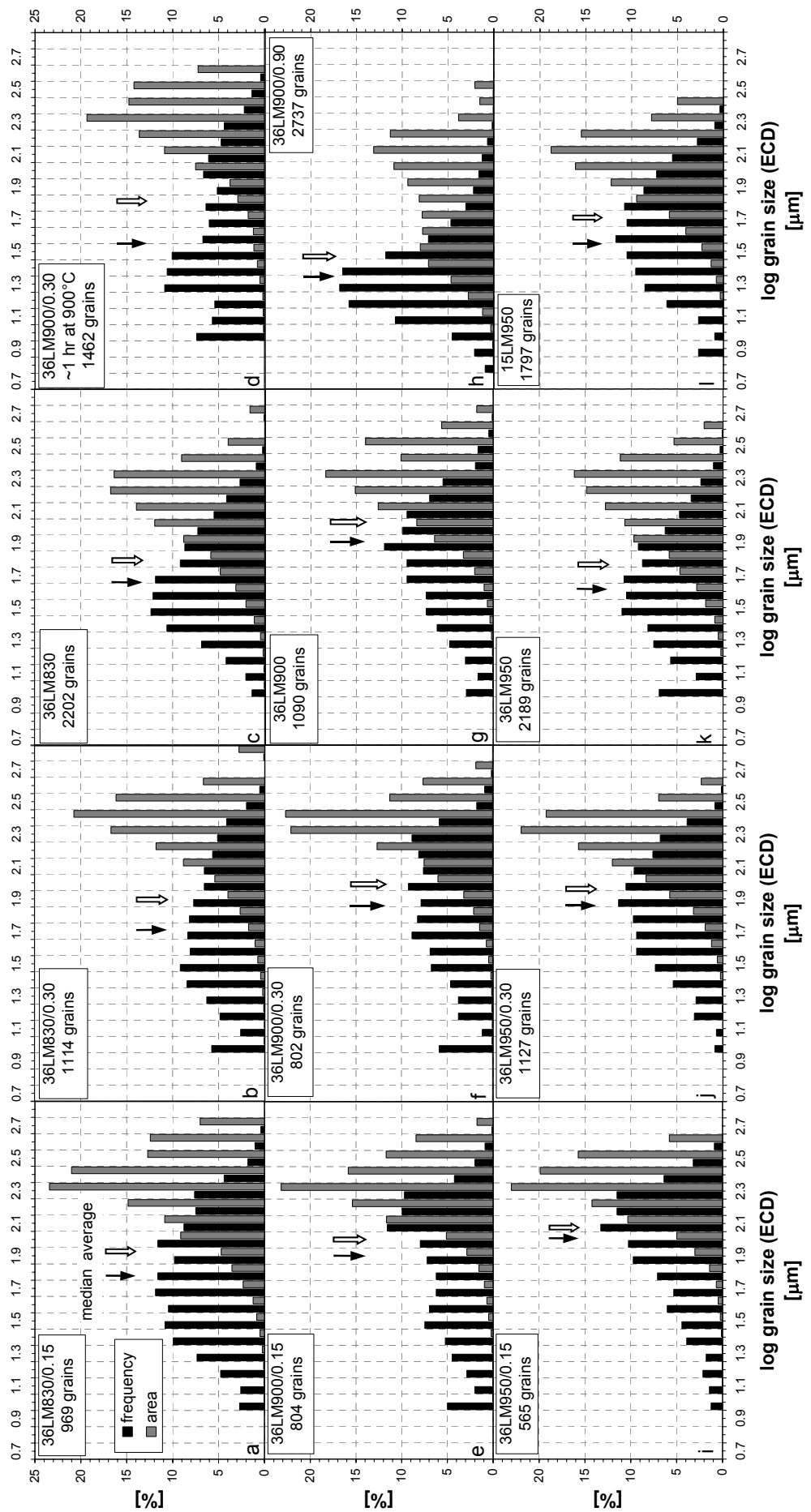


Figure 3.4 (continues on next page).

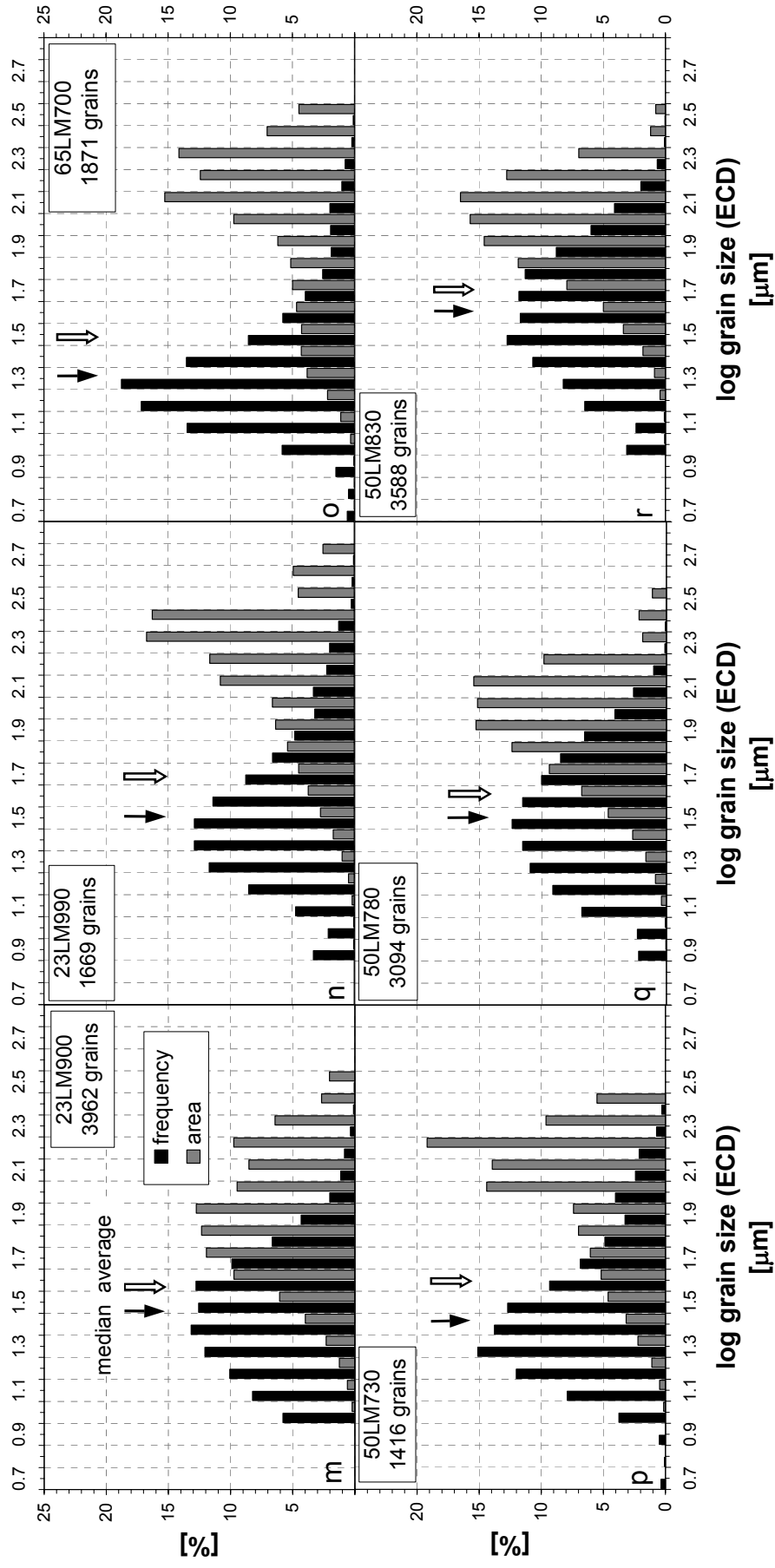


Figure 3.4 (continued). Logarithmic grain size (equivalent circular diameter-ECD) distributions showing ECD frequency (black bars) and area fraction (grey bars) of the deformed samples. Sample number, median (closed arrow) and average (open arrow) grain size are indicated. Where possible, histograms are ordered so that strain is increasing from left to right at constant stress and temperature (a-c, e-h, i-k) or temperature is increasing from left to right at constant stress and strain (m-n, p-r). See table 3.3 and fig. 3.6 for statistical descriptors and other details on the experiments.

Deformed material

Table 3.3 shows that the median grain size and average of $\log d$ are generally close for the deformed samples. In addition, the skewness and kurtosis of the logarithmic grain size distributions of all deformed samples are close to zero. As for a lognormal distribution the median and average of $\log d$ coincides and skewness and kurtosis are zero, this indicates that the grain size distributions of the deformed samples are close to lognormal. However, none of the grain size distributions are exactly lognormal and most distributions are slightly platykurtic and positively skewed at the higher strains. Some trends of mode, median, average, standard deviation and skewness with strain, stress and temperature can be identified.

The area distributions of all deformed samples are negatively skewed with a mode at 71-282 μm , always higher than the mode of the grain size distribution.

Influence of strain

The evolution of the grain size distributions with strain is investigated for strains of 0.15-0.90 at a stress of 35.6 ± 4.0 MPa and temperatures of 830-950°C (figs. 3.4a-c, 3.4e-h, 3.4i-k and table 3.3). The grain size distributions have changed significantly with respect to the starting material heated for ~ 1 hr at 900°C (fig. 3.3b), even at strains as small as 0.15. Except for the distribution of the sample deformed at $T=900^\circ\text{C}$, the distributions are unimodal. Skewness is close to zero or negative and kurtosis is negative. With increasing strain, the grain size distributions become unimodal. The skewness of the distributions increases with strain, changing from negative to positive for $T > 830^\circ\text{C}$ (fig. 3.6). The standard deviation of the grain size distribution decreases with increasing strain (table 3.3, fig. 3.6).

Sample 36LM900/0.90 is deformed to a strain of ~ 0.90 in three steps (cf. experimental method, table 3.2). We assessed the possibility that the heating periods in between the loading steps modified the microstructure by heating sample 36LM900/0.30 to 900°C for ~ 1 hr, which is equivalent to the time required to reach a stable temperature at the beginning of the experiments. The grain size distribution (fig. 3.4d) and delta-histogram of the re-heated sample compared to 36LM900/0.30 (fig. 3.5b) show that heating resulted in a grain size distribution that is bimodal with more grains in the classes below 35 μm than the distribution before heating. Moreover, the flow stress after reloading agrees well with the flow stress at the end of the previous step (fig. 3.1). Hence, heating between subsequent steps does not result in complete annealing of the microstructure nor does it significantly affect the mechanical behavior. The growth of very small grains at best results in a slight overestimation of the number of grains in the classes below 35 μm in the distribution of 36LM900/0.90 (fig. 3.4h).

The evolution of the grain size distribution with strain at a stress of 35.6 ± 4.0 MPa and temperatures 830-950°C is illustrated by the delta-histograms shown in figs. 3.5d-h for samples deformed at 900°C. The delta-histogram in fig. 3.5d shows that for sample 36LM900/0.15 the frequency of grains smaller than 28 μm decreases substantially, while the frequency of grains with sizes above 56 μm increases compared to the starting material heated for ~ 1 hr at 900°C. This indicates that during deformation to a strain of ~ 0.15 , the grain size distribution predominantly changes by the growth of small grains, which causes removal of grains from the smaller grain size classes and an increase of grains in the larger classes. This results in an increase in median and average grain size at a strain of ~ 0.15 with respect to the heated starting material for all investigated temperatures (fig. 3.7a).

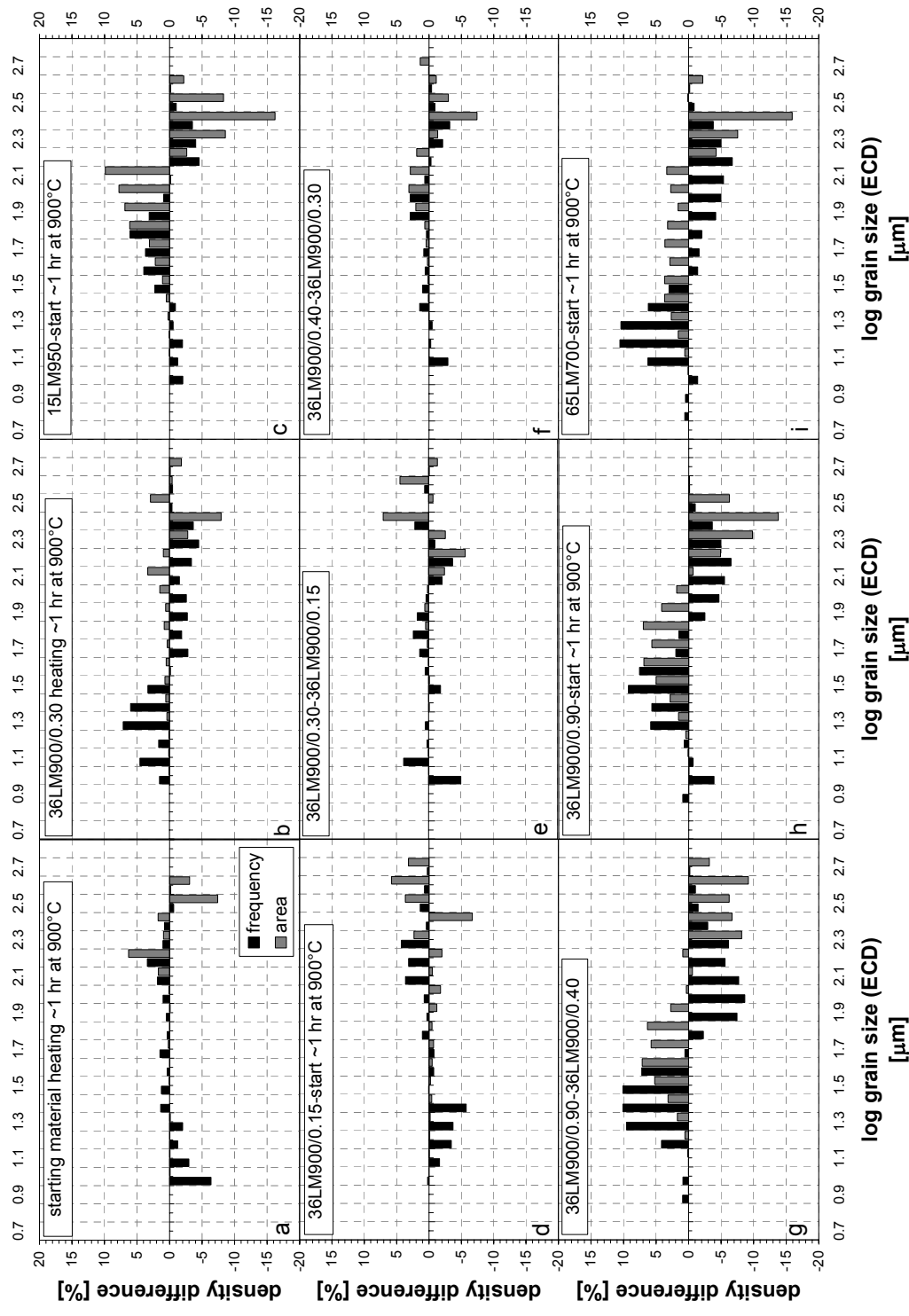


Figure 3.5. Delta-histograms showing differences in ECD frequency (black bars) and area fraction (grey bars) calculated from the logarithmic grain size distributions of fig. 3.3 and 3.4 (corrected for out-of-plain strain where necessary). The delta-histograms show changes in ECD frequency and area fraction due (a) to heating of the starting material, (b) reheating of 36LM900/0.30, (d-h) progressive deformation and (c-i) deformation at different conditions.

The delta-histograms (figs. 3.5e-g) show that as strain increases from ~ 0.15 to 0.90 at 900°C , the frequency of grains in the classes with the smallest grain sizes (below $14\ \mu\text{m}$) remains approximately constant, while the frequency of grains in the classes with the largest grains decreases and the frequency of grains in between the smallest and largest size increases. The smallest grain size class, in which the frequency of grains decreases, becomes smaller (from $112\ \mu\text{m}$ to $56\ \mu\text{m}$) with increasing strain. This indicates that with ongoing deformation, the grain size distribution predominantly changes by the progressive reduction of the larger grains in the distribution, which causes removal of grains from the larger grain size classes and an increase of grains in smaller classes. However, the frequency of the classes with the smallest grains of the distributions remains approximately constant with strain, indicating that grains are removed from these classes by grain growth during deformation compensating the grains added to these classes by nucleation of new grains (cf. fig. 3.2g). Most of the change in frequency that has occurred after a strain of ~ 0.90 (fig. 3.5h) takes place in the strain interval 0.40 - 0.90 (fig. 3.5g). Microstructural alteration during deformation results in an overall decrease of the median and average grain size with strain for all investigated temperatures. The minimum recrystallized area increases with increasing strain for $T=830$ - 950°C (table 3.3). Average grain aspect ratios increase with strain (table 3.3), which is in agreement with the qualitative observation that grains progressively flatten, with their long axis at an angle of more than 45° to the compression direction.

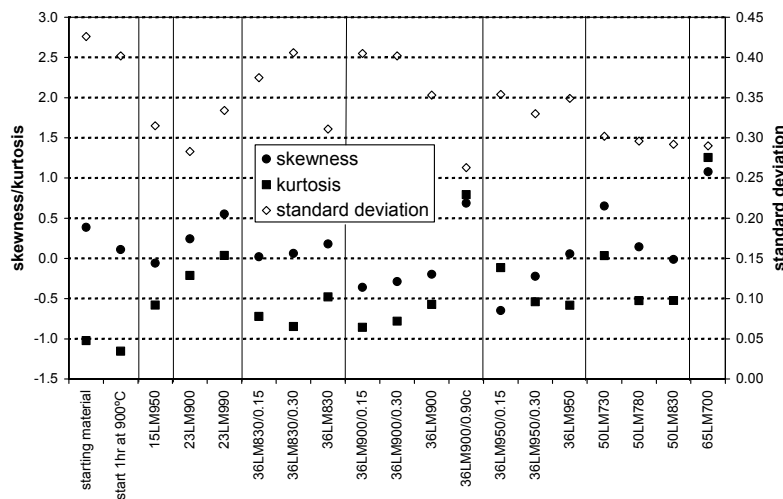


Figure 3.6. Plot of the measured statistical descriptors, i.e. standard deviation, skewness and kurtosis (of $\log d$) for undeformed and deformed samples of Carrara marble. For an ideal lognormal distribution, skewness and kurtosis are zero.

Influence of temperature and stress

The influence of temperature and stress on the grain size distributions of samples deformed to a strain of ~ 0.4 at stresses of 15 - $65\ \text{MPa}$ and temperatures of 730 - 990°C , selecting samples deformed at approximately similar stress and different temperatures or approximately similar temperatures and different stresses (figs. 3.4c, 3.4g, 3.4k, 3.4l, 3.4m-r, table 3.2). There are no trends of standard deviation, skewness or kurtosis with changing temperature or stress that are consistent for all investigated conditions (fig. 3.6).

Median and average grain size increase with increasing temperature at all stresses, except at a stress of $\sim 36\ \text{MPa}$. At this stress, the median and average grain size increase with increasing temperature for $T=830$ - 900°C and then decrease for $T=900$ - 950°C . There is no clear correlation between median and average grain size and stress. It is recalled that the median and average grain size are determined from partially recrystallized grain size distributions, as shown by the labels in fig. 3.7b, indicating the minimum estimated recrystallized area in the samples. The median and average grain size and the minimum estimated recrystallized area do not show a clear correlation.

Delta-histograms (fig. 3.5c, 3.5i) show that the ECD frequency and area fraction of the classes with the largest grains decrease, while the classes with the smallest grains remain approximately constant and the classes in between increase in frequency and area fraction. As mentioned before, this indicates that the distributions have changed with respect to the heated starting material by grain size reduction of the larger grains and grain growth of the smallest grains in the distribution.

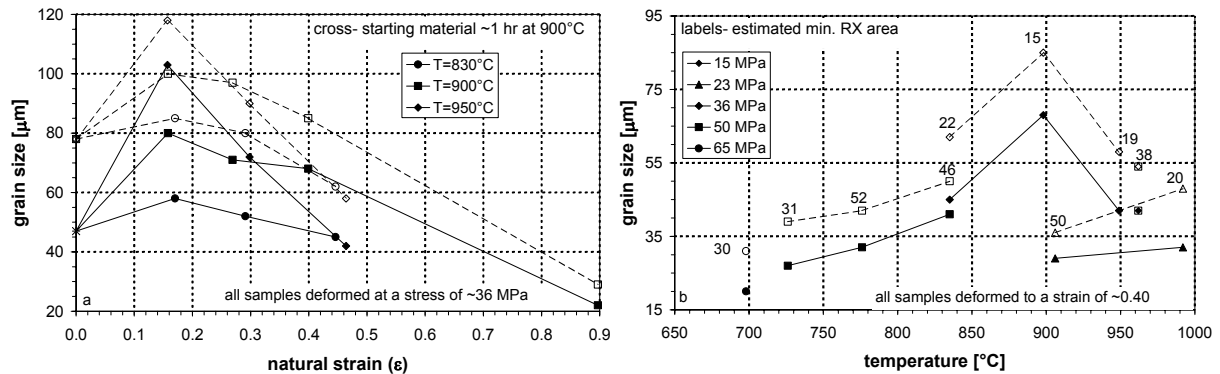


Figure 3.7. Changes of median (open symbols) and average (closed symbols) grain size (a) with strain for $T=830-950^{\circ}\text{C}$ and (b) with temperature at a stress of 15-65 MPa.

3.4 Discussion

3.4.1 Deformation mechanisms

Microstructural observations show widespread evidence for crystal plastic deformation in all deformed samples, such as deformation bands, grain flattening, undulose extinction, subgrains and deformation lamellae in the larger grains (fig. 3.2). In addition, in samples deformed to a strain of ~ 0.4 , equi axed grains as small as $\sim 10\ \mu\text{m}$ are present that do not show evidence for intracrystalline plasticity. This may indicate that grain size sensitive deformation mechanisms also played a role in deformation of the aggregates. According to *Walker et al.* [1990], grains of $\sim 10\ \mu\text{m}$ size can be expected to deform by grain size sensitive mechanisms under the conditions investigated in this study. With increasing strain, a larger contribution of grain size sensitive flow may be expected as more small grains are formed. The microstructures of samples deformed to a strain of ~ 0.15 do not show widespread evidence for the nucleation of small grains and grain growth dominates up to this strain. All stress peaks occur at a strain below ~ 0.20 , mostly around a strain of ~ 0.15 . It is therefore inferred that deformation at the stress peaks is dominated by dislocation creep mechanisms.

In fig. 3.8, peak stresses are plotted against strain rate for different temperatures. The data show high strain rate sensitivity of the peak stress, which is in general agreement with previous studies on the mechanical behavior of marble at high temperature [*Rutter, 1974; Schmid et al., 1980; Covey-Crump, 1998; Pieri et al., 2001a*]. The peak stress data was obtained for a limited range of conditions, which hampers making definite conclusions regarding the rate controlling mechanism during dislocation creep on the basis of the mechanical data. Microstructural evidence that allows such conclusions to be made is lacking as well. However, a high strain rate sensitivity of stress as observed in this study and a changing strain rate sensitivity changes with temperature and/or stress as observed in other studies on Carrara marble [*Rutter, 1974; Schmid et al., 1980; Pieri et al., 2001a*] indicate that the mechanical behavior cannot be accurately described by a single power law creep equation of the type derived for (climb-controlled) dislocation creep [see *Renner and Evans, 2002*].

Rather, it has been suggested that deformation of marble under conditions investigated in this study is controlled by cross slip of dislocations [De Bresser and Spiers, 1990]. We therefore infer that dislocation creep is controlled by cross slip of dislocations in the samples of Carrara marble deformed in this study and that the peak stress data can be best described by a rate equation for cross slip controlled dislocation creep.

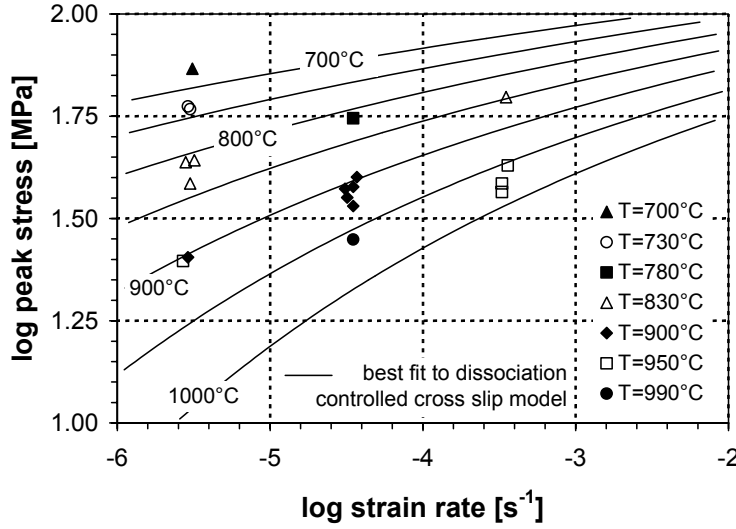


Figure 3.8. Plot of log peak stress versus log strain rate for all experiments. Isotherms for a best fit of the data to a theoretical model for flow by dissociation controlled cross slip of dislocations [De Bresser, 1996] are indicated.

Cross slip is a mechanism capable of dislocation recovery (as is dislocation climb), hence prevents continuous work hardening [Poirier, 1976; De Bresser, 1991]. Models for dislocation cross slip all start from dissociated dislocations forming stacking faults. A detailed evaluation of the current data against these models is beyond the scope of this paper, and is subject of a separate study including additional experiments on Carrara marble [see De Bresser, 1996, abstract- manuscript submitted to *Journal of Geophysical Research* in 2002]. We confine ourselves here to fitting our mechanical data to the dissociation controlled cross slip model of Escaig [1968], in which creep rate ($\dot{\epsilon}_{cs}$) is related to flow stress (σ) by

$$\dot{\epsilon}_{cs} = K \left(\frac{\sigma}{\mu} \right)^2 \exp \left[- \frac{\Delta U_{cs} \left(1 - \frac{\alpha b \sigma}{\gamma} \right)}{kT} \right] \quad (3.1)$$

where γ is the stacking fault energy (in J/m²), α is a geometrical constant, b is the Burgers vector (taken as $b=6.37 \times 10^{-10}$ m), k is the gas constant ($k=1.381 \times 10^{-23}$ J/K) and K is a dimensionless rate constant. ΔU_{cs} represents the activation energy at zero applied stress (in J) described by

$$\Delta U_{cs} = \left(\frac{\mu b^3}{1859(\gamma / \mu b)} \right) \left(\ln \left[\frac{2\sqrt{3}}{16\pi(\gamma / \mu b)} \right] \right)^{0.5} \quad (3.2)$$

where μ is the shear modulus. Best fit of (3.1) to the peak stress data yields $\text{LOG}(K)=8.98 \pm 1.19$, $\gamma=0.17 \pm 0.02$ J/m² and $\alpha=1.41 \pm 0.15$ (we used $\delta\mu/\delta T=-9.7$ and $\mu=34180$ Pa at 0 K and 300 MPa). Isotherms for cross slip controlled dislocation creep have been included in fig. 3.8 using (3.1)-(3.2) with best fit values for K , γ and α .

3.4.2 Evolution of flow stress with strain

The microstructure of Carrara marble evolves with strain and appears to be associated with a change in flow stress. Under the investigated conditions, weakening following the peak in flow stress may be explained as:

- (1) Geometric weakening, due the development of a lattice-preferred orientation (LPO), in particular with progressive alignment of easy slip directions.
- (2) Weakening due to the recovery of dislocations by grain boundary migration consuming grains with high dislocation densities, which leads to a reduction in dislocation density faster than recovery by dislocation climb or cross slip.
- (3) Weakening due to an increase of the importance of grain size sensitive flow mechanisms as a result of the nucleation of small grains by dynamic recrystallization

Texture weakening by alignment of easy slip systems parallel to the shear direction has been proposed as an explanation for the limited rheological weakening (~10%) observed in high strain torsion tests [Pieri *et al.* 2001a]. However, this cannot explain the rheological weakening observed in experiments deformed in axial compression, because the easy slip systems tend to rotate to an orientation perpendicular to the compression direction, effectively making it progressively harder to continue glide of dislocations along the slip planes.

Weakening due to recovery of dislocations by grain boundary migration is put forward by Rutter [1998] to explain the weakening observed in axial compression or extension test on Carrara marble. Although grain boundary migration is widespread in the samples, grain boundary migration is less active at temperatures below ~730°C and sample scale recovery by the consumption of large grains with high dislocation densities is not observed at these temperatures. However, strain weakening is of a similar magnitude at $T=700-730^{\circ}\text{C}$ (experiments 50LM730, 65LM700), which indicates that the weakening cannot be controlled by grain boundary migration.

We will now evaluate the possibility that the observed strain weakening after a strain of ~0.15 may be the result of an increase in the contribution of grain size sensitive deformation mechanisms to the overall creep rate due to the nucleation of small grains by dynamic recrystallization. Comparison of the stress-strain curves with microstructural observations reveals that there is a direct correlation between the onset of strain weakening and nucleation of small grains by dynamic recrystallization after a strain of ~0.15. Up to the peak in stress, grains predominantly grow and flatten without significant nucleation of new grains. In order to quantify the contribution of grain size sensitive flow of grains in the distribution to the overall rheological behavior of Carrara marble, a combined grain size sensitive-grain size insensitive flow law is required. In addition, this flow law needs to be able to account for variations in the grain size distribution (cf. chapter 2). For grain size insensitive flow in Carrara marble, the flow law for dissociation controlled cross slip, given in (3.1)-(3.2), is used. Studies of grain size sensitive deformation in calcite aggregates [Schmid *et al.*, 1977; Walker *et al.*, 1990] indicate that the creep rate for grain size sensitive flow ($\dot{\epsilon}_{gss}$) can be related to flow stress (σ) by

$$\dot{\epsilon}_{gss} = A\sigma^n d^m \exp\left[-\frac{H}{RT}\right] \quad (3.3)$$

where H is the apparent activation enthalpy for grain size sensitive flow (in kJ/mol), R is the gas constant (in kJ/mol), d is grain size (in μm), A is a rate constant (in $\text{MPa}^{-n} \mu\text{m}^{-m} \text{s}^{-1}$, for σ in MPa) and m , n are the empirically-derived grain size and stress exponent,

respectively. Both studies suggest that grain size sensitive flow of calcite rocks occurs by grain boundary sliding accommodated by a combination of dislocation and diffusional processes. The most extensive study is the one performed by *Walker et al.* [1990] on synthetic hot pressed calcite aggregates. They found that $A=10^{4.93}\text{MPa}^{-n}\mu\text{m}^{-m}\text{s}^{-1}$, $H=190\text{ kJ/mol}$, $m=-1.87$ and $n=1.67$.

In our analysis, we adopt the following assumptions. (i) In an individual grain size class, grain size insensitive creep is dominated by dissociation controlled cross slip with a creep rate ($\dot{\epsilon}_{cs}$), described by (3.1)-(3.2), and grain size sensitive creep is dominated by grain boundary sliding with a creep rate ($\dot{\epsilon}_{gss}$) described by (3.3). (ii) Both mechanisms contribute independently to the total creep rate ($\dot{\epsilon}_i$) of grains in an individual grain size class (i), given by $\dot{\epsilon}_i = \dot{\epsilon}_{cs} + \dot{\epsilon}_{gss}$. (iii) The grain size distribution at the peak stress (at $\epsilon=0.1-0.2$) is similar to the distribution analysed at a strain of ~ 0.15 . (iv) Either stress is uniform in the sample with the bulk flow stress (σ) equal to local stresses of grains (σ_i) in individual grain size classes ($\sigma = \sigma_1 = \sigma_2 = \dots = \sigma_i$), or strain rate is uniform with the bulk strain rate ($\dot{\epsilon}$) equal to local strain rates of grains in individual grain size classes ($\dot{\epsilon} = \dot{\epsilon}_1 = \dot{\epsilon}_2 = \dots = \dot{\epsilon}_i$). The uniform stress and uniform strain rate assumptions give upper and lower bounds for the rate of deformation in polycrystalline aggregates [*Freeman and Ferguson, 1986; Wang, 1994*]. If stress is uniform, the bulk strain rate for Carrara marble with a grain size distribution consisting of j classes can be written as the volume average of the strain rate of grains in individual classes with a volume fraction v_i [*Raj and Ghosh, 1981; Freeman and Ferguson, 1986*]

$$\dot{\epsilon} = \dot{\epsilon}_1 v_1 + \dot{\epsilon}_2 v_2 + \dots + \dot{\epsilon}_j v_j = \sum_{i=1}^{i=j} \dot{\epsilon}_i v_i \quad (3.4)$$

or, if strain rate is uniform, the bulk stress can be written as

$$\sigma = \sigma_1 v_1 + \sigma_2 v_2 + \dots + \sigma_j v_j = \sum_{i=1}^{i=j} \sigma_i v_i \quad (3.5)$$

with $v_1 + v_2 + \dots + v_j = \sum_{i=1}^j v_i = 1$. Volume fractions of individual grain size classes were calculated using the StripStar computer program [*Heilbronner and Bruhn, 1998*]. The program uses the so called Schwartz-Saltykov method to calculate volume fractions of individual classes of a three-dimensional grain size distribution from frequencies of grain size distributions based on two-dimensional grain sections, assuming grains are spherical [*Underwood, 1968*]. Bulk flow stresses can be determined directly from (3.5) using (3.1)-(3.3) and the imposed strain rate in the experiments or flow stress can be chosen in (3.1)-(3.3) so that the bulk strain rate from (3.4) equals the imposed strain rate in the experiments. In this way, changes in bulk flow stress can be calculated from changes in grain size distribution for both uniform stress and uniform strain rate assumption. Reliable calculations of strain weakening due to changes in grain size distribution could be made at 830°C , using samples 36LM830/0.15 and 36LM830, and at 900°C , using samples 36LM900/0.15 and 36LM900/0.90. The results are presented in fig. 3.9. Taking into account all uncertainties, notably regarding the applicability of the grain size sensitive flow law to Carrara marble, as well as experimental reproducibility and sample variability, the calculated strain weakening is close to the observed weakening for both uniform stress and strain rate. At this stage, this should not be regarded as undisputable evidence that the strain weakening observed in our experiments is due to an increased contribution of grain size sensitive flow as a result of

changes in grain size distribution. It is merely meant to illustrate that changes in grain size distribution can explain the observed weakening and should be considered as a serious alternative for other weakening mechanisms like the alignment of easy slip systems [Pieri *et al.*, 2001a] or recovery by grain boundary migration [Rutter, 1998].

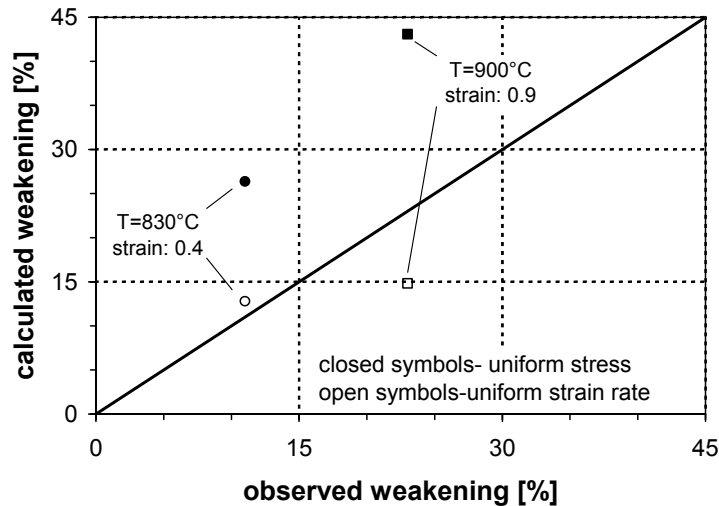


Figure 3.9. Strain weakening of the flow stress relative to the peak stress, calculated using changes in grain size distribution and associated increase of the importance of grain size sensitive flow with increasing strain, plotted against the strain weakening observed in experiments at 830 and 900°C. Calculated strain weakening, assuming uniform stress or strain rate (giving upper and lower bounds), and the observed weakening are in reasonably good agreement for these experiments as the points fall near the line where calculated and observed weakening are similar.

3.4.3 Evolution of dynamically recrystallizing microstructure

The systematic investigation of the effect of deformation of Carrara marble on the microstructure at different strains, temperatures and stresses carried out in this study, provides a picture of the microstructural evolution during transient deformation in the approach to steady state. We make three important inferences based on the microstructural observations, regarding (1) the effect of heating of the starting material prior to deformation, (2) processes altering the microstructure during deformation and (3) the evolution of (recrystallized) grain size as a function of strain.

First, heating of the starting material for ~1 hr at 900°C (roughly equivalent to the time needed to reach a stable temperature before actually starting to load the sample in the experiments) resulted in an increase of the average and median grain size due to minor growth of small grains at the expense of larger grains in the grain size distribution. Because the grain size distributions of the deformed samples are compared to the heated starting material rather than to that of the original block, observed changes in distributions are truly syn-deformational.

Second, grain size distributions are continuously changing during deformation by a combination of growth of the smallest grains and refinement of the larger grains in the distribution. Grain growth predominantly occurs by migration of boundaries of small relatively strain free grains into larger grains. Based on the three distinctive types of microstructural features identified in the results, we infer that grain size reduction occurred by (1) the formation of new grains by progressive subgrain rotation (fig. 3.2e), (2) nucleation of grains behind grain boundary bulges (fig. 3.2g) and (3) dissection of grains by formation of new grain boundaries across larger parts of old grains or by cross cutting of (migrated) new grains (fig. 3.2h). Grain growth and grain size reduction are competing processes during dynamic recrystallization. The relative importance of both processes is dependent on the deformation conditions as evidenced by comparing the samples deformed to strains of ~0.40.

At relatively low temperatures (below $\sim 730^\circ\text{C}$, in samples 50LM730 and 65LM700), core-mantle microstructures (fig. 3.2b) develop and grain size distributions are positively skewed and leptokurtic (figs. 3.4o-p). At relatively high temperatures microstructures with interlocking (e.g. sample 36LM950, fig. 3.2c) or even polygonal shaped grains (e.g. sample 15LM950, fig. 3.2d) develop and grain size distributions are closer to lognormal (fig. 3.4c, 3.4g, 3.4k, 3.4m-n, 3.4q-r, 3.6). This indicates that at high temperatures, relatively rapid grain boundary migration prevents the development of core-mantle structures by rapid growth of nucleated grains (mantle), consuming larger older grains with higher dislocation density (core). From this it is concluded that the relative kinetics of grain growth by grain boundary migration and grain refinement during dynamic recrystallization determines the characteristics of the grain size distribution.

Third, the delta-histograms show that with ongoing deformation, the grain size class with positive frequencies progressively lowers (compare fig. 3.5e-g). Thus not only the complete (old + new grains) grain size distribution is evolving to high strain, but also the recrystallized grain size distribution did not reach steady state. It follows that recrystallized–stress (piezometric) relations based on low strain (~ 0.15) microstructures need to be regarded as characteristic of transient deformation, and hence are not generally applicable. At best the recrystallized grain size obtained from the delta-histograms gives an upper limit of the recrystallized grain size at steady state. In addition, analysis of nucleated small (subgrain size) grains will give a lower limit, as recrystallized grains grow by grain boundary migration after nucleation. These grains will be the smallest in the grain size distribution that develops during steady state as a result of a competition between grain growth and grain size reduction. It is emphasized that individual grains can undergo several cycles of nucleation and growth before a steady state microstructure has developed. It also means that it will be problematic to calibrate separate piezometric relations for rotation and migration recrystallization [cf. *Rutter*, 1995] as grains nucleated from subgrains will continuously grow by grain boundary migration and grains are continuously refined by a combination of subgrain rotation and nucleation behind bulges resulting from grain boundary migration.

3.4.4 Comparison with high strain torsion experiments

Recently, the same type of Carrara marble ('Lorano Bianco' type) has been deformed by *Pieri et al.* [2001a; b] to high shear strains in torsion at conditions that fall in the range of conditions investigated in this study. They claim that at a shear strain of 1 (equivalent to a natural strain of ~ 0.5), recrystallized grains make up only $\sim 5\%$ of the area (in 2-D section) of the sample. The delta-histograms presented in this study show that already at a strain of ~ 0.4 , a higher percentage of the area (15-52%) of the sample has recrystallized at all conditions (table 3.3, fig. 3.5c, 3.5i). *Pieri et al.* [2001a] determined the recrystallized area fraction on the basis of the area fraction made up by new nucleated grains with a size approximately similar to the final recrystallized grain size at high strains (shear strain of ~ 11). Their estimate should be regarded as a minimum because grains are not always reduced to this size and grains may grow after nucleation during dynamic recrystallization. In this study, we determine the recrystallized area fraction from the delta-histograms, indicating alteration of the area distribution with respect to the starting material. The delta-histograms (fig. 3.5d-h) of this study and the grain size distributions analysed by *Pieri et al.* [2001a] show that the grain size distributions continue to change up to very high strains (unattainable in axial compression) and that grain size is progressively reduced. As mentioned before, this means that the microstructural observations in this study are indicative of transient deformation. However, the results can be used to investigate the microphysical processes altering the microstructure during dynamic recrystallization and their effect on grain size distribution. In

addition, inferences on the development of a steady state microstructure can be made as it is likely that the processes active during transient deformation operate during steady state deformation as well.

The amount of weakening observed in the experiments conducted in this study (9-41%) is comparable or higher than the weakening observed by *Pieri et al.* [2001a] in their torsion tests and of similar magnitude as observed by *Rutter* [1995, 1998]. It should be noted that part of the observed weakening in the samples deformed to strains larger than ~ 0.3 may be an artefact of the data processing as deformation in the samples becomes increasingly heterogeneous with increasing strain. *Pieri et al.* [2001a] claim that mechanical steady state is only reached at high strain ($\gamma > 5$, equivalent to a natural strain of ~ 1.6), which is clearly not reached in this study. The weakening observed in the axial compression tests in this study cannot be explained by the progressive alignment of easy slip directions. This means that either the weakening in both studies is not caused by the progressive alignment of easy slip directions or that the weakening in both studies occurs by different mechanisms due to differences in the deformation geometry. However, a mechanism different from alignment of easy slip directions is more likely as it is unclear to us how deformation geometry can affect the weakening mechanism.

3.4.5 Geodynamical implications

The recent high strain torsion tests on anhydrite [*Stretton and Olgaard, 1997*], calcite [*Casey et al., 1998; Pieri et al., 2001a*] and olivine rocks [*Bystricky et al., 2000*] indicate that steady state deformation may be reached only at high strains [*Paterson and Olgaard, 2000*], e.g. shear strains of more than 10 for microstructural steady state in Carrara marble [*Pieri et al., 2001a; b*]. This implies that transient rheological behavior associated with evolving microstructure is important in nature. In practice, it will be difficult to recognize steady state from microstructures of natural rocks, as the results obtained in this study indicate that grain size continuously decreases with ongoing deformation. However, the present study shows that it is possible to calculate the evolution of flow stress during transient deformation from the evolution of grain size distribution, provided that the individual grain size sensitive and grain size insensitive rate equations are well constrained for the material under consideration. If further research supports these findings, the method will provide better constraints for both transient and steady state deformation of natural rocks because changes in grain size distribution due to dynamic recrystallization are accounted for. In addition, a model describing the evolution of the grain size distribution during dynamic recrystallization would offer a way of tracking rheological behavior in nature during deformation from transient to steady state.

In the approach to steady state, grain size distributions of experimentally deformed Carrara marble evolve by a combination of grain size reduction and grain growth acting as competing processes. Both processes need to balance in order to develop a steady state microstructure. This implies that the grain size distribution at steady state depends on the relative kinetics of grain growth and grain size reduction, determined by the deformation conditions. Hence, the steady state grain size distribution can be expected to be a characteristic of true steady state with distribution parameters that are uniquely related to stress and temperature. Our data suggest that the grain size distributions are close to lognormal, although some deviations from an ideal lognormal distribution are present. Considering that the deviations are not systematically with stress or temperature, we infer that in general the distributions may be best described by a lognormal grain size distribution. This is in agreement with models that predict the development of a steady state grain size distribution during dynamic recrystallization based on a competition between nucleation and

growth [Shimizu, 1999]. If the distributions at steady state are approximately lognormal, they can be uniquely described by the median and standard deviation [Aitchison and Brown, 1957], which can then be regarded as microstructural state variables. The development of a unique steady state grain size distribution during dynamic recrystallization by a competition between grain size reduction of large grains, deforming by grain size insensitive (GSI) mechanisms, and growth of small grains, deforming by grain size sensitive (GSS) mechanisms, is consistent with the boundary hypothesis model, proposed by De Bresser *et al.* [1998; 2001].

On the basis of the results presented in this paper, some inferences can be made on the causes for rheological weakening and strain localization in Carrara marble. The results indicate that extensive rheological weakening by a complete switch in deformation mechanism due to grain size reduction associated with dynamic recrystallization is not possible, because at steady state deformation will occur by a combination of GSS and GSI creep mechanisms. Instead, dynamic recrystallization alters the grain size distribution, causing limited weakening due to an increase in the relative contribution of GSS creep mechanisms. It is therefore concluded that in single phase materials, such as Carrara marble, the degree of weakening caused by dynamical recrystallization is probably insufficient to produce significant strain localization [Braun *et al.*, 1999; Rutter, 1999]. This means that in order to explain the strain localization, often observed in natural marble rocks, other weakening mechanisms should be considered [White *et al.*, 1980], such as brittle processes [Bos and Spiers, 2001], or grain growth should be inhibited by the presence of second phases [Olgaard, 1990].

3.5 Summary and conclusions

Cylindrical samples of Carrara marble have been deformed to natural strains of 0.15-0.90 in axial compression at temperatures in the range of 700-990°C, stresses of 15-65 MPa, strain rates of 3.0×10^{-6} - $4.9 \times 10^{-4} \text{ s}^{-1}$ and a confining pressure of 150 or 300 MPa. The aim of the experiments was to investigate the evolution of grain size distribution and rheological behavior as a result of dynamic recrystallization during transient deformation in the approach to steady state. We conclude the following:

1. Under the deformation conditions investigated, Carrara marble shows ductile flow behavior with high strain rate sensitivity of flow stress, if compared at fixed strains. The observed mechanical behavior is in agreement with the results of previous axial compression experiments on Carrara marble for which cross slip controlled dislocation creep was inferred to be the dominant deformation mechanism. Microstructural evidence for dislocation creep and dynamic recrystallization by grain boundary migration and progressive subgrain rotation was found.
2. In general, individual stress-strain curves show a peak stress followed by continuous weakening to natural strains of at least 0.4 at all investigated conditions and up to ~0.9 at 900°C, without reaching true steady state.
3. Measurements of grain sizes on traced micrographs show an evolution of the grain size distribution from bimodal at the start to a positively skewed or roughly lognormal distribution with increasing strain. At strains above ~0.15, the median and average grain size decreases with increasing strain. The recrystallized area, as seen in 2-D sections, ranged from a minimum of 8 to 52%, depending on deformation conditions. The grain size distributions evolved during dynamic recrystallization by a competition of grain

growth due to grain boundary migration and grain size reduction due to progressive subgrain rotation, dissection of grains by new grains or grain boundaries or nucleation of new grains behind grain boundary bulges caused by grain boundary migration.

4. Geometric (“texture”) weakening resulting from alignment of easy slip systems, which has been proposed to occur in torsion tests on Carrara marble, cannot explain the weakening as observed in the current experiments because of the different (axial symmetric) deformation geometry. Moreover, since rates of grain boundary migration were slow in some of the experiments showing strain weakening, it is unlikely that the observed weakening is due to selected removal of dislocations by grain boundary migration.
5. We infer that peak stress and subsequent weakening behavior observed in torsion and compression experiments is probably due to a change in relative importance of diffusion creep with respect to dislocation creep as the number of small grains in the distribution increases with strain. This is quantitatively supported by calculations of weakening resulting from changes in grain size distributions based on a composite flow law, combining grain boundary sliding accommodated by both diffusional and dislocation processes and cross slip controlled dislocation creep. This type of behavior is consistent with the boundary hypothesis model proposed by *De Bresser et al.* [1998; 2001] and implies that both steady state and transient grain size distribution parameters will be uniquely related to stress and temperature. Also consistent with the framework of the boundary hypothesis is the fact that the degree of weakening observed both in our experiments and in torsion tests is minor and probably insufficient to produce significant strain localization.
6. If the present conclusions on Carrara marble apply to other materials, a model describing the evolution of the grain size distribution during dynamic recrystallization would offer a way of tracking rheological behavior in nature during deformation from transient to steady state. The data presented in this paper may form a starting point for formulating such a model.

Chapter 4

The effect of dynamic recrystallization on rheology, microstructure and grain size distribution: Inferences from experiments on polycrystalline halite

4.1 Introduction

Dynamic recrystallization is an important process that can alter the microstructure and mechanical behavior of rock materials during deformation involving dislocation mechanisms. It has been observed, both in experiment and nature, in a wide range of materials important in the Earth, such as olivine [e.g. *Karato et al.*, 1982; *Jaroslow et al.*, 1996], quartz [e.g. *Hirth and Tullis*, 1992; *Stöckhert et al.*, 1999], feldspar [e.g. *Tullis and Yund*, 1985; *Shigematsu*, 1999] and calcite [e.g. *Schmid et al.*, 1980; *Molli et al.*, 2000]. The basic processes involved in dynamic recrystallization are the migration of existing grain boundaries and the formation of new high angle grain boundaries. Grain boundary migration can lead to grain growth during dynamic recrystallization. However, migration recrystallization can also lead to grain size reduction if new grain boundaries are formed at grain boundary bulges. New grain boundaries can also be formed from subgrain boundaries by progressive misorientation of subgrains or by migration of a sub boundary through an area of cumulative lattice rotation. The relative importance of these microphysical processes during dynamic recrystallization is dependent on the deformation conditions [*Poirier*, 1985; *Drury and Urai*, 1990].

Rock deformation studies mainly focus on dynamic recrystallization regarding (1) piezometers that relate recrystallized grain size to the flow stress [*Twiss*, 1977; *Etheridge and Wilkie*, 1979; *White et al.*, 1985], and (2) strain localization associated with rheological weakening. Dynamic recrystallization may result in rheological weakening due to a reduction in grain size, thus promoting grain size sensitive creep, or due to progressive removal of strain hardening substructure by grain boundary migration [*White et al.*, 1980; *Poirier*, 1985; *Rutter and Brodie*, 1988].

We note several problems with the above mentioned focal points. Problems with the calibration and application of recrystallized grain size piezometers are that (i) microstructures observed after laboratory deformation experiments are usually taken to represent steady state without systematically exploring the evolution as a function of strain, (ii) piezometric relations are generally assumed to be temperature independent, while both recent data and models for dynamic recrystallization suggest that temperature plays a role in determining the recrystallized grain size (cf. chapter 3) [*Derby*, 1990; *De Bresser et al.*, 1998; *Shimizu*, 1998], (iii) piezometers calibrated so far have rarely been evaluated against a sound theoretical basis (see chapter 1 for an extensive review of experimental data and models). Failing to address these problems hampers reliable application of piezometers to natural situations, potentially leading to large over- or underestimates of paleo-stresses. Problems with assessment of rheological weakening during dynamic recrystallization are that (i) so far, only the reduction of the average single-valued grain size has been considered, while the contribution of grain size sensitive creep to the overall creep rate is determined by the complete grain size distribution, including median grain size and standard deviation (chapter 2, 3), and (ii) microstructural evolution is usually not considered in direct relation to the flow behavior, except on qualitative grounds.

In this study we address these problems using synthetic polycrystalline halite. The use of polycrystalline halite has some important advantages compared to other materials or rock

analogues. Many of its properties are well known and deformation experiments are relatively easy to conduct in the laboratory. Dry halite deforms by dislocation mechanisms under laboratory conditions [Carter *et al.*, 1993; Watanabe and Peach, 2002]. In addition, water plays an important role in the deformation of polycrystalline halite, allowing active solution-precipitation creep [Spiers *et al.*, 1990] and fluid-assisted grain boundary migration [Urai *et al.*, 1986; Watanabe and Peach, 2002]. Hence, comparison of experiments on dry and wet polycrystalline halite allows quantitative analysis of the effect of solution-precipitation (diffusion) creep and grain boundary migration on the microstructural alteration and mechanical behavior.

The specific aims of the present study are to (1) relate microstructural evolution during dynamic recrystallization to flow behavior, (2) assess rheological weakening of wet polycrystalline halite and quantify the contribution of solution-precipitation creep to the overall diffusion-dislocation creep rate, (3) calibrate a recrystallized grain size piezometer for wet polycrystalline halite using the complete grain size distributions, taking into account recent models including a temperature dependence of the recrystallized grain size

To reach these aims, we have deformed polycrystalline samples of synthetic halite in a triaxial deformation apparatus operating at a confining pressure of 50 MPa. Samples with a water content of >10 ppm ('wet') were deformed at a strain rate of 5×10^{-7} - 1×10^{-4} s⁻¹, temperature of 75-240°C and stress of 7-22 MPa and samples with a water content of ≤ 5 ppm ('dry') were deformed at a strain rate of $\sim 5 \times 10^{-7}$ s⁻¹, temperature of 125 and 175°C and stress of 15 and 20 MPa.

The results give insight in the different microphysical processes operating during dynamic recrystallization, such as grain growth due to grain boundary migration and grain nucleation by progressive subgrain rotation or at grain boundary bulges. The results also show the effect of these processes on the grain size distribution and flow behavior. A piezometer could be calibrated, which allows testing of theoretical models relating recrystallized grain size to stress and temperature. This provides insight into the physical meaning of this piezometric relation. Besides these implications for dynamic recrystallization processes and piezometers, the results provide better constraints for the flow of halite rock in nature.

4.2 Experimental procedure

4.2.1 Sample preparation

Synthetic polycrystalline halite starting material has been produced by cold pressing analytical grade NaCl powder in a piston and cylinder compaction apparatus for 20 min. at ~ 200 MPa and subsequently annealing it in a pressure vessel for one week at 150°C and 100 MPa confining pressure [see Peach, 1991; Peach and Spiers, 1996 for more details]. Before cold pressing, the NaCl powder was placed in a vacuum chamber together with a beaker of water at room temperature. Condensation of water, evaporated from the beaker, resulted in NaCl powder with a small amount (< 0.1 wt%) of water. This method of cold pressing and annealing yielded dense (>99.5% of theoretical density) translucent cylindrical samples of halite rock. Samples were machined to right cylinders of either ~ 50 mm diameter and ~ 120 mm length or ~ 32 mm diameter and ~ 60 mm length. Two samples of ~ 32 mm diameter were machined to lengths of ~ 50 or ~ 40 mm respectively, to allow deformation to strains above values normally attainable in the experimental set-up used. Measurements of the water content of the samples using a Fourier Transform Infrared (FTIR) spectrometer [see Watanabe and Peach, 2002 for details] revealed that the starting material contained 37-290 ppm water ('wet' samples). Selected samples were slowly heated ($\sim 0.1^\circ\text{C}/\text{min.}$) to $T \approx 515^\circ\text{C}$

in flowing Argon gas using a high temperature furnace and were held at that temperature for ~24 hours. This resulted in samples with a water content of ~5 ppm. All samples were stored (before and after deformation) in a low-humidity room (R.H. \leq 15%). A detailed description of the microstructure and grain size distribution of the starting material is given in the results section of this paper.

4.2.2 Apparatus, experimental procedure and data acquisition

The machined cylinders of wet and dry polycrystalline halite have been deformed in axial compression at elevated pressure, using two different triaxial machines with silicone oil as the confining medium. The data in this study have been acquired from two sets of experiments: 1) new experiments on wet samples in a shuttle vessel deformation apparatus (name based on the easily removable piston-sample design), 2) experiments on wet and dry samples in a Heard triaxial deformation apparatus (named after its designer H.C. Heard). This set of experiments also forms part of a separate study by *Watanabe and Peach* [2002].

The shuttle vessel deformation apparatus used for the new experiments consists of an internally heated ~100 MPa pressure vessel mounted in an Instron 1362 servo-controlled testing machine. The apparatus allows axi-symmetric compression of the samples at constant displacement rate, temperature and pressure. Displacement is controlled by the Instron actuator and is measured externally using the Instron linear variable differential transformer (LVDT, 2 μ m resolution). The axial force resulting from sample displacement is measured externally by a 100 kN load cell (accurate to 0.1% of the full-scale output or 0.5% of the indicated load, whichever is greater). Temperature is measured by a chromel-alumel (type K) thermocouple at the top of the sample and is controlled within $\pm 1^\circ\text{C}$ during the experiments. Confining pressure is measured using a diaphragm-type transducer of 100 MPa full scale and servo-controlled within ± 0.5 MPa during the experiments. The samples were sealed from the pressurized silicone oil by a fluorethylene propylene (FEP) jacket and a double metal wire seal tightened against machined O-rings.

Displacement, axial force, temperature and pressure were continuously logged on a chart recorder and a computer during the shuttle vessel experiments. Axial force was corrected for friction effects on the seals between the pressure vessel and pistons, based on a relation between friction and piston position determined in several calibration runs of the apparatus at different displacements rates and temperatures. Sample strain was calculated from the externally measured displacement, corrected for distortion of the apparatus. Stress on the sample was calculated from the friction-corrected axial force, taking the change in cross-sectional area of the sample into account, assuming constant volume and homogeneous deformation. Stress was averaged over a time interval related to the sampling interval to remove electronic noise. All measurements were accurate well within 5%. The samples were deformed to natural strains of 0.3-0.7 at strain rates of 5.3×10^{-7} - 1.3×10^{-4} s^{-1} , temperatures of 75-243°C and a confining pressure of 50 MPa. At the end of the experiments, samples were cooled to a temperature below ~50°C (cooling 250°C to 50°C in ~1.5 hrs) before pressure was vented and the sample was removed from the apparatus. The samples were immediately cut to allow preparation of the thin sections.

Details on the Heard apparatus and experimental procedure employed in the second set of experiments have already been described elsewhere [*Peach*, 1991; *Peach and Spiers*, 1996]. The accuracy of the measurements is comparable with the experiments in the shuttle vessel deformation apparatus. Samples were deformed at a strain rate of $\sim 5 \times 10^{-7}$ s^{-1} , temperature of 125°C and confining pressure of 50 MPa. Natural strains of 0.07, 0.12 and 0.25 were achieved, corresponding to characteristic portions of the stress-strain curves [*Watanabe and Peach*, 2002].

4.2.3 Microstructural analysis

Thin sections of a few millimeters thick were prepared from the starting material and deformed samples following the method described in detail by [Urai *et al.*, 1987]. The method involved sectioning under evaporating oil with a diamond loaded jeweller's saw blade, polishing and etching with slightly undersaturated NaCl solution containing ~0.8wt% FeCl₃.6H₂O. With this method, low angle subgrain boundaries can be qualitatively distinguished from high angle (>10°) grain boundaries based on the intensity of etching [Trimby *et al.*, 2000a].

Microstructural analysis was carried out on the thin sections using a Leica DMRX light microscope, equipped with a Sony DXC-950P video camera. A compilation of gray scale digital photographs was made in incident light using a magnification of 2.5x, covering an area of 22-180 mm² in the center of the sample. High angle grain boundaries visible on the photographs were traced manually on a transparency, which was reduced to A4 size using a copying machine. The A4 page was scanned as a 300 dpi gray scale image on a Hewlett Packard ScanJet 6200C scanner. Quantitative grain size analysis was performed on the scanned image using the image analyzing program Leica QWin Pro Version 2.2 [1997]. Grain area (A_{grain}), the area of grain boundaries on the 2D section plane (A_{gb}), perimeter length of each grain (P_{grain}) and the aspect ratio of individual grains (calculated by dividing the maximum grain intercept length perpendicular to the compression direction by the maximum length parallel to the compression direction) were analyzed in the section plane. The area of individual grains was corrected for the measured area of the manually traced grain boundary by $A_{cor} = A_{grain} + (P_{grain}/P_{tot}) * A_{gb}$, where P_{tot} the total measured grain perimeter. Grain size was calculated and presented as equivalent circular diameters (ECD), using the corrected grain area A_{cor} without any (stereological) correction for sectioning effects. With this method, the number of grains in the lowest class (1 pixel size, equal to the detection limit) of the distribution may be slightly overestimated. Also, in some samples a limited amount of grains could be analyzed due to the large grains present. As a result the number of grains in the highest class may be underestimated in these samples. For all samples, the ECD frequency distribution (referred to as grain size distribution) and distribution of area fraction occupied by a given ECD class (referred to as area distribution) is given in a single frequency histogram.

4.3 Results

4.3.1 Mechanical data

Table 4.1 lists the test conditions and characteristics of all performed experiments. The stress-strain curves of the wet samples of polycrystalline halite are distinctly different from those of the dry samples (fig. 4.1a, b). The dry halite aggregates show continuous work hardening up to a strain of 0.25-0.51 at a strain rate of $5-7 \times 10^{-7} \text{ s}^{-1}$ and temperature of 125-175°C without reaching a steady state flow stress. A general feature of the experiments on the wet samples is the oscillating stress-strain behavior with local (broad) stress peaks followed by stress lows (fig. 4.1a-d). At all strains, flow stresses of the wet samples are significantly lower than the flow stresses of the dry samples at similar deformation conditions.

Table 4.1. Characteristics of all experiments.

test [*]	first stress peak [MPa]	strain at peak	first stress low [MPa]	strain at low	weak. (peak-low) [%] [‡]	flow stress [†] [MPa]	strain rate [†] [s ⁻¹]	T [†] [°C]	nat. strain	exp. dur. [hr]	H ₂ O cont. before (ppm)	H ₂ O cont. after (ppm)	number of grains
starting	-	-	-	-	-	-	-	-	-	-	-	-	887
p40t109dry	-	-	-	-	-	19.7	5x10 ⁻⁷	125	0.25	144.3	-	~5	578
15RS175dry	-	-	-	-	-	15.0	7.2x10 ⁻⁷	167	0.51	329.8	-	~5	-
p40t115	-	-	-	-	-	11.1	5x10 ⁻⁷	125	0.07	43.8	196	32	416
p40t112	12.5	0.10	-	-	-	12.4	5x10 ⁻⁷	125	0.12	72.5	133	28	242
p40t114	10.8	0.10	10.2	0.14	5.6	10.9	5x10 ⁻⁷	125	0.25	144.0	257	36	92
p40t111	11.8	0.09	11.3	0.13	4.2	11.8	5x10 ⁻⁷	125	0.25	143.0	290	36	-
7RS150	4.8	0.07	-	-	-	7.2	5.3x10 ⁻⁷	149	0.29	180.9	37	20	154
7RS200	6.7	0.10	-	-	-	7.5	2.4x10 ⁻⁶	203	0.30	40.8	-	22	176
7RS240	7.1	0.10	6.8	0.12	4.2	7.3	1.6x10 ⁻⁵	243	0.33	6.9	-	22	182
10RS240	9.9	0.14	9.0	0.20	9.0	9.5	1.3x10 ⁻⁴	243	0.34	0.9	-	19	611
11RS125	9.9	0.07	9.6	0.10	3.0	10.8	5.4x10 ⁻⁷	121	0.31	187.4	37	23	526
11RS150a	10.8	0.10	10.0	0.13	7.4	11.3	2.2x10 ⁻⁶	150	0.31	45.1	-	30	364
11RS150b	10.7	0.10	10.4	0.13	2.8	11.3	1.4x10 ⁻⁶	150	0.30	71.3	58	24	357
11RS175	11.6	0.11	10.3	0.18	11.2	10.9	6.6x10 ⁻⁶	174	0.30	14.9	-	12	425
11RS200	12.0	0.20	11.1	0.36	7.5	11.1	2.4x10 ⁻⁵	202	0.36	5.1	-	9	701
13RS125	13.1	0.11	12.3	0.14	6.1	13.3	1.3x10 ⁻⁶	125	0.30	73.2	-	45	515
13RS150	13.6	0.16	12.7	0.23	6.6	13.3	4.5x10 ⁻⁶	150	0.32	21.8	58	30	307
14RS100	14.3	0.13	13.0	0.17	9.0	13.6	5.3x10 ⁻⁷	99	0.29	182.6	-	33	317
14RS150	14.4	0.14	13.3	0.20	7.6	14.4	6.6x10 ⁻⁶	150	0.32	16.0	117	25	340
14RS175	15.3	0.26	13.9	0.44	9.2	13.9	5.0x10 ⁻⁵	171	0.44	3.0	-	9	958
18RS100	20.4	0.18	17.8	0.27	12.7	17.9	2.8x10 ⁻⁶	100	0.29	34.4	-	46	373
18RS125	20.3	0.20	17.6	0.31	13.3	17.7	7.4x10 ⁻⁶	126	0.34	14.6	-	36	660
18RS150	18.8	0.19	17.0	0.31	9.6	17.6	3.6x10 ⁻⁵	148	0.46	4.5	-	13	669
19RS150	19.3	0.23	18.8	0.31	2.6	19.1	4.5x10 ⁻⁵	149	0.68	6.0	-	16	840
22RS75	24.0	0.23	21.7	0.32	10.0	21.7	5.4x10 ⁻⁷	75	0.32	197.9	-	46	738
22RS100	26.0	0.25	22.1	0.37	15.0	22.1	7.5x10 ⁻⁶	99	0.38	17.1	-	10	943
22RS150	22.4	0.32	-	-	-	22.4	3.2x10 ⁻⁵	149	0.32	3.3	-	28	958

* Stress (first number) and temperature (second number) are quoted in the test numbers.

† Flow stress, temperature (T), strain rate and pressure (P) averaged over a strain of 0.01 at the end of the test.

‡ Weakening is calculated by $((\sigma_{peak} - \sigma_{end}) / \sigma_{peak}) \times 100\%$ with σ_{peak} and σ_{end} the flow stress at the peak or at the end of the experiment.

^{||} Experiments from *Watanabe and Peach* [2002], grain size analysis from this study.

Two types of stress-strain curves can be identified for the wet samples deformed to natural strains of 0.3-0.4 (fig. 4.1a-d):

- (1) Curves with a peak or plateau in flow stress, followed by a stress low and subsequent strain hardening to a second peak at a higher stress (e.g. 7RS150, 7RS240 and 11RS125). This type of mechanical behavior occurs at low strain rates and relatively high temperatures.
- (2) Curves with a peak in flow stress, followed by strain softening to a stress low and limited hardening to a second peak at a lower stress (e.g. 14RS100, 18RS150). This type of behavior occurs at strain rates that are higher and temperatures that are lower than for type (1).

Note that at the highest stress investigated ($\sigma > 20$ MPa), the maximum strain achieved in the experiments is insufficient to reach a second stress peak (i.e. the oscillation pattern is

incomplete). At the lower strain rates and relatively high temperatures, the stress-strain curves show at least two complete cycles of a peak stress followed by a stress low. The difference between stress peaks and lows decreases with increasing strain, suggesting an approach to a steady state flow stress (e.g. 7RS240, 11RS175 and 14RS100). The strain required to reach the first stress peak increases with increasing stress or strain rate and with decreasing temperature, although 18RS150 deviates from this general trend (fig. 4.1d).

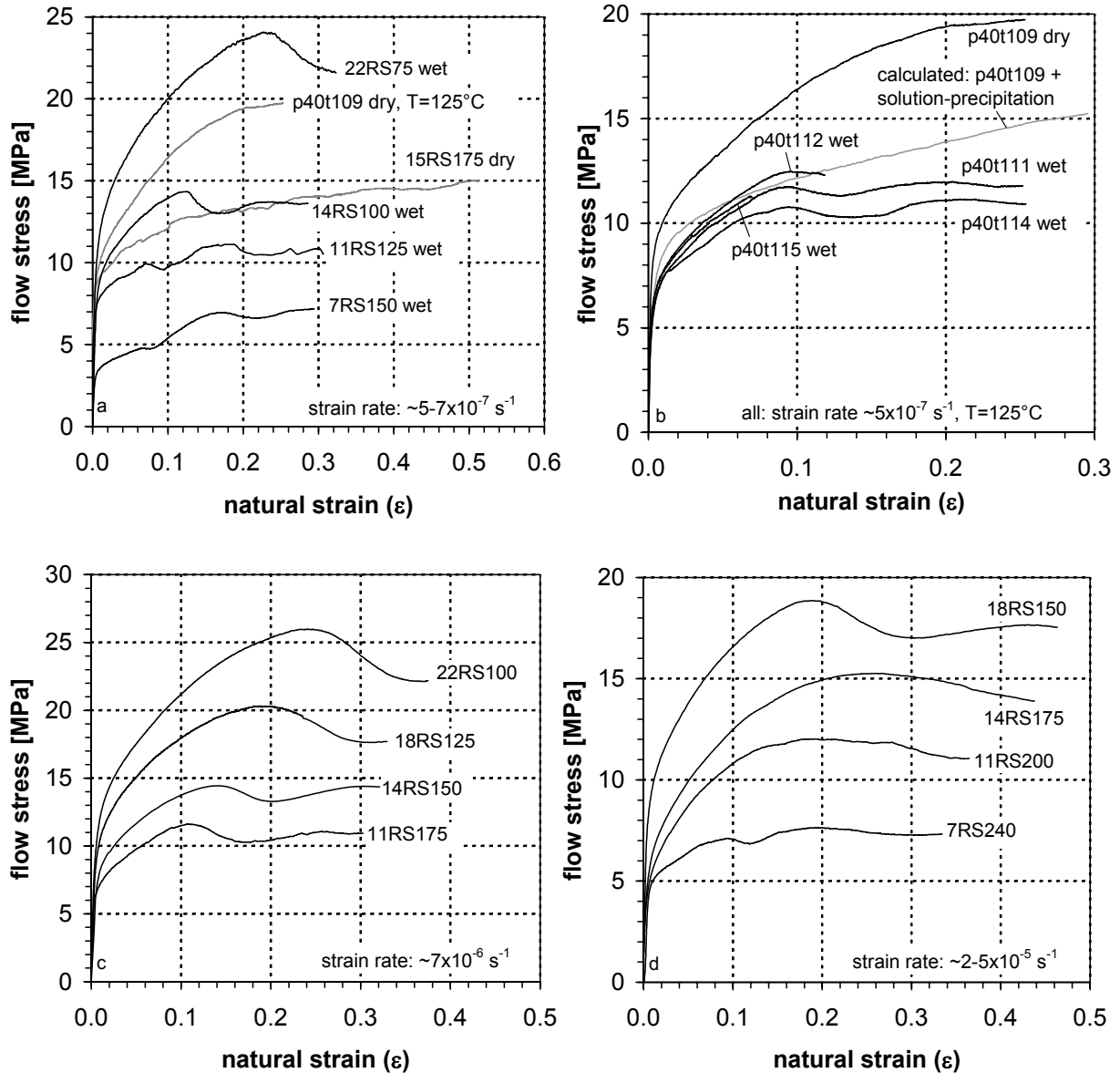


Figure 4.1. Typical stress-strain curves showing (a) the difference between the mechanical behavior of wet ($T=75-150^\circ\text{C}$) and dry polycrystalline halite ($T=125, 175^\circ\text{C}$) at $\dot{\epsilon} \approx 5-7 \times 10^{-7} \text{ s}^{-1}$, (b) the difference between wet and dry polycrystalline halite at $T=125^\circ\text{C}$ and $\dot{\epsilon} \approx 5 \times 10^{-7} \text{ s}^{-1}$. Indicated are stress-strain curves from Watanabe and Peach [2002] (samples deformed to different strains) and the stress-strain curve calculated by adding the contribution of solution-precipitation creep to p40t109 (see discussion), (c) wet polycrystalline halite at $\dot{\epsilon} \approx 7 \times 10^{-6} \text{ s}^{-1}$ and $T=100-175^\circ\text{C}$ and (d) wet polycrystalline halite at $\dot{\epsilon} \approx 2-5 \times 10^{-5} \text{ s}^{-1}$ and $T=150-240^\circ\text{C}$.

The rheological weakening associated with the oscillations, calculated by the relative difference in stress between the first stress peak and the stress at the end of the experiment, is below 15% in all samples and increases with increasing flow stress (table 4.1).

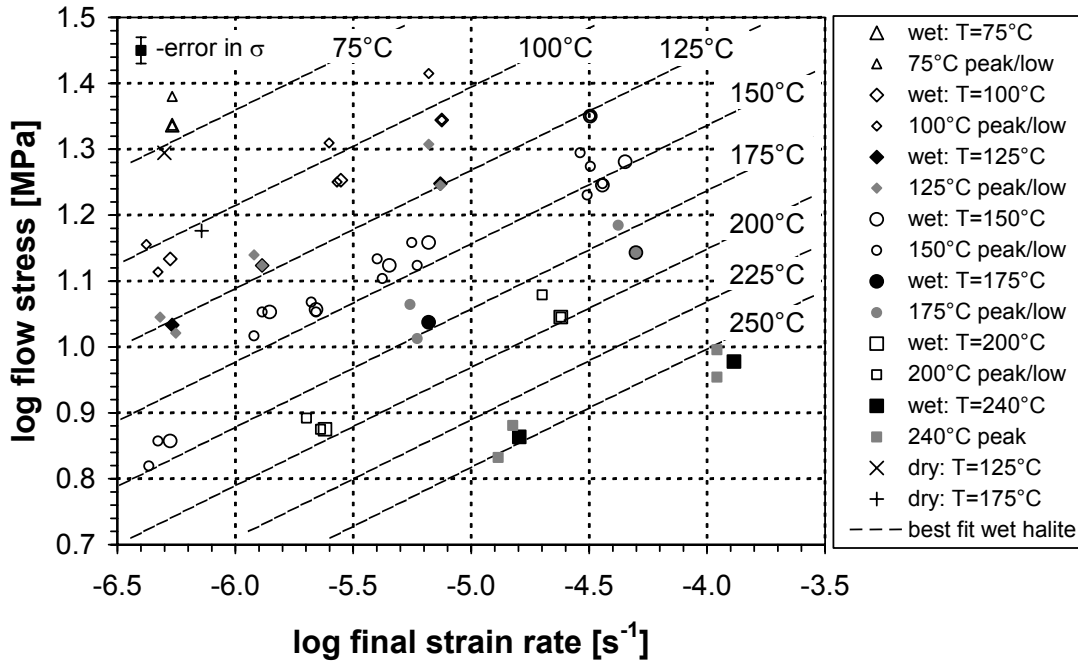


Figure 4.2 Stress versus strain rate data for wet and dry polycrystalline halite. Flow stresses averaged over the last 0.01 strain (large symbols) and stress peaks and lows (small symbols) of the last cycle in the experiments are indicated.

The stress versus strain rate data of all experiments on wet and dry polycrystalline halite are depicted in fig. 4.2. The figure includes flow stresses averaged over the last 0.01 strain in the experiments and the stress peaks and lows of the last cycle in the experiments. Flow stresses increase with increasing strain rate and decreasing temperature at all conditions. The flow stresses of dry polycrystalline halite are a factor ~ 2 higher than the flow stresses of wet polycrystalline halite for the same conditions. For wet polycrystalline halite, the strain rate ($\dot{\epsilon}$) can be related to the flow stress (σ) using a Dorn type power law equation of the type

$$\dot{\epsilon} = A \sigma^n \exp\left(\frac{-Q}{RT}\right) \quad (4.1)$$

Table 4.2 shows values for the rate constant (A in $\text{MPa}^{-n} \cdot \text{s}^{-1}$), stress exponent (n) and apparent activation energy (Q) obtained from a non-linear best fit of the data to (4.1). Only data of the last 0.01 strain in the experiments are used for the fit. Isotherms of (4.1) with the best fit values of A , n and Q are indicated in fig. 4.2.

Table 4.2 The rate constant A , stress exponent n and apparent activation energy Q obtained from a non-linear best fit of the stress-strain rate data for wet polycrystalline halite to a Dorn type power law equation (see text). The flow law parameters, water content and deformation conditions of a selection of previous studies and different types of polycrystalline halite are compared with the values obtained in this study.

material/ composition	H ₂ O (ppm)	P (MPa)	strain rate (s ⁻¹)	temp. (°C)	stress (MPa)	-log(A) (MPa ⁻ⁿ .s ⁻¹)	stress exponent	Q (kJ/mol)	source/ comments
synthetic pure halite	9-46	50	10 ⁻⁴ -10 ⁻⁷	75- 250	7.2- 22.4	1.56 ± 0.54	5.6 ± 0.5	80 ± 6	this study
synthetic pure halite	20-45	200	10 ⁻¹ -10 ⁻⁸	23- 400	1.6-47	0.11 ± 0.82	5.5 ± 0.4	98 ± 8	Heard [1972]
synthetic pure halite	20-45	200	10 ⁻¹ -10 ⁻⁸	23- 400	1.6-47	0.7 ± 0.4	5.8 ± 0.2	96 ± 3	Heard and Ryerson [1986]
natural (>95% halite)*	?	14, 21	10 ⁻⁶ -10 ⁻¹¹	23- 160	8.3-24	3.36-6.03	4.1-6.3	50-83	Wawersik and Zeuch [1986]
natural (>99% halite)†	< 100	2.5- 20.7	10 ⁻⁶ -10 ⁻⁹	50- 200	6.9- 20.7	3.80	5.3	68	Carter et al. [1993]-high $\dot{\epsilon}$, σ
natural (>99% halite)†	<100	2.5- 20.7	10 ⁻⁷ -10 ⁻⁹	100- 200	2.5- 10.3	4.09	3.4	52	Carter et al. [1993]-low $\dot{\epsilon}$, σ
synthetic pure halite	dry	unconf.	10 ⁻³ -10 ⁻⁷	250- 780	0.4- 14.8	0.76	5.7	129	Franssen [1994]- low T regime

* Range of parameters for natural halite from 5 different locations: Salado (New Mexico), West Hackberry and Bayou Choctaw (Louisiana), Bryan Mound (Texas) and Asse (Germany). † Avery Island (Louisiana).

4.3.2 Microstructure

Starting material

The wet (37-290 ppm water) synthetic halite starting material deformed in this study is identical to the material described by Peach [1991] and Peach and Spiers [1996] and is typical of a completely annealed polycrystalline material. It consists of a homogeneous aggregate of polygonal grains (fig. 4.3a). Individual grains lack internal structure and are mostly equidimensional (aspect ratio of ~1, table 4.3). Grain boundaries are straight to gently curved and preferentially intersect at ~120° triple junctions.

Figure 4.3a. Microstructure of undeformed polycrystalline halite (starting material).

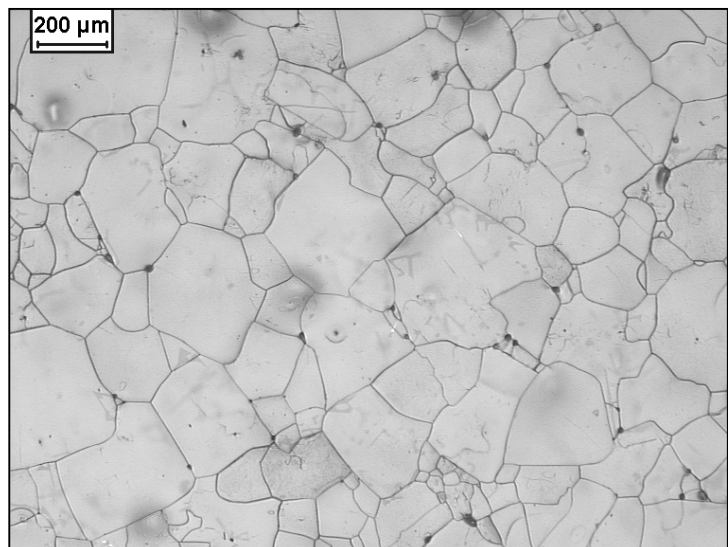


Table 4.3 Statistical descriptors of the grain size distributions analysed.

test [*]	median grain size [μm]	average grain size [μm]	average grain size log-space [μm] (log)	stand. dev. (log d)	min.-max. grain size [μm]	skewness (log d)	av. grain aspect ratio [§]	number of grains
starting material	123	145	118 (2.07)	0.29	19-646	-0.26	1.02	887
p40t109dry	188	218	181 (2.26)	0.29	17-749	-0.62	1.52	578
p40t115	185	217	162 (2.21)	0.36	16-969	-0.51	1.31	416
p40t112	282	419	251 (2.40)	0.47	29-3355	-0.16	1.36	242
p40t114	287	774	331 (2.52)	0.57	43-6801	0.25	1.47	92
7RS150	355	604	231 (2.52)	0.50	38-3170	-0.04	1.42	154
7RS200	269	625	303 (2.48)	0.54	39-4066	0.15	1.55	176
7RS240	380	525	328 (2.52)	0.46	29-2828	-0.39	1.47	182
10RS240	163	219	160 (2.20)	0.36	20-1065	-0.16	1.40	611
11RS125	161	330	179 (2.25)	0.46	42-4550	0.49	1.42	526
11RS150a	322	471	299 (2.47)	0.44	38-2707	-0.23	1.56	364
11RS150b	230	374	226 (2.35)	0.46	30-1971	-0.10	1.54	357
11RS175	202	310	203 (2.31)	0.41	27-2386	-0.09	1.43	425
11RS200	183	259	178 (2.25)	0.39	27-2026	-0.10	1.51	701
13RS125	193	318	203 (2.31)	0.42	28-1868	0.07	1.46	515
13RS150	173	226	169 (2.23)	0.35	17-1063	-0.34	1.59	307
14RS100	158	308	171 (2.23)	0.45	29-3270	0.36	1.60	317
14RS150	159	220	160 (2.20)	0.35	16-1142	-0.04	1.62	340
14RS175	133	216	140 (2.15)	0.41	27-1469	0.14	1.45	958
18RS100	164	331	179 (2.25)	0.49	29-2571	0.18	1.36	373
18RS125	136	188	131 (2.12)	0.37	20-1768	-0.01	1.44	660
18RS150	124	190	132 (2.12)	0.37	19-1172	0.17	1.37	669
19RS150	128	178	126 (2.10)	0.37	20-1126	-0.08	1.44	840
22RS75	97	147	103 (2.01)	0.36	16-1123	0.23	1.61	738
22RS100	116	198	127 (2.10)	0.40	29-1577	0.28	1.34	943
22RS150	156	192	152 (2.18)	0.31	20-794	-0.34	1.50	958

* Stress (first number) and temperature (second number) are quoted in the test numbers.

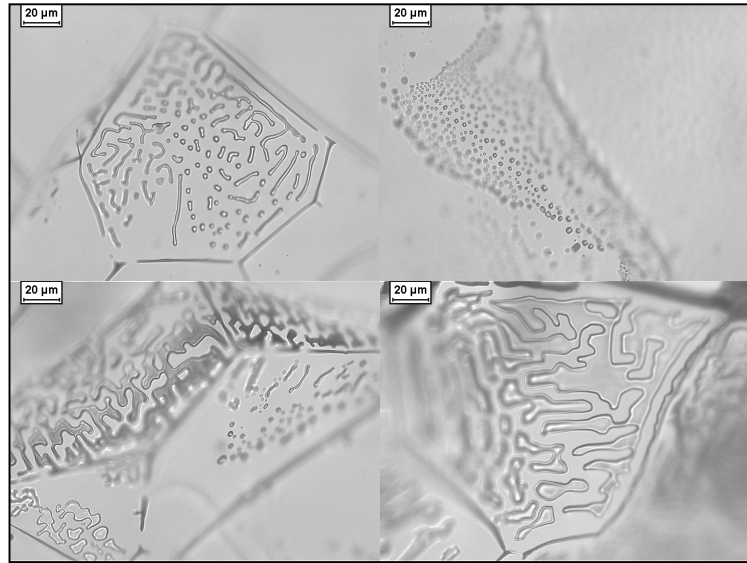
§ Average grain aspect ratio perpendicular to the compression direction are quoted.

|| Experiments from *Watanabe and Peach* [2002], grain size analysis from this study.

Fluids (mainly brine) and possibly some gas are present in isolated inclusions or isolated and interconnected worm-like channels (fig. 4.3b), similar as often observed in natural halite rock [Roedder, 1984; Urai *et al.*, 1987].

The dry (~5 ppm water) synthetic halite starting material deformed by *Watanabe and Peach* [2002] is similar to the wet starting material, but samples are less translucent due to opening of grain boundaries during the heating stage of the sample preparation. The boundaries were closed again during deformation, and samples were translucent after deformation. Grain boundaries contain some fluid and gas bearing spherical inclusions, but connected worm-like channels are less abundant compared to the wet material.

Figure 4.3b. Fluid and gas inclusions at grain boundaries of the undeformed starting material.



Influence of strain

The influence of strain on the microstructure of the wet samples can be systematically investigated at a flow stress of $\sigma \approx 11$ MPa, $T = 125^\circ\text{C}$ and $\dot{\epsilon} \approx 5 \times 10^{-7} \text{ s}^{-1}$ using experiments p40t111-p40t115 performed by *Watanabe and Peach* [2002] (table 4.1, 4.3, fig. 4.1b). In these samples, microstructural evolution is directly related to specific stages of the stress-strain curves, i.e. the microstructures just before the first stress peak (p40t115), just after the peak stress (p40t112) and after 2 oscillations (p40t111, p40t114) are compared.

At a strain of ~ 0.07 , just before the first peak stress (p40t115), grains have flattened with respect to the undeformed material (table 4.3). Many grains have developed internal structure with linear (wavy) etch features at an angle of $\sim 35\text{-}60^\circ$ to the compression direction, although some grains without a clear internal structure are present. Subgrains and small grains of subgrain size are present, predominantly near grain boundaries of large grains (fig. 4.3c). Grain boundaries are more irregular than in the undeformed material and occasional lobate grain boundaries are present (fig. 4.3c).

Figure 4.3c. Lobate grain boundary, subgrains and grains of subgrain size in sample p40t115.

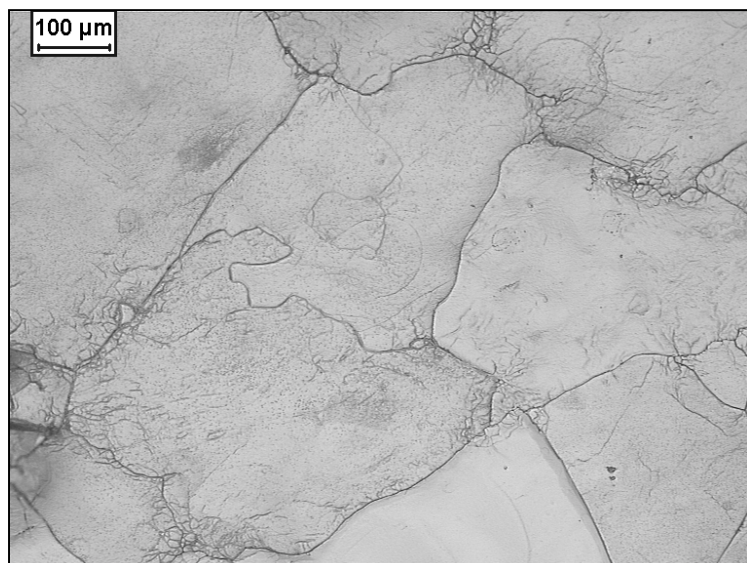
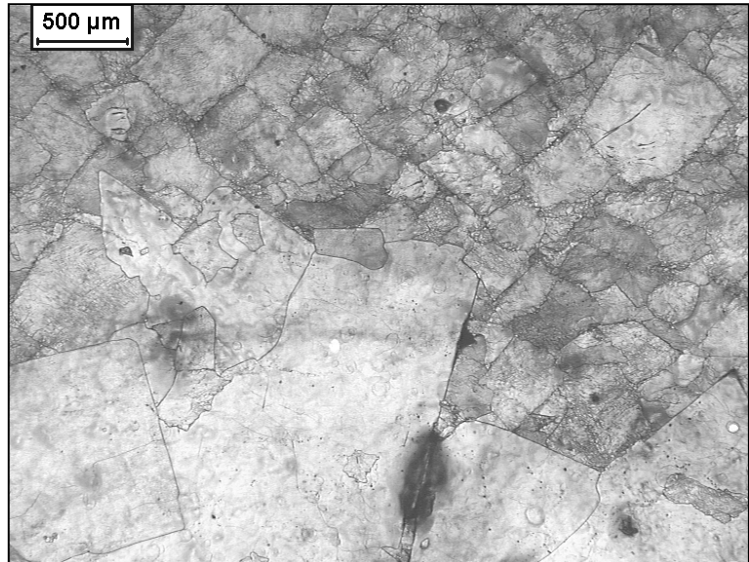


Figure 4.3d. Recrystallization front, dividing sample p40t112 in a recrystallized (bottom) and non-recrystallized (top) part. Compression direction vertical.



At a strain of ~ 0.11 , just after the first peak stress (p40t112), the microstructure is substantially different from p40t115. The sample is divided in a (non-recrystallized) part with a microstructure resembling the microstructure of p40t115 and a (recrystallized) part with a microstructure dominated by large grains with irregular lobate grain boundaries. The boundary (recrystallization front) between the two parts is irregular and runs across the entire sample, roughly perpendicular to the compression direction (fig. 4.3d). In the recrystallized part, the maximum grain size is significantly larger than in the non-recrystallized part. Arrays of fluid inclusions are present in the large grains, indicating the old positions of grain boundaries. This shows that widespread migration of grain boundaries has occurred (fig. 4.3e). Grains with straight crystal faces and $\sim 90^\circ$ angles between faces, typical of euhedral halite, are present (fig. 4.3d, e). The large grains exhibit a shape-preferred orientation with the longest axis of the grains oriented perpendicular to the compression direction. These grains have little internal structure, although some subgrains with irregular subgrain boundaries occasionally are present (fig. 4.3f). In addition, smaller grains full of internal structure, such as linear etch features and small subgrains, are present in the recrystallized part. These grains do not exhibit a strong shape preferred orientation and have a similar appearance as the grains in the sample deformed to a strain of ~ 0.07 . Grains of subgrain size are present, predominantly at grain boundaries (fig. 4.3e).

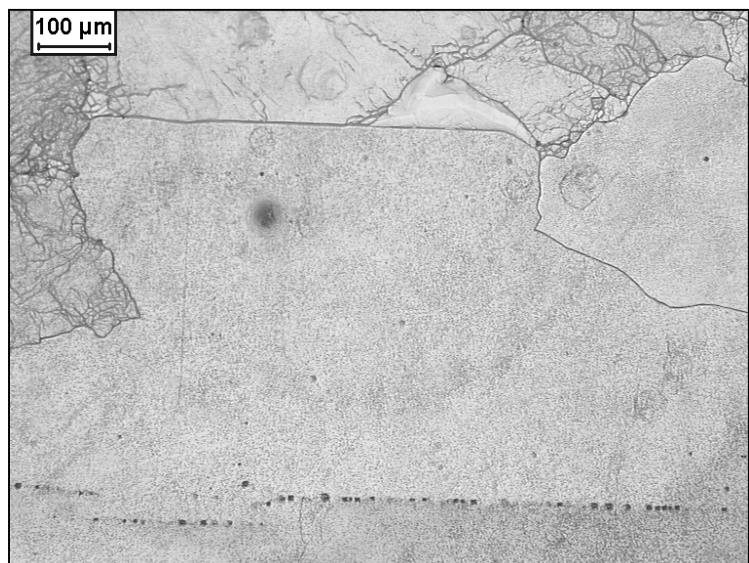
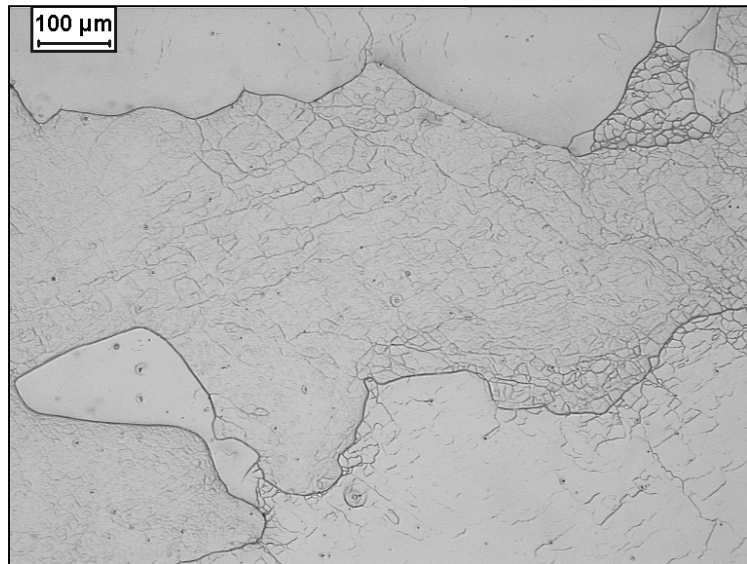


Figure 4.3e. Array of fluid inclusions indicating the old position of a grain boundary before migration in sample p40t112.

Figure 4.3f. Grain boundary of a grain with little internal structure bulging into a grain with well developed internal structure (lower left) and grain with a clear subgrain structure and a grain boundary that follows the subgrain boundaries (upper right) in sample 11RS200.



At a strain of ~ 0.25 , at near steady state after two complete oscillations (p40t114), the sample is completely recrystallized and the distinct recrystallization front has disappeared. The size of both the large grains with little internal structure and the smaller grains full of internal structure is larger than in the recrystallized part of p40t112. Grains of subgrain size are also present. All other features observed in the recrystallized part at a strain of ~ 0.11 are present, but grains with straight faces are more abundant (fig. 4.3g).

The microstructural evolution with increasing strain described for p40t111-p40t115 is characteristic for the investigated wet material and can also be observed at other conditions. Sample 22RS150 just reached the first stress peak at a strain of ~ 0.3 . The microstructure of this sample shows similar features as p40t115 with flattened grains and well developed internal structure. The average aspect ratio is higher due to the larger strain of 22RS150. Sample 22RS75 did not reach the first stress low at a strain of ~ 0.3 and is partly recrystallized with a similar recrystallization front as observed in p40t112. All other samples have been completely recrystallized and exhibit microstructural features as observed in p40t112 and p40t114. In these samples, some grain boundaries of grains with little internal structure form bulges into grains with a well developed internal structure, indicating migration of grain boundaries into grains with well developed internal structure. There are also grains that exhibit a clear subgrain structure and have grain boundaries that follow the subgrain boundaries (fig. 4.3f).

Influence of temperature and stress

The influence of temperature and stress on the microstructure of wet polycrystalline halite can be systematically investigated using samples deformed at approximately constant stress and different temperatures (e.g. 11RS125, 11RS150a, b and 11RS175) and samples deformed at constant temperature and different stresses (e.g. 7RS150, 11RS150a, b, 13RS150 and 14RS150). Only samples that have been completely recrystallized and have reached a (near) steady state flow stress are compared. With increasing temperature and stress, the size of the grains with little internal structure and straight (euhedral) or lobate boundaries (indicating migration) decreases at the expense of the grains full of internal structure. At the highest temperatures and stresses, both types of grains have roughly similar sizes, while at low temperature and stress, the microstructure is dominated by grains with little internal structure. The average aspect ratio does not change systematically with temperature or stress (table 4.3).

Figure 4.3g. Recrystallized microstructure of sample p40t114 (wet). Compression direction vertical.

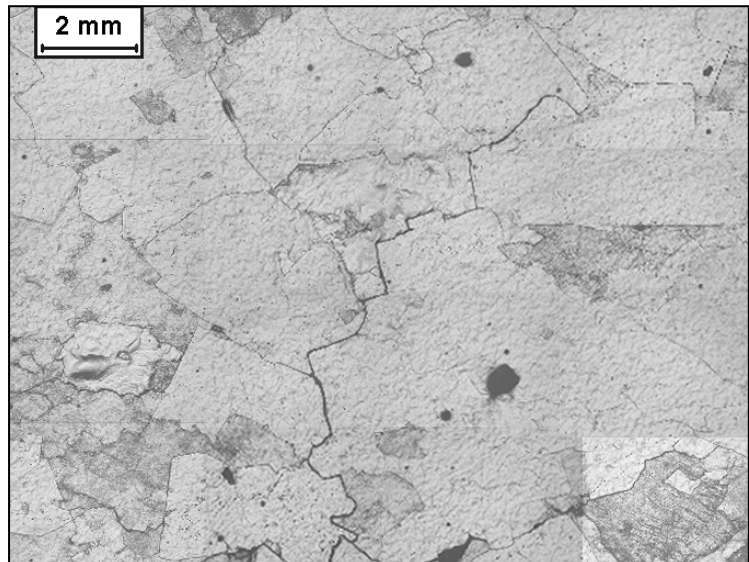
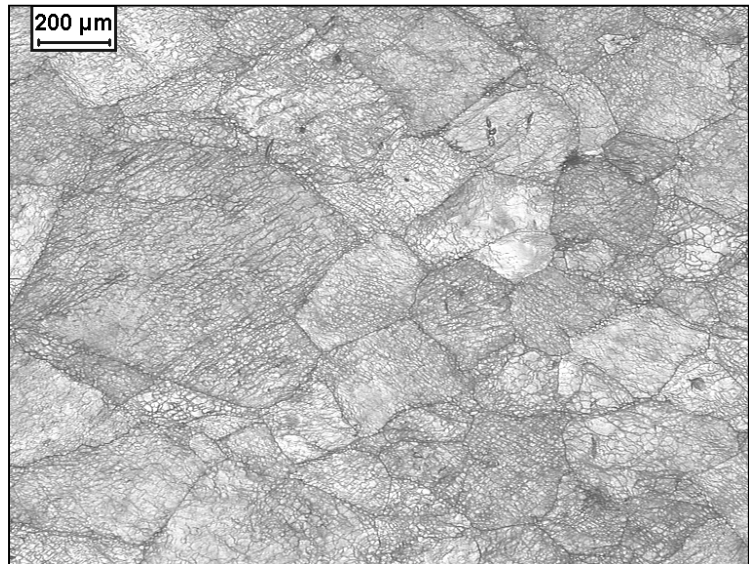


Figure 4.3h. Microstructure of p40t109 (dry). Compression direction vertical.



The microstructure of the wet deformed samples is strikingly different from that of the dry sample deformed at $\dot{\epsilon} \approx 5 \times 10^{-7} \text{ s}^{-1}$ and $T = 125^\circ\text{C}$ (fig. 4.3h). Almost all grains show an internal structure with linear (wavy) etch features at an angle to the compression direction. Grain boundaries generally are irregular and follow the subgrain boundaries. No evidence for migration of boundaries, such as intra-grain arrays of fluid inclusions or lobate grain boundaries, was found. Grains have flattened with respect to the starting material and are full of subgrains. Subgrain size grains are present, predominantly at grain boundaries.

4.3.3 Grain size distributions

The ECD frequency distributions (grain size distribution) and distributions of area fraction occupied by a given ECD class (area distribution) of the starting material and all deformed wet and dry samples are depicted in figs. 4.4-4.7. Statistical descriptors characterizing the number distributions are given in table 4.3.

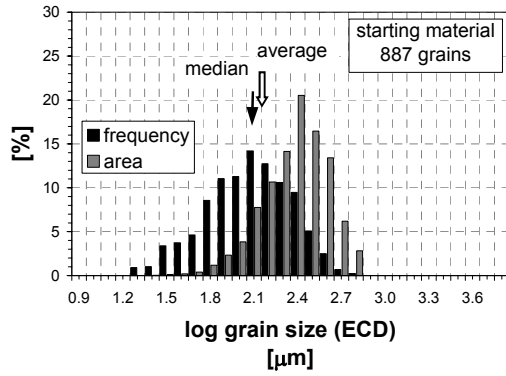


Figure 4.4 ECD frequency distributions (grain size distribution) and distributions of area fraction occupied by a given ECD class (area distribution) of the polycrystalline halite starting material. Grain size presented as equivalent circular diameter (ECD) in log space. Closed arrow indicates median grain size. Open arrow indicates linear average grain size. The grain area distribution shows the total area of grains in a certain grain size class relative to the total grain area in the sample.

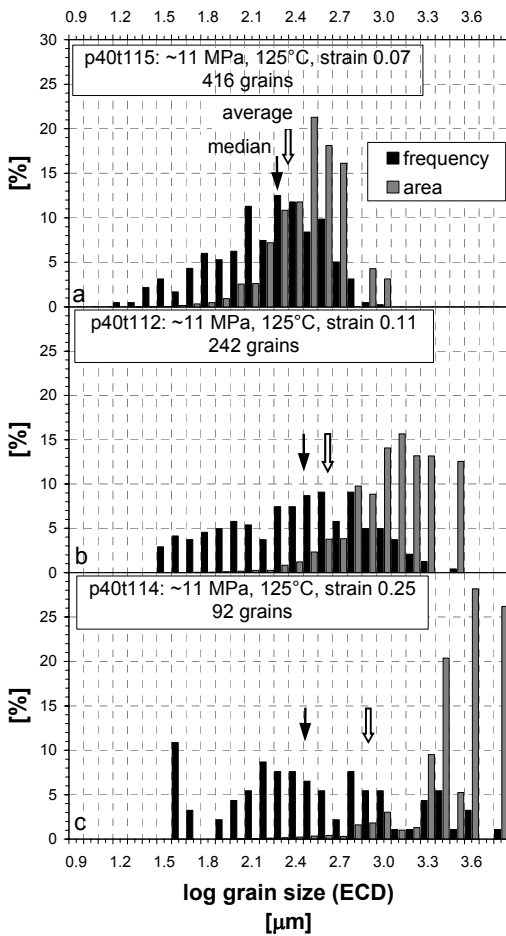


Figure 4.5 ECD frequency distributions (grain size distribution) and distributions of area fraction occupied by a given ECD class (area distribution) of wet polycrystalline halite deformed to different strains at $T=125^{\circ}\text{C}$ and $\dot{\epsilon} \approx 5 \times 10^{-7} \text{ s}^{-1}$ by Watanabe and Peach [2002] (p40t111-p40t115). Arrows and grain area distribution as indicated in fig. 4.4. Samples deformed to specific strains (cf. fig. 4.1b): (a) just before the first peak stress, (b) just after the first peak stress, (c) at a (near) steady state flow stress.

Starting material

The grain size distribution of the starting material is slightly negatively skewed (in log space) with a median grain size of $123 \mu\text{m}$ (fig. 4.4). The linear average grain size is $145 \mu\text{m}$, the average logarithmic grain size ($\log d$) is 2.07, and the standard deviation of $\log d$ is 0.29 (table 4.3). The average $\log d$ and the median grain size are close to each other and the skewness of the logarithmic grain size distribution is relatively small, indicating that the grain size distribution is close to lognormal.

Influence of strain

Fig. 4.5 reveals the influence of strain on the grain size distribution of wet polycrystalline halite at $\sigma \approx 11 \text{ MPa}$, $T=125^{\circ}\text{C}$ and $\dot{\epsilon} \approx 5 \times 10^{-7} \text{ s}^{-1}$. At a strain of ~ 0.07 , just before the first stress peak (p40t115, fig. 4.5a), the logarithmic grain size distribution is more negatively skewed than the starting material. The median, average and maximum grain size are larger than for the starting material. The standard deviation of $\log d$ has also increased compared to the starting material. At a strain of 0.11-0.25, after the first stress peak (p40t112 and p40t114-fig. 4.5b, c), the median, average and maximum grain size increase considerably. The standard deviation also increases considerably and skewness changes from negative to positive. The mode of the area distribution changes increases from $316 \mu\text{m}$ at a strain of 0.07 to $1259 \mu\text{m}$ at a strain of 0.11 and $3981 \mu\text{m}$ at a strain of 0.20.

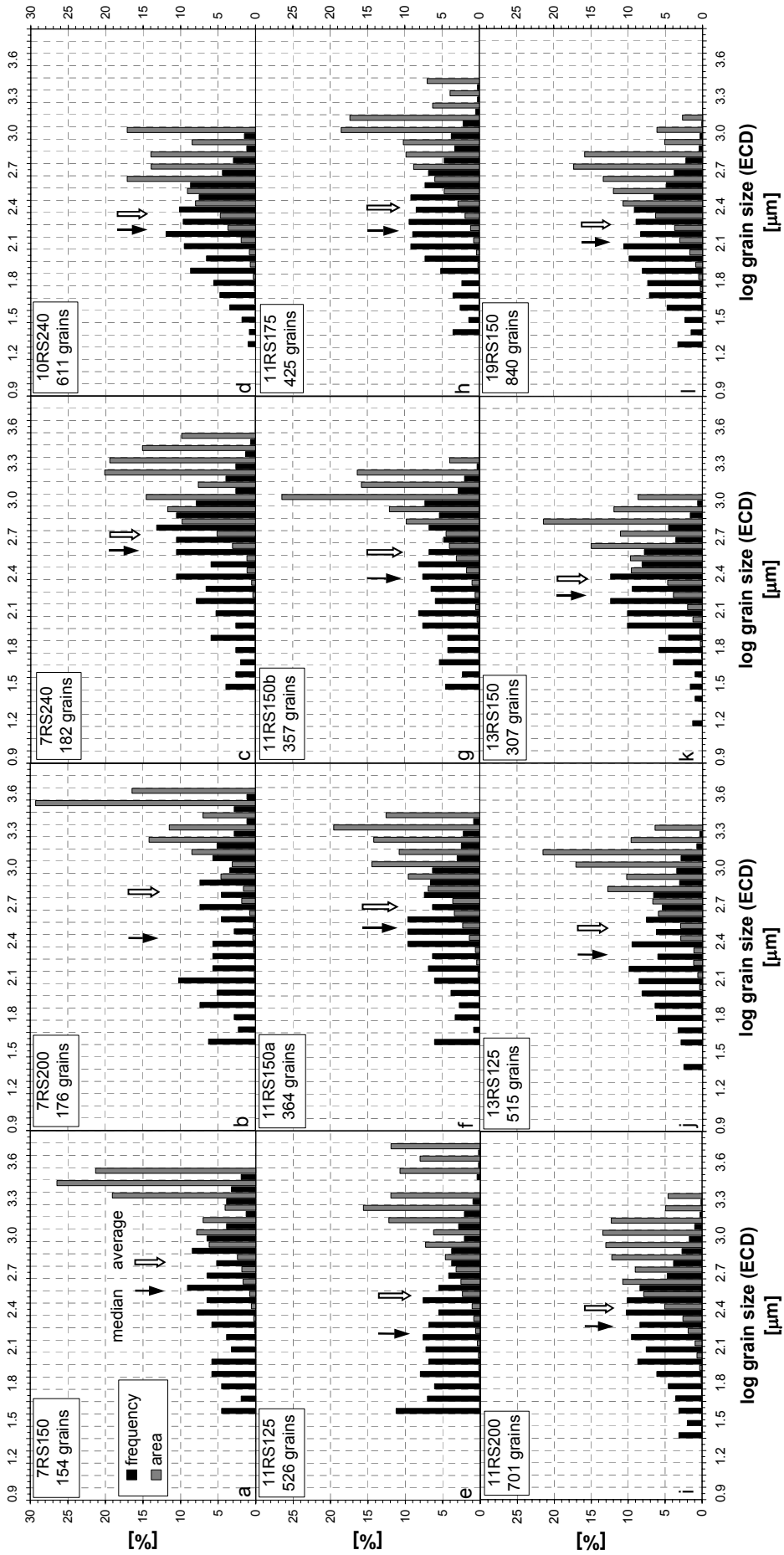


Figure 4.6 (continues on next page).

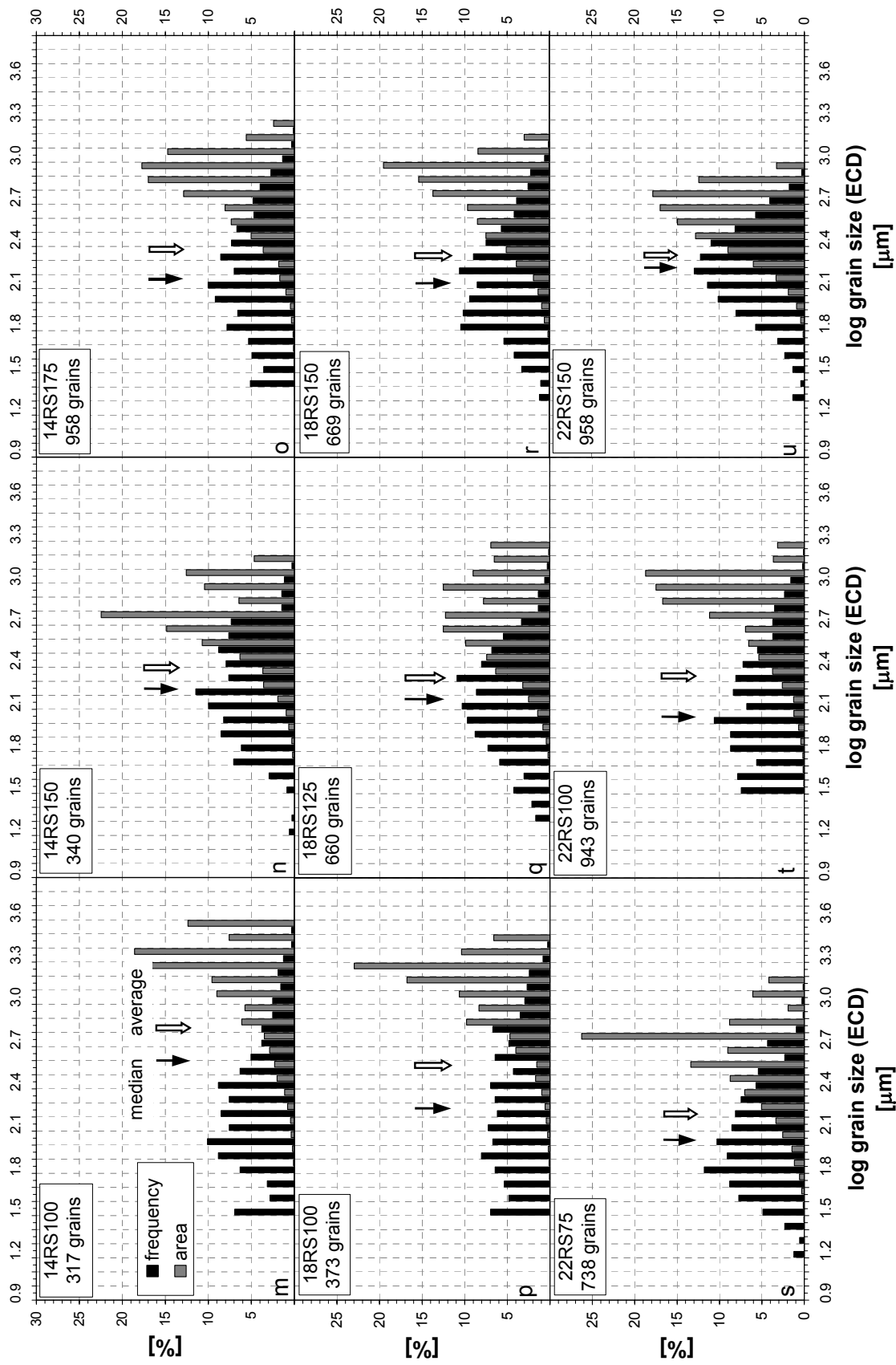


Figure 4.6 ECD frequency distributions (grain size distribution) and distributions of area fraction occupied by a given ECD class (area distribution) of wet polycrystalline halite deformed at different deformation conditions (see table 4.1). Arrows and grain area distribution as indicated in fig. 4.4.

Influence of temperature and stress

The influence of temperature and stress on the grain size distribution can be investigated using the distributions in fig. 4.6. The distributions tend to become more symmetrical and less irregular with increasing temperature and stress. Except for sample 22RS100, the median and average grain size have increased with respect to the starting material. The median and average grain size generally decrease with increasing temperature and stress, although some observations deviate from this trend (table 4.3). Figs. 4.7a and b show the influence of temperature and stress on the median grain size. The standard deviation of $\log d$ decreases with increasing temperature and increasing stress (fig. 4.8). Only samples that have been completely recrystallized are depicted in figs. 4.7 and 4.8. All area density distributions are negatively skewed with a mode that decreases with increasing stress and no clear trend with temperature.

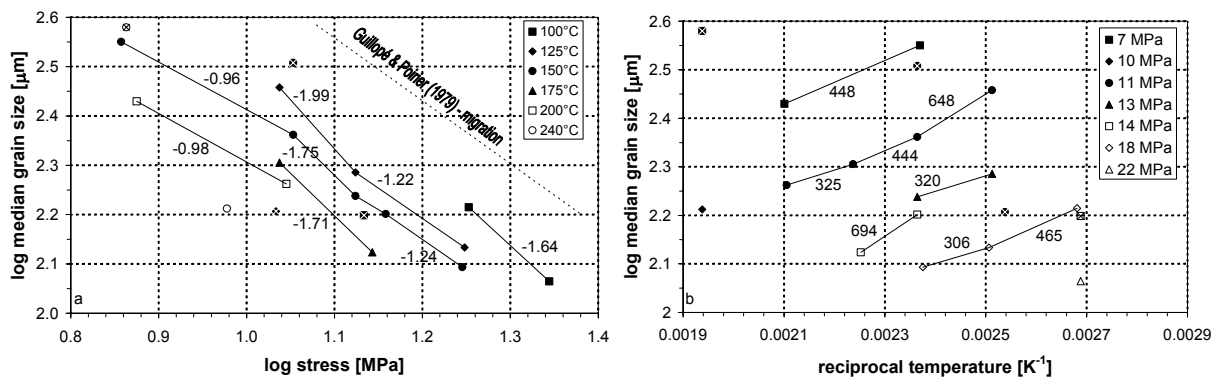


Figure 4.7 The influence of (a) stress and (b) temperature on the median grain size of completely recrystallized wet polycrystalline halite. The median grain size data is used to calibrate a piezometer (see discussion). The solid lines indicate general trends of recrystallized grain size with stress and temperature. Data points that deviate from the general trends (indicated by crosses) have not been interconnected with the other points, and were omitted in calibrating the piezometer.

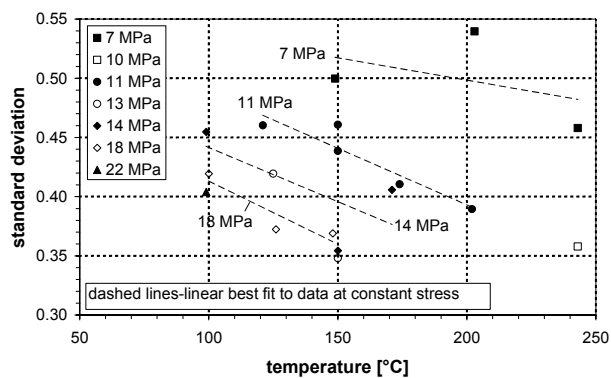


Figure 4.8 The influence of stress and temperature on the standard deviation of logarithmic grain size of completely recrystallized wet polycrystalline halite.

The grain size distribution of deformed dry polycrystalline halite is negatively skewed with a median grain size of 188 μm (fig. 4.9). The linear average grain size is 218 μm , average $\log d$ is 2.26 and the standard deviation of $\log d$ is 0.29 (table 4.3). The median and average grain size are higher than for the starting material. These values and the skewness and standard deviation of $\log d$ are close to the values for the wet material deformed to a strain of 0.07, just before the peak stress (p40t115, fig. 4.5a).

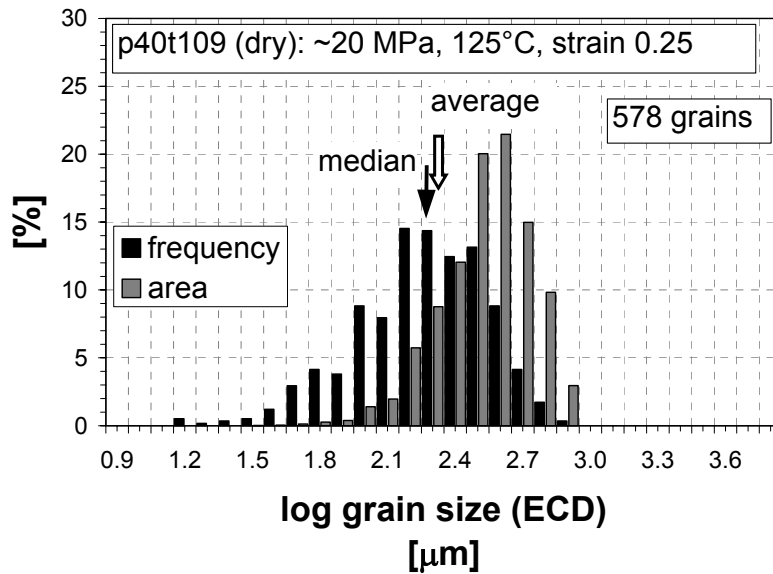


Figure 4.9 ECD frequency distributions (grain size distribution) and distributions of area fraction occupied by a given ECD class (area distribution) of deformed dry polycrystalline halite (p40t109). Arrows and grain area distribution as indicated in fig. 4.4.

4.4 Discussion

In this section we will first discuss the microphysical processes that operate during the deformation of polycrystalline halite. This includes the deformation and recrystallization mechanisms and their effect on the microstructure and flow behavior during transient and steady state deformation. We then use the results to make general inferences on the effect of dynamic recrystallization on rheology, microstructure and grain size distribution with emphasis on the problems and aims mentioned in the introduction. We also briefly address the implications of the results for flow of halite rock in nature.

4.4.1 Deformation and recrystallization mechanisms

The microstructure of deformed wet polycrystalline halite shows widespread evidence for the operation of dislocation processes, such as linear and wavy slip lines and subgrain structure. The wavy slip lines have been attributed to result from cross-slip of screw dislocations by short movement on {100} and {111} planes, bridging parallel {110} slip planes [Skrotzki and Liu, 1982; Senseny et al., 1992; Carter et al., 1993]. In addition, subgrains develop at all investigated conditions, suggesting that climb-controlled recovery was active as well [e.g. Edward et al., 1982]. After the first stress peak, grain boundary migration occurs as evidenced by the presence of lobate grain boundaries and intracrystalline trails of fluid inclusions indicating old positions of grain boundaries. The presence of fluid inclusions on grain boundaries suggests that water plays an important role in the migration of boundaries. Straight (euhedral) crystal faces indicate that grain boundary migration is facilitated by solution-precipitation transfer across grain boundary brine films [Urai, 1983; Urai, 1985]. Several experimental studies have reported these microstructural features in deformed natural and synthetic polycrystalline halite [Urai et al., 1986; Peach and Spiers, 1996; Watanabe and Peach, 2002]. Besides promoting grain boundary migration, solution-precipitation processes may contribute to deformation as well [Urai et al., 1986; Spiers et al., 1990; Bos et al., 2000]. Solution-precipitation creep is likely to be the dominant deformation mechanism in the smaller grains of the wet material. The presence of similar microstructural features in natural halite rock indicates that solution-precipitation creep and fluid assisted grain boundary migration also plays a role in the deformation of halite rock in nature [Urai et al., 1987].

In the wet samples, grain boundary migration leads to grain growth due to the consumption of grains with high stored energy (i.e. the energy associated with dislocations, point defects and subgrain boundaries) by grains with low stored density. At the same time, grain size is reduced due to the nucleation of small grains at grain boundary bulges. Grain size is also reduced due to the nucleation of grains by progressive subgrain rotation as evidenced from the development of subgrain structures in some grains, grain boundaries that follow subgrain boundaries and the presence of subgrain size grains. Qualitative microstructural observations suggest that grain boundary migration is the dominant process modifying the microstructure at all conditions. This is quantitatively supported by grain boundary misorientation measurements on the same material that reveal a discrete boundary hierarchy indicative of migration dominated recrystallization [Trimby *et al.*, 2000b].

The microstructure of deformed dry polycrystalline halite shows similar evidence for active dislocation mechanisms as the microstructure of wet polycrystalline halite, i.e. linear and wavy slip lines and subgrain structure. The microstructure is dominated by grains with a well developed subgrain structure. Qualitative microstructural observations suggest that dynamic recrystallization is minor and dominated by progressive subgrain rotation. This was again quantitatively supported by grain boundary misorientation measurements on the same material that show a continuous boundary hierarchy indicative of subgrain rotation dominated recrystallization [Trimby *et al.*, 2000b]. The average and median grain size of the deformed, dry material is larger than that of the starting material, demonstrating that some grain growth has occurred. Although both the dry and wet materials were produced from halite powder of identical composition, evidence for solution-precipitation processes and extensive grain boundary migration (lobate grain boundaries, large euhedral grains) is absent in the dry material. This indicates that water is the main factor controlling the grain boundary migration rate. Instead of solution-precipitation creep, solid-state diffusion creep mechanisms, such as grain boundary (Coble) or lattice (Nabarro-Herring) diffusion creep, may have been active in small grains.

4.4.2 Flow behavior and microstructural evolution

Stress oscillations

The evolution of flow stress and grain microstructure in the wet samples is characterized by continuous work hardening with flattening of grains and development of subgrain structure up to the first peak stress. Some nucleation of grains by progressive subgrain rotation may have occurred during this stage as evidenced by the presence of small (subgrain size) grains (fig. 4.3c) and a more negatively skewed grain size distribution (table 4.3, fig. 4.5a). The oscillations in flow stress after the first peak stress can be explained by the interaction of fluid assisted grain boundary migration, leading to softening as relatively strain free grains (low internal energy) replace grains full of substructure (high internal energy), recovery and work hardening. It is inferred that the oscillations are mainly controlled by grain boundary migration, as without dynamic recrystallization, work hardening and recovery balance after sufficient strain, resulting in a constant flow stress [Sellars, 1978]. The flow stress increases when work hardening exceeds softening due to recovery and migration recrystallization. The driving force for grain boundary migration, i.e. differences in dislocation energy between adjacent grains, will increase during work hardening. This will lead to an increase in grain boundary migration with a stress peak when hardening and softening processes balance. At relative low temperature and high stress or strain rate, the work hardening rate is high with respect to the softening rate. This means that more strain is required to balance hardening and softening and reach the peak stress. Also, the amount of

weakening due to grain boundary migration is higher than at relatively high temperature and low stress or strain rate (fig. 4.1, table 4.1). Grain boundary migration spreads through the sample with a distinct recrystallization front, dividing the sample in a recrystallized and non-recrystallized part. The driving force for grain boundary migration will diminish when consumption of grains with high dislocation density approaches completion. This will lead to a decrease in grain boundary migration with a stress low when hardening and softening processes balance. After several oscillations, dynamic recrystallization becomes effectively continuous leading to a continuous balance between hardening and softening processes and a steady state flow stress [Sellars, 1978; Watanabe and Peach, 2002].

The dry samples show continuous work hardening with increasing strain at the conditions investigated. Work hardening is accompanied by the development of a clear subgrain structure in almost all grains. The work hardening rate decreases with increasing strain indicating that recovery processes are active to some extent. The microstructure and more negatively skewed grain size distribution of the deformed dry material compared to the starting material indicate that grains have nucleated by progressive subgrain rotation, comparable to the wet sample before the first stress peak.

Contribution of solution precipitation creep to flow behavior

The distinct difference in rheological and microstructural evolution between wet and dry halite can be attributed to the operation of fluid-assisted grain boundary migration. However, despite the absence of significant dynamic recrystallization before the first stress peak, the flow stress of the wet samples is much lower than for the dry samples. This indicates the operation of a process leading to water weakening independently of dynamic recrystallization. In polycrystalline halite this can occur by the enhancement of dislocation mobility (hydrolytic weakening) [Carter *et al.*, 1993] or by solution-precipitation creep [Spiers *et al.*, 1990]. The qualitative microstructural observations of this study, as well as solution-precipitation related microstructures (e.g., overgrowths) revealed by γ -irradiation of natural Asse Speisesalz and Avery Island halite rock [Urai *et al.*, 1987; Spiers and Carter, 1998], indicate that solution-precipitation creep may be important during deformation of wet polycrystalline halite. It is noteworthy that the smaller grains in the grain size distribution of all wet samples fall well in the solution-precipitation creep field of deformation mechanism maps constructed by Spiers and Carter [1998] using the solution-precipitation creep law of Spiers *et al.* [1990] and the climb and cross slip controlled dislocation creep laws of Carter *et al.* [1993].

We now investigate if the observed difference in flow stress can be explained by the contribution of solution-precipitation creep to the overall creep rate of wet polycrystalline halite. In order to quantify this contribution, an estimate of the solution-precipitation creep rate in dense polycrystalline halite is required. The solution-precipitation creep rate in dense material is well constrained and the flow rate can be related to the flow stress by [Spiers and Carter, 1998]

$$\dot{\epsilon}_{ps} = 4.7 \times 10^5 \frac{\sigma}{Td^3} \exp\left(\frac{-24.5}{RT}\right) \quad (4.2)$$

with the flow rate ($\dot{\epsilon}_{ps}$) in s^{-1} , temperature (T) in K, stress (σ) in MPa, grain size (d) in μm and the gas constant (R) in kJ/mol. This flow law has been calibrated on the basis of experiments on porous and dense polycrystalline aggregates of synthetic halite by Spiers *et al.* [1990]. Although the pre-exponential constant of (4.2) does not account for the exact

characteristics of distributed grain size, we use (4.2) as a first-order approach to describe the solution-precipitation creep rate of grains in individual classes of the grain size distribution. The contribution of solution-precipitation can be expected to be higher if the width of the distribution is taken into account (chapter 5).

The effect of solution-precipitation creep on the mechanical behavior can be evaluated using the experiments on the dry and wet sample conducted at $T=125^{\circ}\text{C}$ and $\dot{\epsilon} \approx 5 \times 10^{-7} \text{ s}^{-1}$ (samples p40t109 and p40t115, respectively, fig. 4.1b). Experiment p40t115 was selected, because this experiment was ended before the first stress peak and because microstructural observations indicated that at this point dynamic recrystallization has not significantly altered the microstructure. Because dynamic recrystallization was equally unimportant in the dry sample, differences in mechanical behavior between the two samples can be considered as due to differences in deformation mechanisms and not due to dynamic recrystallization. We assume that the dry sample deformed by dislocation mechanisms alone and that deformation of the wet sample occurred by a combination of dislocation creep (equal to the dry sample) and solution-precipitation creep (given by 4.2). Consequently, at a given stress and temperature, the strain rate in the wet sample will be higher than in the dry sample deforming at the same conditions, due to the contribution of solution-precipitation creep. Thus, more strain will be reached in the same time interval. This strain can be determined at a given stress from the solution-precipitation creep rate using (4.2) and the grain size distribution of p40t115. For this, the approach used to determine the contribution of grain size sensitive mechanisms in deformation of Carrara marble with a distributed grain size is adopted (chapter 3). In this approach, the grain size distribution before the stress peak is analyzed (sample p40t115, fig. 4.5a). The number densities of each grain size class (i) in the distribution (consisting of j classes) are converted to volume fractions (v_i) using the Stripstar computer program [Heilbronner and Bruhn, 1998]. The solution-precipitation creep rate ($\dot{\epsilon}_{ps}$) at a given stress is determined by volume averaging the strain rate in individual grain size classes ($\dot{\epsilon}_i$), given by (4.2), assuming that stress is uniform in the aggregate [Freeman and Ferguson, 1986; Wang, 1994, chapter 2]

$$\dot{\epsilon}_{ps} = \dot{\epsilon}_1 v_1 + \dot{\epsilon}_2 v_2 + \dots + \dot{\epsilon}_j v_j \quad \text{with} \quad \sigma = \sigma_1 = \sigma_2 = \dots = \sigma_j \quad (4.3)$$

The uniform stress assumption gives an upper bound for the rate of deformation in the aggregate [Freeman and Ferguson, 1986; Tullis et al., 1991, chapter 2]. A lower bound would be provided using the assumption that strain rate is uniform in the aggregate. This requires volume averaging of the local stress in individual grain size classes due to both dislocation and solution-precipitation creep mechanisms. However, these local stresses cannot be determined using the stress-strain curve of p40t109 and (4.2). As a consequence, the uniform strain rate bound cannot be calculated. If stress is uniform, within a time interval $\Delta t = t_{x+1} - t_x$, work hardening dislocation flow results in an increment of strain $\Delta \epsilon = \epsilon_{x+1} - \epsilon_x$ and stress increment $\Delta \sigma = \sigma_{x+1} - \sigma_x$, given by the stress-strain curve of p40t109 (fig. 4.1b). Using (4.3), the pressure solution creep rate in the same interval Δt can be approximated by calculating $\dot{\epsilon}_{ps}$ at the average stress $\sigma_x^{av} = (\sigma_{x+1} + \sigma_x) / 2$ in interval Δt (written as $\dot{\epsilon}_{ps}(\sigma_x^{av})$ in the following). The strain increment due to solution-precipitation creep ($\Delta \epsilon_{ps}$) over interval Δt is given by $\dot{\epsilon}_{ps}(\sigma_x^{av}) \Delta t$. The total amount of strain due to solution-precipitation creep (ϵ_{ps}) at a given stress (σ_x) can hence be calculated by summing the strain increments calculated for each stress point on the stress-strain curve of p40t109 up to σ_x .

$$\varepsilon_{ps} = \sum_l^x \Delta \varepsilon_{ps} = \sum_l^x \dot{\varepsilon}_{ps}(\sigma_x^{av}) \Delta t \quad (4.4)$$

This means that at a given stress the stress-strain curve of the dry material shifts by ε_{ps} along the strain axis. This yields a stress-strain curve of the aggregate deforming by a combination of dislocation creep and solution-precipitation creep (fig. 4.1b). The resulting curve is very close to the stress-strain curve of the wet sample p40t115, especially at the end of experiment p40t115. Differences between the calculated stress-strain curve and the curve for p40t115 might be caused by the fact that the final grain size distribution of p40t115 is used in the calculations, and not the evolution towards it. Note in this respect that the correspondence is indeed best at the end of p40t115. Under the assumptions adopted, the water weakening effect in polycrystalline halite prior to the onset of dynamic recrystallization can thus be largely explained by the contribution of solution-precipitation creep to the overall strain rate. Other weakening mechanisms (e.g. intracrystalline) are not necessary, although they cannot be completely excluded on these grounds.

Overall, grain size increases after the first stress peak. Hence, the contribution of grain size sensitive solution-precipitation creep may be expected to decrease after the peak. At least part of the difference in strength between the dry and wet samples is caused by the removal of strain hardening substructure by grain boundary migration. The contribution of solution-precipitation creep to the overall creep rate of the recrystallized material can be calculated using (4.2) and the grain size distribution for p40t114, converted to volume fractions with the Stripstar computer program [Heilbronner and Bruhn, 1998]. This yields a contribution of ~5% to the overall creep rate. However, the distribution of volume fractions of p40t114 calculated by the Stripstar program is far less accurate than for p40t115. This and the fact that (4.2) does not account for variations in standard deviation as mentioned before casts doubt on the accuracy of this estimate. If a contribution of solution-precipitation creep is calculated, using (4.2), on the basis of the median grain size alone (287 μm - p40t114), a value of 67% results, substantially higher than the 5% mentioned above.

On the basis of these quantitative analyses, we infer that solution-precipitation creep plays an important role in the deformation of wet polycrystalline halite, before and after the onset of dynamic recrystallization. In order to accurately describe the flow rate, composite flow laws should therefore be used that incorporate the contributions of solution-precipitation creep as well as dislocation creep. The relative contribution of both deformation mechanisms will be determined by the characteristics of the grain size distribution. Dislocation creep will dominate deformation of the larger grains in the distribution and solution-precipitation creep will dominate deformation of the smaller grains.

4.4.3 Comparison with previous studies

The mechanical data obtained in this study allow calibration of an empirical flow of the type given by (4.1), with a rate constant, stress exponent and apparent activation given in table 4.2. This flow law describes flow of fully recrystallized wet polycrystalline halite under the investigated conditions and incorporates the effect of dynamic recrystallization on the flow behavior. As shown above, it combines the different deformation mechanisms that may operate during steady state deformation, such as cross slip and climb controlled dislocation creep and solution-precipitation creep. The flow law allows comparison with other studies on the mechanical behavior of polycrystalline halite and with values for the apparent activation energy that were measured independently. This can provide further insight in the microphysical processes controlling deformation in polycrystalline halite.

Numerous experimental studies have been performed on natural and synthetic polycrystalline halite, which have been reviewed in several papers [see *Carter and Hansen*, 1983; *Senseny et al.*, 1992; *Carter et al.*, 1993 for reviews]. In table 4.2, flow parameters from a selection of previous studies relevant to this study are compared. In all studies, the parameters were obtained by fitting mechanical data to a power law equation of the type given in (4.1). The deformation conditions imposed in the present study correspond to the high strain rate and stress regime of *Carter et al.* [1993]. The stress exponent for the wet material is close to the value in all the other studies if the high strain rate and stress regime of *Carter et al.* [1993] is considered. The variation in apparent activation energy of the different studies is more pronounced. In fig. 4.10, strain rates of the different studies, calculated using (4.1) with the flow law parameters of table 4.2, are compared for 125 and 175°C. The flow rates of the wet samples in this study are higher than the flow rates for polycrystalline halite in all other studies for a relevant range of stresses, i.e. the wet material is weaker than all other materials tested. At the two investigated temperatures, the strength of the dry samples in this study is lower than predicted by the flow law for dry halite from *Franssen* [1994] and the flow laws for the stronger types of the natural halite rock from *Wawersik and Zeuch* [1986]. All other flow laws predict strengths in between the strength of the dry and wet samples in this study.

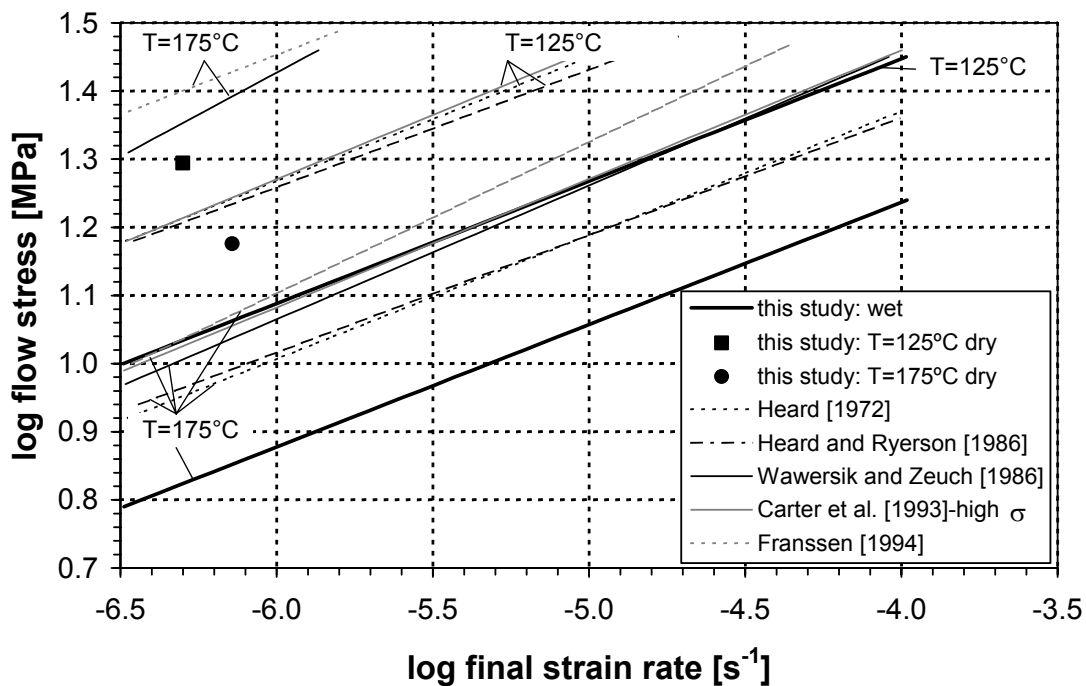


Figure 4.10 Comparison of strain rates for wet polycrystalline halite, given by the flow law from this study, and strain rates for dry polycrystalline halite with strain rates given by flow laws from previous studies, using the flow law parameters in table 4.2.

The difference in flow law parameters and strength between previous studies and the present study can have various causes, including compositional differences, differences in experimental conditions, extrapolation of flow laws beyond the range of experimental conditions and differences in water content. A definite explanation for the differences cannot be given, but we discuss two aspects emerging from this study that are of importance.

First, interpretation of the mechanical behavior in terms of deformation mechanisms is not straightforward. Except for the activation energy found by *Franssen* [1994], the apparent activation energies of all studies (table 4.2) are lower than the activation energy for lattice diffusion of the slowest diffusing chloride anion, measured independently by direct diffusion (205-221 kJ/mol) [*Laurent and Bénard*, 1957, 1958; *Laurance*, 1960; *Barr et al.*, 1965] or estimates of the activation energy for short-circuit diffusion through dislocation cores (pipe diffusion, 103-155 kJ/mol) [*Wawersik and Zeuch*, 1986; *Franssen*, 1994]. This suggests that other processes, such as cross slip of dislocations, may be rate controlling at the investigated conditions [*Skrotzki and Liu*, 1982; *Wawersik and Zeuch*, 1986] or that multiple deformation mechanisms operate [*Carter et al.*, 1993; *Franssen*, 1994]. We have shown in the previous section that solution-precipitation contributes significantly to the overall strain rate in wet polycrystalline halite. Therefore, the activation energy determined from the mechanical data might lie in between the activation energy associated with solution-precipitation creep (24.5 kJ/mol) and the activation energy associated with the rate controlling mechanism in dislocation creep. This again stresses the need to consider composite flow laws for reliable interpretation and description of mechanical data (cf. chapter 2, 5).

Another important point for the interpretation of mechanical data in terms of deformation mechanisms is the influence of strain. Most experimental studies on polycrystalline halite have investigated the mechanical behavior on the basis of stepping experiments with limited strain (typically few percent shortening) in each step or constant stress or strain rate experiments to natural strains of typically ~ 0.1 [see for example *Heard*, 1972; *Senseny et al.*, 1992; *Carter et al.*, 1993]. It is directly obvious from fig. 4.1 that steady state deformation is not reached at these low strains. This means that part of the interpretation of the mechanical data of previous studies may be based on transient deformation. Flow law parameters, such as stress exponent and apparent activation energy, derived from transient data cannot be used to make reliable inferences about active deformation mechanisms during steady state deformation. An additional complication is that for most deformation conditions a strain of ~ 0.1 is insufficient to get past the first stress peak and initiate grain boundary migration in wet polycrystalline halite. Before the first stress peak, the microstructures of wet and dry polycrystalline halite are comparable and it remains unclear if the halite material under investigation will behave similar to the dry or similar to the wet material in this study at higher strains. This is important for the application of laboratory data to the deformation of polycrystalline halite in nature, because the difference in strength between wet and dry polycrystalline halite is considerable (fig. 4.1 a, b).

4.4.4 Grain size distributions in relation to deformation conditions

In wet polycrystalline halite, the onset of dynamic recrystallization correlates with some grains consuming adjacent grains by rapid grain boundary migration. This leads to a marked increase in median, average, and maximum grain size. In addition, nucleation of small grains occurs by progressive subgrain rotation and at grain boundary bulges, leading to an increase in standard deviation of the grain size distribution (series p40t111-p40t115, table 4.3). Nucleation of new grains by both processes occurs concurrently at all conditions. Grains nucleated by progressive subgrain rotation are generally smaller than grains nucleated at grain boundary bulges [cf. *Guillopé and Poirier*, 1979], but subsequent migration hampers a clear distinction between grains originating from progressive subgrain rotation and grains originating from grain boundary bulges. During deformation, dynamic recrystallization continuously reworks the microstructure. Grain growth due to grain boundary migration and grain size reduction due to nucleation of grains act as competing processes. At steady state,

these processes can be expected to be in dynamic equilibrium resulting in a characteristic microstructure and grain size distribution.

Overall the microstructures of wet polycrystalline halite indicate that grain size decreases with increasing stress and temperature. In addition, the size of grains with migrated boundaries, free of substructure, decreases relative to the size of grains full of substructure with increasing stress and temperature. This may be due to a decrease in the rate of grain boundary migration relative to the rate at which substructure develops with increasing stress and temperature, i.e. for low stresses and temperatures grain boundary migration is relatively fast compared to grain size reduction and at these conditions grains can grow to large sizes by grain boundary migration. As a result, the standard deviation of the logarithmic grain size distribution decreases with increasing stress and temperature (fig. 4.8). Consequently, the steady state microstructure and grain size distribution, i.e. the median or average grain size and standard deviation, are uniquely related to the deformation conditions. Moreover, the trend of standard deviation with stress and temperature may be used as an indication of the grain boundary migration rate relative to the rate of grain size reduction during dynamic recrystallization.

Despite minor trends in the skewness with stress and temperature, the distributions are close to lognormal. This means that grain size is best represented by the median of the grain size distribution, which is unaffected by the width of the lognormal grain size distribution [cf. *Ranalli, 1984*]. The median grain size is related to temperature and stress (fig. 4.7a, b). Hence, the microstructure that develops during steady state can be characterized by the distribution parameters, i.e. the median and the standard deviation of the log d . This means the median and standard deviation may act as microstructural state variables, uniquely relating microstructure to deformation conditions. The present study clearly shows that variations in both standard deviation and median grain size should be accounted for in investigations to the effect of dynamic recrystallization on grain size and rheology.

4.4.5 Calibration of a recrystallized grain size piezometer

The systematic variation of stress, temperature and strain rate in this study and complete recrystallization of most wet deformed samples allows calibration of a piezometer, relating recrystallized grain size to flow stress and temperature. The results are evaluated against relevant microphysical models.

Numerous experimental studies on metals, ceramics and rock materials demonstrate that the mean recrystallized grain size (d) and flow stress (σ) are related by a relation of the type $d=K\sigma^{-p}$ where K and p (typically 0.7-1.6) are material- and mechanism-specific constants [*Takeuchi and Argon, 1976; Twiss, 1977; Drury et al., 1985; De Bresser et al., 2001*]. Various models exist that try to explain this relation [*Twiss, 1977; Derby and Ashby, 1987; De Bresser et al., 1998; Shimizu, 1998*]. The *Twiss* [1977] model is based on the assumption that there exists a unique recrystallized grain size at which the total strain energy of dislocations ordered in a recrystallized grain boundary is equal to the stored energy of the dislocations in the enclosed volume. The *Derby and Ashby* [1987] model considers dynamic recrystallization by grain boundary migration with nucleation of grains at grain boundary bulges. In this model, an estimate of the mean grain size is obtained by balancing the rate of bulge nucleation with the mean boundary migration rate [see also *Derby, 1990*]. In the *De Bresser et al.* [1998] model, it is assumed that the recrystallized grain size organizes itself in the boundary between the dislocation and diffusion creep field, regardless of the nucleation mechanism. An expression for the recrystallized grain size could be obtained assuming a constant contribution of diffusion and dislocation creep to the overall creep rate [see also *De Bresser et al., 2001*]. The *Shimizu* [1998] model considers dynamic recrystallization by progressive subgrain

rotation with intracrystalline or grain boundary nucleation of grains. In this model, a steady state recrystallized grain size is formed because of a balance between the rate of nucleation and the (radial) growth rate of the newly created grains [see also *Shimizu*, 1999].

All models predict a relation between stress and temperature and recrystallized grain size, which can be written in general form as (see chapter 1 for more details on the models and equations)

$$\left(\frac{d}{b}\right) = K \left(\frac{\sigma}{\mu}\right)^{-p} \exp\left(\frac{\Delta Q}{aRT}\right) \quad (4.5)$$

where K , p and a are constants and ΔQ is a difference in activation energy of diffusion processes involved, dependent on the characteristics of the model (cf. chapter 1). The *Twiss* [1977] model predicts $1.3 \leq p \leq 1.5$ but does not include activation energy terms (i.e. effectively $\Delta Q=0$ and the relation is temperature independent). However, the model is based on the incorrect application of equilibrium thermodynamics [*Poirier*, 1985; *Derby*, 1990; *De Bresser et al.*, 2001]. In the *Derby and Ashby* [1987] model p is related to the power law stress exponent n by $p=n/2$, $a=2$ and ΔQ represents the difference between the activation energy for lattice and grain boundary diffusion. In the *De Bresser et al.* [1998] model, $p=(n-1)/m$ and $a=m$, where m is the grain size exponent in a diffusion creep equation of the type shown in (4.2), and ΔQ is the difference in between the activation energy for dislocation and diffusion creep. In the *Shimizu* [1998] model, $p=1.25$ and $a=4$ for intracrystalline nucleation or $p=1.33$ and $a=3$ for grain boundary nucleation. For both mechanisms of nucleation, ΔQ is the difference between the activation energy for lattice diffusion that controls climb of dislocations towards sub-boundaries, but not necessarily controls creep, and grain boundary diffusion (chapter 1).

Figures 4.7a and 4.7b show the variation of the median grain size analyzed in this study with stress and reciprocal temperature. We use the median grain size in the evaluation of recrystallized grain size data, because most grain size distributions are close to lognormal. A best fit of all the median grain size data to (4.5) yields poorly constrained values for K , p and $\Delta Q/a$ and a poor correlation coefficient ($R^2=0.72$). Only samples that have been completely recrystallized and were deformed to roughly similar strain are used in this fit (table 4.1, 4.3). The majority of the data shows clear trends with stress and reciprocal temperature. Most slopes in grain size-stress space (indicating $-p$) are between -0.96 and -1.99 and most slopes in grain size-reciprocal temperature space (indicating $(\Delta Q \log(e)/aR)$) are between 306 and 694, giving $5.86 < (\Delta Q/a) < 13.29$ (fig. 4.7a, b). Four data points (indicated by crosses in fig. 4.7a, b) deviate considerably from the general trends. The reason for the deviations remains unclear, but some duplicate experiments and comparison of trends in median and average grain size show that the general trends shown by the majority of the data are robust. If the four deviating points are excluded, a best fit of the median grain size data to (4.5) yields

$$\left(\frac{d}{b}\right) = 10^{0.61 \pm 0.09} \left(\frac{\sigma}{\mu}\right)^{-1.30 \pm 0.07} \exp\left(\frac{8.59 \pm 0.92}{RT}\right) \quad (4.6)$$

where b is the magnitude of the Burgers vector ($b=3.99 \times 10^{-4} \mu\text{m}$) and μ is the shear modulus (taken as $\mu=1.5 \times 10^4 \text{ MPa}$). In this piezometric relation, K , p and Q/a are well constrained and the correlation coefficient is high ($R^2=0.96$).

If we want to evaluate this result against the theoretical models described above, the power law stress exponent for pure dislocation creep (n), the activation energies (Q) for lattice

and boundary diffusion and the grain size exponent (m) in the diffusion creep equation need to be known. The flow law parameters determined in this study (table 4.2) cannot be used, because the mechanical data in this study reflects combined dislocation and solution-precipitation creep while flow law parameters for pure dislocation creep and diffusion creep are required. Because *Carter et al.* [1993] claim that their samples deformed by pure dislocation creep without dynamic recrystallization, we take the flow parameters obtained by *Carter et al.* [1993] for pure dislocation creep (table 4.2). We take the values of their high strain rate and stress regime ($n=5.3$ and $Q=68$ kJ/mol) as the experiments of the present study were conducted under comparable high strain rate and stress conditions. In addition, we take the flow law parameters in (4.2) for the grain size exponent ($m=3$) and the activation energy for grain boundary diffusion ($Q=24.5$ kJ/mol) as we have shown that the wet samples in the present study deform by a combination of dislocation and solution-precipitation creep.

The best fit value of $p=1.30 \pm 0.07$ falls in the range of p -values predicted by the *Twiss* [1977] model, but the temperature dependence of the recrystallized grain size is not predicted by this model. The *Derby and Ashby* [1987] model then predicts $p=2.65$ and $\Delta Q=22$ kJ/mol, if the activation energy for pure dislocation creep is assumed equal to the activation energy for lattice diffusion. Both values differ considerably from the best fit values in (4.6), which means the data do not agree with the *Derby and Ashby* [1987] model. The model predicts an even higher value for ΔQ , if the activation energy for lattice diffusion obtained from independent direct diffusion measurements (205-221 kJ/mol) is considered [*Laurent and Bénard*, 1957; *Laurent and Bénard*, 1958; *Laurance*, 1960; *Barr et al.*, 1965]. The *De Bresser et al.* [1998] model predicts $p=1.43$ and $\Delta Q=15$ kJ/mol. Considering all uncertainties, this value of p is in reasonably good agreement with the data. The value for ΔQ predicted by the *De Bresser et al.* [1998] model is rather high compared to the data, but the model does predict the proper temperature dependence of recrystallized grain size. The *Shimizu* [1998] model predicts $p=1.25$ and $p=1.33$ for intracrystalline and grain boundary nucleation respectively. These values are both in good agreement with the data. However, the *Shimizu* model has been developed for recrystallization dominated by progressive subgrain rotation, while the observations on wet halite are more consistent with migration recrystallization. Further, the model predicts $\Delta Q=45-49$ kJ/mol and $\Delta Q=60-66$ kJ/mol for intracrystalline and grain boundary nucleation respectively, if the activation energy for lattice diffusion obtained from independent direct diffusion measurements (205-221 kJ/mol) is used. These values are much higher than the best fit value in (4.6). Better agreement between ΔQ predicted by the *Shimizu* [1998] model and the data might be obtained if the activation energy for pure dislocation creep from *Carter et al.* [1993] is assumed equal to the activation energy for lattice diffusion. However, it is questionable if this is justified as *Carter et al.* [1993] relate the activation energy for dislocation creep in the high strain rate and stress regime to cross slip of dislocations. Summarizing, the relation between recrystallized median grain size in wet polycrystalline halite and stress or temperature is in reasonable agreement with the *De Bresser et al.* [1998] field boundary model. The agreement with *De Bresser et al.* [1998] model suggests that dynamic recrystallization constrains grain size and rheology to the boundary between the dislocation and solution-precipitation creep fields.

The recrystallized grain size data obtained in the present study can be compared with existing piezometers for halite that were calibrated using experiments on single crystals of halite [*Guillopé and Poirier*, 1979]. They found for migration dominated recrystallization

$$\left(\frac{d}{b}\right) = 176.8 \left(\frac{\sigma}{\mu}\right)^{-1.28} \quad (4.7)$$

and for subgrain rotation dominated recrystallization

$$\left(\frac{d}{b}\right) = 13.4 \left(\frac{\sigma}{\mu}\right)^{-1.18} \quad (4.8)$$

Median grain sizes of this study are lower than predicted by (4.7) for migration recrystallization and much higher than predicted by (4.8) for subgrain rotation recrystallization for all stresses investigated. It is emphasized that *Guillopé and Poirier* [1979] measured linear intercepts, whereas the recrystallized grain size data in this study are presented by the median of the grain size distribution (calculated from the distribution of grain areas). Hence, no definite conclusion can be drawn from direct comparison of the studies. It is important, however, that (4.7) and (4.8) do not include a temperature dependence of recrystallized grain size, while the present data clearly indicate that such a temperature dependence exists.

At this point, it should be emphasized that all models for recrystallized grain size considered regard grain size as a single value (median), while considerable and systematic variation in standard deviation of individual grain size distributions exists (fig. 4.8). Variation in standard deviation can have a pronounced effect on the rheology of materials and should be taken into account in determining reliable flow parameters (chapter 2). The development and testing of a model that can account for variations in standard deviation is the scope of chapter 5 of this thesis.

4.4.6 General implications

We now give some general implications of the results on polycrystalline halite for the effect of dynamic recrystallization on rheology and grain microstructure. We focus on (1) the use of mechanical data to calibrate flow laws and infer active deformation mechanisms, (2) the calibration and application of recrystallized grain size piezometers and (3) the possibility of strain localization due to rheological weakening caused by dynamic recrystallization. We also give some implications of the results for flow of halite rock in nature.

The use of mechanical data to infer deformation mechanisms

In most rock deformation studies, mechanical data is used to calibrate single-mechanism flow laws with one set of flow law parameters, such as stress exponent and activation energy. The present study shows that multiple mechanisms may contribute to the overall strain rate, especially if there is a large spread in grain size. Wet polycrystalline halite shows some distinct microstructural features, e.g. euhedral crystal faces, which can be ascribed to solution-precipitation processes. The operation of multiple deformation mechanisms is therefore relatively easy to detect, despite the fact that the microstructure is dominated by evidence for dislocation processes. In other rock materials, microstructural evidence for diffusion creep might be more difficult to detect and might be overshadowed by evidence for dislocation creep. If multiple deformation mechanisms operate, single-mechanism flow laws, obviously, cannot be used to infer the active deformation mechanisms, because the flow law parameters are the result of the combination of deformation mechanisms. In addition, the microphysical basis for the flow law required to extrapolate mechanical data beyond the range of experimental conditions to natural conditions is lacking. Hence, it is important to consider all deformation mechanisms that may operate during deformation and calibrate composite flow laws on the basis of theoretical flow laws of the

individual deformation mechanisms involved (cf. chapter 2). The present study also illustrates that high strain experiments at constant deformation conditions should be used to calibrate flow laws and interpret mechanical data, because the flow behavior of materials may change significantly after the strain that is usually reached in axial compression deformation experiments.

Calibration and application of recrystallized grain size piezometers

The present study shows that it is important to take the effect of strain and temperature on recrystallized grain size into account in the calibration of piezometers. Clearly, wet polycrystalline halite should be deformed way past the first stress peak and past the onset of grain boundary migration, i.e. to strains \sim of 0.3 for most deformation conditions, in order to obtain results to calibrate a meaningful piezometer. The effect of temperature on recrystallized grain size can be significant and stresses associated with flow of halite rock in nature will be over- or underestimated if temperature is unaccounted for. As shown in figs. 4.1a, b and 4.2, flow stress of wet polycrystalline halite may differ up to a factor \sim 2 at the same median grain size of 164 μm for temperature increasing from 100 to 240°C. Comparison of the piezometer given in (4.6) with existing piezometers for halite given in (4.7) and (4.8) can serve as an example of the fact that in many studies, a temperature dependence of recrystallized grain size remains unrecognized because the role of temperature was not systematically explored [De Bresser *et al.*, 2001]. The present study shows that there is reasonable agreement between the recrystallized grain size data of wet polycrystalline halite and the De Bresser *et al.* [1998] field boundary model. In the De Bresser *et al.* [1998] model, the piezometer is a mathematical expression of the diffusion-dislocation field boundary, if this boundary is defined as a line where the relative contribution of diffusion and dislocation creep to the overall strain rate is constant. This provides a physical meaning to piezometric relations, which is required to reliably apply them to natural situations.

Weakening and localization

It has often been proposed that dynamic recrystallization can lead to rheological weakening by grain size reduction, inducing a switch in deformation mechanism from grain size insensitive dislocation creep to grain size sensitive diffusion creep [White *et al.*, 1980; Rutter and Brodie, 1988; Karato and Wu, 1993] or by progressive removal of strain hardening substructure by grain boundary migration [Poirier, 1980; White *et al.*, 1980; Rutter, 1998]. This has led to the notion that dynamic recrystallization may be the mechanism providing the rheological weakening required to initiate strain localization in nature [e.g. Drury *et al.*, 1991]. Rheological weakening by a switch in deformation mechanism has been disputed for single phase materials, because calibrated recrystallized grain size-stress relations are restricted to the dislocation creep field for most relevant deformation conditions [Etheridge and Wilkie, 1979; Poirier, 1985; Braun *et al.*, 1999] or are confined to the boundary zone between the diffusion and dislocation creep fields [De Bresser *et al.*, 2001]. The present study shows that a switch from dislocation to solution-precipitation is hampered by grain growth due to grain boundary migration, although there is widespread evidence for grain size reduction due to nucleation of grains by progressive subgrain rotation or by bulging of grain boundaries. Therefore, we corroborate that a switch in deformation mechanism and associated major rheological weakening is unlikely to occur in materials in which grain growth is relatively fast, such as wet polycrystalline halite.

Our microstructural observations on samples p40t115 and p40t112 have shown that the observed decrease in flow stress between the first stress peak and first stress low in wet

polycrystalline halite is due to the complete replacement of grains with high internal energy with grains of low internal energy. Despite this distinct difference in the microstructure at the first stress peak and first stress low, bulk weakening of the sample does not exceed 15%. In addition, grain boundary migration does not result in a stable zone where deformation concentrates. Instead, grain boundary migration was observed to spread through the sample resulting in homogeneous deformation with ongoing deformation. Therefore, it is concluded that weakening due to progressive removal of strain hardening substructure by grain boundary migration is insufficient to lead to strain localization in wet polycrystalline halite. Given that halite is a material with high grain boundary migration rates, this conclusion is expected to be generally valid, holding for geological materials with lower migration rates. Strain localization may thus only occur if other weakening mechanisms, such as geometrical softening by the development of a crystallographic preferred orientation [Poirier, 1980], or metamorphic reactions [Visser *et al.*, 1995] operate or if grain growth is inhibited [Olgaard, 1990].

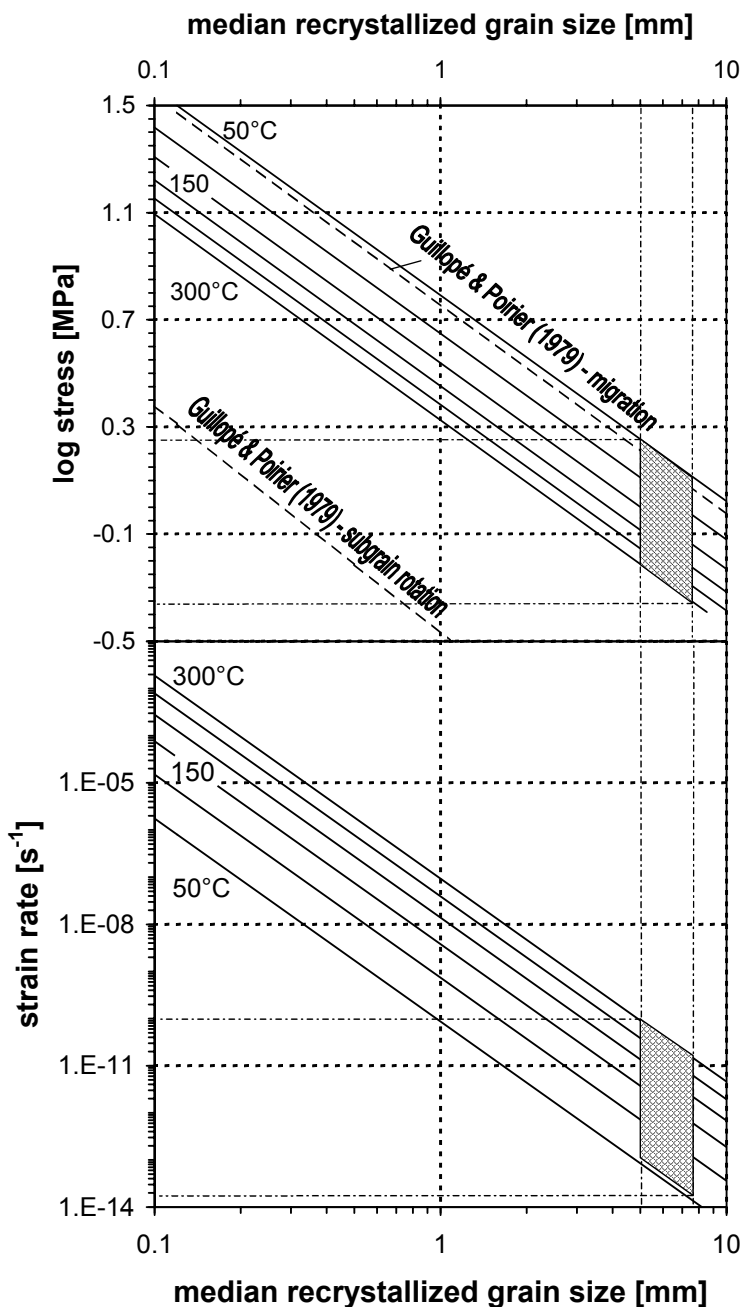


Figure 4.11 Estimate of flow stresses and rate of deformation of halite rock in nature (shaded area) using the piezometer and flow law calibrated in this study. For comparison, piezometers for migration and subgrain rotation dominated recrystallization from Guillopé and Poirier [1979] are indicated.

Deformation of halite in nature

The piezometer and flow law for dynamic recrystallized wet halite can be used to constrain deformation of halite rock under conditions relevant to nature. If the median recrystallized grain size of the halite rock and deformation temperature are known, the piezometer gives an estimate of the flow stress involved, which can be coupled to the rate of deformation using the flow law. This is illustrated in fig. 4.11. Grain sizes of typically ~5 mm (Asse Speisesalz anticlinal salt, *Urai et al.* [1986]), ~6 mm (Gulf of Mexico salt sheets, *Spiers and Carter* [1998]) or ~7.5 mm (Avery Island domal salts, *Carter et al.* [1993]) have been reported for natural halite rock. For these grain sizes and deformation temperatures of 50-300°C, the piezometer predicts flow stresses in the range of 0.4-1.8 MPa and the flow law predicts strain rates in the range of 1×10^{-14} - $9 \times 10^{-11} \text{ s}^{-1}$, depending on temperature. These values are in agreement with estimates of flow stresses and strain rates associated with the flow of halite rock in nature [*Carter et al.*, 1982; *Talbot and Jackson*, 1987; *Carter et al.*, 1993; *Spiers and Carter*, 1998]. It is emphasized that the piezometer for migration dominated recrystallization of *Guillopé and Poirier* [1979] predict flow stresses in the upper part of the stress range, independent of temperature. The present study shows that the piezometer of *Guillopé and Poirier* [1979] tend to overestimate flow stresses, in particular if deformation of the halite rock in nature occurred at higher temperatures ($T > 50^\circ\text{C}$). The piezometer and flow law for wet polycrystalline halite obtained in this study also provides better constraints for flow of polycrystalline halite relevant to geo-engineering applications, such as radioactive waste disposal in salt caverns or borehole closure [*Carter and Hansen*, 1983; *Peach*, 1991; *Aubertin and Hardy Jr.*, 1998].

4.6 Summary and conclusions

Wet (>10 ppm water) and dry (≤ 5 ppm water) polycrystalline halite have been deformed to natural strains of 0.1-0.7 at a strain rate of 5×10^{-7} - $1 \times 10^{-4} \text{ s}^{-1}$, temperature of 75-240°C and stress of 7-22 MPa to investigate the effect of dynamic recrystallization on rheology, microstructure and grain size distribution. The following conclusions can be drawn:

1. At the investigated conditions, wet polycrystalline halite deforms by a combination of climb or cross slip controlled dislocation creep and solution-precipitation creep. Dynamic recrystallization is dominated by fluid-assisted grain boundary migration. Small-sized new grains are formed by a combination of nucleation at grain boundary bulges and progressive subgrain rotation. Dry polycrystalline halite deforms by climb or cross slip controlled dislocation creep alone. Dynamic recrystallization is very limited and involves progressive subgrain rotation with limited grain growth. Extensive grain boundary migration, resulting in lobate or euhedral grains, is absent in the dry material.
2. Wet polycrystalline halite shows work hardening to a peak stress followed by oscillations in flow stress. The oscillations in flow stress can be explained by the operation of fluid-assisted grain boundary migration. Grain boundary migration results in an increase in median grain size and standard deviation. At high strains where mechanical steady state is approached, grain growth and grain size reduction balance, leading to a grain size distribution that is characteristic of the deformation conditions. Dry polycrystalline halite shows continuous work hardening accompanied by grain growth for the investigated strains and deformation conditions. The higher flow strength of the dry samples compared with the wet samples up to the first peak stress (factor 2),

can be explained by the operation of fluid-assisted grain boundary migration and solution-precipitation creep in the wet samples, while the latter process is inactive in the dry material.

3. The (near) steady state mechanical data obtained for the wet polycrystalline halite can be empirically described by a Dorn type power law rate equation with $n=5.6$ and $Q=80$ kJ/mol. The flow law is an improvement of previously available (low strain) flow laws for halite, because it is based on experiments to strains high enough to completely recrystallize most samples. It predicts realistic stress and strain rate under natural conditions. However, the inference of composite flow behavior (dislocation plus solution precipitation creep) adds weight to the importance of using composite flow laws based on a theoretical approach rather than simple empirical relations.
4. Analysis of the recrystallized grain size distributions of all samples revealed that the median grain size and standard deviation of the distribution are dependent on stress and temperature. The recrystallized grain size data are in agreement with the field boundary model from *De Bresser et al.* [1998], suggesting that grain size and rheology of dynamically recrystallizing materials will be confined to the diffusion-dislocation creep boundary. As a consequence, dynamic recrystallization of halite does not lead to major rheological weakening. Development of strain free grains in the material, by relatively fast grain boundary migration only leads to limited rheological weakening in wet polycrystalline halite.

Chapter 5

A model relating grain size distribution to the rheology of dynamically recrystallizing rock materials

5.1 Introduction

From both experimental and theoretical studies, it is well established that the microstructure of a material can be extensively modified by recrystallization during deformation. A relation between flow stress (σ) and the recrystallized grain size (d) that develops during steady state deformation, of the type $\sigma \propto d^{1/p}$ where p is a constant, has generally been found for metals and ceramics [Takeuchi and Argon, 1976; Sellars, 1978; Humphreys and Hatherly, 1996] as well as geological materials [Twiss, 1977; Drury *et al.*, 1985]. Recrystallized grain size versus stress relations for geological materials can be used as a piezometer to estimate the paleo-stress associated with the deformation of dynamically recrystallized tectonites in nature [Christie and Ord, 1980; Etheridge and Wilkie, 1981; White *et al.*, 1985].

Deformation in natural tectonites is often found to be localized in zones of recrystallized rock material. Several mechanisms have been proposed that may cause localization in natural rocks, almost all of them being associated with rheological weakening [e.g., White *et al.*, 1980; Vissers *et al.*, 1995; Jin *et al.*, 1998]. In particular, recrystallized grain size versus stress relations have been repeatedly used in combination with deformation mechanism maps to explore the possibility of weakening and associated strain localization due to grain refinement by dynamic recrystallization [Rutter and Brodie, 1988; Karato and Wu, 1993; Govers and Wortel, 1995]. In such approach, σ - d relations are considered to be independent of the active deformation mechanisms, making a recrystallization induced switch in deformation mechanism from dislocation to diffusion creep possible if the relation transects the boundary between the diffusion and dislocation creep fields. However, evaluation of theoretical models for recrystallized grain size versus stress relations against experimental σ - d data (chapter 1) suggests that dynamic recrystallization and creep behavior cannot be regarded as independent. Rather, a direct relationship between recrystallized grain size and active deformation mechanisms exists, with the recrystallized grain size falling in the boundary between diffusion and dislocation creep fields [cf. De Bresser *et al.*, 2001]. This is explained by the hypothesis that the mechanism boundary acts as an attractor for recrystallized grain size, because small grains deforming by diffusion creep tend to grow towards the field boundary, while large grains deforming by dislocation creep tend to be reduced towards that boundary by dynamic recrystallization. Hence, grain growth and grain size reduction processes will tend to balance during steady state deformation, rendering a dynamically stable recrystallized grain size set up in the neighborhood of the diffusion-dislocation creep field boundary.

One consequence of a direct relationship between recrystallized grain size and active creep mechanisms is that temperature cannot be *à priori* ignored, while conventional σ - d relations usually do not include temperature. So far, experimental support for a temperature dependence of recrystallized grain size is limited, but some experimental evidence has been presented [Mercier *et al.*, 1977; Ross *et al.*, 1980; Tungatt and Humphreys, 1984; De Bresser *et al.*, 1998]. These studies indicate that temperature only weakly influences recrystallized grain size and may be noticed only in studies that systematically explore the role of temperature. This is corroborated by the results obtained from new systematic deformation experiments on natural Carrara marble (chapter 3) and synthetic polycrystalline halite (chapter

4). A possible effect of temperature should be taken into account when using σ - d relations in paleo-piezometry.

Another consequence of the inferred direct relationship between recrystallized grain size and active creep mechanisms is that grain size needs to be distributed to allow grain growth and grain size reduction to occur simultaneously. Dynamically recrystallized rock materials invariably exhibit a grain size distribution that may vary considerably in width (expressed by the standard deviation of the distribution) as well as in median or average grain size (cf. chapters 3 and 4) [Michibayashi, 1993; Dijkstra, 2001]. The importance of this has been demonstrated in chapter 2, where it has been shown that variation in distribution width can have a pronounced effect on the rheology of materials. This effect cannot be ignored. Only recently though, measurement of grain size distribution instead of determination of a single, mean value has become standard [e.g. Heilbronner and Bruhn, 1998; Post and Tullis, 1999; Pieri et al., 2001a]. However, theoretical models for dynamic recrystallization as well as formulations of flow laws used so far generally regard grain size as single-valued, and consequently cannot account for variations in the width of the grain size distribution. Obviously, this gap between the demonstrated effect of grain size distribution and the practical application in σ - d equations that are related to rheological behavior needs to be filled.

Aim now of the present chapter is to develop a model that relates recrystallized grain size to rheology taking the distribution of grain size and temperature into account. We use the composite diffusion-dislocation creep laws derived for materials with a lognormal grain size distribution in chapter 2, and combine these with the field boundary model [De Bresser et al., 1998; 2001 – see also chapter 1]. The result is a model equation that relates median grain size and standard deviation to stress and temperature and incorporates flow parameters for diffusion and dislocation creep. The model is tested against the experimental data obtained on wet polycrystalline halite (chapter 4). The obtained model allows more reliable estimation of deformation conditions in nature since it is not hindered by inconsistencies between extrapolated flow laws and extrapolated σ - d relations. It thereby improves analysis of the role of grain microstructure evolution in weakening and localization.

5.2 Model Development

The model addresses a single phase polycrystalline material with lognormally distributed grain size (see chapter 2), undergoing steady state deformation by GSS and GSI mechanisms that operate as independent, parallel-concurrent processes [Poirier, 1985]. If stress is assumed to be uniform throughout the material, the composite diffusion-dislocation creep law can be written as (chapter 2)

$$\dot{\epsilon}_{\sigma} = \left[\frac{A_{diff} b D_{diff} \mu}{kT} \left(\frac{b}{\exp\left[\left(3 - \frac{1}{2}m\right)\phi^2\right] d_{med}} \right)^m \left(\frac{\sigma_{\sigma}}{\mu} \right) \right] + \left[\frac{A_{disl} b D_{disl} \mu}{kT} \left(\frac{\sigma_{\sigma}}{\mu} \right)^n \right] \quad (5.1)$$

All symbols used are defined in table 2.1 (chapter 2). If strain rate is uniform throughout the material, strain rate can be approximated by a composite flow law of the type

$$\dot{\epsilon}_{\dot{\epsilon}}^{approx} = \left\{ \left[\frac{A_{diff} b D_{diff} \mu}{kT} \left(\frac{b}{\exp\left[\left(3 + \frac{1}{2}m\right)\phi^2\right] d_{med}} \right)^m \left(\frac{\sigma_{\dot{\epsilon}}}{\mu} \right) \right] + \left[\frac{A_{disl} b D_{disl} \mu}{kT} \left(\frac{\sigma_{\dot{\epsilon}}}{\mu} \right)^n \right] \right\} \left\{ \frac{1}{1 - F(\bar{\sigma}_{\dot{\epsilon}}^*, \phi, n, m)} \right\}$$

$$\text{where } \bar{\sigma}_{\dot{\epsilon}}^* = \bar{\sigma}_{\dot{\epsilon}} / \bar{\sigma}_{\dot{\epsilon}}^{int} \quad \text{with} \quad \bar{\sigma}_{\dot{\epsilon}}^{int} = \left(\frac{A_{diff} D_{diff}}{A_{disl} D_{disl}} \right)^{\frac{1}{n-1}} \left(\frac{b}{\exp\left[\left(3 + \frac{1}{2}m\right)\phi^2\right] d_{med}} \right)^{\frac{m}{n-1}} \quad (5.2)$$

In (5.2), $F(\bar{\sigma}^*, \phi, n, m)$ represents a function with three parameters that are related to the stress exponent (n), grain size exponent (m) and standard deviation (ϕ). It needs to be incorporated to keep the error between the approximated strain rate and the true strain rate, determined numerically, at acceptable levels for high values of n ($n \approx 5$) and ϕ ($\phi \approx 1.2$). Its exact meaning and values for $m=2$, $3 < n < 5$ and $0 < \phi < 1.2$ are given in chapter 2. Flow laws (5.1) and (5.2) describe bounds on the rate of deformation in a single phase material with a distributed grain size, in a similar manner as uniform stress or strain rate provide bounds on the rate of deformation in polyphase materials [Raj and Ghosh, 1981; Tullis et al., 1991]. Both flow laws incorporate a diffusion creep term that is dependent on the median grain size and standard deviation of the lognormal grain size distribution, and a dislocation creep term that is grain size insensitive.

As a next step, we apply the field boundary model formulated for single-fixed grain size [De Bresser et al., 1998; 2001], which assumes that the steady state grain size d that develops during dynamic recrystallization is set up in the boundary between the diffusion and dislocation creep fields. This concept is easily envisaged if a single-phase polycrystal is considered with a specific grain size distribution consisting of small grains and large grains. The small grains dominantly deform by diffusion creep and are likely to grow, while the large grains dominantly deform by dislocation creep and are likely to be reduced by dynamic recrystallization. If this rationale holds, both deformation mechanisms will have a contribution to the overall creep rate and because diffusion and dislocation creep mechanism are parallel-concurrent [Poirier, 1985], their strain rates are additive. At the boundary, both mechanisms contribute equally, but the recrystallized grain size might adjust itself to a different relative contribution of diffusion and dislocation creep [De Bresser et al., 2001], written as

$$\dot{\epsilon}_{diff} / \dot{\epsilon}_{disl} = U \quad (5.3)$$

This expression has already been used to derive a relation between stress, temperature and the recrystallized grain size (chapter 1), but can now be modified using (5.1) or (5.2) to include grain size distribution (assuming a lognormal shape of the distribution, characterized by median d and standard deviation ϕ in log-space). If stress is uniform, substitution of (5.1) in (5.3) yields

$$\left(\frac{\sigma}{\mu} \right) = \left(\frac{A_{diff} D_{0diff}}{U A_{disl} D_{0disl}} \right)^{\frac{1}{n-1}} \left(\frac{b}{\exp\left[\left(3 - \frac{1}{2}m\right)\phi^2\right] d_{med}} \right)^{\frac{m}{n-1}} \exp\left(\frac{Q_{disl} - Q_{diff}}{(n-1)RT} \right) \quad (5.4)$$

If strain rate is uniform through the aggregate, the physical meaning of (5.3) is not straightforward, because bulk strain rate is not an the independent variable but dependent on the distribution of stress in the polycrystal. The volume average of the stress in individual grains determines the overall creep rate (chapter 2) and therefore the contributions of the diffusion and dislocation creep rate to the overall creep rate cannot be simply expressed as a ratio. However, this problem only arises if both mechanisms contribute significantly to the overall creep rate. The diffusion and dislocation creep terms in (5.2) describe the pure

diffusion and dislocation creep rate if strain rate is uniform. This means that the position of lines (in σ - d space) parallel to the field boundary can be determined by (5.3), but that these lines may not be used to quantify the relative contribution of both mechanisms to the overall creep rate. Substitution of (5.2) in (5.1) yields

$$\left(\frac{\sigma}{\mu}\right) = \left(\frac{A_{diff} D_{0diff}}{U A_{disl} D_{0disl}}\right)^{\frac{1}{n-1}} \left(\frac{b}{\exp\left[\left(3 + \frac{1}{2}m\right)\phi^2\right] d_{med}}\right)^{\frac{m}{n-1}} \exp\left(\frac{Q_{disl} - Q_{diff}}{(n-1)RT}\right) \quad (5.5)$$

It should be emphasized at this point that U in expressions (5.4) and (5.5) is not necessarily a constant for all deformation conditions, as U will be determined by the relative rates of grain size reduction and grain growth processes. However, for sufficiently small ranges of deformation conditions, U may be assumed constant. Full evaluation of the magnitude of U and its dependence on deformation conditions can only be performed using models that describe evolution of grain size distribution due to the different microphysical processes involved in dynamic recrystallization [e.g. *Derby and Ashby, 1990; Shimizu, 1998*], which is beyond the scope of this paper.

Equations (5.4) or (5.5) now form an improved relationship between recrystallized grain size and flow stress, taking into account a lognormal distribution of grain size. The relation is directly linked to the active creep mechanisms via the parameters n and Q_{disl} (for dislocation creep) and m and Q_{diff} (for diffusion creep), respectively. Note that (5.4) and (5.5) are temperature dependent as long as the two activation energy terms are not equal.

Table 5.1 Selected experiments and grain size distribution data for experimentally deformed and fully recrystallized wet polycrystalline halite (cf. chapter 4).

test	flow stress [†]	strain rate [†]	temp. [†]	natural strain	median grain size	standard deviation for ln(d)
	[MPa]	[s ⁻¹]	[°C]		[μm]	
7RS150	7.2	5.3 x 10 ⁻⁷	149	0.29	355	1.15
7RS200	7.5	2.4 x 10 ⁻⁶	203	0.30	269	1.24
7RS240	7.3	1.6 x 10 ⁻⁵	243	0.33	380	1.05
10RS240	9.5	1.3 x 10 ⁻⁴	243	0.34	163	0.82
11RS125	10.8	5.4 x 10 ⁻⁷	121	0.31	161	1.06
11RS150a	11.3	2.2 x 10 ⁻⁶	150	0.31	322	1.01
11RS150b	11.3	1.4 x 10 ⁻⁶	150	0.30	230	1.06
11RS175	10.9	6.6 x 10 ⁻⁶	174	0.30	202	0.95
11RS200	11.1	2.4 x 10 ⁻⁵	202	0.36	183	0.90
13RS125	13.3	1.3 x 10 ⁻⁶	125	0.30	193	0.97
13RS150	13.3	4.5 x 10 ⁻⁶	150	0.32	173	0.80
14RS100	13.6	5.3 x 10 ⁻⁷	99	0.29	158	1.05
14RS150	14.4	6.6 x 10 ⁻⁶	150	0.32	159	0.82
14RS175	13.9	5.0 x 10 ⁻⁵	171	0.44	133	0.93
18RS100	17.9	2.8 x 10 ⁻⁶	100	0.29	164	0.97
18RS125	17.7	7.4 x 10 ⁻⁶	126	0.34	136	0.86
18RS150	17.6	3.6 x 10 ⁻⁵	148	0.46	124	0.85
22RS100	22.1	7.5 x 10 ⁻⁶	99	0.38	116	0.93

[†] Flow stress, temperature, strain rate and pressure averaged over a strain of 0.01 at the end of the test are quoted.

5.3 Evaluation of the model using data on wet polycrystalline halite

We will now test the model given by (5.4) and (5.5) against the data for wet polycrystalline halite, obtained in chapter 4. Most of the wet polycrystalline halite samples were completely recrystallized and are therefore favored above the partially recrystallized samples of Carrara marble (chapter 3) in evaluating the model. Details on the experimental method and data on wet polycrystalline halite have been described in detail in chapter 4. Only samples that have completely recrystallized and have been deformed to roughly similar strain are used (table 5.1). The standard deviations determined for the logarithmic grain size $^{10}\log(d)$, quoted in table 4.3, are converted to standard deviations for natural logarithmic grain size $\ln(d)$ to allow direct substitution in (5.4) and (5.5). In this way, the distributions analyzed in chapter 4 are approximated by a lognormal grain size distribution. This is a viable approach as shown by the example distribution of fig. 5.1.

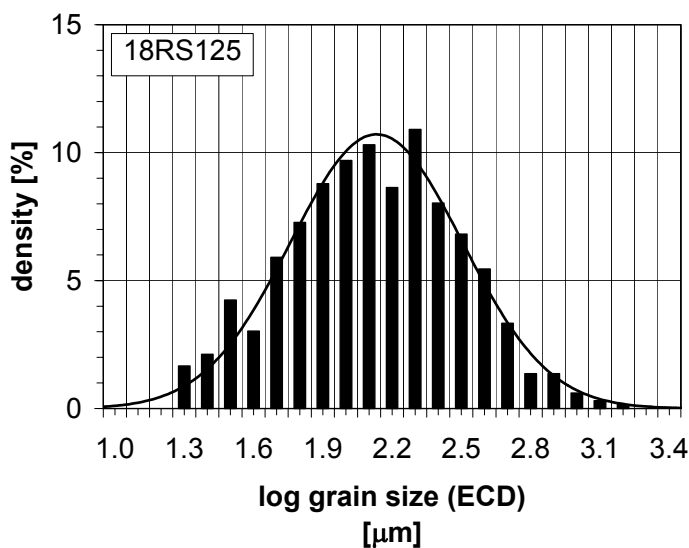


Figure 5.1 Grain size distribution for a representative fully recrystallized sample of wet polycrystalline halite compared with an ideal, continuous lognormal grain size distribution.

In order to test the model, flow law parameters for pure diffusion creep and pure dislocation creep for polycrystalline halite are required (assuming that the effect of grain boundary migration on pure dislocation creep is limited). Analysis of mechanical data and microstructures of deformed dry polycrystalline halite indicates that it predominantly deforms by dislocation creep processes, without evidence for significant contribution of diffusion creep mechanisms (chapter 4). *Carter et al.* [1993] claim that samples of Avery Island natural halite deformed by pure cross slip controlled dislocation creep at conditions (high strain rate, high stress) similar to the conditions for which our recrystallized grain size data was obtained. Accordingly, the flow law defined by *Carter et al.* [1993] is taken as representing pure dislocation creep. Flow law parameters are given in table 5.2. In contrast, wet polycrystalline halite shows widespread evidence for dislocation creep as well as solution-precipitation processes. The flow law for solution-precipitation creep in dense aggregates of wet synthetic polycrystalline halite is well defined [*Spiers et al.*, 1990; *Spiers and Carter*, 1998]. Using this flow law, we have shown in chapter 4 that the difference in strength between the dry and wet polycrystalline halite samples could be largely explained by the joint activity of solution-precipitation creep and dislocation creep mechanisms in the wet material, as opposed to the single dislocation creep deformation of the dry samples. The solution-precipitation creep law of *Spiers and Carter* [1998] thus can be taken as representative of diffusion creep in wet polycrystalline halite aggregates. Accordingly, the flow parameters are used as input for the

model (table 5.2). In order to calculate the rate constant A_{diff} , we assume that the grain size distribution of the material used to calibrate the solution-precipitation flow law is similar to the grain size distribution of the starting material in the present study (fig. 4.4). This is a realistic assumption as the sample preparation procedure described in chapter 4 was very similar to that used to produce the material the flow law was calibrated for [Spiers *et al.*, 1986]. It does mean, however, that A_{diff} is different for the uniform stress and uniform strain rate case, because of differences in the distribution terms containing median grain size and standard deviation (compare (5.1) and (5.2), see table 5.2).

Table 5.2 Constants and flow law parameters for solution-precipitation creep [Spiers *et al.*, 1990; Spiers and Carter, 1998] and cross slip controlled dislocation creep [Carter *et al.*, 1993] in polycrystalline halite used for the evaluation of the presented model against experimental data on wet polycrystalline halite.

parameter	value	dimensions	source/remarks
$A_{diff} \frac{\pi\delta}{b} D_{0diff}$	1.90×10^{-3}	-	for uniform stress, calculated using the rate constant from Spiers and Carter [1998] and values for b and μ from Frost and Ashby [1982]
$A_{diff} \frac{\pi\delta}{b} D_{0diff}$	1.05×10^{-1}	-	for uniform strain rate, calculated using the rate constant from Spiers and Carter [1998] and values for b and μ from Frost and Ashby [1982]
Q_{diff}	24530	J.mol ⁻¹	Spiers <i>et al.</i> [1990]
m	3	-	Spiers <i>et al.</i> [1990]
$A_{disl} D_{0disl}$	1.87×10^{-3}	-	calculated using the rate constant and stress exponent quoted in Carter <i>et al.</i> [1993] and values for b and μ from Frost and Ashby [1982] for $T=100^\circ\text{C}$
Q_{disl}	68100	J.mol ⁻¹	Carter <i>et al.</i> [1993]
n	5.3	-	Carter <i>et al.</i> [1993]
b	3.99×10^{-10}	m	Frost and Ashby [1982]
μ	1.5×10^{10}	Pa	Frost and Ashby [1982] for $T=300$ K, small temperature dependence neglected
k	1.381×10^{-23}	J.K ⁻¹	
R	8.314	J.mol ⁻¹ .K ⁻¹	

5.3.1 Deformation mechanism maps of grain size versus stress including a distribution term

Figure 5.2a shows the distribution data from table 5.1 plotted in a deformation mechanism map for stress versus the distribution term $\exp((3-1/2m)\phi^2)d_{med}$ for the case of uniform stress (5.1), with $m=3$ (table 5.2). Strain rate contours are indicated as well. The map is drawn for $T=150^\circ\text{C}$, but distribution data for the temperature range $125-175^\circ\text{C}$ are included. The field boundary is defined as the region where both diffusion and dislocation creep contribute for more than 10% to the overall strain rate, indicated by the lines with $U=0.11$ and $U=10$. In addition, the position of the line where both mechanisms contribute equally to the overall strain rate ($U=1$) is indicated. All the distribution data fall in the diffusion-dislocation creep field boundary.

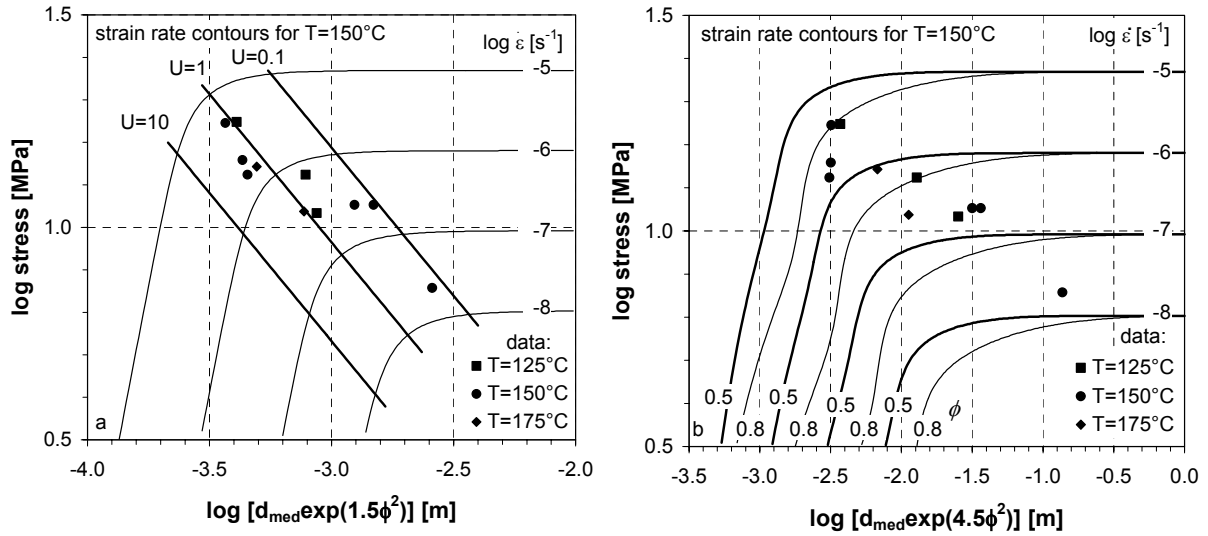


Figure 5.2 Deformation mechanism maps of stress versus the distribution term with strain rate contours for $T=150^\circ\text{C}$. Experimental data of wet polycrystalline halite for $T=125\text{--}175^\circ\text{C}$ (table 5.1) are superimposed. (a) Uniform stress case with lines for $U=0.11$, 1 and 10 denoting 10, 50 and 90% contribution of diffusion creep. (b) Uniform strain rate case with strain rate contours for $\phi=0.5$ and $\phi=0.8$.

A map similar to that of fig. 5.2a can be drawn for uniform strain rate with strain rate contours that differ with standard deviation (fig. 5.2b), using the distribution term $\exp((3+1/2m)\phi^2)d_{med}$ with $m=3$. As shown in chapter 2, the width of the boundary region spreads out considerably with increasing standard deviation. However, the accuracy of the composite flow law given by (5.2) decreases with increasing standard deviation due to a reduced effectiveness of the error-reducing function $F(\bar{\sigma}^*, \phi, n, m)$ (as can be observed by the irregularity of the contours at $\phi=0.8$). The $U=0.11$, 1 and 10 lines are not included in the map, because for uniform strain rate these are merely lines parallel to the field boundary and do not indicate the contribution of diffusion creep to the overall strain rate as in the uniform stress case (section 5.2). The map can be used, however, to show that the distribution data also falls in the region where both mechanisms contribute significantly to the overall strain rate (field boundary) for uniform strain rate, consistent with the results of fig. 5.2a. Note at this point that strain rate contours have been drawn for standard deviations ($\phi=0.5$ and $\phi=0.8$) that are low in comparison with the distribution data (table 5.1), because the error in strain rate increases towards higher standard deviations. As the width of boundary region spreads with increasing standard deviation (compare contours for $\phi=0.5$ and $\phi=0.8$), the data will be positioned even further into the boundary for higher standard deviations.

5.3.2 Deformation mechanism maps of stress versus strain rate

The flow laws given in (5.1) and (5.2) can be written in normalized form (chapter 2) as

$$S = \left[C \left(\frac{\sigma}{\mu} \right) + \left(\frac{\sigma}{\mu} \right)^n \right] \left[\frac{1}{1 - F(\bar{\sigma}^*, \phi, n)} \right] \quad (5.6)$$

$$\text{where } S = \frac{\dot{\epsilon}kT}{A_{disl}bD_{disl}\mu} \quad \text{and} \quad C = \frac{A_{diff}D_{0diff}}{A_{disl}D_{0disl}} \left(\frac{b}{X} \right)^m \exp\left(\frac{Q_{disl} - Q_{diff}}{RT} \right)$$

In this expression, $X = \exp[(3-m/2)\phi^2]d_{med}$ and $F(\bar{\sigma}^*, \phi, n) = 0$ for uniform stress and $X = \exp[(3+m/2)\phi^2]d_{med}$ and $F(\bar{\sigma}^*, \phi, n)$ represents the same function as in (5.2) for uniform strain rate. The advantage of (5.6) is that universal deformation mechanism maps can be constructed of normalized strain rate S to the normalized stress (σ/μ) for different values of C containing the median grain size and standard deviation. This allows data of different stress, temperature and grain size distribution to be plotted in a single diagram.

Fig. 5.3a and 5.3b show universal mechanism maps drawn for wet polycrystalline halite for uniform stress and strain rate (calculated using the flow law parameters of table 5.2). For uniform stress, the position of the $U=0.11$, 0.1 and 10 lines is fixed for all standard deviations and indicate a 90, 50 or 10% contribution of diffusion creep to the overall strain rate. For uniform strain rate, the position of the $U=0.11$, 0.1 and 10 lines are not included because of reasons mentioned before. Values of S for the distribution data of table 5.1 have been calculated using (5.6) and the data are indicated on both maps. The distribution data plot close to the boundary region for uniform stress and in the boundary for uniform strain rate. In addition, the slope of the best fit line through the data points is sub-parallel (slope: 4.58 ± 0.39) to the lines with a constant value of U denoting the diffusion-dislocation creep boundary zone (slope: 5.3, equal to stress exponent n).

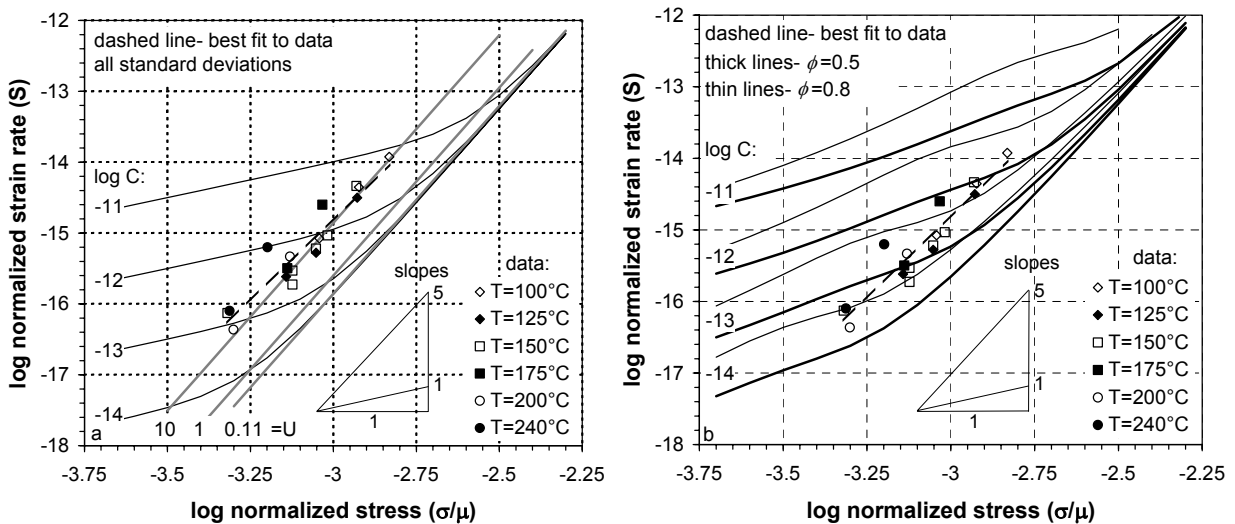


Figure 5.3 Deformation mechanism map of normalized strain rate S versus normalized stress σ/μ with contours of the normalized parameter C . Experimental data of wet polycrystalline halite (table 5.1) and best fit line through the data are superimposed. (a) Uniform stress with lines for $U=0.11$, 1 and 10 denoting 10, 50 and 90% contribution of diffusion creep. (b) Uniform strain rate with C contours for $\phi=0.5$ and $\phi=0.8$.

In comparing the position of the data points on the maps with that of the lines of constant U , a point of caution should be made. The C contours on the map are calculated using best fit values for the flow law parameters (cf. 5.6). However, the position of the data points on the maps is dependent on the values of these flow law parameters, as S and C of the data are calculated using the same flow law parameters. The use of slightly different values for the flow law parameters, within the error bars resulting from the quality of fit of the mechanical data to the flow equations, may move the data relative to the lines of constant U ,

i.e. into or away from the field boundary of the maps. This stresses the need for accurate diffusion and dislocation creep laws for the material that is analyzed. The best results can be expected for a complete analysis of flow laws and distribution data for a single material, which is a prerequisite for accurate estimates of values for U .

5.4 Discussion

In this chapter, a model is advanced that relates the grain size distribution that develops during dynamic recrystallization to rheology. The model uses composite diffusion-dislocation creep laws for materials with a lognormal grain size distribution. The model is based on the hypothesis that the grain size distribution of dynamically recrystallizing materials tends to organize itself in the boundary between the diffusion and dislocation creep fields (chapter 1). In this, the boundary is taken as the region where both mechanisms contribute significantly (but not necessarily equal) to the overall strain rate. The requirements for this to happen are that (1) grain size is distributed, (2) diffusion creep contributes significantly to the strain rate of (small) grains that nucleate during dynamic recrystallization, and (3) grains are allowed to grow by normal grain growth or by grain boundary migration during dynamic recrystallization. The mechanical and microstructural results obtained from experiments on natural Carrara marble (chapter 3) and synthetic polycrystalline halite (chapter 4) have shown that these requirements are generally fulfilled, at least in these two, relatively pure single phase materials.

The new set of data on wet polycrystalline halite, covering a systematic range in strain rate, temperature and stress, has been selected to test the model formulated in this chapter, taking into account the complete grain size distributions. As far as we are aware, such analysis has not been performed before, which seems a deficiency since distributed grain sizes are standard in rock and other materials. Grain size distributions are taken as approximately log-normal in our analysis, supported by measurements on a variety of rock materials [e.g., *Ranalli*, 1984; *Michibayashi*, 1993; *Newman*, 1994; *Post and Tullis*, 1994; *Shimizu*, 1999; *Dijkstra*, 2001; chapters 3, 4]. The halite data are in agreement with the model. Several points, however, need further discussion. These are (1) the consequence for paleopiezometry of incorporating standard deviation in σ - d relations, (2) the implications in terms of rheological weakening, and (3) the limitations of the model.

5.4.1 Consequences of incorporating standard deviation in σ - d relations

The present analysis differs from conventional methods used to calibrate a relation between recrystallized grain size and stress and temperature by the incorporation of the distribution parameters, standard deviation and median grain size, in the distribution term $\exp((3 \pm 1/2 m) \phi^2) d_{med}$. Because conventional relations only use a single value for the grain size [e.g., *Derby and Ashby*, 1990; *Shimizu*, 1998; *De Bresser et al.*, 2001], paleo-stresses calculated from earlier piezometric relations may be over- or underestimated. This is illustrated in fig. 5.4, which shows the variation in estimated paleo-stress (expressed as σ_2/σ_1) between materials with different standard deviation (ϕ_1 and ϕ_2) of the lognormal grain size distribution for the uniform stress case using $n=3$ (e.g. olivine, see table 2.3) and $m=3$ (grain boundary diffusion creep). As an example, ϕ_1 may indicate the standard deviation of the material used to calibrate the piezometer and ϕ_2 may indicate the standard deviation of a natural tectonite to which the piezometer is applied. In this case, conventional relations that do not account for variations in standard deviation will only predict accurate paleo-stresses if

$\phi_1 = \phi_2$ ($\sigma_2/\sigma_1=1$). The error in estimated stress may be up to one order of magnitude ($\sigma_2/\sigma_1=0.1$) for realistic variations in standard deviation (e.g. $\phi_1=0.8$ and $\phi_2=1.2$).

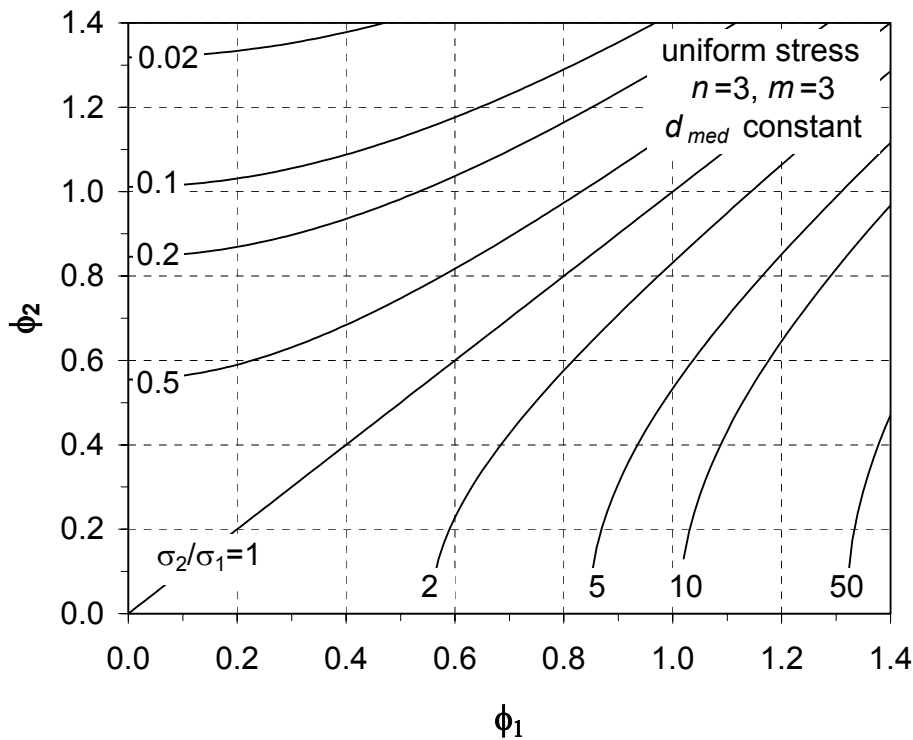


Figure 5.4 Illustration of the effect of variations in standard deviation of the lognormal grain size distribution (ϕ_1 and ϕ_2) on paleo-stress estimates in nature. Piezometers that do not account for differences in standard deviation may significantly over- or underestimate ($\sigma_2/\sigma_1 \neq 1$) paleo-stresses of natural tectonites.

If the boundary hypothesis advanced by *De Bresser et al.* [1998; 2001] is valid, the model given by (5.4) and (5.5) provides a physical basis for piezometers, constraining the grain size distribution to the diffusion-dislocation creep boundary. In contrast, conventional piezometers that relate recrystallized grain size to stress (and in some cases temperature) are usually fully empirical and unrelated to the active creep mechanisms. The model does not assume *a priori* a specific recrystallization mechanism (e.g. migration recrystallization, *Derby and Ashby*, [1990], or rotation recrystallization, *Shimizu*, [1998]). Through the underlying assumptions, the model implicitly requires the recrystallized grain size distribution to be expressed in a distribution characteristics term $\exp((3 \pm 1/2)m)\phi^2 d_{med}$ (with median grain size d_{med} , standard deviation ϕ , and $m=2$ or $m=3$ for diffusion creep controlled by volume or grain boundary diffusion, respectively). Consequently, an important implication of the model is that recrystallized grain size is not uniquely related to stress and temperature, as predicted by conventional models. Instead, stress and temperature only determine the magnitude of the distribution characteristics term. This is an important issue, because the standard deviation of the recrystallized grain size distribution is often dependent on the deformation conditions (see table 5.1 and chapters 3 and 4). Conventional models cannot account for a variation in standard deviation and would predict erroneous stresses and strain rate based on a single value for grain size.

5.4.2 Implications for rheological weakening

A direct consequence of the model is that the rheology of dynamically recrystallizing materials is constrained to the diffusion-dislocation creep boundary for all deformation conditions, as was originally proposed by *De Bresser et al.* [2001] for materials with a single-valued grain size. Using (5.3), the steady state creep rate of dynamically recrystallizing materials ($\dot{\epsilon}_{rx}$) assuming uniform stress can be written as

$$\dot{\epsilon}_{rx} = \dot{\epsilon}_{diff} + \dot{\epsilon}_{disl} = (U + I)\dot{\epsilon}_{disl} \quad (5.6)$$

This means that for uniform stress, assessment of U and the experimentally calibrated flow law parameters for the dislocation creep part of (5.1) or (5.2) suffices to constrain the rheology of a specific material under natural conditions. As a consequence, a complete switch in deformation mechanism from dislocation to diffusion creep may not occur as recrystallized grain size is constrained to the diffusion-dislocation creep boundary. This has also been pointed out by *De Bresser et al.* [2001] for a single-valued grain size (chapter 1). These authors conclude that rheological weakening due to dynamic recrystallization may be limited and insufficient to cause strain localization in nature. The present model incorporates the effect of the width of the grain size distribution, and gives nuances to this conclusion. For uniform strain rate, the diffusion-dislocation creep boundary may spread out considerably with increasing standard deviation (chapter 2, see also fig. 5.2b). This means that even if grain size organizes itself in the diffusion-dislocation creep boundary, rheological weakening due to dynamic recrystallization may be larger than expected on the basis of a single-valued grain size. The amount of weakening depends on the change in standard deviation and median grain size due to dynamic recrystallization. Considering the fact that for uniform strain rate the boundary may spread out over orders of magnitude in stress for large standard deviations (chapter 2, fig. 5.2b, see also *Freeman and Ferguson*, [1986]), weakening may be considerable without a complete switch in deformation mechanism. The uniform stress and uniform strain rate case provide bounds on the rate of deformation in real polycrystals [*Raj and Ghosh*, 1981; *Freeman and Ferguson*, 1986]. For uniform stress, (5.6) predicts minor weakening (a factor 2, if $U=1$ corresponding to an equal contribution of diffusion and dislocation creep, cf. section 1.4.4), but weakening may be expected to be larger if strain rate is assumed uniform. This means that rheological weakening may be expected to be larger than predicted by (5.6). Accurate assessment of rheological weakening due to dynamic recrystallization in real polycrystalline materials needs to account for distributed grain size.

5.4.3 Final remarks

The data on wet polycrystalline halite are found to be in agreement with the proposed model relating recrystallized grain size distribution to the rheology controlled by diffusion as well as dislocation mechanisms. Further experimental support for the model should come from other systematic data on the mechanical behavior and grain size distribution of single materials. In this, focus should be on calibrating microphysically based pure diffusion and dislocation creep (end-member) laws for a single material, as the model incorporates flow law parameters for both mechanisms. In addition, microphysical models for the processes involved in dynamic recrystallization, such as grain boundary migration and progressive subgrain rotation, can provide independent proof for the model. One final remark on the limitation of the model refers to the single, pure phase nature of the materials considered in the field boundary hypothesis. The requirements for the model outlined in section 5.4.1 might not be fulfilled in polyphase materials or materials with impurities inhibiting grain growth.

5.5 Conclusions

1. We have proposed a model that relates the grain size distribution to rheology of dynamically recrystallizing materials. The model is based on the notion that grain size tends to organize itself in the boundary between the (grain size sensitive) diffusion and (grain size insensitive) dislocation creep fields. It uses composite diffusion-dislocation flow laws for materials with a lognormal grain size distribution, uniquely characterized by the median grain size and standard deviation of the distribution in log-space.
2. The model can be used as a piezometer that relates the recrystallized grain size distribution to temperature as well as stress. This relation can be used to constrain the rheology of rock materials in nature. It differs from conventional piezometers that uniquely relate recrystallized grain size (as a single value) to flow stress and (in some cases) temperature. Instead, it implies that the standard deviation of the distribution should be taken into account if reliable paleo-stress estimates are to be obtained from piezometers.
3. Experimental data on wet polycrystalline halite, consisting of mechanical data together with detailed analysis of the grain size distribution of fully recrystallized samples, show good agreement with the formulated model. Support from experimental data for other materials is required now to assess the general applicability of the model.
4. If the model generally holds, the earlier suggestion that dynamic recrystallization in single phase, pure materials cannot result in rheological weakening and associated localization [*De Bresser et al.*, 2001] requires examination, since the distributed nature of grain size broadens the transition zone between in deformation mechanisms.
5. The present results highlight the need to consider grain size distributions rather than treating grain size as a single value, if accurate constraints on deformation of rock materials in nature are to be obtained.

Chapter 6

Conclusions and recommendations for further research

6.1 General conclusions and innovative aspects

In this thesis, the relationship between dynamic recrystallization, grain size distribution and rheology of Earth materials has been investigated. The general conclusions and innovative aspects, in relation to the research aims specified in the introductions, are:

On flow laws that incorporate grain size distribution:

1. Theoretical composite diffusion-dislocation flow laws were derived that incorporate median and standard deviation of a continuous lognormal grain size distribution. The flow laws provide an improved basis for the extrapolation of mechanical data to nature, the interpretation of experimental data in terms of deformation mechanisms and the assessment of the effect of syn-deformational changes in grain size distribution, for example by dynamic recrystallization, on rheology.
2. Application of the flow laws to polycrystalline olivine deforming under natural conditions revealed that strain rates can change by orders of magnitude due to variation in standard deviation at fixed median grain size. This is unaccounted for by conventional flow laws that include a single-valued grain size.

On the effect of dynamic recrystallization on rheology and grain size distribution:

3. Deformation experiments on natural Carrara marble and synthetic polycrystalline halite were performed at a systematic range of deformation conditions and strains. In addition, the grain size distributions of all samples were analyzed. It was shown that dynamic recrystallization of Carrara marble results in progressive reduction of the average grain size with increasing strain, associated with progressively decreasing flow stress. In wet polycrystalline halite, the microstructural development was dominated by dynamic recrystallization involving fluid-assisted grain boundary migration, resulting in an increase in grain size with respect to the starting material. After the onset of grain boundary migration in wet polycrystalline halite, corresponding to a peak in stress-strain behavior, oscillations in flow stress were observed that decrease in amplitude with increasing strain, leading to a (near) steady state flow stress at high strain..
4. The experiments revealed that during dynamic recrystallization, grain size distributions evolve by a competition of processes leading to grain growth, such as grain boundary migration, and processes leading to grain size reduction, such as nucleation of new grains by progressive subgrain rotation and at grain boundary bulges. It was inferred that these processes balance at steady state, leading to a recrystallized grain size distribution that is close to lognormal. The median and standard deviation of the distribution are characteristic of the deformation conditions.
5. Analysis of the mechanical data and qualitative microstructural observations on deformed samples of Carrara marble and wet polycrystalline halite showed that

dislocation deformation mechanisms as well as grain size sensitive (diffusion) creep mechanisms were active in the deforming samples. Thus, composite flow laws of grain size insensitive (dislocation) creep and grain size sensitive (i.e. solid state diffusion, grain boundary sliding or solution-precipitation) creep incorporating grain size distribution are required to adequately describe deformation and assess rheological weakening of dynamically recrystallizing materials.

6. Minor rheological weakening due to progressive grain size reduction in Carrara marble and due to continuous removal of strain hardening substructure by grain boundary migration in wet polycrystalline halite has been observed. This suggests that dynamic recrystallization will only result in minor rheological weakening.

On evaluation of models for dynamic recrystallization and the role of temperature and strain:

7. Experimental data on Carrara marble and wet polycrystalline halite showed that the recrystallized grain size distribution in these materials is dependent on temperature as well as stress. The grain size distribution evolves with strain by a combination of grain boundary migration, progressive subgrain rotation and nucleation at grain boundary bulges. It follows that the grain size distribution of high strain, fully recrystallized samples must be used to evaluate models for dynamic recrystallization.
8. Recrystallized grain size data of wet polycrystalline halite, plotted on a deformation mechanism map, fall in the boundary region between solution-precipitation creep and dislocation creep. The data lend support to a model that assumes that dynamic recrystallization adjusts grain size and rheology to the boundary between grain size sensitive (diffusion) and grain size insensitive (dislocation) creep [De Bresser *et al.*, 1998; 2001].

On the incorporation of distributed grain size in models for dynamic recrystallization:

9. A quantitative relationship between the median and standard deviation of a lognormal grain size distribution and the rheology of dynamically recrystallizing materials deforming by dislocation and diffusion creep was formulated. Recrystallized grain size distribution data of wet halite were found to be in agreement with the model.
10. The model implies that recrystallized grain size cannot be uniquely related to stress and temperature without taking the width of the grain size distribution into account. This shows that grain size distributions need to be considered if recrystallized grain size piezometers are used to estimate paleo-stresses in natural tectonites.

6.2 Recommendations for further research

On flow laws that incorporate grain size distribution:

1. In the derivation of flow laws for distributed grain size, either stress or strain rate was assumed uniform throughout the material. The flow laws derived for these two cases are generally considered to describe bounds for the rate of deformation in real polycrystals. However, these bounds may widely divert if the grain size distribution of the material shows a large standard deviation (chapter 2). Hence, there is scope for the derivation of

a single flow law that accurately constrains deformation in real polycrystals. Further research should focus on the way that distribution of stress and strain rate in polycrystals leads to bulk deformation and how bulk deformation can be described by a single flow law. This may require numerical modeling of deformation on the aggregate scale [e.g. *Jinich et al.*, 1978; *Ghosh and Raj*, 1981; *Tullis et al.* 1991]. It may also provide a way of avoiding the rather elaborate derivation of a flow law for uniform strain rate for a given material.

2. In the theoretical flow laws incorporating distributed grain size, grain size is taken as lognormally distributed. Although many rock materials indeed exhibit a lognormal grain size distribution, other distributions may be important as well. The effect of approximating grain size distributions by a lognormal distribution rather than some other distribution should be (numerically) investigated by comparing stress and strain rate of rock materials using the exact distributions encountered in nature [cf. *Freeman and Ferguson*, 1986] with the stress and strain rate predicted by the flow laws in this thesis.
3. In order to fully assess the improvements and accuracy of the flow laws for distributed grain size, they should be tested against synthetic materials that can be manufactured with different lognormal grain size distributions.

On the effect of dynamic recrystallization on rheology and grain size distribution:

4. Many previous rock deformation studies regard grain size as single-valued. More experimental data on the deformation behavior of materials in combination with analysis of the complete grain size distribution are needed to accurately assess the effect of dynamic recrystallization on rheology and grain size distribution. It is suggested to develop experimental programs that can provide such data.
5. The possibility of strain localization and rheological weakening due to dynamic recrystallization processes requires further attention, focusing on the effect of distributed grain size. It is recommended to perform research projects that combine deformation experiments with (numerical) modeling of the effect of microphysical processes operating during dynamic recrystallization on the strength of polycrystalline aggregates.

On evaluation of models for dynamic recrystallization and the role of temperature and strain:

6. In many rock deformation studies, samples are deformed to low strains or exposed to changing deformation conditions during the experiments (e.g. strain rate stepping experiments), with small strains in individual steps. The latter experiments provide a wealth of mechanical data, but do not allow systematic investigation of the role of strain and temperature on microstructure development. However, if previous models for dynamic recrystallization as well as the modified model derived in this thesis are to be further evaluated against experimental data, fully recrystallized (high strain) samples without stepping history are needed, for which the role of temperature is systematically investigated. Torsion testing and direct shear experiments are suitable for this.
7. This study clearly demonstrates the importance of accurate calibration of flow laws for pure diffusion creep and pure dislocation creep. Individual studies that have performed

such calibration for a single Earth material are lacking. Consequently, in this thesis flow laws from different studies, using materials from different sources, had to be used to evaluate models for dynamic recrystallization. There is scope for a well-designed study on one material with a very fine grain size to investigate grain size sensitive flow, and on the same material with a very coarse grain size to study grain size insensitive flow. The latter material may be obtained by normal grain growth of the corresponding fine material, although methods must also be employed to manufacture fine materials that can be shown to remain fine at high strains and temperatures.

On the incorporation of distributed grain size in models for dynamic recrystallization:

8. It is proposed to further develop models for dynamic recrystallization by focusing on modeling the effect of different microphysical processes operating during dynamic recrystallization on the grain size distribution. This would provide an independent microphysical basis for the quantitative relationship between grain size distribution parameters and the rheology of dynamically recrystallizing materials developed in the present study.
9. Existing piezometric relations based on recrystallized grain size are in need of revision to account for grain size distribution and temperature. In those cases that samples are still available, a re-evaluation of the microstructure with measurement of the complete grain size distribution is strongly advised.

References

- Ahrens, L.H., Lognormal-type distributions-III, *Geochim. Cosmochim. Acta*, **11**, 205-212, 1957.
- Aitchison, J., and J.A.C. Brown, *The lognormal distribution, with special reference to its use in economics*, Cambridge University Press, Cambridge, 1957.
- Aubertin, M., and H.R. Hardy Jr., *The mechanical behavior of salt: Proceedings of the fourth conference*, 658 pp., 1998.
- Avé Lallemant, H.G., Experimental deformation of diopside and websterite, *Tectonophysics*, **48**, 1-27, 1978.
- Barr, L.W., J.A. Morrison, and P.A. Schroeder, Anion diffusion in crystals of NaCl, *J. Appl. Phys.*, **36**, 624-631, 1965.
- Bassi, G., Factors controlling the style of continental rifting: insights from numerical modelling, *Earth Planet. Sci. Lett.*, **105**, 430-452, 1991.
- Beaumont, C., P.J.J. Kamp, J. Hamilton, and P. Fullsack, The continental collision zone, South Island, New Zealand: Comparison of geodynamical models and observations, *J. Geoph. Res.*, **101**, 3333-3359, 1996.
- Bilde-Sørensen, J.B., and D.A. Smith, Comment on "Refutation of the relationship between denuded zones and diffusional creep", *Scripta Metall. Mater.*, **30**, 383-386, 1994.
- Bos, B., C.J. Peach, and C.J. Spiers, Slip behaviour of simulated gouge-bearing faults under conditions favouring pressure solution, *J. Geoph. Res.*, **105**, 16699-16717, 2000.
- Bos, B., and C.J. Spiers, Experimental investigation into the microstructural and mechanical evolution of phyllosilicate-bearing fault rock under conditions favouring pressure solution, *J. Struct. Geol.*, **23**, 1187-1202, 2001.
- Braun, J., J. Chéry, A. Poliakov, D. Mainprice, A. Vauchez, A. Tomassi, and M. Daignières, A simple parameterization of strain localization in the ductile regime due to grain size reduction: A case study for olivine, *J. Geoph. Res.*, **104**, 25167-25181, 1999.
- Bystricky, M., K. Kunze, L. Burlini, and J.-P. Burg, High shear strain of olivine aggregates: Rheological and seismic consequences, *Science*, **290**, 1564-1567, 2000.
- Carter, N.L., and F.D. Hansen, Creep of rocksalt, *Tectonophysics*, **92**, 275-333, 1983.
- Carter, N.L., F.D. Hansen, and P.E. Senseny, Stress magnitudes in natural rocksalt, *J. Geoph. Res.*, **87**, 9289-9300, 1982.
- Carter, N.L., S.T. Horseman, J.E. Russel, and J. Handin, Rheology of rocksalt, *J. Struct. Geol.*, **15**, 1257-1271, 1993.
- Carter, N.L., and M.C. Tsenn, Flow properties of continental lithosphere, *Tectonophysics*, **136**, 27-63, 1987.
- Casey, M., K. Kunze, and D.L. Olgaard, Texture of Solnhofen limestone deformed to high strains in torsion, *J. Struct. Geol.*, **20**, 255-267, 1998.
- Cepeda, L.E., J.M. Rodriguez-Ibabe, J.J. Urcola, and M. Fuentes, Influence of dynamic recrystallization on hot ductility of aluminium killed mild steel, *Mater. Sci. Tech.*, **5**, 1191-1199, 1989.
- Chopra, P.N., and M.S. Paterson, The experimental deformation of dunite, *Tectonophysics*, **78**, 453-473, 1981.
- Chopra, P.N., and M.S. Paterson, The role of water in the deformation of dunite, *J. Geoph. Res.*, **89**, 7861-7876, 1984.
- Christie, J.M., and A. Ord, Flow stress from microstructures of mylonites: Example and current assessment, *J. Geoph. Res.*, **85**, 6253-6262, 1980.
- Coble, R.L., A model for boundary diffusion controlled creep in polycrystalline materials, *J. Appl. Phys.*, **34**, 1679-1682, 1963.

References

- Covey-Crump, S.J., Evolution of mechanical state in Carrara marble during deformation at 400° to 700° C, *J. Geoph. Res.*, **103**, 29781-29794, 1998.
- Cox, S.F., M.A. Etheridge, and B.E. Hobbs, The experimental ductile deformation of polycrystalline and single crystal pyrite, *Econ. Geology*, **76**, 2105-2117, 1981.
- De Bresser, J.H.P., Intracrystalline deformation of calcite, Ph. D. thesis, Utrecht University, Utrecht, 1991.
- De Bresser, J.H.P., Influence of pressure on the high temperature flow of Carrara marble, *EOS Trans. AGU*, **77**, F710, 1996.
- De Bresser, J.H.P., C.J. Peach, J.P.J. Reijns, and C.J. Spiers, On dynamic recrystallization during solid state flow: Effects of stress and temperature, *Geoph. Res. Lett.*, **25**, 3457-3460, 1998.
- De Bresser, J.H.P., and C.J. Spiers, High-temperature deformation of calcite single crystals by r^+ and f^+ slip, in *Deformation Mechanisms, Rheology and Tectonics*, edited by R.J. Knipe, and E.H. Rutter, Geological Society Special Publication, , 285-298, London, 1990.
- De Bresser, J.H.P., J.H. Ter Heege, and C.J. Spiers, Grain size reduction by dynamic recrystallization: Can it result in major rheological weakening ?, *Int. J. Earth Sci.*, **90**, 28-45, 2001.
- De Meer, S., and C.J. Spiers, On mechanics and kinetics of creep by intergranular pressure solution, in *Growth, Dissolution and Pattern Formation in Geosystems*, edited by B. Jamtveit, and P. Meakin, , 345-366, Amsterdam, 1999.
- De Meer, S., and C.J. Spiers, Diffusive properties of fluid-filled grain boundaries measured electrically during active pressure solution, *Earth Planet. Sci. Lett.*, **in press**, 2002.
- Dell'Angelo, L.N., and D.L. Olgaard, Experimental deformation of fine-grained anhydrite: Evidence for dislocation and diffusion creep, *J. Geoph. Res.*, **100**, 15425-15440, 1995.
- Derby, B., Dynamic recrystallization and grain size, in *Deformation processes in minerals, ceramics and rocks*, edited by D.J. Barber, and P.D. Meridith, , 354-364, London, 1990.
- Derby, B., The dependence of grain size on stress during dynamic recrystallisation, *Acta Metall. Mater.*, **39**, 955-962, 1991.
- Derby, B., and M.F. Ashby, On dynamic recrystallization, *Scripta Metall.*, **21**, 879-884, 1987.
- Dijkstra, A.H., Deformation and melt in natural mantle rocks: The Hilti Massif (Oman) and the Othris Massif (Greece), Ph.D. thesis, Utrecht University, Utrecht, 2001.
- Drury, M.R., F.J. Humphreys, and S.H. White, Large strain deformation studies using polycrystalline magnesium as a rock analogue, part II: Dynamic recrystallization mechanisms at high temperatures, in *Experiments in solid state physics relevant to lithospheric dynamics*, edited by Y. Gueguen, and H. Kern, *Physics Earth Planet. Int.*, **40**, 208-222, 1985.
- Drury, M.R., and J.L. Urai, Deformation-related recrystallization processes, *Tectonophysics*, **172**, 235-253, 1990.
- Drury, M.R., R.L.M. Vissers, D. Van der Wal, and E.H. Hoogerduijn Strating, Shear localisation in upper mantle peridotites, *Pure Appl. Geoph.*, **137**, 439-460, 1991.
- Durham, W.B., and C. Goetze, Plastic flow of oriented single crystals of olivine. 1. Mechanical data, *J. Geoph. Res.*, **82**, 5737-5753, 1977.
- Edward, G.H., M.H. Etheridge, and B.E. Hobbs, On the stress dependence of subgrain size, *Textures and Microstructures*, **5**, 127-152, 1982.
- Escaig, B., Sur le glissement dévié des dislocations dans la structure cubique à faces centrées, *J. Phys.*, **29**, 225-239, 1968.
- Etheridge, M.A., and J.C. Wilkie, Grain size reduction, grain boundary sliding and the flow strength of mylonites, *Tectonophysics*, **58**, 159-178, 1979.

- Etheridge, M.A., and J.C. Wilkie, An assessment of dynamically recrystallized grain size as a paleopiezometer in quartz-bearing mylonite zones, *Tectonophysics*, **78**, 475-508, 1981.
- Evans, B., and D.L. Kohlstedt, Rheology of rocks, in *Handbook of physical constants. Part 3-rock physics and phase relations*, edited by T.J. Ahrens, , 148-165, Washington, DC, 1995.
- Fernández, M., and G. Ranalli, The role of rheology in extensional basin formation modelling, *Tectonophysics*, **282**, 129-145, 1997.
- Fliervoet, T.F., Deformation mechanisms in fine grained quartzo-feldspathic mylonites, Ph.D. thesis, Utrecht University, Utrecht, 1995.
- Franssen, R.C.M.W., The rheology of synthetic rocksalt in uniaxial compression, *Tectonophysics*, **233**, 1-40, 1994.
- Freeman, B., and C.C. Ferguson, Deformation mechanism maps and micromechanics of rocks with distributed grain sizes, *J. Geoph. Res.*, **91**, 3849-3860, 1986.
- Friedman, M., and N.G. Higgs, Calcite fabrics in experimental shear zones, *American Geophysical Union Geophysical Monographs*, **24**, 11-17, 1981.
- Frost, H.J., and M.F. Ashby, *Deformation-mechanism maps: The plasticity and creep of metals and ceramics*, 166 pp., Pergamon Press, Oxford, 1982.
- Furlong, K.P., Thermal-rheologic evolution of the upper mantle and the development of the San Andreas fault system, *Tectonophysics*, **223**, 149-164, 1993.
- Ghosh, A.K., and R. Raj, Grain size distribution effects in superplasticity, *Acta Metall.*, **29**, 607-616, 1981.
- Glover, G., and C.M. Sellars, Recovery and recrystallisation during high temperature deformation of α -iron, *Metall. Trans.*, **4**, 765-775, 1973.
- Govers, R., and M.J.R. Wortel, Extension of stable continental lithosphere and the initiation of lithospheric scale faults, *Tectonics*, **14**, 1041-1055, 1995.
- Gradshteyn, I.S., and I.M. Ryzhik, *Table of integrals, series and products*, 1160 pp., Academic Press, 1980.
- Griggs, D.T., Deformation of rocks under high confining pressures-I. Experiments at room temperature, *J. Geol.*, **44**, 541-577, 1936.
- Gueydan, F., Y.M. Leroy, and L. Jolivet, Grain-size sensitive flow and shear stress enhancement at the brittle-ductile transition of the continental crust, *Int. J. Earth Sci.*, 2001.
- Guillopé, M., and J.P. Poirier, Dynamic recrystallization during creep of single-crystalline halite: An experimental study, *J. Geoph. Res.*, **84**, 5557-5567, 1979.
- Hacker, B.R., A. Yin, J.M. Christie, and G.A. Davis, Stress magnitude, strain rate, and rheology of extended middle continental crust inferred from quartz grain sizes in the Whipple Mountains, California, *Tectonics*, **11**, 36-46, 1992.
- Hacker, B.R., A. Yin, J.M. Christie, and A.W. Snoke, Differential stress, strain rate, and temperatures of mylonitization in the Ruby mountains, Nevada: implications for the rate and duration of uplift, *J. Geoph. Res.*, **95**, 8569-8580, 1990.
- Han, J.-H., and D.-Y. Kim, Determination of three-dimensional grain size distribution by linear intercept measurement, *Acta Mater.*, **46**, 2021-2028, 1998.
- Hashin, Z., Theory of mechanical behavior of heterogeneous media, *Appl. Mech. Rev.*, **17**, 1-9, 1964.
- Heard, H.C., Steady-state flow in polycrystalline halite at pressure of 2 kilobars, in *Flow and fracture of rocks*, edited by H.C. Heard, I.Y. Borg, N.L. Carter, and C.B. Raleigh, Geophysical Monograph, **16**, 191-210, 1972.
- Heard, H.C., and C.B. Raleigh, Steady state flow in marble at 500° to 800°C, *Geol. Soc. Am. Bull.*, **83**, 935-956, 1972.

References

- Heard, H.C., and F.J. Ryerson, Effect of cation impurities on steady-state flow of salt, in *Mineral and Rock Deformation: Laboratory Studies*, edited by B.E. Hobbs, and H.C. Heard, Geophysical Monograph Series, , 99-115, Washington, 1986.
- Heilbronner, R., and D. Bruhn, The influence of three-dimensional grain size on the rheology of polyphase rocks, *J. Struct. Geol.*, **20**, 695-705, 1998.
- Hill, R., A self-consistent mechanics of composite materials, *J. Mech. Phys. Solids*, **13**, 213-222, 1965.
- Hirth, G., and J. Tullis, Dislocation creep regimes in quartz aggregates, *J. Struct. Geol.*, **14**, 145-159, 1992.
- Humphreys, F.J., and M. Hatherly, *Recrystallization and related annealing phenomena*, 497 pp., Pergamon, 1996.
- Jacka, T.H., and L. Jun, The steady-state crystal size of deforming ice, *Annals of Glaciology*, **20**, 13-18, 1994.
- Jaoul, O., Multicomponent diffusion and creep in olivine, *J. Geoph. Res.*, **95**, 17631-17642, 1990.
- Jaroslow, G.E., G. Hirth, and H.J.B. Dick, Abyssal peridotite mylonites: implications for grain-size sensitive flow and strain localization in the oceanic lithosphere, *Tectonophysics*, **256**, 17-37, 1996.
- Jin, D., S. Karato, and M. Obata, Mechanism of shear localization in the continental lithosphere: inference from the deformation microstructures of peridotites from the Ivrea zone, northwestern Italy, *J. Struct. Geol.*, **20**, 195-209, 1998.
- Jinoch, J., S. Ankern, and H. Margolin, Calculations of stress-strain curve and stress and strain distributions for an α - β Ti-8Mn alloy, *Mater. Sci. Eng.*, **34**, 203-211, 1978.
- Kameyama, M., D.A. Yuen, and H. Fujimoto, The interaction of viscous heating with grain-size dependent rheology in the formation of localized slip zones, *Geoph. Res. Lett.*, **24**, 2523-2526, 1997.
- Karato, S., M.S. Paterson, and J.D. FitzGerald, Rheology of synthetic olivine aggregates: Influence of grain size and water, *J. Geoph. Res.*, **91**, 8151-8176, 1986.
- Karato, S., M. Toriumi, and T. Fujii, Dynamic recrystallisation of olivine single crystals during high temperature creep, *Geoph. Res. Lett.*, **7**, 649-652, 1980.
- Karato, S., M. Toriumi, and T. Fujii, Dynamic recrystallization and high-temperature rheology of olivine, in *High pressure research in geophysics*, edited by S. Akimoto, and M. Manghnani, Advances in Earth and Planetary Sciences, **12**, 171-189, Tokyo, 1982.
- Karato, S., and P. Wu, Rheology of the upper mantle, *Science*, **260**, 771-778, 1993.
- Kern, H., and H.-R. Wenk, Calcite texture development in experimentally induced ductile shear zones, *Contrib. Mineral. Petrol.*, **83**, 231-236, 1983.
- Kirby, S.H., Tectonic stresses in the lithosphere: Constraints provided by the experimental deformation of rocks, *J. Geoph. Res.*, **85**, 6353-6363, 1980.
- Kirby, S.H., Rheology of the lithosphere, *Reviews of Geophysical Space Physics*, **21**, 1458-1487, 1983.
- Kirby, S.H., and C.B. Raleigh, Mechanisms of high-temperature solid-state flow in minerals and ceramics and their bearing on the creep behavior of the mantle, *Tectonophysics*, **19**, 165-194, 1973.
- Knipe, R.J., Deformation mechanisms- recognition from natural tectonites, *J. Struct. Geol.*, **11**, 127-146, 1989.
- Koch, P.S., Rheology and microstructures of experimentally deformed quartz aggregates, Ph.D. thesis, University of California, Los Angeles, 1983.
- Kohlstedt, D.L., B. Evans, and S.J. Mackwell, Strength of the lithosphere: Constraints imposed by laboratory experiments, *J. Geoph. Res.*, **100**, 17587-17602, 1995.

- Kohlstedt, D.L., and M.S. Weathers, Deformation-induced microstructures, paleopiezometers, and differential stresses in deeply eroded fault zones, *J. Geoph. Res.*, **85**, 6269-6285, 1980.
- Kretz, R., Grain size distribution for certain metamorphic minerals in relation to nucleation and growth, *J. Geol.*, **74**, 147-173, 1966.
- Kronenberg, A.K., and J. Tullis, Flow strengths of quartz aggregates: grain size and pressure effects due to hydrolytic weakening, *J. Geoph. Res.*, **89**, 4281-4297, 1984.
- Kurtz, S.K., and F.M.A. Carpay, Microstructure and normal grain growth in metals and ceramics. Part I. Theory, *J. Appl. Phys.*, **51**, 5725-5744, 1980.
- Langdon, T.G., Identifying creep mechanisms at low stresses, *Mater. Sci. Eng. A*, **283**, 266-273, 2000.
- Laurance, N., Self-diffusion of the chloride ion in sodium chloride, *Phys. Rev.*, **120**, 57-62, 1960.
- Laurent, J.F., and J. Bénard, Autodiffusion des ions dans les cristaux uniques des halogénures de potassium et des chlorures alcalines, *J. Phys. Chem. Solids*, **3**, 7-19, 1957.
- Laurent, J.F., and J. Bénard, Autodiffusion des ions dans les halogénures alcalins polycristallins, *J. Phys. Chem. Solids*, **7**, 218-227, 1958.
- Luton, M.J., and C.M. Sellars, Dynamic recrystallisation in nickel and nickel-iron alloys during high temperature deformation, *Acta Metall.*, **17**, 1033-1044, 1969.
- McDonnell, R.D., Deformation of fine-grained synthetic peridotite under wet conditions, Ph.D. thesis, Utrecht University, Utrecht, 1997.
- McDonnell, R.D., C.J. Peach, and C.J. Spiers, Flow behavior of fine-grained synthetic dunite in the presence of 0.5 wt% H₂O, *J. Geoph. Res.*, **104**, 17823-17845, 1999.
- Mercier, J.-C.C., D.A. Anderson, and N.L. Carter, Stress in the lithosphere: Inferences from steady state flow of rocks, *Pure Appl. Geoph.*, **115**, 199-226, 1977.
- Michibayashi, K., Syntectonic development of a strain-independent steady-state grain size during mylonitization, *Tectonophysics*, **222**, 151-164, 1993.
- Miralles, L., M. Sans, J.J. Pueyo, and P. Santanach, Recrystallization salt fabric in a shear zone (Cardona diapir, southern Pyrenees, Spain), in *Salt, Shale and Igneous Diapirs in and around Europe*, edited by B. Vendeville, Y. Mart, and J.-L. Vigneresse, Geological Society, London, Special Publications, **174**, 149-167, London, 2000.
- Molli, G., P. Conti, G. Giorgetti, M. Meccheri, and N. Oesterling, Microfabric study on the deformational and thermal history of the Alpi Apuane marbles (Carrara marbles), Italy, *J. Struct. Geol.*, **22**, 1809-1825, 2000.
- Nabarro, F.R.N., Report of a Conference on Strength of Solids, pp. 75-90, The Physical Society, Bristol, 1948.
- Nabarro, F.R.N., Diffusional viscosity of a polycrystalline solid, *J. Appl. Phys.*, **21**, 437-443, 1950.
- Nabarro, F.R.N., *Theory of crystal dislocations*, 821 pp., Dover Publications, Inc., 1987.
- Newman, J., The influence of grain size and grain size distribution on methods for estimating paleostresses from twinning in carbonates, *J. Struct. Geol.*, **16**, 1589-1601, 1994.
- Nieh, T.G., J. Wadsworth, and O.D. Sherby, *Superplasticity in metals and ceramics*, 273 pp., Cambridge University Press, Cambridge, 1997.
- Olgaard, D.L., The role of second phase in localizing deformation, in *Deformation Mechanisms, Rheology and Tectonics*, edited by R.J. Knipe, and E.H. Rutter, Geological Society of London Special Publication, **54**, 175-181, London, 1990.
- Ord, A., and J.M. Christie, Flow stresses from microstructures in mylonitic quartzites of the Moine Thrust zone, Assynt area, Scotland, *J. Struct. Geol.*, **6**, 639-654, 1984.
- Parrish, D.K., and A.F. Gangi, A nonlinear least squares technique for determining multiple-mechanism, high-temperature creep flow laws, in *Mechanical behavior of crustal rocks*,

References

- edited by N.L. Carter, M. Friedman, J.M. Logan, and D.W. Stearns, Geophysical Monograph Series, , 287-298, Washington D.C., 1981.
- Parrish, D.K., A.L. Krivz, and N.L. Carter, Finite-element folds of similar geometry, *Tectonophysics*, **32**, 183-207, 1976.
- Passchier, C.W., and R.A.J. Trouw, *Microtectonics*, 289 pp., Springer-Verlag, 1996.
- Paterson, M.S., and D.L. Olgaard, Rock deformation tests to large shear strains in torsion, *J. Struct. Geol.*, **22**, 1341-1358, 2000.
- Peach, C.J., Influence of deformation on the fluid transport properties of salt rocks, Ph. D. thesis, Utrecht University, Utrecht, 1991.
- Peach, C.J., and C.J. Spiers, Influence of crystal plastic deformation on dilatancy and permeability development in synthetic salt rock, *Tectonophysics*, **256**, 101-128, 1996.
- Pfiffner, O.A., Deformation mechanisms and flow regimes in limestones from the Helvetic zone of the Swiss Alps, *J. Struct. Geol.*, **4**, 429-442, 1982.
- Pieri, M., L. Burlini, K. Kunze, I. Stretton, and D.L. Olgaard, Rheological and microstructural evolution of Carrara marble with high shear strain: results from high temperature torsion experiments, *J. Struct. Geol.*, **23**, 1393-1413, 2001a.
- Pieri, M., K. Kunze, L. Burlini, I.C. Stretton, D.L. Olgaard, J.-P. Burg, and H.-R. Wenk, Texture development of calcite by deformation and dynamic recrystallization at 1000 K during torsion experiments of marble to large strains, *Tectonophysics*, **330**, 119-140, 2001b.
- Poirier, J.P., On the symmetrical role of cross-slip of screw dislocations and climb of edge dislocations as recovery processes controlling high-temperature creep, *Revue Phys. Appl.*, **11**, 731-738, 1976.
- Poirier, J.P., Shear localization and shear instability in materials in the ductile field, *J. Struct. Geol.*, **2**, 135-142, 1980.
- Poirier, J.P., *Creep of crystals- High-temperature deformation processes in metals, ceramics and minerals*, 260 pp., Cambridge University Press, Cambridge, 1985.
- Post, A., and J. Tullis, A recrystallized grain size piezometer for experimentally deformed feldspar aggregates, *Tectonophysics*, **303**, 159-173, 1999.
- Post, R.L., High-temperature creep of Mt. Burnet dunite, *Tectonophysics*, **42**, 75-110, 1977.
- Raj, R., and A.K. Ghosh, Micromechanical modelling of creep using distributed parameters, *Acta Metall.*, **29**, 283-292, 1981.
- Ranalli, G., Grain size distribution and flow stress in tectonites, *J. Struct. Geol.*, **6**, 443-447, 1984.
- Ranalli, G., *Rheology of the earth*, 413 pp., Chapman & Hall, Ottawa, 1995.
- Renner, J., and B. Evans, Do calcite rocks obey the power-law creep equation ?, in *Deformation mechanisms, rheology and tectonics 2001*, Geological Society of London Special Publication, *in press*, 2002.
- Roedder, E., The fluids in salt, *Amer. Mineral.*, **69**, 413-439, 1984.
- Ross, J.V., H.G. Avé Lallemant, and N.L. Carter, Stress dependence of recrystallized-grain and subgrain size in olivine, *Tectonophysics*, **70**, 39-61, 1980.
- Ross, J.V., and K.C. Nielson, High-temperature flow of wet polycrystalline enstatite, *Tectonophysics*, **44**, 233-261, 1978.
- Rutter, E.H., The influence of temperature, strain-rate and interstitial water in the experimental deformation of calcite rocks, *Tectonophysics*, **22**, 311-334, 1974.
- Rutter, E.H., Experimental study of the influence of stress, temperature, and strain on the dynamic recrystallization of Carrara marble, *J. Geoph. Res.*, **100**, 24651-24663, 1995.
- Rutter, E.H., Use of extension testing to investigate the influence of finite strain on the rheological behaviour of marble, *J. Struct. Geol.*, **20**, 243-254, 1998.

- Rutter, E.H., On the relationship between the formation of shear zones and the form of the flow law for rocks undergoing dynamic recrystallization, *Tectonophysics*, **303**, 147-158, 1999.
- Rutter, E.H., and K.H. Brodie, The role of tectonic grain size reduction in the rheological stratification of the lithosphere, *Geol. Rundschau*, **77**, 295-308, 1988.
- Rutter, E.H., and K.H. Brodie, Rheology of the lower crust, in *Continental lower crust*, edited by D.M. Fountain, R. Arculus, and R.W. Kay, , 201-267, Amsterdam, 1992.
- Sah, J.P., G.J. Richardson, and C.M. Sellars, Grain-size effects during dynamic recrystallization of nickel, *Metal Sci.*, **8**, 325-331, 1974.
- Schmid, S.M., The Glarus Overthrust: Field evidence and mechanical model, *Eclogae Geol. Helv.*, **68**, 247-280, 1975.
- Schmid, S.M., J.N. Boland, and M.S. Paterson, Superplastic flow in fine grained limestone, *Tectonophysics*, **43**, 257-291, 1977.
- Schmid, S.M., R. Panozzo, and S. Bauer, Simple shear experiments on calcite rocks: Rheology and microfabric, *J. Struct. Geol.*, **9**, 747-778, 1987.
- Schmid, S.M., M.S. Paterson, and J.N. Boland, High temperature flow and dynamic recrystallization in Carrara marble, *Tectonophysics*, **65**, 245-280, 1980.
- Schückher, F., Grain size, in *Quantitative microscopy*, edited by R.T. DeHoff, and F.N. Rhines, McGraw-Hill Series in Materials Science and Engineering, , 201-265, New York, 1968.
- Sellars, C.M., Recrystallization of metals during hot deformation, *Phil. Trans. R. Soc. Lond. A*, **288**, 147-158, 1978.
- Senseny, P.E., F.D. Hansen, J.E. Russel, N.L. Carter, and J. Handin, Mechanical behaviour of rocksalt: Phenomenology and micromechanism, *International Journal of Rock Mechanics*, **29**, 363-378, 1992.
- Shigematsu, N., Dynamic recrystallization in deformed plagioclase during progressive shear deformation, *Tectonophysics*, **305**, 437-452, 1999.
- Shimizu, I., Stress and temperature dependence of recrystallized grain size: A subgrain misorientation model, *Geoph. Res. Lett.*, **25**, 4237-4240, 1998.
- Shimizu, I., A stochastic model of grain size distribution during dynamic recrystallization, *Philos. Mag. A*, **79**, 1217-1231, 1999.
- Skrotzki, W., and Z.G. Liu, Analysis of the cross slip process in alkali halides, *Phys. Stat. Sol. A*, **73**, 225-229, 1982.
- Spiers, C.J., and N.L. Carter, Microphysics of rocksalt flow in nature, in *Fourth Conference on the Mechanical Behavior of Salt*, edited by M. Aubertin, and H.R. Hardy Jr., pp. 115-128, Trans. Tech. Publications, Hannover, Germany, 1998.
- Spiers, C.J., P.M.T.M. Schutjens, R.H. Brzesowsky, C.J. Peach, J.L. Liezenberg, and H.J. Zwart, Experimental determination of constitutive parameters governing creep of rocksalt by pressure solution, in *Deformation Mechanisms, Rheology and Tectonics*, edited by R.J. Knipe, and E.H. Rutter, Geological Society Special Publication, **54**, 215-227, 1990.
- Spiers, C.J., J.L. Urai, G.S. Lister, J.N. Boland, and H.J. Zwart, The influence of fluid-rock interaction on the rheology of salt rock, pp. 131, Office for Official Publications of the European Communities, Luxembourg, 1986.
- Stöckhert, B., M.R. Brix, R. Kleinschrot, A.J. Hurford, and R. Wirth, Thermochronometry and microstructures of quartz - a comparison with experimental flow laws and predictions on the temperature of the brittle-plastic transition, *J. Struct. Geol.*, **21**, 351-369, 1999.
- Stone, D.S., Scaling laws in dislocation creep, *Acta Metall. Mater.*, **39**, 599-608, 1991.

References

- Stretton, I.C., and D.L. Olgaard, A transition in deformation mechanism through recrystallization: Evidence from high strain, high temperature torsion experiments, *EOS Trans. AGU*, **78**, F723, 1997.
- Takeuchi, S., and A.S. Argon, Steady-state creep of single-phase crystalline matter at high temperature, *J. Mat. Sci.*, **11**, 1542-1566, 1976.
- Talbot, C.J., and M.P.A. Jackson, Internal kinematics of salt diapirs, *AAPG Bulletin*, **71**, 1068-1093, 1987.
- Talbot, C.J., and E.A. Rogers, Seasonal movements in a salt glacier in Iran, *Science*, **208**, 395-397, 1980.
- Thorvaldsen, A., The intercept method-2. Determination of spatial grain size, *Acta Metall.*, **45**, 595-600, 1997.
- Trimby, P.W., M.R. Drury, and C.J. Spiers, Misorientations across etched boundaries in deformed rocksalt: a study using electron backscatter diffraction, *J. Struct. Geol.*, **22**, 81-89, 2000a.
- Trimby, P.W., M.R. Drury, and C.J. Spiers, Recognising the crystallographic signature of recrystallisation processes in deformed rocks: a study of experimentally deformed rocksalt, *J. Struct. Geol.*, **22**, 1609-1620, 2000b.
- Tsenn, M.C., and N.L. Carter, Upper limits of power law creep of rocks, *Tectonophysics*, **136**, 1-26, 1987.
- Tullis, J., and R.A. Yund, Dynamic recrystallization of feldspar: A mechanism for ductile shear zone foliation, *Geology*, **13**, 238-241, 1985.
- Tullis, T.E., F.G. Horowitz, and J. Tullis, Flow laws of polyphase aggregates from end-member flow laws, *J. Geoph. Res.*, **96**, 8081-8096, 1991.
- Tungatt, P.D., and F.J. Humphreys, The plastic deformation and dynamic recrystallization of polycrystalline sodium nitrate, *Acta Metall.*, **32**, 1625-1635, 1984.
- Twiss, R.J., Theory and applicability of a recrystallized grain size paleopiezometer, *Pure Appl. Geoph.*, **115**, 227-244, 1977.
- Twiss, R.J., and C.M. Sellars, Limits of the applicability of the recrystallized grain size paleopiezometer, *Geoph. Res. Lett.*, **5**, 337-340, 1978.
- Underwood, E.E., Particle size distribution, in *Quantitative Microscopy*, edited by R.T. DeHoff, and F.N. Rhines, McGraw-Hill Series in Materials Science and Engineering, , 149-200, New York, 1968.
- Underwood, E.E., *Quantitative stereology*, 264 pp., Addison-Wesley, Marietta, Georgia, 1970.
- Urai, J.L., Water assisted dynamic recrystallization and weakening in polycrystalline bischofite, *Tectonophysics*, **96**, 125-157, 1983.
- Urai, J.L., Water-enhanced dynamic recrystallization and solution transfer in experimentally deformed carnallite, *Tectonophysics*, **120**, 285-317, 1985.
- Urai, J.L., C.J. Spiers, C.J. Peach, R.C.M.W. Franssen, and J.L. Liezenberg, Deformation mechanisms operating in naturally deformed halite rocks as deduced from microstructural investigations, *Geol. Mijnbouw*, **66**, 165-176, 1987.
- Urai, J.L., C.J. Spiers, H.J. Zwart, and G.S. Lister, Weakening of rock salt by water during long-term creep, *Nature*, **324**, 554-557, 1986.
- Van den Berg, A.P., P.E. Van Keken, and D.A. Yuen, The effects of a composite non-Newtonian and Newtonian rheology on mantle convection, *Geophys. J. Int.*, **115**, 62-78, 1993.
- Van den Berg, A.P., D.A. Yuen, and P.E. Van Keken, Rheological transition in mantle convection with a composite temperature-dependent, non-Newtonian and Newtonian rheology, *Earth Planet. Sci. Lett.*, **129**, 249-260, 1995.

- Van der Wal, D., Deformation processes in mantle peridotites, Ph.D. thesis, Utrecht University, Utrecht, 1993.
- Van der Wal, D., P. Chopra, and J.D. FitzGerald, Relationships between dynamically recrystallized grain size and deformation conditions in experimentally deformed olivine rocks, *Geoph. Res. Lett.*, **20**, 1479-1482, 1993.
- Van Hunen, J., A.P. Van den Berg, and N.J. Vlaar, A thermo-mechanical model of horizontal subduction below an overriding plate, *Earth Planet. Sci. Lett.*, **182**, 157-169, 2000.
- Vissers, R.L.M., M.R. Drury, E.H. Hoogerduijn Strating, C.J. Spiers, and D. Van der Wal, Mantle shear zones and their effect on lithosphere strength during continental breakup, *Tectonophysics*, **249**, 155-171, 1995.
- Walker, A.N., E.H. Rutter, and K.H. Brodie, Experimental study of grain-size sensitive flow of synthetic, hot-pressed calcite rocks, in *Deformation mechanisms, rheology and tectonics*, edited by R.J. Knipe, and E.H. Rutter, Geological Society Special Publication, , 259-284, 1990.
- Wang, J.N., The effect of grain size distribution on the rheological behavior of polycrystalline materials, *J. Struct. Geol.*, **16**, 961-970, 1994.
- Wang, Z.-C., and S. Ji, Diffusion creep of fine-grained garnetite: implications for the flow strength of subducting slabs, *Geoph. Res. Lett.*, **27**, 2333-2336, 2000.
- Wang, Z.-C., S. Mei, S. Karato, and R. Wirth, Grain growth in CaTiO₃-perovskite + FeO-wüstite aggregates, *Phys. Chem. Minerals*, **27**, 11-19, 1999.
- Watanabe, T., and C.J. Peach, Electrical impedance measurement of plastically deforming halite rocks at 125°C and 50 MPa, *J. of Geoph. Res.*, *in press*, 2002.
- Wawersik, W.R., and D.H. Zeuch, Modelling and mechanistic interpretation of creep of rock salt below 200°C, *Tectonophysics*, **121**, 125-152, 1986.
- Weertman, J., Dislocation climb theory of steady-state creep, *Trans. Am. Soc. Metals*, **61**, 681-694, 1968.
- White, S.H., Grain and sub-grain size variations across a mylonite zone, *Contrib. Mineral. Petrol.*, **70**, 193-202, 1979.
- White, S.H., S.E. Burrows, J. Carreras, N.D. Shaw, and F.J. Humphreys, On mylonites in ductile shear zones, *J. Struct. Geol.*, **2**, 175-187, 1980.
- White, S.H., M.R. Drury, S.E. Ion, and F.J. Humphreys, Large strain deformation studies using polycrystalline magnesium as a rock analogue, part I: Grain size paleopiezometry in mylonite zones, in *Experiments in solid state physics relevant to lithospheric dynamics*, edited by Y. Gueguen, and H. Kern, *Physics Earth Planet. Int.*, **40**, 201-207, 1985.
- Wolfenstine, J., O.A. Ruano, J. Wadsworth, and O.D. Sherby, Refutation of the relationship between denuded zones and diffusional creep, *Scripta Metall. Mater.*, **29**, 515-520, 1993.
- Zhang, S., S. Karato, J.D. FitzGerald, U.H. Faul, and Y. Zhou, Simple shear deformation of olivine aggregates, *Tectonophysics*, **316**, 133-152, 2000.
- Zhong, S., and M. Gurnis, Mantle convection with plates and mobile, faulted plate margins, *Science*, **267**, 838-843, 1995.

Papers and abstracts

- Ter Heege, J.H., J.H.P. de Bresser and C.J. Spiers, The influence of dynamic recrystallization on the grain size distribution and rheological behaviour of Carrara marble deformed in axial compression, in *Deformation mechanisms, rheology and tectonics 2001*, Geological Society of London Special Publication, *in press*, 2002 (chapter 3).
- Ter Heege, J.H., J.H.P. de Bresser and C.J. Spiers, Composite flow laws for crystalline materials with continuously distributed grain size: Theory and application to olivine, *J. Geoph. Res.*, *submitted*, 2002 (chapter 2).
- De Bresser, J.H.P., J.H. Ter Heege, and C.J. Spiers, Grain size reduction by dynamic recrystallization: Can it result in major rheological weakening ?, *Int. J. Earth Sci.*, **90**, 28-45, 2001 (section 1.4, modified).
- Ter Heege, J.H., J.H.P. de Bresser and C.J. Spiers, Incorporating grain size distributions in flow laws: Implications for rheology, in *Deformation mechanisms, rheology and tectonics 2001 abstract volume*, Noordwijkerhout, 65, 2001 (chapter 2).
- Ter Heege, J.H., J.H.P. de Bresser and C.J. Spiers, The effect of grain size distribution on rheology, *EOS Trans. AGU*, **81**, F1208, 2000 (chapter 2).
- De Bresser, J.H.P., J.H. ter Heege and C.J. Spiers, The influence of strain and temperature on the recrystallized grain size distribution of experimentally deformed Lorano marble, *EOS Trans. AGU*, **81**, F1188, 2000 (chapter 3).
- Ter Heege, J.H., J.H.P. De Bresser, and C.J. Spiers, The role of microstructure in determining rheology, in *Geophysical Research Abstracts*, **1**, 69, European Geophysical Society, 1999 (chapter 2).
- Ter Heege, J.H., J.H.P. de Bresser and C.J. Spiers, The effect of grain size distribution and dynamic recrystallization on rheology, *Deformation mechanisms, rheology and microstructures 1997 abstract volume*, Neustadt an der Weinstraße, 143, 1997 (chapter 2 & 5, modified).

Samenvatting

Grootschalige geodynamische processen (subductie, mantel convectie) worden voor een belangrijk deel gecontroleerd door de manier waarop gesteenten in de mantel en korst van de aarde vervormen (deformeren) als gevolg van aanwezige krachten. Deze krachten kunnen bijvoorbeeld veroorzaakt door plaatbewegingen. Onder de hoge temperatuur en druk die in de mantel en korst van de aarde heersen deformerende aanwezige gesteenten vaak in vaste toestand ('vloeiën'). Het gedrag van gesteenten onder invloed van opgelegde krachten (rheologie) kan beschreven worden met behulp van vloeiwetten, die de snelheid van vervorming (deformatie) relateren aan de opgelegde kracht, temperatuur en druk. De meeste vloeiwetten zijn gecalibreerd met behulp van experimenten in laboratoria waarbij materialen (o.a. gesteenten) onder hoge temperatuur en druk vervormd worden. De vloeiwetten kunnen vervolgens gebruikt worden om de rheologie van gesteenten in de natuur te bepalen, mits de invloed van alle processen die optreden tijdens deformatie op de rheologie bekend zijn. Gezien het grote verschil tussen deformatiesnelheden in de natuur en de deformatiesnelheden die haalbaar zijn in laboratoria, is een nauwkeurige bepaling van het effect van de (microfysische) processen die optreden essentieel voor een betrouwbare beschrijving van de rheologie van gesteenten onder natuurlijke omstandigheden.

Gesteenten die in de natuur voorkomen bestaan vrijwel altijd uit kristallen van verschillende grootte. De meeste gesteenten hebben dus een specifieke korrelgrootteverdeling met zowel kleine als grote kristallen. Deze kleine en grote kristallen kunnen tegelijkertijd volgens verschillende mechanismen deformeren, waarbij het mechanisme waardoor kleinere kristallen deformeren korrelgrootteafhankelijk is en het mechanisme waarmee grotere kristallen deformeren korrelgrootteonafhankelijk is. Daarbij is ook van belang dat gedurende deformatie van gesteenten de korrelgrootteverdeling aanzienlijk kan veranderen als gevolg van het groeien van kleine korrels of het vormen van nieuwe kleine korrels (dynamische rekristallisatie). Als het korrelgrootteafhankelijke deformatiemechanisme optreedt, wordt de rheologie van gesteenten mede bepaald door de korrelgrootteverdeling. Dit alles betekent dat voor een nauwkeurige beschrijving van de rheologie van gesteenten, vloeiwetten zowel met korrelgrootteafhankelijke als korrelgrootteonafhankelijke deformatie rekening moeten houden en dat het effect van dynamische rekristallisatie in ogenschouw genomen dient te worden. Desalniettemin missen bestaande vloeiwetten vaak een gedegen microfysische basis en zijn ze opgesteld voor een enkel deformatiemechanisme, zodat ze niet gebruikt kunnen worden voor een combinatie van deformatiemechanismen. Verder wordt korrelgrootte vaak als een constante in de wetten gebruikt, in plaats van de vereiste korrelgrootteverdeling.

Dit proefschrift heeft als doel de vloeiwetten die de rheologie van gesteenten onder hoge temperatuur en druk beschrijven te verbeteren door bestaande vloeiwetten zo aan te passen dat ze rekening houden met korrelgrootteverdelingen en een combinatie van deformatiemechanismen. Het heeft verder tot doel de invloed van dynamische rekristallisatie op de rheologie van gesteenten en op de evolutie van korrelgrootteverdeling tijdens deformatie te bepalen.

In hoofdstuk 1 komen de problemen aan de orde met vloeiwetten die de rheologie van gesteenten trachten te beschrijven. Daarbij wordt aangetoond dat het effect van dynamische rekristallisatie op de rheologie van aardse materialen nog niet afdoende behandeld is, ondanks de aanzienlijke hoeveelheid bestaand onderzoek met betrekking tot dit onderwerp. Hiermee wordt het kader van dit promotieonderzoek vastgesteld.

In hoofdstuk 2 wordt een theoretische vloeiwet voor het korrelgrootteafhankelijke deformatiemechanisme 'diffusiekruij' afgeleid, waarin korrelgrootte als een lognormale verdeling voorkomt. De vloeiwet wordt gecombineerd met een theoretische vloeiwet voor het korrelgrootteonafhankelijke deformatiemechanisme 'dislocatiekruij', hetgeen een

gecombineerde diffusie-dislocatie vloeiwet voor materialen met een korrelgrootteverdeling oplevert. Met deze vloeiwet kan de invloed van de mediaan en breedte (standaard deviatie) van een korrelgrootteverdeling op de rheologie systematisch worden onderzocht. De vloeiwet wordt gebruikt om de invloed van een variërende standaard deviatie op de deformatiesnelheid van gesteente dat volledig bestaat uit het in de mantel veel voorkomende mineraal olivijn, te bepalen. Hieruit blijkt dat de deformatiesnelheid orders van grootte kan veranderen als gevolg van veranderingen in standaard deviatie. Bestaande vloeiwetten met één waarde voor de korrelgrootte zijn niet in staat deze verandering te beschrijven. Dit laat zien dat de nieuwe vloeiwetten een betere basis bieden voor het extrapoleren van gegevens over deformatie van gesteenten van condities in het laboratorium naar de natuur. Alsmede helpen de vloeiwetten bij de interpretatie van deformatiemechanismen die optreden in laboratoriumexperimenten en maken ze het mogelijk het effect van dynamische rekristallisatie op de rheologie beter te bepalen.

Hoofdstuk 3 beschrijft een experimenteel onderzoek naar het effect van dynamische rekristallisatie op de korrelgrootteverdeling en de rheologie van marmer dat in Carrara, Italië in de natuur voorkomt. In dit onderzoek zijn cilindrische monsters van het gesteente systematisch in verschillende mate verkort (15-35% van de oorspronkelijke lengte) bij een temperatuur tussen 700 en 990°C en bij een (gas) druk van 150 of 300 MPa. De deformatiesnelheid is systematisch gevarieerd tussen verschillende experimenten (3.0×10^{-6} - $4.9 \times 10^{-4} \text{ s}^{-1}$). Het is gebleken dat de marmer een sterkte van 15-65 MPa (kracht per oppervlakte) heeft onder deze omstandigheden. De microstructuur en korrelgrootteverdeling van de oorspronkelijke marmer uit de natuur en van alle verkorte (gedeformeerde) monsters zijn in detail geanalyseerd. In de microstructuur van de deformede monsters zijn veel aanwijzingen voor een actieve rol van dislocatiekruip te vinden. Ook zijn er aanwijzingen voor het migreren van korrelgrenzen en het vormen van nieuwe kleine korrels, kenmerkend voor dynamische rekristallisatie. Uit analyse van de monsters die in verschillende mate gedeformerd zijn is gebleken dat voor verkortingen boven 15%, de gemiddelde korrelgrootte afneemt met toenemende verkorting (deformatie). Dit ging gepaard met een afname in sterkte van de marmer. De microstructuur en sterkte van de marmer veranderde tot aan de maximale verkorting mogelijk in het deformatieapparaat (een constante microstructuur en sterkte tijdens deformatie werd niet bereikt). Uit analyse van de korrelgrootteverdelingen bij de verschillende verkortingen is afgeleid dat tegelijkertijd korrels groeien en nieuwe korrels gevormd worden gedurende dynamische rekristallisatie. De (geringe) afname in sterkte tijdens deformatie wordt waarschijnlijk veroorzaakt door een toename van korrelgrootteafhankelijke deformatie, als gevolg van de afname in gemiddelde korrelgrootte. Een berekening van de te verwachten afname in sterkte door de veranderingen in korrelgrootteverdeling met behulp van bestaande vloeiwetten voor korrelgrootteafhankelijke en korrelgrootteonafhankelijke deformatie voorspelt ongeveer dezelfde afname als waargenomen in de experimenten. Dit geeft aan dat de afname in sterkte door verkleining van korrels als gevolg van dynamische rekristallisatie waarschijnlijk niet voldoende is om deformatie te localiseren. Localisatie van deformatie komt veelvuldig in de natuur voor, bijvoorbeeld in schuifzones. Er wordt vaak beweerd dat deze zones ontstaan doordat korrelgrootte wordt gereduceerd als gevolg van dynamische rekristallisatie, maar gezien de resultaten van dit onderzoek lijkt dit onwaarschijnlijk.

Hoofdstuk 4 behandelt een vergelijkbaar experimenteel onderzoek, maar dan op synthetisch gefabriceerd haliet gesteente met verschillend watergehalte. Ook hier is de invloed van dynamische rekristallisatie op de microstructuur, korrelgrootteverdeling en rheologie onderzocht. Van dit materiaal zijn cilindrische monsters met relatief hoog water gehalte in verschillende mate verkort (5-60% van de oorspronkelijke lengte) bij een temperatuur tussen 75 en 240°C en bij een (olie) druk van 50 MPa. De deformatiesnelheid is

weer systematisch gevarieerd tussen verschillende experimenten (5×10^{-7} - $1 \times 10^{-4} \text{ s}^{-1}$), hetgeen een sterkte van 7-22 MPa opleverde. Monsters met een relatief laag water gehalte zijn verkort bij een constante deformatiesnelheid ($\sim 5 \times 10^{-7} \text{ s}^{-1}$), bij een temperatuur van 125 of 175°C en bij een (olie) druk van 50 MPa, hetgeen een sterkte van respectievelijk 20 of 15 MPa opleverde. De microstructuur en korrelgrootteverdeling van het oorspronkelijke materiaal en van de gedeformeerde monsters is wederom geanalyseerd. De microstructuur van gedeformeerd haliet gesteente met relatief hoog watergehalte laat aanwijzingen zien voor dislocatiekruip en oplossing- en precipitatieprocessen. Ook zijn er aanwijzingen voor dynamische rekristallisatie, met migratie van korrelgrenzen als gevolg van oplossing- en precipitatieprocessen. De sterkte van het gesteente oscilleert tijdens deformatie, maar wordt uiteindelijk vrijwel constant in de meeste experimenten (vooral bij hoge temperatuur en een lage deformatiesnelheid). De constante sterkte bij hoge verkorting is altijd iets kleiner dan de (piek) sterkte bij kleine verkorting. De microstructuur van gedeformeerd haliet gesteente met relatief laag watergehalte laat in geringe mate aanwijzingen zien voor dynamische rekristallisatie, voornamelijk in de vorm van nieuwe kleine korrels. Uit het toepassen van gecombineerde vloeiwetten (hoofdstuk 2) op de laboratorium gegevens kan geconcludeerd worden dat deformatie in haliet gesteente met relatief hoog watergehalte plaatsvindt door korrelgrootteafhankelijk dislocatiekruip en korrelgrootteafhankelijk drukoplossing. De gerekristalliseerde korrelgrootte van haliet gesteente met relatief hoog watergehalte wordt bepaald door zowel de kracht op het monster als de temperatuur. De korrelgrootte gegevens komen het beste overeen met voorspellingen van een model voor dynamische rekristallisatie, ontwikkeld met de aanname dat korrelgrootte en rheologie bepaald worden door een balans tussen korrelgrootte reductie en korrelgroei, waarbij zowel dislocatiekruip als drukoplossing optreden.

In hoofdstuk 5 wordt een model voor dynamische rekristallisatie gepresenteerd dat is afgeleid van het model dat het beste de korrelgrootte gegevens in haliet gesteente met relatief hoog watergehalte voorspelt (hoofdstuk 4). In het aangepaste model wordt de theoretische vloeiwet voor diffusiekruip met lognormale korrelgrootteverdeling (hoofdstuk 2) gelijkgesteld aan de theoretische vloeiwet voor dislocatiekruip. Dit levert een model op dat de gerekristalliseerde korrelgrootteverdeling relateert aan deformatiecondities en vloeiwetparameters. Het model is getest met de korrelgrootte gegevens van haliet gesteente met relatief hoog watergehalte (hoofdstuk 4). De gegevens komen goed overeen met de voorspellingen van het model, hetgeen laat zien dat bij het vaststellen van de relatie tussen korrelgrootte en deformatiecondities, rekening gehouden dient te worden met de (varierende) standaard deviatie van de korrelgrootteverdeling. In bestaande modellen voor dynamische rekristallisatie wordt dit niet gedaan.

Korte samenvatting voor de leek

Onderzoek naar de sterkte en vervorming van materialen kent brede toepassing in veel onderzoeksgebieden, zoals materiaalkunde en aardwetenschappen. In de diepe aarde, onder hoge druk en temperatuur, breken stenen niet, maar vloeien ze in vaste toestand net zoals ijzer kan vervormen bij kamertemperatuur en atmosferische druk. Dit is erg belangrijk, want de snelheid waarmee stenen in de diepe aarde vervormen bepaald voor een groot deel hoe gebergten als de Alpen of Himalaya gevormd worden. Met geavanceerde apparatuur in het laboratorium kunnen we de omstandigheden die diep in de aarde heersen nabootsen. We kunnen dan nauwkeurig onderzoeken hoe sterk gesteenten onder deze omstandigheden zijn en hoe snel ze kunnen vervormen. Tijdens het vervormen van gesteenten onder deze omstandigheden verandert de interne structuur van de gesteenten, zoals de korrelvorm en -grootte (rekristallisatie). Nu is gebleken dat onder bepaalde omstandigheden de korrelgrootte bepaald wordt door de kracht en temperatuur waarmee stenen vervormd worden: Hoe groter de kracht en temperatuur, hoe kleiner de korrelgrootte. Dit gegeven kan gebruikt worden om te bepalen welke krachten er gepaard gaan met het ontstaan van gebergten door de korrelgrootten van gesteenten in de natuur te bepalen. Dit vereist echter wel dat de resultaten uit het laboratorium naar natuurlijke omstandigheden geextrapoleerd worden. In het onderzoek zijn relaties tussen de korrelgrootteverdeling en de kracht of snelheid waarmee stenen vervormd worden onderzocht en nauwkeurig vastgesteld. Dit is gedaan door marmer en steenzout te vervormen onder hoge druk en temperatuur en te bepalen hoe de interne structuur verandert door de vervorming. De resultaten van het onderzoek maken het mogelijk om laboratorium gegevens betrouwbaar te extrapoleren naar natuurlijke omstandigheden. Daardoor is nu beter vast te stellen hoe snel stenen in de aarde vervormen en welke kracht er opgetreedt als gebergten gevormd worden.

Dankwoord

Nu mijn promotie tegen het einde aanloopt, is de tijd daar voor een korte terugblik en een lang dankwoord. Ondanks veel goede voornemens bij het begin, heb ik volgens mij toch het klassieke promotietraject doorlopen met een rustig begin en een exponentieel toenemende werkdruk aan het einde. Desalniettemin kan ik terugkijkend toch constateren dat ik er zeer veel plezier in heb gehad en dat het voor mij in ieder geval zeer de moeite waard is geweest. Dit is vooral te danken aan de goede en constructieve atmosfeer in het HPT lab. Jammer is wel dat ik de best mogelijke werkomgeving aan het begin van mijn (hopelijk) wetenschappelijke carrière heb gehad.

Ontegengesteld schuldig aan deze goede werkomgeving zijn mijn begeleiders Chris Spiers en Hans de Bresser. Gedurende mijn promotie is Chris altijd een bron van inspiratie geweest. Zijn begeleiding op de universiteit, maar even vaak na kantooruren in een restaurant in Utrecht waren altijd zeer waardevol en hebben mijn promotieonderzoek naar een veel hoger plan gebracht. Chris, I hope you can find the time to do more research in the future again. Chris zijn oog voor details en streven naar wetenschappelijke perfectie waren soms lastig maar altijd terecht. Wat mij altijd blij heeft verrast is dat Chris bij de voor mij meest gecompliceerde materie nog een tijd voor humor kon vinden. Dankzij hem zal ik ook nooit meer met een strak gezicht iemand 'my apparatus' kunnen laten zien. Chris, I hope we're going to score a lot with the science in this thesis. Many thanks !

Met Hans heb ik een lange en zeer intensieve periode achter de rug met veel begeleiding, veldwerken, congressen en andere uitstapjes. Ik ben nog net niet met hem op vakantie geweest, maar wie weet wat de toekomst brengt. De samenwerking met Hans heb ik altijd als positief ervaren, behalve dan misschien die keer dat ik als vervent alpinist Hans moest lossen op de flanken van de Pyreneeën. Ik heb Hans leren kennen als iemand met een tomeloze energie en vrijwel onaflatende inzet in alles wat hij doet. Mijn onderzoek heeft van deze energie enorm geprofiteerd. In mijn ogen kent Hans geen verschil in benadering van een student tijdens tweedejaars veldwerk en een professor van een prestigieuze universiteit. Volgens mij een uitstekende eigenschap. Misschien is Boxtel toch een prima kweekvijver voor goede wetenschappers, voor gezelligheid is dat al bewezen. Ik heb met Hans met name veel plezier gehad tijdens het begeleiden van tweedejaars studenten. Helaas lijken mijn trucs om Hans te verleiden tot nog een 'ultimo' uitgeput, maar ik ben weer inspiratie aan het opdoen voor mijn promotiefeest. Hans, het was bijna 'in a gadda da vida' voor mij !

Naast mijn begeleiders zijn Colin Peach, HPT technici Peter van Krieken, Gert Kastelein en Eimert de Graaff, Jaap Liezenberg, en secretaresse Magda Marthens ook verantwoordelijk voor de goede sfeer in het HPT lab. Colin was altijd bereid me met raad en daad bij te staan en heeft menig probleem met computers of apparaten in het lab opgelost. Bovendien bleef hij altijd vriendelijk bij mijn elektronische onwetenschap en was het goed met hem vertoeven tijdens menig HPT uitje en jaarlijkse HPT barbecue. Peter is nauw bij mijn onderzoek betrokken geweest en ik heb menig uurtje samen met hem in het lab doorgebracht. Ook heeft hij mijn mobiliteitsprobleem aan het eind van mijn promotie opgelost door me zijn flitsende bolide te verkopen. Gert zijn tomeloze energie en snelheid van handelen hebben menig technisch probleem als sneeuw voor de zon doen verdwijnen. Voordat ik met mijn ogen kon knippen, stond de oplossing van het probleem al op mijn bureau, aangevuld met een levendige verklaring of anekdote. Eimert stond altijd klaar om bij te springen met voltmeter en gereedschapskist. Ik ben blij dat hij het dreigend inferno in Bilthoven heeft weten te voorkomen. Jaap heeft de slijpplaten van de zoutmonsters gemaakt met een precisie en kwaliteit die ik nooit had kunnen evenaren. Magda was onmisbaar, zeker aan het einde van mijn promotie. Zij heeft veel praktische problemen voor me opgelost en altijd met oprechte belangstelling in mijn handel en wandel. Allen hartelijk bedankt !

Veel AiO's, postdocs en stafleden hebben bijgedragen aan een aangenaam verblijf op het IvA. Allereerst wil ik Bart Bos bedanken. Met Bart heb ik het overgrote deel van mijn promotie de kamer gedeeld. Toch jammer dat we door Hans uit ons riante onderkomen met uitzicht op de HPT tuin zijn verjaagd, maar die rekening wordt nog wel vereffend (regel jij de pek en veren?). Bart was altijd in voor een zinnige of onzinnige discussie over onderzoek, dingen die 'den hemel schrijnend' waren of het vreemde gedrag van uithofkonijnen en andere passanten. Ik moet helaas toegeven dat de discussies om 4 uur in de Gasterij of 't Pandje wel meer onzinnig dan zinnig zal zijn geweest zijn. Vaak kwam klinkend gezang uit onze kamer, waarbij zelfs repertoire als Britney Spears niet geschuwd werd. Bij Bart zijn dingen nooit zeker zolang er niet uitgebreid over gediscussieerd is en dat hielp altijd dingen te relativiseren of in het juiste perspectief te zien. Vervelend genoeg lijkt Bart de laatste tijd niet meer gehinderd te worden door enige kennis van zaken. Siese de Meer was altijd in voor een gezellig praatje over van alles en nog wat en natuurlijk altijd aanwezig op de jaarlijkse HPT barbecue en de vele HPT 'piss-ups'. Ik kan me niet herinneren dat ik ooit eerder De Gasterij of 't Pandje heb verlaten dan Siese. In het begin van mijn promotie werden deze escapades altijd opgeluisterd door Rob McDonnell. Ik wil verder Martyn Drury bedanken voor al zijn relevante vragen en de broodnodige kritische noot bij al te lyrisch gedrag over de 'boundary hypothese' en Bernard de Jong voor het scherp houden van de geest en een onaflatende reeks onvergetelijke uitspraken ('standing wave in a spherical enclosure'). Tony, Hans, Otto en Paul worden bedankt voor hand en span diensten, slijplaten en de voorkant van dit proefschrift. Vele memorabele activiteiten en personen hebben mijn pad gekruist. Ik wil Marga, Kike, Andor, Arjan, Fraukje, Armelle, Marije, René, Paul M., Pat, Rian, Saskia ten G., Xiangmin, Stan W., Herman, Frederic, Rinus, Reinoud, Jeroen van H., Abir, Stan S., Marleen, Bert, Rob G., Quintijn, Max, Jeroen de S., Paul F., Sander, Margret, Menno en Edith bedanken voor de interesse in mijn werk en voor het plezier tijdens de vrijdagmiddagfestiviteiten, de VMSG Alpenexcursie, de begeleiding van het Pyreneeënveldwerk en squash. En voor de koffie natuurlijk.

Zeker zo belangrijk voor het slagen van mijn promotie zijn mijn vrienden geweest. Geen gezonde geest zonder een gezond sociaal leven. Ik wil Esther ('je kunt het'), Remco ('afspraak bij de marmot'), Fred en Vivian ('kerstmaaltijd'), Jan-Berend en Meta ('het is maar een promotie'), Michiel ('hoe gaat ie'), Leon ('ik breng je met de wagen'), Peter-Paul ('is het nou nog niet af, hoofd'), Suzanne ('profiteurs'), Vian ('zak met hooi'), Jeroen ('op zuid') en Mathijs ('is dat nou die belangrijke professor') bedanken voor hun steun en niet aflatende interesse in mijn wel en wee. Zonder jullie had ik er nooit lol in gehouden en was dit een propedeutisch examen geweest. En dan de Hut ! Goed voor menig feest, excursie en spelletjesavond, maar nooit zonder tientallen emails en nooit op de afgesproken plek ('zeg ken jij de mosselman'). Martijn ('leuk is het allang niet meer'), Jan-Willem, Luuk, Jolt, Saskia en Eveline, we moeten nodig weer eens op excursie ('Islands in the stream') ! Ook dank aan mijn oud-huisgenoten van IBB 139 en zaalvoetbal teamgenoten: Leve Kampong 4 !

Vele studenten hebben mij gezelschap gehouden en geholpen tijdens HPT barbecues, veldwerken, Edje Educatorium maaltijden en onderwijshallunches. Ik heb het contact met hun altijd zeer op prijs gesteld. Helaas, het zijn er teveel om op te noemen en ik bedank een ieder die mij geholpen heeft. Toch wil ik een aantal personen specifiek noemen: Arthur en André (de EOS collectie is voor jullie), Martine (succes !), Sam, Joris, Noor, Juliette en Annemieke.

Natuurlijk heb ik de belangrijkste personen tot het laatste bewaard. Mijn ouders, Hans en Hennie, steun en toeverlaat en uiteindelijk hoofdverantwoordelijk voor de totstandkoming van dit proefschrift. En mijn zussen en vriendinnen, Marieke, Rimke en Noortje. Nooit te beroerd om hun desolate broer van een goed gesprek, een hapje of drankje te voorzien. Wat jullie voor mij betekend hebben hoop ik ooit nog terug te kunnen geven. Ook Mark, Pieter en Jasper, bedankt voor jullie belangstelling.

Curriculum Vitae

Jan ter Heege was born on the 14th of February 1972 in Rossum (Gld). He attended secondary school in Zaltbommel from 1984-1990. In 1990, he graduated from secondary school and started to study geology at the Utrecht University. In the course of his study, he developed a strong interest in experimental rock deformation and took several specialization courses in this subject. He graduated in 1996 after completing a research project in the HPT laboratory of the Utrecht University on pressure solution in gypsum. In 1997, he started the Ph.D. project described in this thesis.

The author enjoying the benefits of Alpine orogeny.

